This is to certify that the
dissertation entitled

OPTIMAL DESIGN AND PERFORMANCE OF LONGITUDINALLY SPLICED PRECAST/PRESTRESSED CONCRETE BRIDGES

presented by

Pimpida Surakomol

has been accepted towards fulfillment
of the requirements for the

Ph.D. degree in Department of Civil and Environmental Engineering

Major Professor's Signature

12/16/05

Date

MSU is an Affirmative Action/Equal Opportunity Institution

OPTIMAL DESIGN AND PERFORMANCE OF LONGITUDINALLY SPLICED PRECAST/PRESTRESSED CONCRETE BRIDGES

VOLUME I

By

Pimpida Surakomol

A DISSERTATION

Submitted to
Michigan State University
in partial fulfillment of the requirements
for the degree of

DOCTOR OF PHILOSOPHY

Department of Civil and Environmental Engineering

2005

ABSTRACT

OPTIMAL DESIGN AND PERFORMANCE OF LONGITUDINALLY SPLICE PRECAST/PRESTRESSED CONCRETE BRIDGES

By

Pimpida Surakomol

Design of spliced precast/prestressed concrete girder bridges through continuous post-tensioning has gained renewed interest; however, information, as well as design and analysis tools, to assess the feasibility of these systems during the preliminary design phase are limited. In this study, nonlinear structural optimization analyses were integrated with sequential time-dependent design and analysis procedures, to evaluate the performance of single- and two-span continuous spliced precast/prestressed girder bridges was studied and aids for their preliminary design. Common construction methods were investigated to asses their effect on system efficiency and achievable span lengths. Component and system optimization procedures were coupled and used as a tool to develop optimal girder shapes for negative, or pier, segments on two-span continuous systems. Optimal design solutions for pre- and post-tensioned strands and their locations along the span, and maximum span lengths, were obtained and presented in the form of design charts. The solutions satisfied a common objective of minimum construction cost or a set multicriteria objective functions that yielded compromise solutions for different single objective functions. Studies provided a better understanding of the issues and parameters in this bridge design type and the developed design aids can be a great asset to expedite their design potentially resulting in its wider use by transportation agencies.

Acknowledgements

I would like to express my sincere appreciation and special thanks to my advisor, Professor Rigoberto Burgueño. I am grateful for his guidance and support through the course of this study. He provided inspiration and helped me greatly in this dissertation. Without his bright idea and his strong encouragement, this work would not be possible.

In addition, I would like to thank Professor Ronald S. Harichandran, Professor Parviz Soroushian, and Professor Mohammad Najafi for being in my dissertation committees and for helpful ideas.

Furthermore, I also would like to thank Professor William Saul for always guiding me through these years. I also would like to thank my supervisor, Dr. Khaled Soubra, for always understanding and supporting me for both work and study.

Also, I would like to give my appreciation to my parents Kosol and Pimphan, my sister Rose, and my brother Eddy and Oak for their encouragement, support, love and care. Finally, I would like to thank Kriengkrai for giving me the motivation to finish this dissertation. My life would not be at this point without any support from these people.

TABLE OF CONTENTS

LIST OF TABLES

LIST OF FIGURES

LIST OF SYMBOLS

α	The angle between the effective post-tensioning strands and the horizontal reference of lowest post-tensioned profile.
α_1	The coefficient of horizontal distance from splicing location to the center of pier.
β	The coefficient of eccentricity at the end of girder.
β_1	The coefficient of eccentricity at the mid-span of girder.
ε_p	The time-dependent change in strain at location of prestressing steel (tension positive).
ε_{pf}	The value of strain corresponding to the computed stress.
ε_{po}	The different in the strain between the concrete and prestressed reinforcement.
ε_{SD}	The shrinkage strain for deck.
ε_{SG}	The shrinkage strain for girder.
ε_{sh}	The shrinkage strain for steam-cured concrete.
ε_{st}	The shrinkage strain at time t.
ε_t	The total concrete strain at time t.
σ_{1da}	The bottom girder compression stress constraint
σ_{2da}	The Bottom girder compressive stresses

σ_{3da}	The bottom girder stress constraint
σ_{4da}	The compression stress limit under full service load
σ_{b1n}	The girder bottom stress along the negative segment
σ_{b2n}	The girder bottom stress along the negative segment after first staged post-tensioning
σ_{b3n}	The girder bottom stress along the negative segment after deck and splice placement
σ_{b4n}	The girder bottom stress along the negative segment after second staged post-tensioning
σ_o	The concrete stress at time t = 0.
σ_t	The concrete stress at time t.
φ_D	The creep coefficient for deck.
φ_G	The creep coefficient for girder.
φ_{t,t_o}	The creep coefficient at time t due to load applied at time t_o.
ϕV_n	The nominal shear strength provided by concrete, prestressing and reinforcement.
A_{gn}	The girder gross area along the negative segment
A_{PRET}	The pre-tensioned strands.
A_{PS}	The cross-sectional area of prestressing steel.
A_{ps}	The prestressing steel.

A_{psn}	The total pre-tensioned area in the negative segment
A_{PT}	The post-tensioned strands area in the section.
A_v	The area of web reinforcement within a distance *S*.
A_{vf}	The total area of all shear reinforcement including post-tensioning strands and mild reinforcement crossing the shear plane.
b'	The width of a web of a flanged member.
b_1	The bottom flange width
b_2	The top flange width
b_e	The effective bridge width.
b_f	The beam flange width.
C	The permissible pressure at the splice contact area = 0.
C_B	The beam cost
C_{CD}	The concrete deck cost
C_f	The compressive force in the girder flange.
C_o	The chloride concentration at the surface
C_{PS}	The pre-tensioning cost
C_{PT}	The post-tensioning cost
C_t	The compression force in the deck.
C_{TS}	The temporary support cost
d	The distance from extreme compressive fiber to centroid of prestressing force.

d_p	The effective depth.
D_c	The diffusion coefficient
D_w	The web depth
e	The eccentricity of prestressing steel relative to centroid of composite section (down positive).
E_D	The modulus of elasticity for deck.
E_G	The modulus of elasticity for girder.
E_O	The modulus of elasticity at time t_o.
E_p	The elastic modulus of prestressing steel.
E_{PS}	The modulus of elasticity of prestressing steel.
e_{ob}	The vertical distance at the center pier of beam.
e_{pn}	The net eccentricity of pre-tensioning strands along the negative segment measured from the neutral axis of the section
erf()	The error function, in practice x is equal to the depth of concrete over the steel reinforcement.
F	The total post-tensioning forces in the section.
$F_1(x)$	The economics multicriteria optimization
$f(x_i)$	The minimization of total structural costs
$F_1(x)_{min}$	The Economics Multi-criteria
$f_1(x)$	The minimum superstructure cost
$f_2(x)$	The minimum number of pre-tensioned strands

$f_3(x)$	The minimum number of post-tensioned strands
f_c	The girder compressive strength.
f_c'	The final high-strength concrete compressive strength
f_{cd}	The deck compressive strength.
f_{cd}'	The concrete compressive strength of deck at the final age
f_{cdp}	The change in concrete stress at center of gravity of prestressing steel due to permanent loads.
f_{cgp}	The sum of concrete stress at center of gravity of prestressing tendon due to prestressing force at transfer and the self-weight of member at maximum moment.
f_{cgp1}	The sum of concrete stress at center of gravity of prestressing tendon due to post-tensioning force and removal of temporary support.
f_{cgp2}	The sum of concrete stress at center of gravity of post-tensioning tendon due to pre-tensioned strands and girder self-weight.
f_{ci}'	The concrete compressive strength at release
f_d	The stress due to unfactored dead load at extreme fiber section.
f_{pc}	The compressive stress in concrete at centroid of cross section resisting externally applied loads.
f_{pe}	The compressive stress in concrete due to effective prestress forces at extremely fiber of section.
$f_{pe,final}$	The pre-tensioned stress at the final stage

f_{pe1n}	The effective prestress in the pre-tensioned strands after pre-tensioning
f_{pe2n}	The effective prestress in the pre-tensioned strands after placing the deck
f_{pe3n}	The effective prestress in the pre-tensioned strands after post-tensioning
f_{pe4n}	The effective prestress in the pre-tensioned strands after applying the live load
f_{pof}	The effective prestress in the post-tensioned strands after post-tensioning
f_{pof1}	The effective pre-stress in the first post-tensioned strands after first post-tensioning
f_{pof2}	The effective prestress in the second post-tensioned strands after second post-tensioning
f_{poff}	The effective prestress in the post-tensioned strands after applying the live load
f_{poff1}	The effective prestress in the first post-tensioned strands after second post-tensioning
f_{ps}	The prestressing steel.
f_{pu}	The specified tensile strength of prestressing steel.
f_{py}	The yield strength of prestressing steel.
f_y	The yield strength of reinforcement.
H	The relative humidity.
h_f	The slab thickness.

h_w	The girder web height.
I	The moment of inertia about the centroid of the cross-section.
I_D	The moment of intertia of deck about their own centroids.
I_G	The moment of intertia of girder about their own centroids.
k_C	The factor for the effect of volume/surface of component.
k_f	The factor for effect of concrete strength.
k_S	The size factor which is based on PCI equation (1977).
L	The total span length of each span
L_1	The end segment length
M	The total expected maintenance costs.
M_{cn}	The construction load moment along the negative segment
M_{cr}	The moment causing flexural cracking at the section due to externally applied loads.
M_{dn}	The deck moment along the negative segment
M_{gn}	The girder moment along the negative segment
M_{hn}	The haunch moment along the negative segment
M_{lln}	The live load moment due to truck and lane loadings
M_{max}	The maximum factored moment at section due to externally applied load.
M_n	The nominal design moment.
M_{post1}	The primary moment due to first staged post-tensioning

M_{post2}	The primary moment due to second staged post-tensioning
M_{postn}	The primary moment due to post-tensioning
M_{rn}	The removal moment due to temporary support removal
M_{sec1}	The secondary moment due to first staged post-tensioning
M_{sec2}	The secondary moment due to second staged post-tensioning
M_{sectn}	The secondary moment due to post-tensioning
n	The modular ratio of deck concrete to girder concrete.
N	The number of identical prestressing tendons.
npo	The total number of post-tensioning strands on beam
$npo1$	The total number of post-tensioned strands in the girder for single-stage post-tensioning construction or a first stage post-tensioning operation for two-staged post-tensioning construction
n_{po2}	The total number of second staged post-tensioned strands
npr_{1i}	The number of bottom pre-tensioning strands on end segments at i^{th} row
npr_{2i}	The number of bottom pre-tensioning strands on mid-span segments at i^{th} row
npr_{i1}	The number of bottom pre-tensioned strands on end-segments at row i^{th}
npr_{i2}	The number of top pre-tensioned strands on the mid-span segments at row i^{th}
$nprt_1$	The number of top pre-tensioning strands on end-segments

$nprt1$	The number of top pre-tensioned strands on the end-segments
$nprt_2$	The number of top pre-tensioning strands on mid-segment
$nprt2$	The number of bottom pre-tensioned strands on the mid-segment
P_c	The permanent net compressive force normal to the shear plane.
pra	The splice location
R	The removal cost.
R_F	The anchor loss.
S	The beam spacing.
S_b	The bottom sectional modulus
S_{bgn}	The bottom section modulus along the negative segment
S_C	The first area moment of the transformed deck section about the centroid of the composite section.
S_f	The maximum soffit thickness
S_t	The top sectional modulus
t	The maturity of concrete (days).
T	The depth of compression.
t_1, t_2	The bottom flange thicknesses
t_3, t_4	The top flange thicknesses
t_i	The age of concrete when load is initially applied (days).
t_w	The web thickness

V_c The shear strength provided by concrete.

V_{ci} The shear strength.

V_{cw} The shear strength.

V_i The factored shear force at section due to externally applied loads.

V_n The nominal shear resistance of the interface.

V_p The shear force provided by post-tensioning.

V_s The web reinforcement shear.

V_u The factored shear force at the section considered.

x The distance from the concrete surface to the steel surface

x_A The stress at the anchorage.

y_a The vertical distance from the bottom extreme fiber of the girder to the net centroid of the equivalent post-tensioned duct at end segments

y_b The vertical distance from the N-A to the net centroid of post-tensioned duct at the middle of end segment

y_{bb} The vertical distance from the bottom extreme fiber to the net centroid of the post-tensioned duct at the mid-segment

y_c The vertical distance from the neutral axis to the net centroid of the equivalent post-tensioning duct at the splice location

y_d The vertical distance from the neutral axis to the net centroid of the equivalent post-tensioning duct at the negative pier location

Y_t The distance from centroidal axis of gross section.

1 Introduction

1.1 Overview

A spliced precast prestressed girder bridge is defined as a type of superstructure in which separate precast concrete beam-type elements are longitudinally joined, typically using post-tensioning, to a continuous girder. Among the reasons to use spliced girders are the reduction of substructure units due to increased span lengths, reduction of girder units due to increased girder spacing, and functionality and aesthetic improvements by reducing superstructure depth.

Spliced girder bridges have a proven track record, with more than 250 spliced girder bridges having been constructed in the US, some of them dating back as early as 1952 (Castrodale and White 2004). In spite of their past and continued use, the application of this technique is not widespread. A significant reason for limited utilization of spliced girders is the ambiguity in their design and analysis, rooted in the consideration of various issues with which the designer of conventional precast prestressed concrete girders is typically not familiar. In addition, the information available in the literature regarding the design, analysis and construction of spliced girder bridges is limited, as the experience, information, and methods used on these projects have tended to be job-specific, and the knowledge gained has not been made widely available for use on similar projects (Castrodale and White 2004). A recently completed NCHRP research program on extending the span of bridges using precast prestressed concrete girders (Castrodale and White 2004) will certainly improve the state of knowledge on the design

of spliced girder bridges, as the effort has successfully led to recommendations on LRFD design procedures, standard details, and design examples.

While the design requirements for spliced girder bridges are not significantly different from conventional prestressed concrete design, the analysis procedure must take additional considerations. Among the most relevant are staged construction, multiple stressing stages, and combined pre-tensioning and post-tensioning. Thus, the design of spliced girder bridges involves greater complexity than is required for conventional precast/prestressed concrete girder designs. The design is generally executed using a computer program or a series of spreadsheets. Unfortunately, design guides, aides, and examples of spliced girder bridges to help designers are not readily available or address only limited portions of the design (Castrodale and White 2004).

The design of spliced girder bridges depends on several parameters that significantly influence performance and cost. The most relevant are time dependent effects, splicing locations, construction sequences, girder segment geometries, number of beams, and number or profiles of pre-tensioned and post-tensioned reinforcement. Normally most design variables are determined based on the designer's judgment and on a trial and error processes. Consequently there is no guarantee of obtaining the most efficient and/or economical design, which requires more time and effort to explore, and which typical projects cannot afford.

Since design of spliced girder bridges involves a number of design considerations, the use of mathematical optimization methods can provide a systematic approach to arrive at appropriate design solutions. Computational optimization techniques (Arora 2004) can thus be used as a tool to develop the configuration and sectional optimization

of spliced girder bridges and serve as a guide to produce design aids. Design aids can depict the relations between girder shape, girder spacing, pre-tensioning and post-tensioning requirements, splicing locations, pier segment geometries, initial and final concrete compressive strengths, and tendon profiles. Bridge engineers would find benefits in design charts and tables, which are based on optimal solutions that will help expedite the design process. As a result the system can be more widely used by state highway agencies and bridge consulting firms.

1.2 Precast Prestressed Concrete Bridge Construction

Precast Prestressed concrete bridges have become the preferred type of bridge construction; approximately 46% of today's bridges are of this type, primarily for reasons of economy, savings in life-cycle costs and their fast construction (Tanase et al. 2002). In spite of this appeal, precast bridge construction has been mostly limited to simply supported spans primarily due to the ease of construction.

This approach, however, is not in alignment with current design trends toward continuous systems to allow for greater span lengths, eliminate deck joints, and reduce intermediate piers for safety and cost. The use of precast prestressed concrete bridge for longer spans, for instance, greater than approximately 46 meters (150 feet), has been limited due primarily to transportation constraints. Consequently, for medium span bridges, steel plate girders are typically the favored solution, although they have the drawback of higher material, construction, and maintenance costs. In order to overcome these drawbacks and to have an alternative to compete with steel superstructures, methods to achieve continuity with precast prestressed girders have become of great interest to increase the spanning capabilities of precast concrete bridges.

Several methods have been proposed to achieve the continuity of precast prestressed girders (Anderson 1973, Tadros et al. 1993 and Tadros et al. 1995). The most common are the use of mild steel reinforcement in the deck, the splicing of prestressing strands, and the use of longitudinal posttensioning (Anderson 1973). Of these methods, splicing of girder segments through post-tensioning, commonly referred to as longitudinal girder splicing, appears to have the greatest potential for extending span ranges for precast prestressed concrete girder bridges (Castrodale and White 2004).

1.3 Extending the Span Ranges of Precast Bridges

Design options for extending the span lengths of conventional precast/prestressed concrete girder bridges can be divided into groups which include material related methods; design enhancement methods; the post-tensioning method; and spliced girder construction.

Many options related to the enhancement of material properties have been used for extending span length. Using lightweight concrete by reducing the density of girder and deck concrete has been widely used to reduce the weight of concrete bridges for design purposes as well as to minimize transportation limits. Bridge decks constructed with lightweight concrete have been found to have equal or better durability than normal weight concrete deck (Castrodale and White 2004). However when using lightweight concrete girders, the increased prestress losses and the reduced modulus of elasticity must be considered. The use of high strength concrete can also be used to extend span length and the workability of concrete. It may not directly affect the increase of span length, but it does increase the allowable stress limits. This option has an increased cost compared to the use of standard strength concrete. The increase in strand size can also

help increase the span length of precast/prestressed concrete girder bridges. The 42% increase in strand area from 12.7 mm (0.5 in.) diameter to 15.24 mm (0.6 in.) diameter strand can significantly increase the achievable maximum span length for bridge girders, especially when use in conjunction with high strength concrete girder (Castrodale and White 2004).

Enhancement of design parameters or procedures can also increase the span length of bridges. Modified standard girder sections are used very often since it is less expensive than proposed new beam sections, however, the designer should confer with the local producer before proposing modification to standard forms. Modified girder sections will increase the girder sectional properties. If the side forms for the standard girders can be adjusted, all horizontal dimension changes can be easily achieved. Besides increasing girder properties, the increase in top and bottom flange depth allows an additional row of pre-tension strands or post-tensioning to be placed in the flanges. These modifications are considered as economical methods since existing forms are utilized to modify sections with minimum effort and cost. This girder modification will help increase the section capacity dramatically and should be considered as a first alternative to extend the span length before proposing a new girder section.

In recent years, several new girder cross-sections have been developed and used since they have been shown to be more efficient than standard girders for project specific needs. However, this option should be used only if many girders and many similar projects are anticipated to use the new girder types. Otherwise formwork costs are relative high and the producer may be reluctant to bid the job competitively. Furthermore, design of continuous live loads on the girder and use of temporary supports

to shore the girders during deck placement can also help gain additional span lengths for prestressed concrete bridges. Moreover, the LRFD specifications (AASHTO LRFD 2003) allow designers to use refined methods to compute live load distributions for girder designs, which can lead to reduced live load demands and as a result an increase in girder span length.

Utilizing post-tensioning in precast prestressed concrete girder bridges is the most efficient way to increase the span length beyond conventional simple spans. However, the design and construction of post-tensioned girders is more complicated and the design and construction cost is higher. Post-tensioning can be done for a single girder component or to longitudinally splice several girders. Post-tensioning is typically applied to final girder cross-section (i.e., girder plus deck) where the composite section is already achieved; therefore it is more efficient than conventional prestressed concrete girders where pre-tensioning is applied to the noncomposite girder section.

The combination of post-tensioning and pre-tensioning for the splicing of precast girders can lead to spans that are much longer than typical simply-supported prestressed concrete girders. With the use of combined pre-tensioning and post-tensioning, girder sections have become longer, heavier, and deeper. Consequently, their length and weight may exceed the allowable limits for shipment and/or erection. In order to overcome these drawbacks and to have an alternative to compete with steel superstructures, methods to achieve continuity by making smaller precast prestressed girders continuous through post-tensioning have become of great interest to increase the spanning capabilities of this bridge system. Thus, this method allows for longer spans and has recently gained the most attention.

1.4 Spliced Precast Prestressed Girder Bridges

Longitudinally spliced precast prestressed girder bridges (SGB) have been built since 1960. However, they are not commonly used because of limited experience, limited information since most projects are job-specific (Castrodale and White 2004), the added complexity in their design and analysis, and the relatively fewer available design guidelines.

Nowadays, spliced girder bridges are primarily used only for specific projects where the custom beam sections were used to substitute long-span structural steel bridges due to the construction schedule, maintenance, and fabrication cost issues of concern during the design process.

The solution of longitudinally splicing girders can be applied for single- and multi-span bridges. Standard sections used for simply supported bridges are used for section lengths under positive moment. These segments are thus typically called positive or field segments. Pier or negative segments normally consist of custom-designed sections for segments over intermediate supports used for continuous bridge solutions. "Drop-in" segments are usually used in long continuous spans located between the pier segment and field segment (Figure 1-1). Multi-span bridges typically consist of "pier" and "field" segments, while single-span systems consist of field segments only.

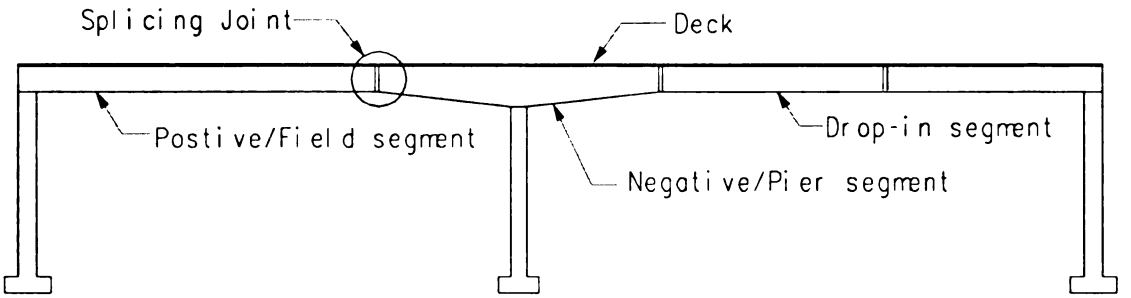

Figure 1-1 *Components of spliced precast/prestressed concrete girder bridge Systems*

All standard precast/prestressed concrete girders currently available in the market are developed for use in simple span bridges. In general, continuous systems lead to higher negative moment demands than simple spans. While peak moments can be reduced by varying the pier spacing and relative span lengths (Ronald 2001), current practice used for custom pier segments is to increase the flexural stiffness and strength in this region by gradually thickening the bottom flange, producing a curved haunch with a constant sized bottom flange, or using a girder with a variable web depth.

The significant form modification of custom-designed pier segments limits the wide implementation of this concept due to the high cost of girder fabrication. In order to make spliced girder bridges more economical in comparison to steel plate girders, the use of standard precast/prestressed sections for typical pier segments needs to be developed and optimized to reduce cost. Thus, the development of standardized haunched girders for pier segments has been identified as a research need by the Concrete Bridges Committee of the National Cooperative Highway Research Program - NCHRP 517 (Castrodale and White 2004).

The design of spliced girder bridges was greatly propelled forward by the work of Tadros et al. (1992) who studied the analysis and design of two-span spliced girder bridges using prismatic I-beams sections. Later Tadros et al. (1995) studied methods to create continuity in precast girder bridges by using high strength threaded-rod splicing and pretensioned strand splicing. Holombo et al. (2000) studied the performance of precast prestressed spliced girder bridges under seismic loads and provided guidelines to detail reinforcement at piers, bentcap, and joints; as well as discussing design aspects relating their seismic analysis. Roland (2001) evaluated key aspects on the design and construction of post-tensioned bulb-tee girder bridges and provided specific recommendations for future projects. Among the information provided by Roland are material properties for design, creep and shrinkage parameters, allowable stress and ultimate strength design considerations, etc. In addition, several recent spliced girder bridge projects have been published (Caroland et al. 1992, Fitzgeral and Stelmack 1996, Janssen and Spaans 1994) providing key aspects of their design, analysis and construction to convey knowledge on this bridge type from the experience. The state-of-the-art knowledge on spliced girder design and analysis has been recently documented through an NCHRP study in (Castrodale and White 2004) in NCHRP Report 517. This report summarizes current approaches to increasing the spanning capabilities of prestressed concrete girders and identifies longitudinal splicing through post-tensioning as the most effective method. In addition, the work identified load-and-resistance-factor-design procedures for spliced girder bridges, including standard details and design examples.

The analysis and design tools currently available for spliced girder bridges are limited. Most design work on these systems is made through custom spreadsheets or use of the CONSPLICE software (LEAP 2004). The design of spliced girder bridges depends on several design variables (e.g., time dependent effects, prestress locations and requirements, beam spacing, etc.) that significantly influence performance and cost. Normally, most design variables are determined based on the designer's judgment through a trial and error process. This approach requires considerable time and effort to explore solutions and establish an understanding of the system parameters; something that typical projects in a preliminary design phase cannot afford.

In spite of the design knowledge and analysis tools available for spliced girder bridges, no design aids that can expedite the design process are available. Implementation of mathematical optimization algorithms can eliminate trial-and-error design procedures and thus lead to the design of more efficient systems. Optimization techniques have been used effectively to develop design aids charts and design tables for determining section dimensions and prestress requirements. Bridge engineers would find benefits in design charts and tables that are based on optimal solutions, to expedite the design process. As a result spliced girder bridges can be more widely used by state highway agencies and bridge consulting firms.

Technical research committees have also identified the need to develop standard segments that can be used efficiently in the negative moment area of spliced post-tensioned bridges in order to cost-effectively increase the span range for precast/prestressed girder bridges. Thus, the current challenge for the industrialization of

post-tensioned SGB is the development of analysis, design, and construction procedures that make use of standard precast girder shapes for pier and field segments.

1.5 Structural Optimization of Civil Infrastructure

Mathematical optimization algorithms can be implemented in order to make a system more efficient and to eliminate the trial and error design procedures. These methods can result in significant cost savings, performance improvements and ease of design by providing guidance and insight into optimal solutions.

Bridge systems may be associated with three levels of optimization: (1) components, (2) transverse and longitudinal configurations, and (3) structural systems. Component optimization design variables consist of cross-section dimensions of the girders, slab, and diaphragms, and details for the prestressed and nonprestressed reinforcements. Configuration optimization design variables deal with the number of girders (or girder spacing), number of spans, position of intermediate supports, and support conditions (simple span, continuous span, or frame). System optimization consists in exploring different bridge superstructure solutions such as slab on precast girders, cell box girder, steel girder, etc.

In general, component optimization deals with the study of optimal dimensioning and section sizing of beams. Component optimization for prestressed concrete girders has been broadly studied through several efforts sponsored by state highway agencies for developing standard positive sections in addition to the AASHTO standard sections.

The use of structural optimization for spliced girder bridge design is limited. Component optimization studies for SGB have been done for prismatic I-Beam sections

for medium span lengths as follows. Lounis et al. (1997) investigated the feasibility of using existing I-beam sections (e.g., AASHTO-PCI standard girders, AASHTO-PCI Bulb-Tee girders, Florida DOT standard bulb-tee girders, Nebraska university standard girders, and Canadian prestressed concrete institute standard girders) for both pre-tensioned and post-tensioned construction. The results showed that no single standard section set can be considered to be optimal for all structural systems, therefore, a new set of I-beam sections were proposed based on the optimal analyses for use in both positive and negative segments in two equal continuous span arrangements.

In the studies by Lounis et al. (1997), only one construction sequence was investigated which is a single-staged post-tensioned applied after deck pouring. In addition, the splice location was fixed. These conditions may not yield optimal system results. For example, the positive and negative segment lengths were fixed, which consequently restricts other possible variables such as the number and layout for the pre-tensioning and post-tensioning reinforcement. Also, the girder sections were considered to be prismatic along the span without any modification to the pier segment. Finally, only one post-tensioning stage was investigated, which may not be an efficient construction process.

Configuration optimization includes the effect of number of spans, pier locations, number of girders, pre-tensioning and post-tensioning requirements, and beam spacing. In addition, configuration optimization can also include the substructure. Since the number of supports is commonly reduced for SGB, the total cost of the system construction will also be reduced.

The only studies to date on configuration optimization on spliced girder bridges have been done for simple spans using I-beam sections. This type of study has been done only for 1.8 meter (72") deep I-beams, which are the most widely used precast sections throughout the country. These precast sections included the Ohio modified 1.8 meter (72"), the New England BT1800, the AASHTO Type VI, The PCI BT 72", and the Caltrans BT 1850. The purpose of this study was to obtain the maximum span length of three equal segments spliced into a simple span bridge system (Collett and Saliba 2002). In these studies, prestressed I-beams were analyzed using a custom spreadsheet and using the program CONSPLICE PT (LEAP 2004) to analyze the post-tensioning process. This study was useful in providing quantifiable limits on the performance achieved by post-tensioning and splicing for standard 1.8 meter (72") beams used in states. However, the results from this studied were based on trial and error on a custom spreadsheet, therefore no guarantee of obtaining the optimal solutions. In addition, the maximum achievable span length, which is the purpose of this study, was determined by fixing the splice locations which may not yield the optimal maximum achievable span length.

In spite of the analysis and design optimization work noted above, at this time there are no available design aids to determine the pre- and post- tensioning requirements for spliced girder bridges or ways to determine the effective configuration of girders and system. The use of optimization techniques can thus be used as a tool for the development of these design aids. Design aids can simplify the analysis and design of spliced girder bridges by providing guidance on variable sensitivity and reduce effort in the design process. The availability of design aids for spliced girder bridges can be a

great asset to bridge engineers to expedite the design process of this bridge system as an alternative during the preliminary design phase.

1.6 Objective and scope of dissertation

The research objective pursued in this study was to understand performance of spliced precast/prestressed concrete girder bridges (SGB) to improve their design by means of *single* and *multi-criteria* optimization through the use of standard or *new optimal pier segments* with *optimal construction sequence* including the *time-dependent effects*.

The research approaches used in this study can be summarized into four main parts as represented in the following flowchart.

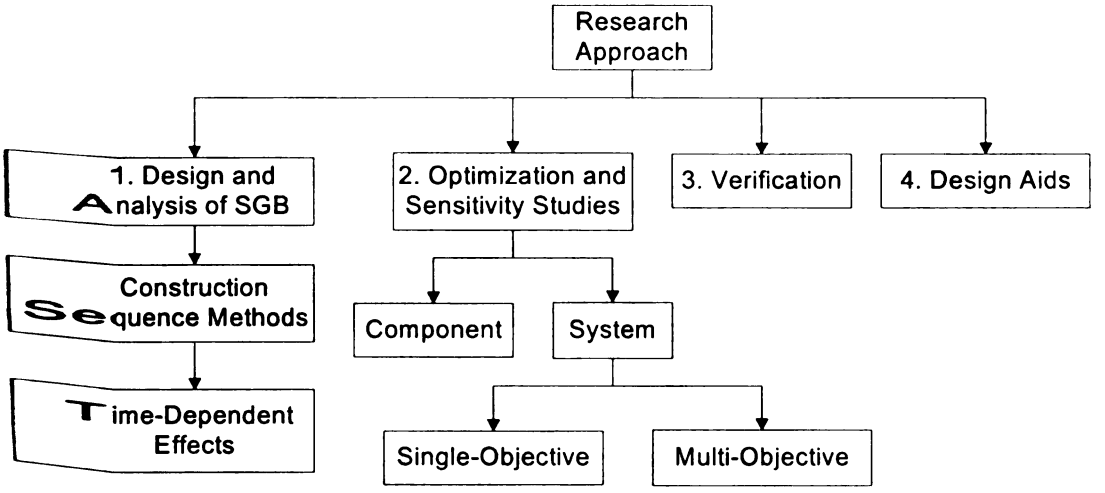

Figure 1-2 *Summary of research approaches*

The detail scope of and approach to the conducted research was as follows:

1) Investigation of design and analysis of optimal construction procedures to maximize efficiency in single- and multi-span structures.

Design and analysis of spliced girder bridge were investigated to study on different construction methods to obtain optimal solutions. The three most commonly used construction methods for SGB were considered in the studies. These construction methods were single-stage post-tensioning after deck pouring, single-stage post-tensioning before deck pouring, and multi-staged post-tensioning. The main difference between these construction methods was the sequence of post-tensioning required to achieve system continuity.

The optimal construction was also used to determine the maximum achievable span length of single- and multi-span spliced girder bridge to investigate the viability of replacing typical existing multi-span highway bridges with spliced girder bridges. Our goal is to replace existing two-span highway bridges (Figure 1-3) with the single-span spliced girder bridges (Figure 1-4) to eliminate the intermediate pier.

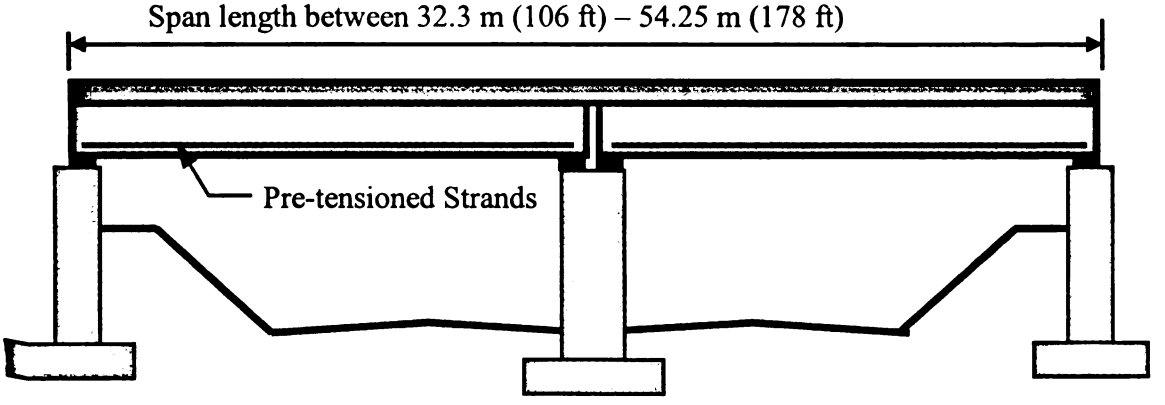

Figure 1-3 *Typical existing 2-span highway bridge*

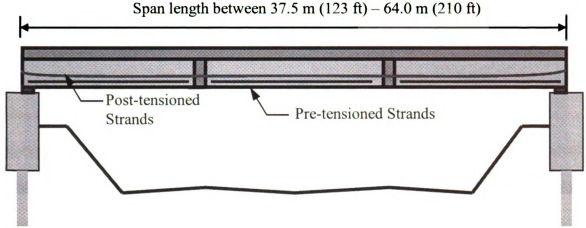

Figure 1-4 *Single-span spliced girder bridge*

The elimination of substructure unit could reduce the construction cost dramatically especially for the multi-span bridges since their intermediate piers can be removed. Consequently, our objective is to study the viability of replacing existing typical existing three to four-span highway bridges (Figure 1-5) with the two-span continuous spliced girder bridges (Figure 1-6).

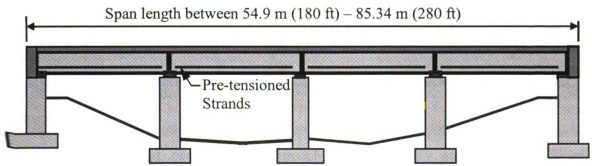

Figure 1-5 *Typical existing 4-span highway bridge*

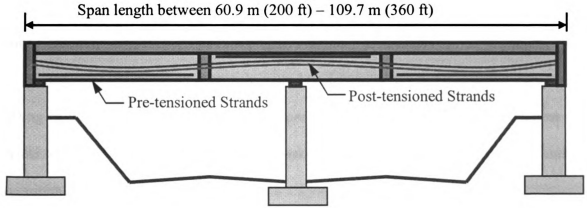

Figure 1-6 *Two-span continuous spliced girder bridge*

2) Investigation of time-dependent effects on spliced precast/prestressed girder bridge systems.

The objective was to investigate and compare time-dependent prestress losses on spliced girder bridges using the currently recommended code models. The simplified method from the AASHTO-LRFD specifications (AASHTO 2003) and the age-adjusted concrete modulus approach of the CEB-FIP 90 recommendations (CEB-FIP 1990) were chosen and compared in this study.

In order to determine the best method to describe the actual behavior of time-dependent losses in SGB, time-dependent effects were integrated in the finite element analyses. Time-dependent losses were considered and checked at each critical construction stage.

3) Implementation of optimization approach and sensitivity approach for spliced precast/prestressed girder bridges.

The objective is to use structural optimization to evaluate the goodness of a design, to study the sensitivity of different variables, to understand the system better, to

obtain the maximum achievable span length, and to study efficiency of different girders for SGB.

Component optimization approach is used to determine the optimal dimensioning or sizing of girders and *configuration/system optimization* is used to determine the best or more efficient splice location, girder spacing, pre-tensioning and post-tensioning requirements and profiles.

4) Development of an optimal standard negative section over intermediate piers.

The main goal of this task was to investigate the best method to obtain a standard negative segment for system cost efficiency. New standard negative sections used for multi-span bridges were developed based on an integrated component and configuration optimization approach that allowed obtaining the most efficient section. Section optimization processes were performed to obtain the dimensions of negative sections and were coupled with the configuration optimization in order to obtain the best geometry solution for a given span length with the most efficient beam at the pier location.

Four methods to increase the section depth over the pier section were considered, namely (1) the use of existing standard positive sections with an additional concrete block (soffit) attached to the underside of the beam; (2) new optimal non-prismatic negative section with variable web; (3) new optimal non-prismatic negative section with variable soffit and constant web; and (4) new optimal prismatic section used over positive and negative moment regions.

5) Development of a single- and multi-objective optimization approach for spliced precast/prestressed girder bridges.

The bridge geometry, beam section dimensions, and material properties with different construction sequences were selected as parameters for component and configuration optimization of SGB. Different objective functions, such as minimum construction cost, minimum post-tensioning, minimum concrete volume, and minimum pre-tensioning were considered and compared through a single-objective optimization formulation to obtain the best optimal solutions. Multicriteria optimization methods combined all the single-objective functions as a main objective group such as economy, safety, and geometric requirements and results were based on multi-objective optimization approaches.

Time-dependent effects were part of the optimization process. Therefore, the optimized solution obtained for the SGB system included both short and long-term effects. Construction sequences are not considered as a design variable in the optimization. Rather, the results from the multi-objective optimization processes for each construction sequence were compared. Thus, each construction method was analyzed separately. This follows from the fact that realistic and/or practical construction procedures will depend on the contractor's preference.

6) Investigation of the life-cycle-cost of spliced precast prestressed concrete bridge structures affected by chloride ingression.

The aim here was to investigate the durability and life-cycle cost of spliced girder bridges under chloride attack, and describe the importance of considering durability at the design stage. Parametric studies to increase the concrete clear cover of the precast prestressed concrete girder were used to evaluate the service life of the structure. Strength requirements and durability were simultaneously considered during the design

process. Thus a compromise between the strength and serviceability requirements versus the life-cycle-cost of spliced girder bridges was achieved.

7) Verification of optimal results obtained from the optimization studies

The objective was to verify obtained optimal results from the optimization process compared with the results of a documented design in NCHRP 517 Report and published journal papers. This result verification is used to proof that optimal solutions are acceptable and can be used to develop design aids for the preliminary design of spliced girder bridges.

8) Development of design aids for the preliminary design of spliced girder bridges.

The objective was to use optimal results from the above-mentioned analyses to create simplified design aids for the preliminary design of single-span and two-span continuous spliced precast/prestressed girder bridges. The design aids are in the form of table and graphs that indicate the best parameter values for minimum construction cost.

The organization and outline of the dissertation is as follows:

Chapter 1 provides an introduction to precast/prestressed concrete bridge construction and spliced precast/prestressed concrete girder bridges (SGB). Current application of structural optimization in precast/prestressed concrete and SGB are briefly reviewed. Outstanding research needs and the motivation behind this work are discussed, and followed by the research scope and approach.

Chapter 2 presents the design and analysis approaches for spliced precast/prestressed concrete bridges. The major design criteria used for the analysis and construction sequence of SGB are briefly presented. The approaches and models currently recommended for time-dependent prestress losses as well as the identification of critical

construction stages are reviewed. The available standard section and non-standard section are evaluated for use in SGB construction. Finally, the analysis of durability in combination with the life-cycle cost of spliced prestressed girder bridge structures attacked by chloride is presented.

Chapter 3 reviews the optimization approaches used for single- and multi-objective optimization of SGB. An overview of the mathematical algorithms used for solving constrained optimization problems is presented. The weighted objective approach and ε-constraint method for solving multi-objective optimization problems are reviewed. The concept of generating the pareto optimum set as well as compromise programming to select the best solution in multi-objective problems are presented. Descriptions of single- and multi-objective functions are discussed in general. Lastly, the implementation of the optimization process for SGB in this study is briefly discussed.

Chapter 4 describes the optimal system design of single-span SGB. The optimization problem formulation for different construction sequence methods of SGB for single- and multi-objective optimization are demonstrated to obtain optimal solutions for maximum achievable span lengths. Parametric studies on material unit weights of the concrete deck and concrete girder are investigated to determine their influence in increasing span length. The durability of SGB due to the chloride ingress is evaluated in terms of concrete cover and then used to determine the service life and life-cycle-cost of the bridge system.

Chapter 5 focuses on the investigation of optimal system designs for two-span continuous SGB. Component optimization formulation for new pier segments are implemented and evaluated to obtain a new pier/negative segment for overall cost

efficiency. Optimal pier segments are used in single- and multi-objective optimization problems to obtain optimal solutions for maximum achievable span lengths. Sensitivity analyses on material unit weight of the concrete deck and concrete girder were investigated to determine the best method to increase span length.

Chapter 6 presents the development of aids for the preliminary design of spliced girder bridges consisting of documented design examples and design charts. Design aids were developed by using the nonlinear structural optimization analyses implemented in a custom automated program written in Matlab (Mathworks 2004). Both single- and multi-objective optimization formulations were used to obtain the optimized solutions. Design and construction limit state requirements were used as constraints in the optimization processes.

Chapter 7 summarizes and concludes the current research efforts for the single- and multi-objective optimization for spliced girder bridges and provides recommendations for future research.

2 Design and Analysis of Spliced Precast/Prestressed Girder Bridges

2.1 Introduction

Design of longitudinally spliced precast/prestressed concrete girder bridges through continuous post-tensioning, or spliced girder bridges (SGB), has gained renewed interest since their spanning range can exceed 48.77 m (160 ft) and are more efficient and cost-effective than steel plate-girder designs. Additionally, using SGB can reduce total project cost due to substructure reduction, fewer number of girders, and increased safety by elimination of shoulder piers and minimization of superstructure depth.

Spliced girder bridges have been constructed in the US since 1952 (Castrodale and White 2004), however their use are very limited and not common. A significant reason for their limited use is the ambiguity in their design and analysis, additional issues with which the designer of conventional precast/prestressed concrete girders is typically not familiar. In addition, the information available in the literature regarding their design, analysis and construction is limited; as the experience, information, and methods used on these projects have tended to be job-specific and the knowledge gained has not been made widely available for use on similar projects (Castrodale and White 2004).

This chapter presents an overview on the design and analysis approaches for spliced precast/prestressed concrete bridges. The major design criteria used in structural analyses and construction sequence methods of SGB are briefly presented. Issues related to equivalent post-tensioning loading, time-dependent losses and construction sequence

methods are reviewed. Lastly, durability issues in combination with the life-cycle cost of spliced prestressed girder bridge structures attacked by chloride are presented.

2.2 Spliced Precast Prestressed Girder Bridge Systems

Girder splicing is a method in which more than one pre-tensioned precast concrete segment is longitudinally spliced to produce span lengths greater than the girder segments. Each segment is connected by full-length post-tensioning. The series of girders are temporarily simply supported between the piers and the abutments and connection, or splicing, is achieved in the field.

The splicing solution can be applied for single-span and multi-span bridges. Typical standard sections used for simply supported bridges are used for section lengths under positive moment. These segments are thus called "positive" or "field" segments. A single-span spliced-girder bridge (SSSGB) system is normally composed of three conventional positive girder segments as shown in Figure 2-1, where the end girder segments may have different lengths depending on the splicing location.

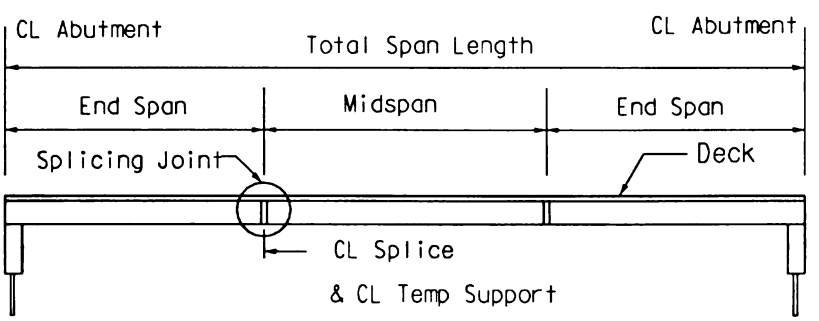

Figure 2-1 *Three-segment single-span spliced precast/prestressed girder bridge*

Multi-span continuous spliced girder bridges (CSGB) consists of positive/field segments and "negative" or "pier" segments. Negative segments can be either prismatic segment as shown in Figure 2-2 or nonprismatic segment as shown in Figure 2-3. A two-span CSGB system is normally consisted of custom-designed sections used for continuous bridge solutions for segments over intermediate supports. The nonprismatic segment has a deeper section over the pier location and is tapered down to match the positive standard section at the splice location.

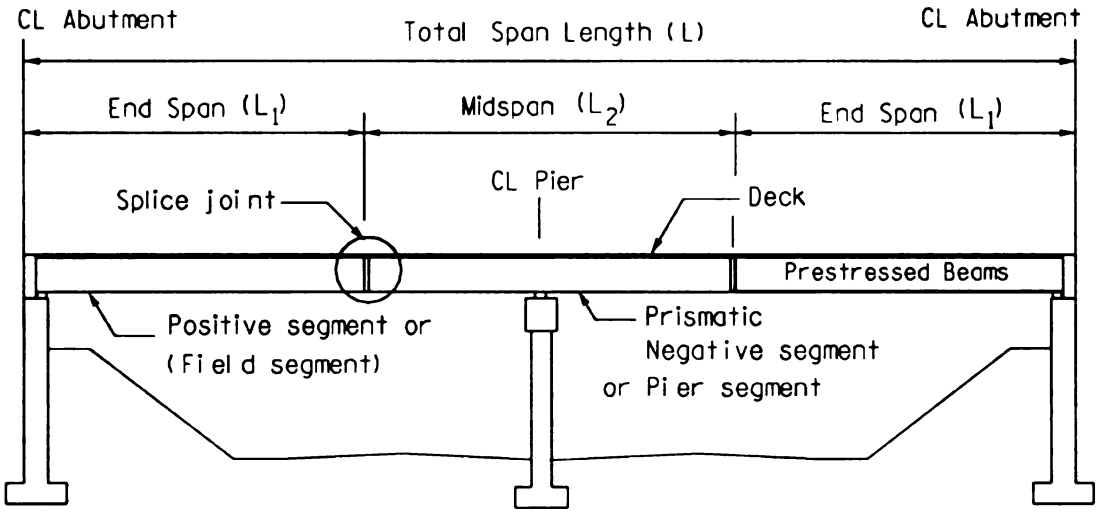

Figure 2-2 *Two-span spliced precast/prestressed bridge with prismatic pier segment*

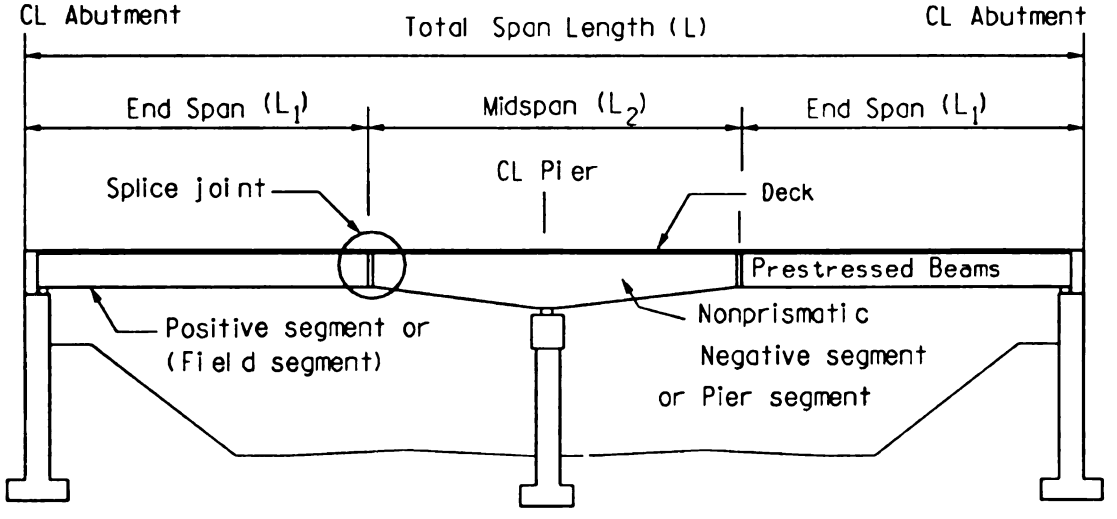

Figure 2-3 *Two-span spliced precast/prestressed bridge with nonprismatic pier segment*

2.3 Girder Cross-Sections

There are several types of standard and newly developed girder cross-sections used for spliced precast/prestressed girder bridges. Some of them are chosen and set by local practice or project-specific requirements. Normally the deeper standards girder sections, i.e., AASHTO type VI, PCI-BT-72, and NEBT 1800, are used in spliced systems since they can span longer distances than shallow sections. Some states, i.e., Florida, Washington, and Nebraska, have developed their own sections for job-specific projects in order to accommodate their span length needs.

2.3.1 Standard sections

Currently, only standard precast/prestressed concrete girders are used under positive moments in simple spans. While these sections can be utilized in spliced girder construction, some researchers have developed new standard sections to be used more efficiently in both positive and negative regions in continuous SGBs. However, there is no evidence that these new standard sections are being commonly made.

Available standard sections in the market used for SGB include AASHTO I-girders and PCI-Bulb Tee girders. Normally, standard sections used in SGB should not be too shallow in order to benefit from the eccentricity effects of post-tensioning tendons. In addition, the dimension of standard sections may need to be modified to accommodate post-tensioning ducts (i.e., widening of the web). In spite of the combination of pre-tensioning and post-tensioning, the sizes of flanges are not necessarily large. Generally, the bottom flange of the spliced prestressed section is used

to accommodate the pre-tensioning strands for positive segments, while the top flange is used to accommodate pre-tensioning strands for negative segments.

Several standard sections have been specifically developed by some states for their particular design and construction requirements. These sections include the modified Washington WS2400 girder, the modified Florida bulb-tee PCI-BT 78 and PCI-BT 96 girders, and trapezoidal box beams. These new standard sections were developed to increase the span length for job-specific projects.

I-girder and Bulb-Tee girders are used in SGB more often than box beams due to their lighter weights. Box beams have two webs, thus their sections are very heavy. Consequently, their span lengths are much shorter than I-girders or PCI Bulb-Tee girders for the same girder depth.

2.3.2 Non-standard sections

For multi-span spliced girder bridges, additional moment and shear resistances at interior supports is required. Segments over the interior supports are called negative or pier segments. These segments can be custom-designed with deep sections using haunches or can be of constant depth girders to carry the high negative bending moments and high shear demands.

Use of constant depth girder sections for the entire bridge span length is more economical. However, when the bottom flange compressive stresses, or web shear stresses at interior supports are not very high, modified standard girder sections can be used. Modifications of standard girders include thickening the web at locations of high moment and shear, using the benefit of end-block sections, or adding an additional slab

to the bottom flange at interior support locations. These modifications still maintain a constant section depth.

When design requirements are very high the modifications of the cross-section usually demand having a deeper section (haunched) over the interior supports (Castrodale and White 2004). Increase in girder depth at interior supports provides additional moment and shear capacity that help satisfy the design requirements. However, these increased depth haunched pier segments might become very heavy for highway transportation.

The construction cost of a haunched section is higher than that of a standard girder. Typically, haunched sections have a linear taper due to ease of construction. Curved, or parabolic, haunches can also be used but they require more intricate formwork, which can dramatically increase construction cost.

Currently, there are several available options for achieving haunched sections for I- and Bulb-Tee girders. These options are listed in the following.

a) Haunched section with constant web

Existing standard girder forms can be used with slight modifications on the slope of the existing bottom flange. The haunched section is accomplished by varying the bottom soffit flange from the standard bottom flange thickness at the splice location to its deepest section over the interior support, or pier.

This method allows the fabricator to utilize existing forms as part of the haunched section, thus fabrication is less complicated than other haunching approaches. However, the increased height of a haunched bottom flange adds significant weight to the section and the deep flange thickness may not be attractive.

b) Haunched section with constant bottom flange

This approach requires using special formwork and the girders are normally custom fabricated. Web height is varied along the haunched section while the bottom flange remains of constant depth along the length of the segment. Even though the bottom flange has a constant depth, it must be large enough to resist the large negative bending moments over interior supports.

The most attractive feature of this option is the reduced weight of the haunched segment. This can lead to savings in transportation costs. The girder segment weight is much lighter since only the web height is varied.

2.4 Splice Location

The location of splices generally depend on site characteristic, maximum limits for girder shipping weight and segment length, fabrication, erection, and/or structural issues. When the girders are transported through several states they have to satisfy the shipping weight and length limits of all states on the route. Some states limit the weight of the girder not to exceed 587 kN (132 kips), in addition to weight limits of 89 kN (20 kips) for the axles of trucks (Castrodale and White 2004). In addition to limits on transportation shipping weight and length, available lifting equipment limits should also be considered.

Splice locations should not be located near mid-span, but rather towards the end of the span. Splice locations can yield different maximum achievable span lengths for the same beam type with different splice locations. Thus, the splice location should be carefully considered in the design phase.

2.5 Structural Loads

The analysis and design of post-tensioned spliced girder bridges is very similar to the analysis and design of segmental bridges. However, it is different from conventional precast/prestressed concrete girder bridges primarily in terms of its staged construction. A time-dependent analysis of the spliced girder system is required to properly accumulate the actions and reactions at each stage of erection. Additional issues that are required differently from conventional prestressed concrete design are multiple stressing stages, combined pre-tensioning and post-tensioning, and time-dependent losses. Thus, the design of spliced girder bridges involves greater complexity than for conventional precast/prestressed concrete girder designs. Their design is thus generally executed using computer programs, such as the commercial program CONSPLICE PT (LEAP 2005), or a series of custom spreadsheets developed by design offices.

The loads in the spliced precast/prestressed girders are a consequence of the construction stages. Each load case is considered individually and accumulated, and loads on the structure are thus classified as non-composite loads and composite loads.

2.5.1 Non-composite loads

Non-composite dead loads include the weights of girders, deck, optional stay-in-place deck forms, and construction loads. Beam spacing has a direct influence on the deck, haunch, and construction loads. All distributed loads are assumed to be applied over the effective tributary area for each girder. Girder and haunch loads are taken as beam line loads. The weight density of normal-weight concrete for girders and deck are assumed to be 2400 kg/m^3 (150 lb/ft^3). For sensitivity analyses, light-weight concrete

was considered, with weight densities of 1762 kg/m^3 (110) to 2243 kg/m^3 (140 lb/ft^3). Uniform 50 mm (2-in.) girder/deck matching haunches are assumed over the top flange width for construction tolerance and variation in road camber. Corrugated metal stay-in-place deck forming is assumed to be 0.77 kN/m^2 (16 lb/ft^2). Construction design loads were thus resulting from temporary loading during placement of the concrete deck and taken as 0.96 kN/m^2 (20 lb/ ft^2).

2.5.2 Composite loads

Composite dead loads included the weight of the girder splice joint, the weight of intermediate diaphragms, the removal of temporary supports, the weight of barriers, the weight of future wearing surface, and vehicular live loads. Composite dead loads were assumed to be equally distributed to all girders in the superstructure cross-section.

Loads from splice joints and temporary diaphragms are not immediately transferred to the superstructure during construction since they are supported by temporary supports. After post-tensioning is applied and the temporary supports are removed, these loads are applied to the composite beam. These "support loads" are based on the assumption that the bridge is lifted off the temporary supports after post-tensioning.

For a single-span SGB, the three continuous segments are thus analyzed as a simple single-span system with two point loads applied at the temporary support locations. Temporary support reactions include all non-composite dead loads and the splice joint weight. These are calculated as half of the weight from the end and middle girder segments.

For a multi-span continuous SGB, the spliced segments are analyzed as a continuous system with point loads applied at the temporary support locations. Reactions at the temporary supports depend on the construction sequence. Secondary reactions due to the continuous system will be induced at the intermediate pier. Temporary support reactions include all non-composite dead loads and the splice joint weight. For a two-span continuous system, these are calculated as half of the weight from the end together with a quarter of the weight of the middle girder segment.

Design live loads are based on the ASSHTO-LRFD bridge design specifications (AASHTO 2003). Design live loads are selected from either the design HL-93 truck loads in combination with the design lane load or the design tandem loads in combination with a design lane load (ASSHTO 2003). The live load used in the design is based on the maximum load combination effect. The dynamic allowance impact factor (IM) is only applied to the design truck as specified in the AASHTO specifications. Live load demands are based on the load distribution factors for either exterior or interior beams as given in the AASHTO-LRFD specifications.

2.5.3 Post-tensioning loads

Normally, post-tensioned tendon profiles are arranged in the form of parabolic curves, therefore their eccentricity (distance measured from the girder neutral axis to the post-tensioning cable) changes along the span length. To simplify the calculations of the loads introduced by these curved cables, the forces caused by post-tensioning and their eccentricity profile along the length can be represented by equivalent loads.

Equivalent loads for prismatic sections are commonly available and defined in multiple references. However, much less information is available on equivalent loads for

nonprismatic sections. In the following sections the equivalent loads of post-tensioning loads on prismatic and nonprismatic sections are outlined for documentation purposes.

a) Single-span girder using a prismatic section

The post-tensioning profile of a single-span girder is defined by a single quadratic curve (see Figure 2-4) and the resulting load from the post-tensioning cable can be modeled by the equivalent loads shown in Figure 2-5. Equivalent loads include horizontal forces, vertical forces, and moments at the external supports; and uniformly distributed transverse forces along the tendon profile. The uniformly distributed transverse forces are generated by the curvature in the tendon profile.

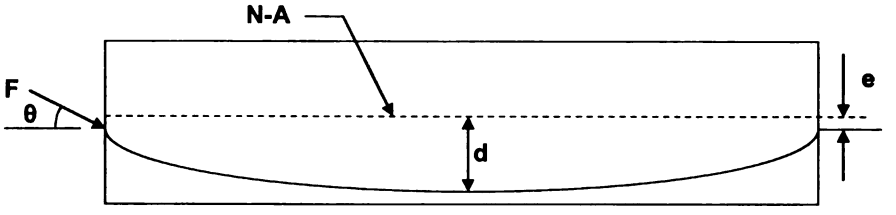

Figure 2-4 *Post-tensioned profile of single-span using prismatic section*

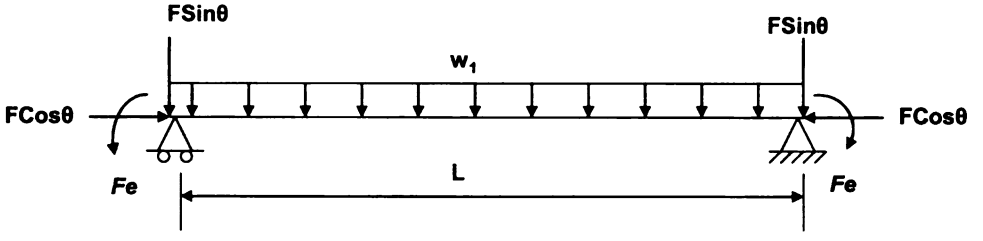

Figure 2-5 *Equivalent loads and fixed end moments of single-span using prismatic section*

Uniform loads w_1 represent transverse forces that occur along the span as shown in Figure 2-5. The distance measured from the neutral axis to the lowest point of tendon

profile is defined as d. The angle between the horizontal reference line and the post-tensioning strand location at $x = 0$ is defined as θ. The magnitude of the equivalent uniform load due to the post-tensioning cable curvature is given by:

$$w_1 = \frac{8F(d-e)}{L^2}. \tag{2-1}$$

b) Two-span continuous girder system using a prismatic section

The two-span continuous spliced girder system dealt with in this dissertation is composed of two continuous spans and is assumed to be symmetry about the center of the pier. Therefore only one half of the system is dealt with herein. The symmetric profile of a post-tensioned tendon along three prismatic continuous girders in the two-span system is assumed to be made of three different quadratic curves as shown in Figure 2-6. The first curve (Curve 1) is measured from the end span to a distance αL. The second curve (Curve 2) is defined between the location at αL, measured from the endspan, and the location at $\alpha_1 L$, measured from the center of the pier. The third curve (Curve 3) is defined along the segment a distance $\alpha_1 L$ from the pier to pier location itself. Assuming quadratic parabolic curves for all parts, the eccentricities of post-tensioning strands are used to define the locations of the quadratic curves. The eccentricity at $X = 0$ is defined as $e(X = 0) = \beta e_{OB}$. The eccentricity at $X = \alpha L$ is defined as $e(X = \alpha L) = \beta_1 e_{OB}$. The eccentricity at $X = L$ is defined as $e(X = L) = e_{OB}$. The terminology used for the post-tensioning parabolic curve profiles is illustrated in Figure 2-6.

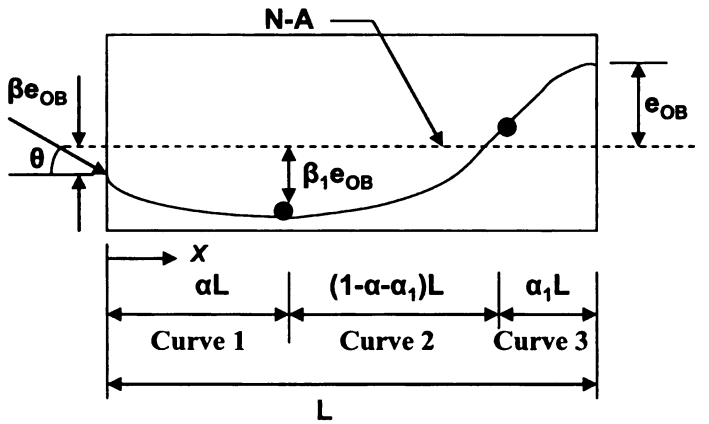

Figure 2-6 *Post-tensioned profile of two-continuous span using prismatic section*

The equivalent distributed loads and fixed-end moments of the post-tensioning profile of a two-span continuous system using a prismatic beam is illustrated in Figure 2-7. Three uniform transverse loads (w_1, w_2 *and* w_3) represent the pressure from the quadratic tendon profile on the symmetric portion of the two-span girder system. The angle between the horizontal reference line and the post-tensioning strands at $X = 0$ is defined as θ. This θ angle is used to determine the vertical end force ($FSin\theta$) and horizontal end force ($FCos\theta$) due to the post-tensioning forces at the end of the spans, while the end moments (m_{BA} and $F_{\beta eoB}$) are determined by multiplying the horizontal end force with the eccentricity at each of the end spans.

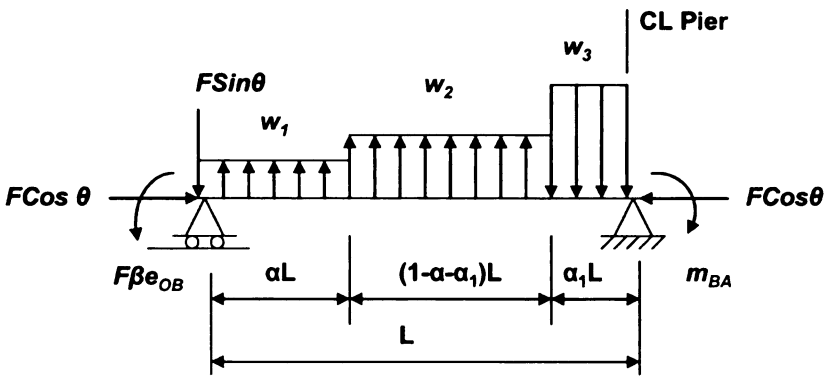

Figure 2-7 *Equivalent loads and fixed end moments of two-continuous span using prismatic section*

The magnitude of the equivalent distributed loads and moments can be shown to be given by the expression in Equation (2-2) through Equation (2-5) below:

$$w_1 = \frac{2F(\beta - \beta_1)e_{0B}}{(\alpha L)^2}, \tag{2-2}$$

$$w_2 = \frac{2Fe_{0B}}{L^2}\left[\frac{\beta_2 - \beta_1}{(1 - 2\alpha - 2\alpha_1 + \alpha^2 + 2\alpha\alpha_1 + \alpha_1^2)}\right], \tag{2-3}$$

$$w_3 = \frac{2Fe_{0B}(\beta_2 - 1)}{\alpha_1^2 L^2}, \tag{2-4}$$

$$m_{BA} = -Fe_{OB}[-\beta\alpha^2 + (1 + \alpha + \alpha_1)^2 - \alpha_1(1 - \alpha) - \beta_1(3 - 3\alpha_1 + \alpha_1^2 + 2\alpha - \alpha\alpha_1)]^{0.25}, \tag{2-5}$$

where F = total post-tensioning force; β = coefficient of eccentricity at the end of the positive segment; β_1 = coefficient of eccentricity at the mid-span of the positive segment; e_{0B} = vertical eccentricity at the center of the pier segment; α = coefficient of horizontal distance from span end to the mid-span of the positive segment; α_1 = coefficient of horizontal distance from splicing location to the center of the pier.

The sign convention for the eccentricity values assumes that they are positive below the neutral axis. The coefficients of β and β_1 are between 0 and -1 while e_{0B} is a negative value. Consequently, the uniform loads w_1 and w_2 are oriented upward and w_3 is oriented downward (see Figure 2-7). Finally the value of $|\beta_1|$ must be greater than $|\beta|$ to satisfy the requirements for a quadratic curve requirement.

c) Two-continuous span using nonprismatic section

Pier segments are increased in height for larger negative moment capacity, consequently a continuous system is typically composed of prismatic positive segments and non-prismatic negative segments. The profile for the post-tensioning tendon along a non-prismatic continuous girder is also assumed to be made of three different quadratic curves on one half of a symmetric structure as shown in Figure 2-8. At the haunched section the neutral axis is assumed to shift in proportion to the height/depth of the haunched section. The tendon profile is defined by three continuous quadratic curves as shown in Figure 2-8. The eccentricity at $X = 0$ is defined as $e(X = 0) = e_1$. The eccentricity at $X = \alpha L$ is defined as $e(X = \alpha L) = e_2$. The eccentricity at $X = (1-\alpha_1 L)$ is defined as $e(X = (1-\alpha_1 L)) = e_3$. The eccentricity at $X = L$ is defined as $e(X = L) = e_4$. Finally, the angle between the horizontal reference and the haunch neutral axis is defined as ψ.

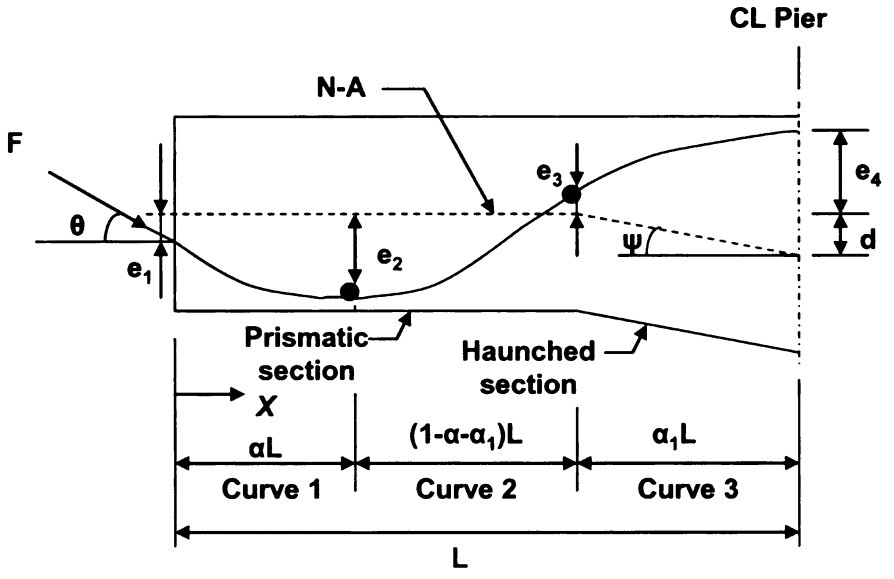

Figure 2-8 *Post-tensioned profile of two-continuous span using a non-prismatic section*

The equivalent transverse loads and fixed-end moments for the post-tensioning of a two-span continuous girder using a non-prismatic pier segment is illustrated in Figure 2-9. The distance measured from the lowest point of the haunched neutral axis of the pier segment to the prismatic neutral axis is represented by d in Figure 2-8. The angle between the horizontal reference line and the post-tensioning strands at the beam end is defined as θ (see Figure 2-8). This angle θ is used to determine the vertical end force ($FSin\theta$), horizontal end force ($FCos\theta$) and segment end moments (m_{BA} and $F_{\beta eoB}$), similar to the end forces in the prismatic section. Three uniform transverse loads (w_1, w_2, *and* w_3) represent the pressure from the post-tensioning strand onto the beam as shown in Figure 2-9. The values for the uniform loads are given by:

$$w_1 = \frac{2F(e_1 - e_2)}{(\alpha L)^2}, \qquad (2\text{-}6)$$

$$w_2 = \frac{2F}{L^2}\left[\frac{e_3 - e_2}{(1 - 2\alpha - 2\alpha_1 + \alpha^2 + 2\alpha\alpha_1 + \alpha_1^2)}\right], \tag{2-7}$$

$$w_3 = \frac{2F(e_4 - e_3)}{\alpha_1^2 L^2}, \tag{2-8}$$

where e_1 = eccentricity at the end of the positive segment; e_2 = eccentricity at the mid-span of the positive segment; e_3 = eccentricity at the splice location; and e_4 = eccentricity at the center of the pier segment measured from the centroid of the prismatic section.

It should be noted that that the post-tensioning strand in the non-prismatic segment leads to two additional concentrated forces ($2FSin\psi$ and $FSin\psi$) at the ends of this element as shown in Figure 2-9.

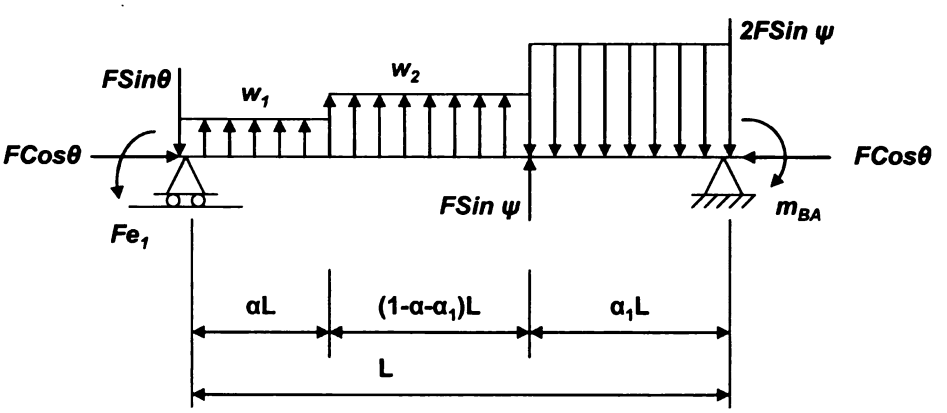

Figure 2-9 *Equivalent loads and fixed end moments of two-continuous span using a non-prismatic section*

The sign convention for the eccentricity values is positive below the N-A line. Therefore, the uniform loads w_1 and w_2 are oriented upward and w_3 is oriented downward. Notations for all other variables are the same as described in Section 2.5.3(b).

2.6 Flexural Criteria

2.6.1 Service limit state

Service limit states include checking concrete stresses in the girder, deck and splice elements. These stresses are calculated from the applied moments on individual girder segments, the moment applied to the entire spliced girders, and the forces caused by prestress loads.

Flexural limit states for both tension and compression stresses are provided in the AASHTO-LRFD specifications (AASHTO 2003) for conventional prestressed concrete and segmental construction. Limit stresses on joints are defined according to segmental construction while limit stresses at all other locations follow conventional prestressed concrete construction.

There are two load combinations considered for full service loads after final construction; these are the Service Limit State I (SLS-I) and Service Limit State III (SLS-III) conditions. The difference between these limit states is the live load factor, which is equal to 1.0 for SLS-I and 0.8 for SLS-III. Service limit state I is used to check the concrete compression stress limit while service limit state III is used to check the concrete tension stress limit under full service loads. Full service loads include the girder self-weight, deck load, non-composite dead load, temporary pier removal, construction dead load, and live load. Top deck stresses, and top and bottom girder stresses at these limit states are checked against allowable concrete stress as defined in Table 2-1 (AASHTO 2003).

Table 2-1 *Allowable concrete stress limits for critical construction stages*

Critical Construction Stages	Stress Type	Girder concrete	Deck concrete
Pre-Tensioning Strand Release	Compression	$0.6f'_{ci}$	
	Tension	-200 psi	
Deck/Splice Concrete	Compression	$0.6f'_c$	
	Tension	-200 psi	
Post-Tensioning/Barriers	Compression	$0.6f'_c$	$0.6f'_{cd}$
	Tension	$-0.0914\sqrt{f'_c}$(MPa)	$-0.0914\sqrt{f'_{cd}}$ (MPa)
		$-0.24\sqrt{f'_c}$ (ksi)	$-0.24\sqrt{f'_{cd}}$ (ksi)
Final Condition – after losses	Compression1	$0.6\phi_w f'_c$	$0.6\phi_w f'_{cd}$
	Compression 2	$0.45f'_c$	$0.45f'_{cd}$
	Compression 3	$0.4f'_c$	$0.4f'_{cd}$
	Tension 1	$-0.0724\sqrt{f'_c}$ (MPa)	
		$-0.19\sqrt{f'_c}$ (ksi)	

Two additional flexural limit states for spliced girder bridges were recommended in the recent NCHRP 517 Report (Castrodale and White 2004) that deal with compression stress limits for partial service load at the final construction stage. These two limit states differ in the load combination to be considered. The first one, referred to as *Compression 2* in the NCHRP 517 Report, considers all the loads from the SLS-I except the live load with all other loads using a unit load factor. The second additional limit state, named *Compression 3*, considers all the SSL-I loads but with a unit load factor for the live load and a load factor of 0.5 for all other loads. The limit stresses for the Compression 1 and Compression 2 checks (see Table 2-1) are those recommended by the NCHRP 517 Report.

2.6.2 Strength limit state

The design of spliced girder bridges is typically controlled by the service limit state. However, the strength limit state still needs to be checked. Spliced girders should be checked at critical sections for their flexural and shear capacities. The strength limit state is checked at final conditions.

Assessment of strength limit state is based on the AASHTO-LRFD recommendations in Article 5.73 (AASHTO 2003) using the simplified strain-compatibility analysis approach provided in the PCI Bridge Design Manual (PCI 2002). Girders for spliced systems tend to have large amounts of post-tensioning strands. Consequently, the compression zone might extend into the web of the girder. Current AASHTO-LRFD specifications (AASHTO 2003) do not consider the different strength of concrete in the deck and in the girder properly. Therefore, a simplified strain-compatibility analysis is best suitable to evaluate the flexural capacity of spliced girder bridges (Castrodale and White 2004).

Strain compatibility analysis is an iterative approach that can be used to determine the flexural capacity of a cross-section at its normal strength limit state. First, the depth of the flexural compression zone, c, is assumed. Decompression strain ε_{po} is the difference in strain between the concrete and prestressed reinforcement and can be defined as $\varepsilon_{cu} = f_{po}/E_p$. The prestressing strain is computed from the curvature $\acute{o} = \varepsilon_{cu}/c$ plus the decompression strain. The value of f_{po} should be less than the value of the jacking force f_{pj}. The ultimate compressive strain, ε_{cu}, in the concrete at the top of deck is assumed equal to 0.003 (see ASSHTO-LRFD Article 5.7.2.1). The total depth of concrete

equivalent stress block is computed as $a = \beta_1/c$, where β_1 is the factor based on the concrete compressive strength. The stress in the prestressing steel is computed using the modified Ramberg-Osgood equation:

$$f_{ps} = E_p \varepsilon_{pf} \{A + \frac{1 - A}{[1 + (B\varepsilon_{pf})^C]^{\frac{1}{C}}}\} \leq f_{pu}, \tag{2-9}$$

where E_p is the elastic modulus of the prestressing steel; ε_{pf} is the strain corresponding to the computed stress; and parameters A, B, and C can be varied to define the shape of the stress-strain curve. For example, A = 0.0334, B = 116.4 and C = 12 when the stress is equal to 1675 MPa (243 ksi) at 1% strain and equal to 1862 MPa (270 ksi) at 3.5 % strain.

The location of effective depth, d_p, of the total prestressed reinforcement, which includes the pre-tensioned and post-tensioned strands, is estimated by

$$d_p = \frac{d_{pPT} A_{PT} + d_{pPRET} A_{PRET}}{A_{PT} + A_{PRET}}. \tag{2-10}$$

The total compression force in the top flange, web and deck are compared with the tension force. The depth of the compression zone, c, is adjusted until the compression and tension forces are equal, i.e., until section force equilibrium is satisfied.

When the concrete stress block extends into the web, all of the flange and part of the top web are in compression. The tension force in the section is then calculated by:

$$T = (A_{PT} + A_{PRET}) f_{ps}, \tag{2-11}$$

where A_{PRET} is the area of pre-tensioned strands; A_{PT} is the area of post-tensioned strands; and f_{ps} is the prestressing steel stress. The compression force in the deck, C_t, is calculated as:

$$C_t = 0.85 f'_{cd} b_e h_f, \tag{2-12}$$

where f'_{cd} is the deck compressive strength; b_e is the effective bridge width; and h_f is the slab thickness. The compressive force, C_f, in the girder flange is defined as:

$$C_f = 0.85 f'_c b_f h_w, \tag{2-13}$$

where f'_c is the girder concrete compressive strength; b_f is the beam flange width; and h_w is the girder web height. The nominal design moment, M_n, for the section is then defined as:

$$M_n = 0.85 f_{cd} b_e h_f (d_p - \frac{h_f}{2}) + 0.85 f_c b_f h_w (d_p - h_f - \frac{h_w}{2}). \tag{2-14}$$

There is no reduction factor ($\phi = 1$) for the factored moment, see AASHTO-LRFD Article 5.5.4.2.1 (AASHTO 2003). The maximum reinforcement limit needs to be checked to satisfy $c/d_e < 0.42$ according to AASHTO-LRFD Article 5.7.3.3.1 (AASHTO 2003). Normally the minimum reinforcement requirement is satisfied since there is a large amount of reinforcement provided in the section. Finally, according to the NCHRP 517 report (Castrodale and White 2004), the fatigue limit state does not need to be considered since the member is designed to satisfy the limiting tensile stress at the Service III limit state according to AASHTO-LRFD Article 5.5.3.1 (AASHTO 2003).

2.7 Shear Criteria

The shear forces on the system include those from the girder, deck, haunch, future wearing surface, removal of temporary supports and live load including impact factor. Factored shear loads are determined from service loads multiplied by the appropriate load factors. Load factors for composite live load and composite dead load are 1.75 and 1.5, respectively. The load factor for all other dead loads is 1.25. There are several critical shear sections needed to be checked, which include the end block and the splice locations. The considerations and relevant formulation for these shear checks are presented in the next senctions.

2.7.1 Vertical shear at splice location

Shear at the spliced locations must be considered since the sections at the faces of the splice are weak. The shear capacity of the splice is determined by using the interface shear method outlined in AASHTO-LRFD Article 5.8.4 (AASHTO 2003). The nominal shear resistance of the interface is computed as:

$$V_n = cA_{cv} + \mu[A_{vf} f_y + P_c], \tag{2-15}$$

where A_{cv} is the area of concrete in the shear transfer zone, which is defined as the web width multiplied by the difference between the total section depth and the section depth in tension; A_{vf} is the area of all shear reinforcement including post-tensioning strands and mild reinforcement crossing the shear plane; μ is the friction coefficient = $0.6 \times \lambda$, where $\lambda = 1$ for normal weight concrete; c is the permissible pressure at the splice contact

area = 0.075; P_c is the permanent net compressive force normal to the shear plane and is defined as $f_{pe}A_{ps}$; and f_y is the yield strength of reinforcement.

The nominal shear resistance must be greater than the factored shear demand, or $\phi V_n \geq V_u$, where $\phi = 0.9$. Since spliced girder bridges contain large amounts of post-tensioning strands in their section, the shear resistance of the splice is normally adequate. Although other reinforcement in the section is typically neglected, the post-tensioning strands usually provide more than the needed resistance. Thus, most of the time, a shear key is not required to provide additional shear resistance at the splice location (Castrodale and White 2004). In addition, the inclination of the post-tensioning tendon force crossing the splice helps increase the shear capacity of the section as defined by the shear resistance component V_p (AASHTO 2003).

2.7.2 Vertical shear at end blocks

The shear capacity at the end blocks for the spliced girder bridge is calculated in the same way as for conventional prestressed concrete bridges. The shear capacity is thus defined as (AASHTO 2003):

$$\phi V_n = \phi(V_c + V_s + V_p). \qquad (2\text{-}16)$$

The component $V_p = F \sin\alpha$ is the shear force provided by the post-tensioning with α being the angle between the effective post-tensioning strands and the horizontal reference of the lowest post-tensioning strand profile, and F being the total post-tensioning force in the section.

The component V_c is the shear strength provided by concrete and shall be taken as the lesser of the values of V_{ci} or V_{cw}. The shear strength, V_{ci} is computed by:

$$V_{ci} = 0.6\sqrt{f_c'}b'd + V_d + \frac{V_i M_{cr}}{M_{\max}}, \tag{2-17}$$

but need not be less than $1.7\sqrt{f_c'}b'd$ (psi) and d need not be less than $0.8h$. The distance d is that from the extreme compressive fiber to the centroid of the prestressing force in inches. The variable b' is the width of a web of a flanged member in inches. V_i is the factored shear force at the section due to externally applied loads occurring simultaneously with M_{max}. M_{max} is the maximum factored moment at the section due to externally applied loads. V_i and M_{max} are computed from the load combination causing maximum moment at the section. The moment causing flexural cracking at the section due to externally applied loads, M_{cr}, is computed by:

$$M_{cr} = \frac{I}{Y_t}(6\sqrt{f_c'} + f_{pe} - f_d), \tag{2-18}$$

where I is the moment of inertia about the centroid of the cross-section, Y_t is the distance from centroidal axis of the gross sections, f_{pe} is the compressive stress in the concrete due to effective prestress forces at the extreme fibers, f_d is the stress due to unfactored dead load at the extreme fiber; and f'_c is the compressive strength of concrete at 28 days.

The shear strength, V_{cw}, is computed by:

$$V_{cw} = (3.5\sqrt{f_c'} + 0.3f_{pc})b'd + V_p, \tag{2-19}$$

where f_{pc} is the compressive stress in concrete at the centroid of cross section resisting externally applied loads The shear strength provided by web reinforcement is taken as:

$$V_S = \frac{A_v f_{sy} d}{s}, \tag{2-20}$$

where A_v is the area of web reinforcement within a distance s . The total nominal shear strength can then be determined by adding the components of post-tensioning contribution (V_p) with the shear web reinforcement capacity (V_s), and the shear capacity from the concrete (V_{ci} or V_{cw}).

2.8 Construction Sequence Methods

Construction process is an important element in the design of spliced girder bridges since the application of post-tensioning to the structure at different stages can yield different stress requirements and thus result in different component and system dimensions and/or arrangements.

The two most common construction methods currently used for spliced girder bridges are single-stage post-tensioning and multi-stage post-tensioning. The main difference between these two construction methods is the sequence of post-tensioning application required to achieve system continuity.

In traditional spliced girder bridges, prestressing forces are applied once at the beginning stage of the construction to balance the self-weight of the girder. The amount of prestressing forces are usually determined to make sure that the total concrete top and bottom fibers stresses on the girders should be less than the allowable values. When the deck load is applied prior to continuously post-tensioning the girders, the prestressing

forces should be ample enough to balance this additional deck load. Post-tensioning forces can be applied in single or multiple stages depending on the sequencing of the deck casting.

2.8.1 Single-span system with single-stage post-tensioning construction method

In this method, the precast/prestressed beams are first installed on temporary supports at the site. Spliced joints and diaphragms are then poured and cured. Either a cast in place deck or a precast deck can be added once the splice and diaphragms have developed enough strength to resist partial loads. Full longitudinal post-tensioning is applied to connect all segments. The temporary supports are removed once the deck develops enough strength to achieve composite action with the beams. Wearing surfaces and barriers are then added prior to traffic opening.

Two separate analyses were used to evaluate stress demands from this construction process. The first analysis considered non-composite girder sections hinged at closure joints. The second analysis considered the composite girder with first-stage post-tensioning and live load demands. The results from these analyses were superimposed to approximate ultimate structural behavior. Stresses were calculated for each stage of erection and accumulated.

2.8.2 Single-span system multi-stage post-tensioning construction method

For this construction process the precast/prestressed beams are again assumed to be installed on temporary supports at the site. Spliced joints and diaphragms are then poured and cured. *Partial* longitudinal post-tensioning is applied to make the girders

continuous prior to the addition of a composite deck. A second stage of post-tensioning is applied after the deck is cast to provide residual compression in the deck for serviceability and deflection control. Temporary supports are removed once the deck develops enough strength to become composite with the beams. Superimposed dead loads are applied prior to the application of live loads.

Three separate analyses were used to determine demands from this construction process. The first analysis considered the non-composite section hinged at closure joints. The second analysis considered the non-composite girder in a continuous system with equivalent externally applied loads to represent the first post-tensioning stage. The third analysis considered the composite girders with second stage post-tensioning equivalent forces and live load demands. Analysis results were superposed after each stage to obtain the total stress state at each stage.

2.8.3 Two-span continuous system with single-stage post-tensioning construction method

Single-stage post-tensioning has been the favorable construction method for spliced prestressed girder bridge since it is faster and less complex (Lounis et al 1997). Only one stage of post-tensioning forces are applied after pouring the deck. This permits construction to be faster since there is no need to apply additional post-tensioning forces. However, this construction method does not consider for the case of future deck replacement. Since all the girders are subjected to the entire post-tensioning forces in a single event after casting the deck, they will likely be overstressed if the deck is removed.

This construction method is done by applying a single post-tensioning operation after the deck has been cast. The prestressed beams are first placed on temporary supports at the site. Spliced joints and diaphragms are then poured and cured. Either a cast in place deck or a precast deck can be added once the splice and diaphragms have developed enough strength to resist partial loads.

Temporary supports are used to hold the girders during placement of the deck concrete and before all segments are longitudinally connected. After the girders are erected, the support towers are adjusted to touch the bottom of each girder without applying any significant force to them. Temporary supports will resist the partial deck weight until full longitudinal post-tensioning is applied to connect all segments.

Once the deck concrete reaches enough strength to achieve composite action with the beams the temporary supports are removed. The force that was carried by the temporary supports (i.e., reactions) are then resisted by the continuous full-span structure. The total stresses caused by dead loads together with the support loads are less than in systems without temporary supports. Therefore, the structure requirements are expected to be less. Wearing surfaces and barriers are then added prior to traffic opening.

To evaluate stress demands resulting from this construction process, two separate analyses were performed. The first analysis considered the non-composite girder sections hinged at closure joints. The second analysis considered the composite girder with first-stage post-tensioning and live load demands. The results from these analyses were then superimposed to obtain the total structural response. Load patterns and

moment diagrams for the single-stage post-tensioning construction precess are illustrated in Table 2-2.

Positive segments were analyzed as simple spans while negative segments were analyzed as cantilevers from the pier, even though in reality they will most likely be supported from a temporary support close to the pier center line. This assumption was made in order to obtain the maximum negative moment over the pier. Temporary supports were assumed to be unconnected to the beam, thus serving as compression only supports. Girder pre-tensioning forces were selected between the range of zero allowable tension and allowable compression at the bottom fiber of the girder section.

Additional deck and joint loads are assumed to be superposed to the system after the beams are erected. Stresses in the deck were not considered at this stage since the slab has not developed enough strength. Therefore, top and bottom stresses in the precast girders are based on noncomposite section properties.

Post-tensioned splicing forces will induce secondary moments at the pier location. Once the temporary supports are removed, the released reactions will create additional demands on the system. Top and bottom stresses on the precast girders and the cast-in-place deck were determined using composite section properties. Different live load patterns need to be explored to obtain the maximum positive and/or negative moments at the desired locations. Truck and lane loads also need to be compared against the effects caused by tandem and lane loads to obtain the maximum live load demands.

Table 2-2 *Load patterns and moment diagrams of single-stage post-tensioning construction method*

Days	Event/Loads	Load patterns and moment schematics
1	Transfer Pre-tension/ Girder Self Weight & Pre-tensioning loads	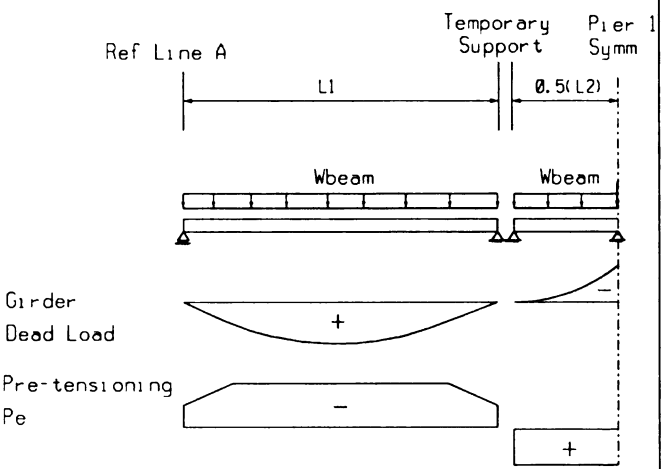
30	Set Girders on Falsework	SAME AS ABOVE
50	Pour splice, diaphragms	SAME AS ABOVE
80	Pour CIP deck/ Fluid weight of deck	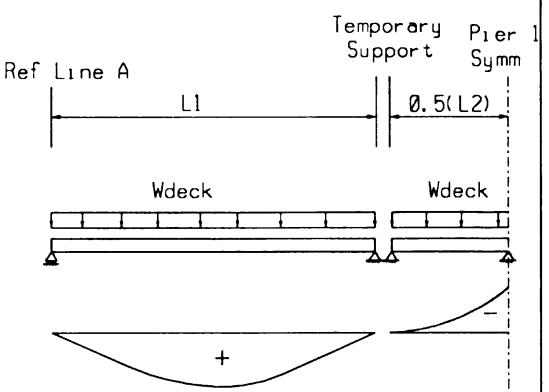

Table 2-2 *Load patterns and moment diagrams of single-stage post-tensioning construction method (Cont...)*

90	Post-tensioning force	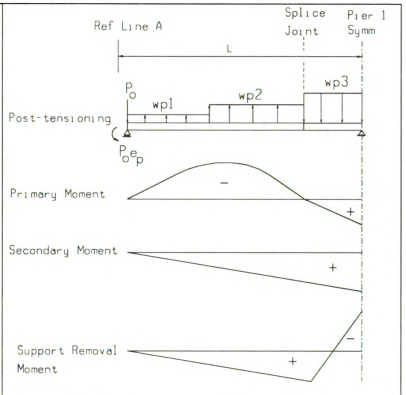
110	Place barrier (Superimposed dead load)	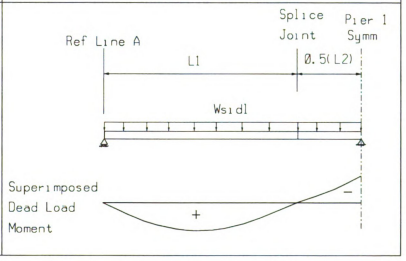

Table 2-2 *Load patterns and moment diagrams of single-stage post-tensioning construction method (Cont...)*

120	Open to full traffic Live load per girder	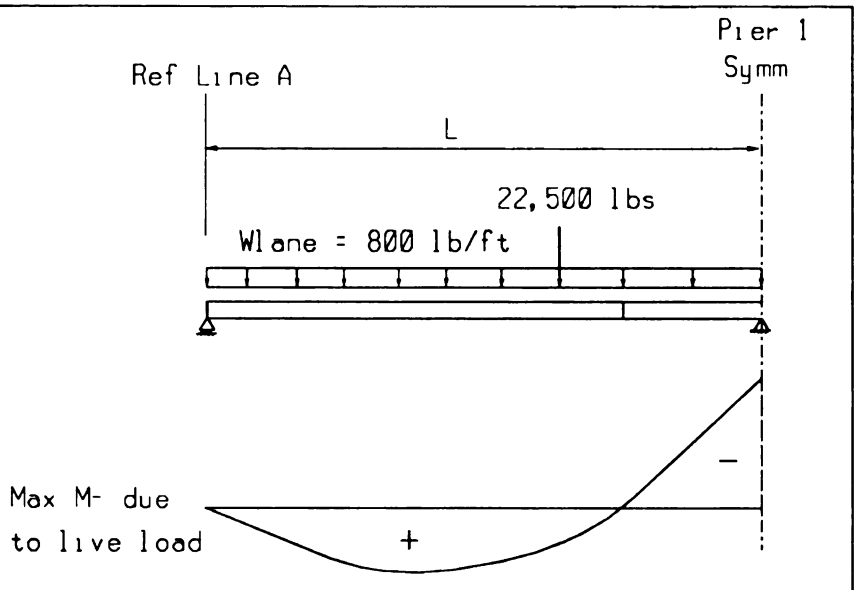

2.8.4 Two- span continuous system with multi-stage post-tensioning construction method

Multi-stage post-tensioning construction can be used to reduce girder demands resulting in reduced girder depths. By applying the post-tensioning forces at different stages, or at least at two stages, the stresses in the girder are redistributed and kept within allowable limits. Using this incremental technique, the resulting girder sections for this construction process are expected to be shallower than those obtained from single-stage construction.

When future maintenance or replacement of the bridge deck is anticipated in a given region, this has to be considered during the design phase. Especially for the case when entire deck replacement is expected to occur during the bridge life-time. In this case, a multi-staged post-tensioned construction method is suitable since it eliminates, or alleviates, overstress conditions in the girder after the deck is removed.

For this method, the precast/prestressed beams are installed on temporary supports at the site. Spliced joints and diaphragms are then poured and cured. *Partial* longitudinal post-tensioning is applied to make the girders continuous prior to the addition of a composite deck. The second stage of post-tensioning is applied after the deck is cast to provide residual compression in the deck for serviceability and deflection control. Temporary supports are removed once the deck develops enough strength to become composite with the beams. Superimposed dead loads are applied prior to the application of live loads.

Typically, the lower post-tensioning tendons are stressed in the first stage while the higher tendons are stressed in the subsequent stages. This tendon stressing scheme can help improve the pre-compression stress state in the deck and allow second stage tendons to be easily accessed.

The stress demands developed through this construction were determined from three separate analyses. The first analysis considered the non-composite section hinged at closure joints. The second analysis considered the non-composite girder in a continuous system with equivalent externally applied loads to represent the first post-tensioning stage. The third analysis considered the composite girders with the second post-tensioning stage equivalent forces and live load demands. Analysis results were superposed after each stage to obtain the total stress state at a given stage. Load Patterns and moment diagrams for the multi-stage post-tensioning construction process are illustrated in Table 2-3.

Table 2-3 *Load patterns and moment diagrams of multi-stage post-tensioning construction method*

Days	Events/Loads	Load patterns and moment schematics
1	Transfer Pre-tension/Girder Self Weight & Pre-tensioning loads	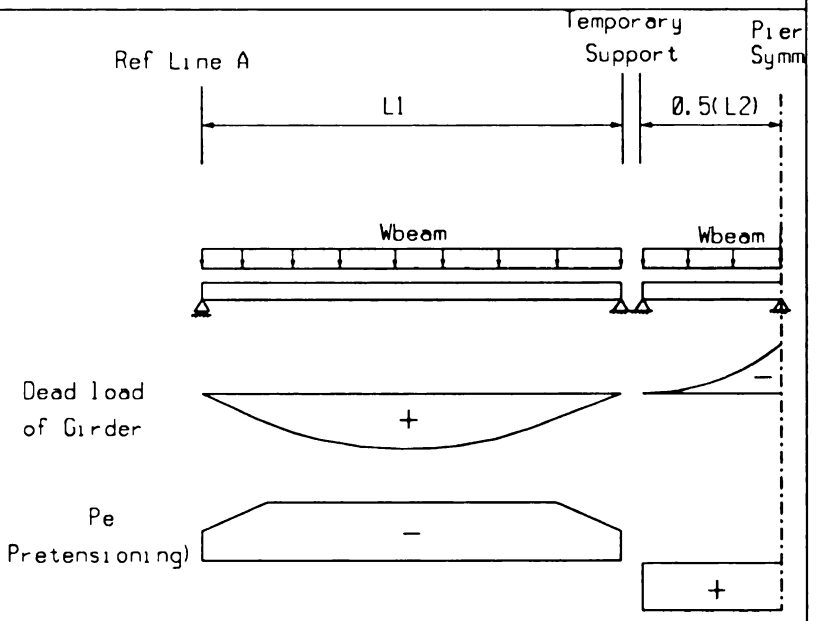
30	Set Girders on Falsework	SAME AS ABOVE
50	Pour splice, diaphragms	SAME AS ABOVE

Table 2-3 *Load patterns and moment diagrams of multi-stage post-tensioning construction method (Cont...)*

80	First stage post-tensioned force	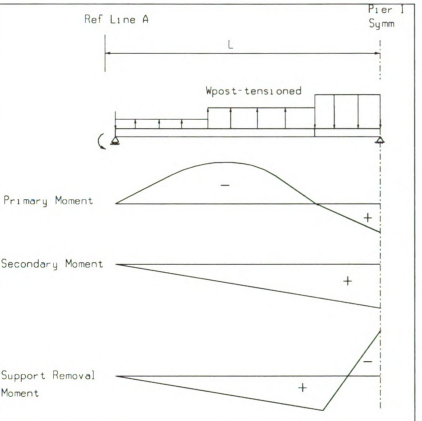
90	Pour CIP deck/ Fluid weight of deck	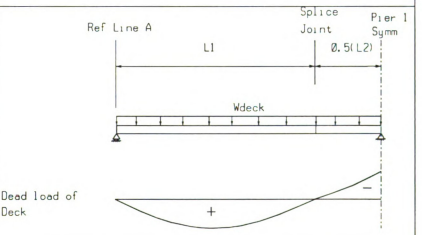

Table 2-3 *Load patterns and moment diagrams of multi-stage post-tensioning construction method (Cont...)*

120	Second stage post-tensioned force	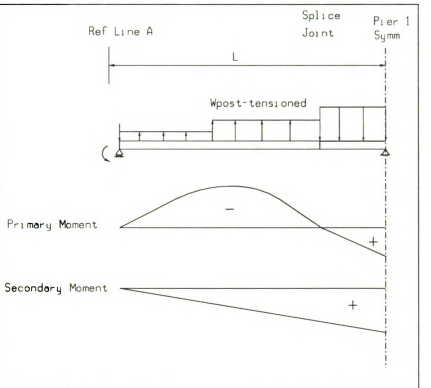
130	Place barrier and superimposed dead load	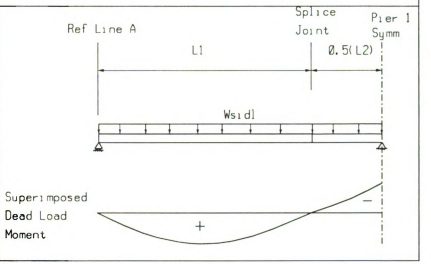

Table 2-3 *Load patterns and moment diagrams of multi-stage post-tensioning construction method (Cont...)*

140	Open to full traffic Live load per girder	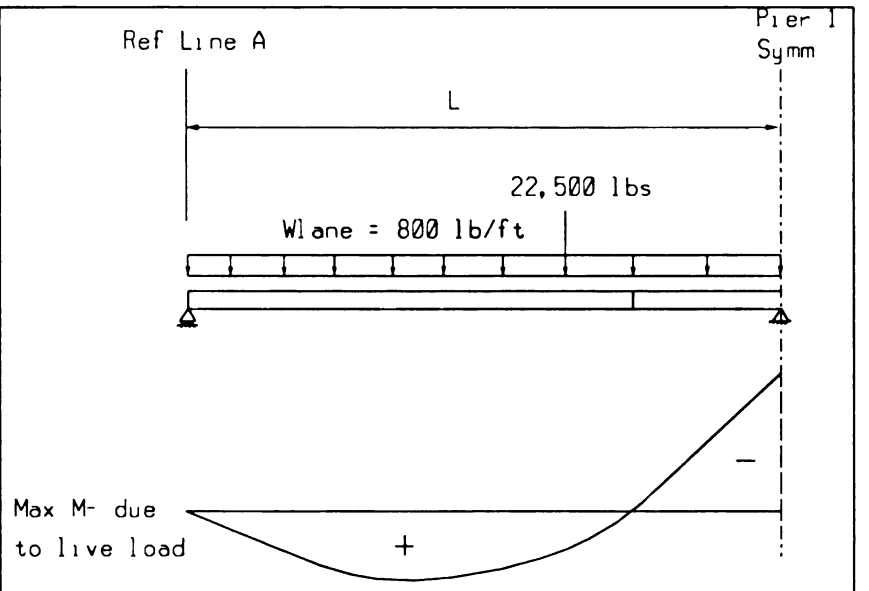

The disadvantages of applying post-tensioning in multiple stages are that the post-tensioning anchorage access must be maintained and some portion of the deck cannot be cast until all the tendons are installed, stressed and grouted. On bridges that have girders post-tensioned at the abutments, the backfill and casting of diaphragms will have to be delayed until all post-tensioning stages are done.

2.9 Stress Demands at Critical Construction Stages

Stress constraints for the service limit state include girder and deck flexural stress limits. Three locations across the composite girder-deck section are checked along the span length of beam on each critical stage to guarantee that all stresses satisfied the constraints, i.e., they should be within the prescribed limits. These locations are the top and bottom flexural fibers of the girder and the top of the deck.

2.9.1 Single-stage post-tensioning construction methods

There are 7 critical stages for a single-stage post-tensioning construction method. Stresses at each critical construction stage, as listed in Table 2-4, need to be checked against the allowable compression and tension stresses. The construction stages summarized in Table 2-4 have been associated with an assumed time schedule. This time schedule was proposed based on typical highway bridge projects with precast concrete. It is understand that this schedule may vary dependent on the nature of the projects state procedures, or other unforeseen events. These issues are addressed later in the implementation and discussion of results in Chapter 4 and 5.

Table 2-4 *Construction sequence for single-staged post-tensioning in spliced girder bridges*

Stage	Time (days)	Action	Critical Tensioning	
			Pre-T	Post-T
1	-	Stress Pre-tensioning strands		
2	0	Cast girder segments		
3	1	Release pre-tensioning strands	X	
4	50	Erect girder segments		
5	60	Place deck and splice concrete	X	
6	75	Stress post-tensioning strands	X	X
7	100	Add barriers		X
8	140	Apply live load		
9	15000	Add FWS		
10	27500	After all prestress losses	X	X

2.9.2 Multi-stage post-tensioned construction methods

There are 10 critical stages for a multi-stage post-tensioned construction method. Stresses at each critical construction stage, as listed in Table 2-5, need to be checked against the allowable compression and tension stresses.

Table 2-5 *Construction sequence for multi-staged post-tensioning in spliced girder bridges*

Stage	Time (days)	Action	Critical Tensioning	
			Pre-T	Post-T
1	-	Stress Pre-tensioning strands		
2	0	Cast girder segments		
3	1	Release pre-tensioning strands	X	
4	50	Erect girder segments		
5	80	Stress 1st post-tensioning strands	X	X
6	90	Place deck and splice concrete	X	X
7	120	Stress 2nd post-tensioning strands	X	X
8	130	Add barriers		X
9	140	Apply live load		
10	15000	Add FWS		
11	27500	After all prestress losses	X	X

2.10 Time-dependent Prestress Losses

Time dependent effects can significantly affect the accuracy of calculated stresses and deflections, particularly in systems employing multi-stage construction, such as segmental bridges and spliced girder bridges. Unconservative estimates of these effects can underestimate tendon requirements and member stress resultants.

Normally, SGB rely on large amounts of post-tensioned, pre-tensioned, and passive reinforcement, consequently the effect of reinforcement on the creep behavior of SGB components may play an important role and should not be ignored in the analysis, particularly of negative sections.

Time-dependent prestress loss sources in pre-tensioned and post-tensioned concrete structures include steel relaxation, concrete shrinkage and concrete creep. Time dependent effects affect the accuracy of calculated stresses and deflections and can have a significant influence on composite prestressed members (Ronald 2001). The ultimate

creep and shrinkage coefficients used in an analysis typically determine the number of tendons employed to satisfy stress limit states (Ronald 2001).

There are several creep and shrinkage models currently used in bridge design practice. These methods are those recommended by the American Concrete Institute Committee 209 (ACI 2002), the American Association of State Highway and Transportation Officials (AASHTO 2003) and the code from the Comite Euro-International du Beton and the Federation Internationale de la Precontrainte (CEB-FIP 1990).

2.10.1 Creep and shrinkage prestress losses - AASHTO /ACI

The methods of determining creep and shrinkage herein are taken from Collins and Mitchell (1991). These methods are based on recommendation of the AASHTO-LRFD code (AASHTO 2003), the ACI-209 recommendations (ACI 1992) and additional published data by Rusch et al. (1983), Bazant and Wittman (1982), and Ghali and Favre (1986).

a) Creep coefficient

The creep coefficient $\phi(t,t_i)$ is defined in AASHTO-LRFD Section 5.4.2.3.2 (AASHTO 2003) as follows:

$$\phi(t,t_i) = 35.k_c k_f (1.58 - \frac{H}{120}) t_i^{-0.118} \frac{(t-t_i)^{0.6}}{10+(t-t_i)^{0.6}}, \qquad (2\text{-}21)$$

where:

k_f= factor for the effect of concrete strength

$$k_f = \frac{1}{0.67 + (\frac{f_c'}{62})} \text{ [MPa] or } k_f = \frac{1}{0.67 + (\frac{f_c'}{9})} \text{ [ksi].} \quad (2\text{-}22)$$

k_c = factor for the effect of volume/surface of component, which is based on PCI equation (1977):

$$k_c = [\frac{t}{\frac{26e^{0.36(V/S)} + t}{t}}][\frac{1.8 + 1.77e^{-0.54(\frac{V}{S})}}{2.587}], \quad (2\text{-}23)$$

where H = relative humidity; t = maturity of concrete (days); t_i = age of concrete when load is initially applied (days); f_c' = specified compressive strength at 28 days (ksi); S = surface area that is exposed to atmospheric drying; and V = concrete volume that is exposed to atmospheric drying. If the information of humidity (H) is not available, it may be taken from AASHTO-LRFD Fig. 5.4.2.3.3-1 (AASHTO 2003).

b) Shrinkage strain

The strain due to shrinkage is taken as defined in AASHTO-LRFD Section 5.4.2.3.3 (AASHTO 2003) as follows:

i) Shrinkage strain for moist cured concrete:

$$\varepsilon_{sh} = -k_s k_h (\frac{t}{t+35}) 0.51 \times 10^{-3}; \quad (2\text{-}24)$$

ii) Shrinkage strain for steam-cured concrete

$$\varepsilon_{sh} = -k_s k_h (\frac{t}{t+55}) 0.56 \times 10^{-3}; \quad (2\text{-}25)$$

where t = drying time (days); and k_s = size factor, and is given by:

$$k_s = [\frac{\frac{t}{26e^{0.36(\frac{V}{S})} + t}}{\frac{t}{45+t}}][\frac{1064 - 94(\frac{V}{S})}{923}]. \quad (2\text{-}26)$$

For H < 80%:

$$k_h = (\frac{140 - H}{70}), \quad (2\text{-}27)$$

and for H > 80%:

$$k_h = \frac{3(100 - H)}{70}. \quad (2\text{-}28)$$

c) Relaxation losses

To determine prestressing losses due to steel relaxation tensile reinforcement and strands are assumed to be lumped at a single location with an effective distance to the passive reinforcement (d_s) and effective distance to the prestressing reinforcement (d_p). The average stress in the prestressing steel is then:

$$f_{ps} = f_{pu}(1 - k\frac{c}{d_p}), \quad (2\text{-}29)$$

where k is the factor of yielding and ultimate strength and is defined as follows:

$$k = 2(1.04 - \frac{f_{py}}{f_{pu}}). \quad (2\text{-}30)$$

The neutral axis depth for the prestressed section can then defined by considering section equilibrium. For a T-section the neutral axis depth is given by:

$$c = \frac{A_{ps} f_{pu} + A_s f_y - A_s' f_y' - 0.85 \beta_1 f_c' (b - b_w) h_f}{0.85 f_c' \beta_1 b_w + k A_{ps} \frac{f_{pu}}{d_p}}, \quad (2\text{-}31)$$

While for a rectangular-section, it is given by

$$c = \frac{A_{ps} f_{pu} + A_s f_y - A_s' f_y'}{0.85 f_c' \beta_1 b + k A_{ps} \frac{f_{pu}}{d_p}}, \quad (2\text{-}32)$$

where A_{ps} = are of prestressing steel; f_{pu} = specified tensile strength of prestressing steel; and f_{py} = yield strength of prestressing steel.

The AASHTO-LRFD (AASHTO 2003) guidelines for prestress losses, which were adopted from the ACI-209 recommendations (ACI 1992), were developed based on a single loss value at the centroid of the prestressing force, and this single loss value is assumed to be uniformly distributed across the girder section.

An excessively conservative value of creep or shrinkage can make the allowable stress design approach nearly impossible without reducing span length or using deeper members. On the other hand, unconservative values of creep or shrinkage will yield unconservative estimates of tendon requirements and may lead to serviceability problems. Rational analyses that offer flexibility in material and geometric variables may yield accurate results. When mix-specific data are not available, estimates of shrinkage and creep may be made using either the AASHTO specifications, or the CEB-FIB 90 or ACI -209 recommendations.

2.10.2 CEB-FIP 90

The time-dependent strain in concrete can be expressed as the sum of elastic and creep strains due to initial stresses, elastic and creep strains due to changes in stress and the shrinkage strain (Wollmann et. al 2003). The total concrete strain at time t is expressed as follows (Wollmann et. al 2003):

$$\varepsilon_t = \frac{\sigma_o}{E_o}(1+\varphi_{t,t_o}) + \frac{\sigma_t - \sigma_o}{E}(1+\mu\varphi_{t,t_o}) + \varepsilon_{s,t}, \qquad (2\text{-}33)$$

where ε_t = total concrete strain at time t; σ_0 = concrete stress at time t = 0; σ_t = concrete stress at time t; $\varphi_{t,to}$= creep coefficient at time t due to load applied at time t_o; ε_{st} = shrinkage strain at time t; μ = aging coefficient = 0.7; and E_o= modulus of elasticity at time t_o = 0.

The first term in Equation (2-33) represents the elastic and creep strain due to a stress σ_0 applied at time t_o. The second term represents the elastic and creep strain due to stress changes from time t_o to time t. The last term represents the shrinkage strain at time t.

The aging coefficient, μ, is a function of load history and of the time-dependent concrete properties. The coefficient accounts for the reduced creep of concrete loaded at a greater age. Generally, the upper bound for μ is 1.0, where the load history is a single step stress increment $\Delta\sigma = \sigma_t - \sigma_o$ applied at time $t = t_o$ with no further changes (Bazant 1972 and Dilger 1982). The aging coefficient is defined as (Bazant 1972 and Dilger 1982):

$$\mu = \frac{E_o}{(\sigma_t - \sigma_o)\varphi_{t,t_o}} \int_{t_o}^{t} \frac{1}{E(\tau)} \frac{d\sigma(\tau)}{d\tau} [1 + \varphi(t,\tau)] d\tau - \frac{1}{\varphi_{t,t_o}}. \quad (2\text{-}34)$$

Bazant (Bazant 1972) has shown that when the change in stress is increased by creep and shrinkage, a value of 0.7 and 0.9 is appropriate to use for the loading at age 10 days and 100 days, respectively. Generally, creep and shrinkage properties are subject to large scatter and cannot be determined with great accuracy. Due to the variability of the creep properties, high accuracy for the aging coefficient is not required since normally the aging coefficient is multiplied by the creep coefficient. The assumption of a constant aging coefficient makes creep and shrinkage calculation simpler and can be reduced to the solution of linear equation (Wollmann et. al 2003).

The component forces due to section forces acting on the composite section and distances of deck and girder are illustrated in Figure 2-10.

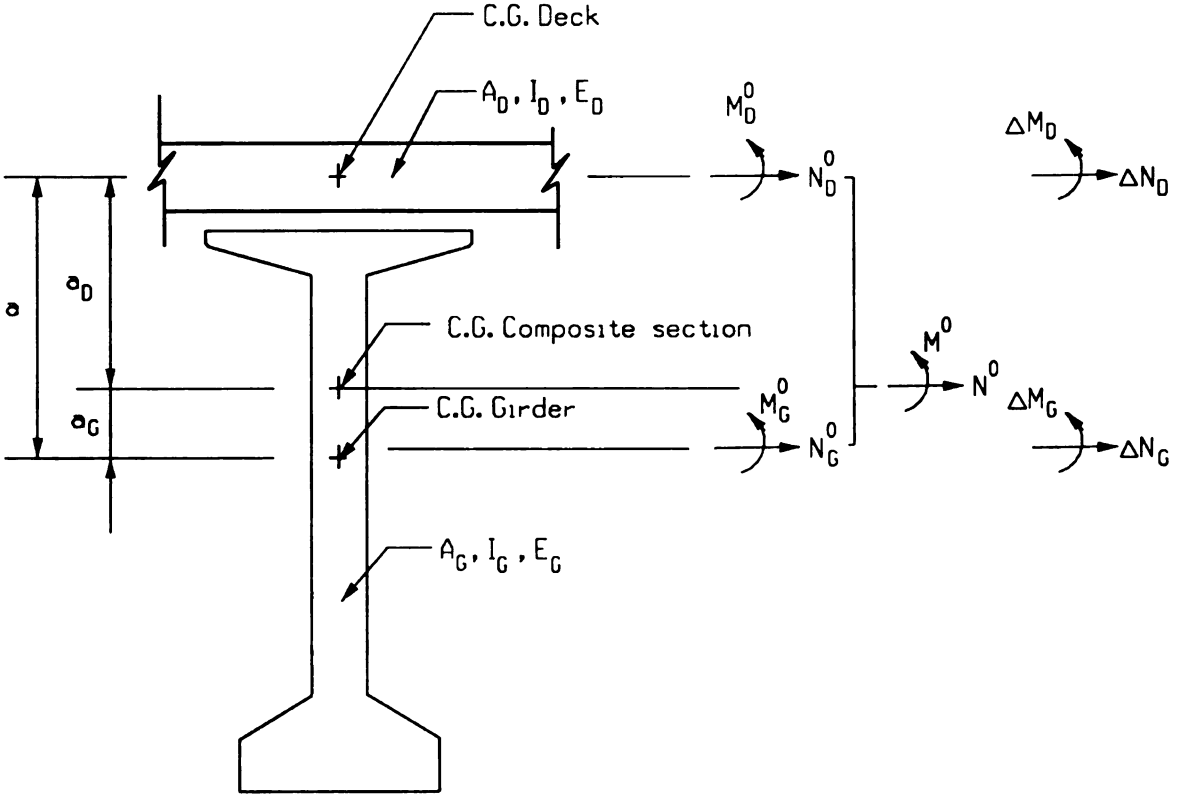

Figure 2-10 *Component forces and centroid distances on composite girder/deck section*

The modular ratio, n, of deck concrete to girder concrete is defined as:

$$n = \frac{E_D}{E_G}. \tag{2-35}$$

where E_D and E_G are the modulus of elasticity for deck and girder, respectively.

The area of transformed composite section, A_c, includes the girder area A_G and the transformed deck area A_D, and can be defined as:

$$A_c = A_G + nA_D. \tag{2-36}$$

The distance a_D between centroid of deck and centroid of composite section is determined by:

$$a_D = \frac{A_G}{A_c} a. \tag{2-37}$$

The distance a_G between the centroid of girder and the centroid of the composite section is given by:

$$a_G = \frac{nA_D}{A_c} a, \tag{2-38}$$

where a is the distance the between centroid of the deck and the centroid of the girder.

The first area moment, S_c, of the transformed deck section about the centroid of the composite section is defined as:

$$S_c = nA_D a_D, \tag{2-39}$$

where a_D is the distance between centroid of the deck and the centroid of the composite section.

The moment of intertia of the transformed composite section I_c is then defined as:

$$I_c = I_G + nI_D + aS_c, \tag{2-40}$$

where I_D and I_G is the moment of intertia of the deck and girder about their own centroids, respectively.

The component axial forces (N_D *and* N_G) and component moment forces (M_D *and* M_G) due to the moment (M) and axial force (N) acting on the composite section can be found by integrating the resultant stress distribution over the respective portions of the cross section. The expressions for the component forces are as follows (Wollmann et. al 2003).

The axial load in the deck due to axial and moment forces on the composite section is determined by:

$$N_D = \frac{nA_D}{A_C} N - M \frac{S_C}{I_C}. \tag{2-41}$$

The axial load the girder due to axial and moment forces of composite section is determined by:

$$N_G = \frac{A_G}{A_C} N + M \frac{S_C}{I_C}. \tag{2-42}$$

The moment in deck due to a moment force on the composite section is determined by:

$$M_D = M \frac{nI_D}{I_C}. \tag{2-43}$$

The moment in the girder due to a moment force on the composite section is given by:

$$M_G = M \frac{I_G}{I_C}. \tag{2-44}$$

With time, strains and curvature will change due to creep and shrinkage, which causes the build-up of a self-equilibrating state of stress over the cross-section. This time-dependent change can be described by eight unknown quantities: $-\Delta M_D$, ΔN_D, ΔM_G, ΔN_G, K_D, ε_D, K_G, *and* ε_G. Since there are eight unknown quantities, eight equations are needed. Two equations can be obtained from compatibility requirements by assuming plane sections remain plane and perfect bond between deck and girder.

Curvature of deck, K_D, and curvature of girder, K_G, due to long term effects are assumed to be equal and defined as:

$$\kappa_G = \kappa_D = \kappa. \tag{2-45}$$

The time-dependent strain for deck, ε_D, is determined from the time-dependent strain on the girder, ε_G, and the curvature, K, at the distance between centroid of deck and centroid of girder.

$$\varepsilon_D = \varepsilon_G - \kappa a. \tag{2-46}$$

Two more equations (equation 2-47 and equation 2-48) can be obtained from equilibrium requirements on axial forces and moments. Axial equilibrium in the composite section can be defined as follows:

$$\Delta N_D + \Delta N_G = 0, \tag{2-47}$$

where ΔN_D is the time-dependent change of axial loads in the deck; and ΔN_G is the time-dependent change of axial loads in the girder.

Moment equilibrium in the composite section can be expressed as follows:

$$\Delta M_D + \Delta M_G + \Delta N_G a = 0, \tag{2-48}$$

where ΔM_D is the time-dependent change of moments in the deck, ΔM_G is the time-dependent change of moments in girder, and a is the distance between the centroid of the deck and the centroid of the girder.

Even though stresses will change with time, there is no resultant force on the composite section due to these changes because they are self-equilibrating. The two equilibrium conditions expressed in Equations 2-47 and 2-48 are true only for a statically determinate system where long-term deformations do not cause a change in section forces. For an indeterminate structure, Equations 2-47 and 2-48 need to be modified to include terms for the time-dependent redundant forces.

The remaining four equations (2-49 through 2-52) are given by the constitutive relations describing the time-dependent strains only. The initial strains are not included in these equations and they are expressed as given by Wollmann et al. (2003) below:

The time-dependent strain in the deck, ε_D, is determined by:

$$\varepsilon_D = \frac{N_D^0}{E_D A_D}\varphi_D + \frac{\Delta N_D}{E_D A_D}(1+\mu\varphi_D) + \varepsilon_{SD}, \tag{2-49}$$

where ε_{SD} is the shrinkage strain for the deck; N_D^0 is the axial load in the deck at the beginning of composite action; φ_D is the creep coefficient for the deck; E_D is the modulus of elasticity of the deck; and A_D is the area of deck.

The time-dependent strain in the girder, ε_G, is defined as:

$$\varepsilon_G = \frac{N_G^0}{E_G A_G}\varphi_G + \frac{\Delta N_G}{E_G A_G}(1+\mu\varphi_G) + \varepsilon_{SG}, \tag{2-50}$$

where ε_{SG} is the shrinkage strain for the girder; N_G^0 is the axial load in girder at the beginning of composite action; φ_G is the creep coefficient for the girder; E_G is the modulus of elasticity of the girder; and A_G is the area of the girder.

The curvature of the deck due to long-term effects, K_D, is given by:

$$\kappa_D = \frac{M_D^0}{E_D I_D}\varphi_D + \frac{\Delta M_D}{E_D I_D}(1+\mu\varphi_D), \tag{2-51}$$

where M_D^0 is the moment in the deck at the beginning of composite action; I_D is the moment of the inertia of the deck about its own centroid; and μ is the aging coefficient.

The curvature of the girder due to long-term effects, K_G, is given by:

$$\kappa_G = \frac{M_G^0}{E_G I_G}\varphi_G + \frac{\Delta M_G}{E_G I_G}(1+\mu\varphi_G), \tag{2-52}$$

where M_G^0 is the moment in the girder at the beginning of composite action and I_G is the moment of inertia of the girder about its own centroid.

The input data required for the solution of the system of four equations (Equation 2-50 to Equation 2-53) are the cross-section and material properties (E_D, E_G, A_D, A_G, I_D, I_G *and* a), the creep producing stress resultants ($N_D^0, N_G^0, M_D^0, M_G^0$), and the concrete creep and shrinkage parameters ($\varphi_D, \varepsilon_{sD}, \varphi_G, \varepsilon_{sG}, \mu$). Solving this system of equations with a spreadsheet or numerical analysis programs is simple.

The effect of prestress and prestress losses can be easily implemented in the system of equations (Equation 2-49 to Equation 2-51). The initial prestress force is considered with the creep-producing stress resultants M_D^0, M_G^0, N_D^0 and N_G^0. Prestress losses are initially estimated by estimating the time-dependent change in strain ε_p at the

location of the tendons or strands. The forces acting on the composite section due to prestress losses are then given by Equation (2-53) through Equation (2-54) (Wollmann et. al 2003).

The change of axial load due to prestress losses, ΔN^P, is defined as:

$$\Delta N^P = A_{PS}(\Delta f_R - E_{PS}\varepsilon_P), \tag{2-53}$$

where A_{ps} = cross-sectional area of the prestressing steel; E_{ps} = modulus of elasticity of the prestressing steel; ε_P = time-dependent change in strain at the location of the prestressing steel (tension positive); and Δf_R = prestress loss due to strand relaxation.

The change in moment due to prestress losses, ΔM^P, is defined as:

$$\Delta M^P = \Delta N^P e, \tag{2-54}$$

where e = eccentricity of the prestressing steel relative to the centroid of the composite section (down positive).

The force ΔN^P and ΔM^P can be decomposed into component forces $\Delta N_D^P, \Delta M_D^P, \Delta N_G^P$, and ΔM_G^P in the deck and girder, respectively. The component forces due to prestress losses are self-equilibrating with the change in tendon force. Time-dependent strains and curvatures including the effects of prestress losses are given by (Wollmann et al. 2003) and are outlined next.

The time-dependent strain in the deck, ε_D, including prestress losses is determined by:

$$\varepsilon_D = \frac{N_D^0}{E_D A_D}\varphi_D + \frac{\Delta N_D + \Delta N_D^P}{E_D A_D}(1 + \mu\varphi_D) + \varepsilon_{SD}. \tag{2-55}$$

The time-dependent strain in the girder, ε_G, including prestress losses is defined by:

$$\varepsilon_G = \frac{N_G^0}{E_G A_G}\varphi_G + \frac{\Delta N_G + \Delta N_G^P}{E_G A_G}(1 + \mu\varphi_G) + \varepsilon_{SG}. \tag{2-56}$$

The curvature of the deck due to long-term effects, K_D, including prestress losses is determined by:

$$\kappa_D = \frac{M_D^0}{E_D I_D}\varphi_D + \frac{\Delta M_D + \Delta M_D^P}{E_D I_D}(1 + \mu\varphi_D). \tag{2-57}$$

The curvature on the girder due to long-term effects, K_G, including prestress losses is given by:

$$\kappa_G = \frac{M_G^0}{E_G I_G}\varphi_G + \frac{\Delta M_G + \Delta M_G^P}{E_G I_G}(1 + \mu\varphi_G). \tag{2-58}$$

2.11 Simplified Estimate of Prestress Loss Components

The estimate prestress losses according to the "refined" simplified method of the AASHTO-LRFD code (LRFD 2003) and the recommendations from the NCHRP 517 report (Castrodale and White 2004) are presented in this section. The principles of the refined method of the AASHTO-LRFD Specifications only provide total losses and has no provisions for computing losses at stages prior to the final conditions. The recommendations from the NCHRP 517 report account for the interaction of pre-tensioning and post-tensioning in prestress loss computation.

2.11.1 Relaxation prestress losses at release

The prestress losses of pre-tensioned strands due to the relaxation at the release stage can be defined as follows (AASHTO-LRFD Article 5.9.5.4.4b-2):

$$\Delta f_{PR1} = \frac{\log(24t)}{40}[\frac{f_{pj}}{f_{py}} - 0.55]f_{pj}, \tag{2-59}$$

where Δf_{PR1} is the relaxation prestress loss at release; f_{pj} is the stress in the strand during the jacking operation; f_{py} is the yield strength of the strand; and t is the time at which prestress is released.

2.11.2 Shrinkage prestress losses

The prestress losses in this section are the estimation of time-dependent shrinkage losses at the final condition according to AASHTO-LRFD. The intermediate shrinkage prestress losses can be determined by multiplying the final shrinkage losses with a time factor as shown in equation (2-62).

Shrinkage prestress losses at the final stage of pre-tensioned strands can be determined as follows (AASHTO-LRFD Article 5.9.5.4.2):

$$\Delta f_{PSR} = (17 - 0.15H) \qquad \text{(ksi)}, \tag{2-60}$$

where Δf_{PSR} is the shrinkage prestress loss and H is the humidity. Shrinkage prestress losses at the final stage of post-tensioning can be defined as follows:

$$\Delta f_{PSR} = (13.5 - 0.123H) \qquad \text{(ksi)}. \tag{2-61}$$

The time factor of shrinkage losses to determine prestress losses at intermediate stages is based on AASHTO-LRFD Equation 5.4.2.3.3-1 as follows:

$$\Delta k_{SHt} = \frac{t}{35.0 + t}. \tag{2-62}$$

2.11.3 Creep prestress losses

NCHRP project 12-57 (Castrodale and White 2004) recommended that the creep losses equation from AASHTO-LRFD Article 5.9.5.4.3 (AASHTO 2003) be modified to include the effects of post-tensioned strands. The creep loss formulas outlined in this section are for the losses at the final stage. Intermediate creep prestress losses can be determined by multiplying the final creep losses with a time factor as it will be shown later.

Creep prestress losses at the final stage of pre-tensioned strands can be determined as by the following expression:

$$\Delta f_{PCR} = 12 f_{cgp} - 7\Delta f_{cdp} + 7 f_{cgp1}, \tag{2-63}$$

where Δf_{PCR} is the creep loss from pre-tensioned strands; f_{cgp} is the summation of concrete stresses at center of gravity of the prestressing strands due to the prestressing force at transfer and the member self-weight at maximum moment; f_{cdp} is the change in concrete stresses at center of gravity of the prestressing steel due to the permanent loads; f_{cgp1} is the summation of concrete stresses at center of gravity of the prestressing tendon due to the post-tensioning force and the removal of temporary support.

The summation of concrete stresses at the center of gravity of the prestressing tendon due to prestressing force at transfer and the member self-weight at maximum moment is defined as follows:

$$f_{cgp} = \frac{F_p}{A} + \frac{F_p e^2}{I} - \frac{M_{GDL} e}{I}, \tag{2-64}$$

where A is the gross area of the girder; I is the gross girder moment of inertia; F_p is the total prestress force due to pre-tensioning; M_{GDL} is the moment due to girder selfweight; and e is the eccentricity of the pre-tensioning strands measured from the neutral axis of noncomposite section to the centroid of the pre-tensioning strands.

The change in concrete stresses at the center of gravity of the prestressing steel due to permanent loads is given by:

$$f_{cdp} = (\frac{M_{DDL} + M_{NCDL}}{I})e + \frac{M_{CDL} e_c}{I_c}, \tag{2-65}$$

where M_{DDL} is the moment due to the deck selfweight; M_{NCDL} is the moment due to the girder/deck haunch weight; M_{CDL} is the moment due to construction loads; e_c is the eccentricity of the pre-tensioning strands measured from the neutral axis of composite section to centroid of the pre-tensioning strands; and I_c is the composite girder/deck moment of inertia.

The summation of concrete stresses at center of gravity of the pre-tensioning strands due to post-tensioning forces and removal of temporary supports is defined as follows:

$$f_{cgp1} = \frac{F_{PT}}{A_c} + \frac{F_{PT} e_{PT} e_c}{I_c} - \frac{M_{REM} e_c}{I_c}, \tag{2-66}$$

where F_{PT} is the total prestress force due to post-tensioning; A_c is the composite area of the section; e_{PT} is the eccentricity of the post-tensioning strand measured from the

neutral axis of the composite section to the centroid of the post-tensioning strands; and M_{REM} is the moment due to removal of temporary supports.

Creep prestress losses at the final stage of post-tensioned strands can be determined by:

$$\Delta f_{PCR} = 12 f_{cgp} - 7\Delta f_{cdp} + 7 f_{cgp2}, \tag{2-67}$$

where Δf_{PCR} is the creep loss for post-tensioning strands; f_{cgp} is the summation of concrete stresses at center of gravity of the post-tensioning tendons due to post-tensioning forces and removal of temporary supports; f_{cdp} is the change in concrete stress at center of gravity of the post-tensioning strands due to permanent loads; and f_{cgp2} is the summation of concrete stresses at the center of gravity of the post-tensioning tendon due to pre-tensioned strands and girder self-weight.

The summation of concrete stresses at the center of gravity of the post-tensioning tendon due to post-tensioning forces and the removal of temporary supports is determined as follows:

$$f_{cgp} = \frac{F_{PT}}{A_c} + \frac{F_{PT} e_{PT}^2}{I_c} - \frac{M_{REM} e_{PT}}{I_c},$$

(2-68)

where F_{PT} is the total prestress force due to post-tensioning; A_c is the composite area of the section; e_{PT} is the eccentricity of the post-tensioning strand measured from the neutral axis of the composite section to the centroid of the post-tensioned strands; and M_{REM} is the moment due to the removal of temporary supports.

The change in concrete stress at center of gravity of the post-tensioning strands due to permanent loads is defined by:

$$f_{cdp} = (\frac{M_{DDL} + M_{NCDL}}{I})e_{PT} + \frac{M_{CDL}e_{PT}}{I_c}. \quad (2\text{-}69)$$

The summation of concrete stresses at center of gravity of the post-tensioning tendon due to pre-tensioning strands and girder self-weight is determined by:

$$f_{cgp2} = \frac{F_{PRE}}{A} + \frac{F_{PRE}e_{PT}e}{I} - \frac{M_{self}e_{PT}}{I}, \quad (2\text{-}70)$$

where F_{PRE} is the total prestress force due to pre-tensioning; and M_{self} is the moment due to the girder self-weight.

The time factor to determine the prestress losses due to creep at intermediate stages is based on AASHTO-LRFD Equation 5.4.2.3.2-1 as follows:

$$\Delta k_{CRt} = \frac{t^{0.6}}{10.0 + t^{0.6}}. \quad (2\text{-}71)$$

2.11.4 Elastic shortening prestress losses

Instantaneous elastic shortening prestress losses at the initial stage of pre-tensioning strands can be determined as follows (AASHTO Article 5.9.5.2.3):

$$\Delta f_{PES} = \frac{E_P}{E_{ci}} f_{cgp}, \quad (2\text{-}72)$$

where Δf_{PES} is the elastic shortening losses on the pre-tensioning strands; f_{cgp} is the summation of concrete stress at the center of gravity of the prestressing tendon as

described in Equation (2-63); E_p is the elastic modulus of the pre-tensioning strands; and E_{ci} is the elastic modulus of girder concrete at the initial stage.

Elastic shortening prestress losses at the initial stage of post-tensioning strands is defined by:

$$\Delta f_{PES} = (\frac{N-1}{2N})\frac{E_P}{E_{ci}} f_{cgp}, \tag{2-73}$$

where Δf_{PES} is the elastic shortening losses on the pre-tensioning strands; N is the number of post-tensioning ducts; f_{cgp} is the summation of concrete stresses at the center of gravity of the post-tensioning tendon due to post-tensioning forces and removal of temporary supports, as described in Equation (2-68).

2.11.5 Relaxation prestress losses at final condition

Prestress losses due to steel relaxation at the final stage of pre-tensioning strands is based on AASHTO-LRFD section 5.9.5.4 and can be determined for stress-relieved strands as follows:

$$\Delta f_{PR2} = 20 - 0.4\Delta f_{PES} - 0.2(\Delta f_{PSR} + \Delta f_{PCR}), \tag{2-74}$$

where Δf_{PR2} is the final relaxation loss at the final stage for the pre-tensioning strands; Δf_{PES} is the elastic shortening prestress loss; Δf_{PSR} is the shrinkage prestress loss; and Δf_{PCR} is the creep loss.

Relaxation prestress loss for low-relaxation strands at the final stage of pre-tensioning strands is based on AASHTO-LRFD section 5.9.5.4.4c-1 and is given by:

$$\Delta f_{PR2} = 0.3 \times (20 - 0.4\Delta f_{PES} - 0.2(\Delta f_{PSR} + \Delta f_{PCR})), \tag{2-75}$$

where Δf_{PR2} is the final relaxation loss at the final stage for low-relaxation pre-tensioning strands.

Relaxation prestress loss at the final stage for post-tensioning strands is based on AASHTO-LRFD section 5.9.5.4.4c-2 and is given by:

$$\Delta f_{PR2} = 0.3 \times (20 - 0.30\Delta f_{PF} - 0.4\Delta f_{PES} - 0.2(\Delta f_{PSR} + \Delta f_{PCR})), \quad (2\text{-}76)$$

where Δf_{PR2} is the final relaxation loss at the final stage for the post-tensioning strands.

2.11.6 Additional elastic shortening prestress losses due to post-tensioning

The stressing of post-tensioning tendons causes additional, or secondary, elastic shortening prestress losses in the girder segments and they are defined as follows (Castrodale and White 2004):

$$\Delta f_{PES2} = \frac{E_P}{E_c} f_{cgp1}, \quad (2\text{-}77)$$

where N is the number of post-tensioning ducts; E_c is the elastic modulus of the girder concrete at the stage in question; E_p is the elastic modulus of prestress steel; and Δf_{cgp1} is the summation of concrete stresses at center of gravity of the prestressing tendon due to the post-tensioning forces and the removal of temporary supports as defined in Equation (2-65).

2.11.7 Friction prestress losses

Friction prestress losses from post-tensioning at the segment midspan are computed by (AASHTO Article 5.9.5.2.2):

$$\Delta f_{PF} = f_{pj}(1 - e^{-(kx+\mu\alpha)}), \quad (2\text{-}78)$$

where Δf_{PF} is the friction prestress loss; k is wobble coefficient; μ is the friction coefficient; α is the angle between the post-tensioning tendon and the horizontal axis; x is half of the girder length; and Δf_{pj} is the jacking stress.

2.11.8 Anchorage set prestress losses (NCHRP 517 report)

Anchor set prestress losses are those that occur on each post-tensioned tendon when it is pulled into the anchorage seating. The constant rate of friction loss, R_F, for estimating friction losses from post-tensioning can be computed as recommended in the NCHRP 517 report (Castrodale and White 2004) corresponding to the location at midspan, x, as follows:

$$R_F = \frac{\Delta f_{PF}}{x}. \tag{2-79}$$

The stress at the anchorage is reduced based on the distance, X_A, that the anchorage is extended and is calculated as follows (Castrodale and White 2004):

$$x_A = \sqrt{\frac{A_{SET} E_P}{R_F}}, \tag{2-80}$$

where A_{SET} is the length of the anchorage set and E_P is the elastic modulus of the post-tensioning strands.

The anchor prestress loss, Δf_A, is then calculated by using the following equation:

$$\Delta f_A = 2 x_A R_F. \tag{2-81}$$

2.12 Total Prestress Losses at Critical Construction Stages

The construction sequence of SGB can yield different prestress loss components for the pre-tensioned and post-tensioned strands at each stage, and thus they need to be

individually considered for each critical construction stage case. This section presents the critical construction stages for the different construction sequences that need to be considered for the change in prestress losses.

The total prestress losses of the pre-tensioned and post-tensioned strands at the critical construction stages of single-stage post-tensioning applied after deck casting (see Section 2.11) are summarized in Table 2-6.

Table 2-6 *Prestress losses during single-stage post-tensioning after deck casting*

Pre-tensioned strands (Δf_{PRET})	
Critical construction stage	**Components of prestress loss**
Release of pre-tensioned strands	$\Delta f_{PES1} + \Delta f_{PR1}$
Placement of deck and splice concrete	$\Delta f_{PES1} + k_{CR1}\Delta f_{PCR} + k_{SH1}\Delta f_{PSR} + \Delta f_{PR2}$
Stressing of post-tensioning tendons	$\Delta f_{PES1} + k_{CR2}\Delta f_{PCR} + k_{SH2}\Delta f_{PSR} + \Delta f_{PR2} + \Delta f_{PES2}$
Final conditions after losses	$\Delta f_{PES1} + \Delta f_{PCR} + \Delta f_{PSR} + \Delta f_{PR2} + \Delta f_{PES2}$
Post-tensioned strands (Δf_{PT})	
Critical construction stage	**Components of prestress loss**
Stressing of post-tensioning tendons	$\Delta f_{PF} + \Delta f_{PA} + \Delta f_{PES}$
Final conditions after losses	$\Delta f_{PF} + \Delta f_{PA} + \Delta f_{PES} + \Delta f_{PCR} + \Delta f_{PSR} + \Delta f_{PR2}$

The total prestress losses of the pre-tensioned and post-tensioned strands at the critical construction stages of multi-stage post-tensioning applied after deck casting are summarized in Table 2-7.

Table 2-7 *Total prestress losses during multi-staged post-tensioning*

Pre-tensioned Strands (Δf_{PRET})	
Critical construction stage	**Components of prestress loss**
Release of pre-tensioned strands	$\Delta f_{PES1} + \Delta f_{PR1}$
Stressing of 1st post-tensioning tendons	$\Delta f_{PES1} + k_{CR1}\Delta f_{PCR} + k_{SH1}\Delta f_{PSR} + \Delta f_{PR2} + \Delta f_{PES2}$
Placement of deck and splice concrete	$\Delta f_{PES1} + k_{CR2}\Delta f_{PCR} + k_{SH2}\Delta f_{PSR} + \Delta f_{PR2} + \Delta f_{PES2}$
Stressing of 2nd post-tensioning tendons	$\Delta f_{PES1} + k_{CR3}\Delta f_{PCR} + k_{SH3}\Delta f_{PSR} + \Delta f_{PR2} + \Delta f_{PES2} + \Delta f_{PES3}$
Final conditions after losses	$\Delta f_{PES1} + \Delta f_{PCR} + \Delta f_{PSR} + \Delta f_{PR2} + \Delta f_{PES2} + \Delta f_{PES3}$
Post-tensioned Strands (Δf_{PT})	
Critical construction stage	**Components of prestress loss**
Stressing of 1st post-tensioning tendons	$\Delta f_{PF} + \Delta f_{PA} + \Delta f_{PES1}$
Stressing of 2nd post-tensioning tendons	$\Delta f_{PF} + \Delta f_{PA} + \Delta f_{PES1} + \Delta f_{PES2}$
Final conditions after losses	$\Delta f_{PF} + \Delta f_{PA} + \Delta f_{PES1} + \Delta f_{PES2} + \Delta f_{PCR} + \Delta f_{PSR} + \Delta f_{PR2}$

The pre-tensioned stress at the final stage after subtracting all prestress losses at each critical stage is defined as:

$$f_{pe,final} = f_{pi} - \Delta f_{PRE}, \tag{2-82}$$

where f_{pi} is the initial pre-tensioning stress and Δf_{PRE} is the total prestress loss on the pre-tensioning strands as defined in Table 2-6 and Table 2-7.

The post-tensioned stress at the final stage after subtracting all prestress losses at each critical stage is given by:

$$f_{pe,final} = f_{po} - \Delta f_{PT}, \tag{2-83}$$

where f_{po} is the initial post-tensioning stress and Δf_{PT} is the total prestress loss on the post-tensioning strands as defined in Table 2-6 and Table 2-7.

2.13 Life-Cycle Cost of Spliced Prestressed Concrete Bridges

Precast/prestressed concrete bridges have become the preferred type of bridge construction, primarily for reasons of economy, savings in life-cycle costs and their fast construction. Due to large and increasing costs associated with repairing concrete structures, the durability of a structure should be considered during the design stage in order to lengthen the structure service life. Normally, when structures are designed, minimizing the initial cost is the first priority and the durability of the structure is considered as part of the design specifications, which is not clearly specified. However, the overall economy of a structure is measured in terms of its life-cycle cost, which includes the initial cost of the structure plus its maintenance cost.

There are several methods to lengthen the service life of concrete structures, including using sealers, use of concrete admixtures, using coatings, and increasing concrete clear cover. However, only parametric studies on the increase of concrete clear cover on the slab and the precast/prestressed concrete girder are used herein since these

options must be defined during the design process, unlike other parameters that can be applied later when structure is complete.

Only limited research has been conducted concerning durability in combination with life-cycle cost of concrete structures. Especially, the economical consequences of the choice of parameters that can lengthen the service life of a structure in the design phase has been neglected.

In order to provide cost-effective structures, it is necessary to predict the expected service life of a structure in the design phase. When the expected service life is calculated, and the maintenance and repair costs are assumed, the life-cycle-cost per year can be determined.

2.13.1 Life-cycle cost criteria

The overall economy of a structure is measured in terms of life-cycle cost. This includes the initial cost of the structure (I) plus the total expected maintenance costs (M) and the removal cost (R). Precast/prestressed concrete bridges built in accordance with specification requirements should require very little, if any, maintenance. Fatigue problems are minimal because traffic loads induce only minor stresses. Prestressed concrete structures built in the late 1950s have withstood heavy traffic and severe weathering for nearly 50 years and yet have required practically no major maintenance.

The life-cycle cost per year can be determined by dividing the total life-cycle cost by the design life-span years. The life-cycle cost per year can be used to compare design alternatives with different concrete covers. The cost for one-time maintenance and the number of expected maintenance interventions before replacing the existing

bridge should also be part of the life-cycle cost analysis. Typically, maintenance cost is 0.5 to 1.2 times the structure's initial cost.

Initial cost can be developed based on the design strength requirements, while life-cycle cost incorporates all costs that could occur during the life time of the structure. The initial cost of a new bridge is normally higher than that of an existing bridge, but its maintenance cost should be much less. In addition, the life-cycle cost of new bridge structures should be much smaller than that of old bridges.

2.13.2 Effect of chloride ingress on concrete structures

Chloride ingress is a common cause of deterioration in concrete bridges. The presence of chloride ions initiates corrosion of the reinforcement (or rebar), which reduces the service life of the structure as well as causing a reduction in its structural capacity. The shortage of concrete cover is the primary cause of concrete deterioration since the chloride ions can reach the steel faster (Yoshiki et. al 2001)

Chlorides are well known for their ability to penetrate and destroy passive films on reinforcement. Micro pores and gel water, which are generally formed in concrete, serve as a route for the movement of chloride ions. The pore structure in concrete depends on the type of concrete, mix proportion and its quality. Corrosion in concrete depends on the supply of oxygen and water as well as chloride content. Chloride permeability depends on quality of concrete, concrete types, water cement ratio, construction conditions, etc. Concrete may be exposed to chloride by the presence seawater or deicing salts. Chlorides, either alone or combined with carbonation, are the primary cause of concrete corrosion.

When chloride ions penetrate into the concrete and reach the surface of the steel reinforcement, the chloride ions break the inert film in the reinforcement surface and starts corroding it. As corrosion continues, corrosion products build-up around the reinforcing steel. These corrosion products occupy from 2 to 14 times the volume of the original steel, creating an expansive force that is sufficient to cause the concrete to crack. On the surface around the crack of the concrete, a large quantity of chloride ions has already penetrated into the concrete around the reinforce bar. Therefore, repair done by coating and/or replacing the concrete cover is neither effective nor long lasting (Stephen et. al 1998).

2.13.3 Reinforcement corrosion initiation period

The corrosion initiation period refers to the time during which steel is destroyed and the reinforcement starts actively corroding. The time to initiation is a function of the quality and the amount of concrete cover, the environment, the effective chloride diffusivity properties of the concrete, the concentration of chlorides on the surface, and the chloride threshold for the reinforcement.

Normally, structures can be classified as submerged components, splash-zone components, and superstructure components (Stephen et al. 1998). For submerged components there is a constant supply of water and chloride ions on the surface of the concrete. However, corrosion of the steel is limited by the lack of dissolved oxygen in the water. In splash-zone components there is a constant supply of chloride and ample supply of oxygen. Thus splash-zone components have a higher corrosion rate than submerged components. For superstructure components, chlorides come from deicing

salts. The corrosion rate for superstructure components depends on the surrounding environment and will change over time.

If the environment boundary is kept at a constant chloride concentration, *Co*, the initial concentration being zero throughout the medium, then the chloride concentration solution at a distance x and time t can be determined by (Berke and Hicks 1994):

$$C(x,t) = Co(1 - erf\frac{x}{2\sqrt{D_c t}}), \tag{2-84}$$

where *erf* is the error function; x is equal to the depth of concrete over the steel reinforcement; C_o is the surface chloride concentration; D_c is the concrete diffusion coefficient; and t is the time in days. Equation 2-84 is most suited for evaluating submerged and splash zone components.

The diffusion coefficient of chloride ions in concrete, *Dc*, is known to depend on the concrete's pore structure, which is related to the water/cement ratio, cement type, mix proportion and overall concrete quality. The water/cement ratio is a major factor influencing the diffusion coefficient. The smaller the water/cement ratio is, the smaller the diffusion coefficient (Ababneh et al. 2003).

If the environment changes with time, the surface chloride concentration also changes and a new relation that allows surface build-up of chloride ions should be used. When a linear build-up of chloride ions over time is assumed, the chloride concentration solution at a distance x and time t can be obtained as follows (Stephen et al. 1998):

$$C(x,t) = kt\{(1 + \frac{x^2}{2Dt})erfc(\frac{x}{2\sqrt{Dt}}) - (\frac{x}{\sqrt{\pi Dt}})e^{\frac{-x2}{4Dt}}\}. \tag{2-85}$$

When a square root build-up of chloride ions over time is assumed, the chloride concentration solution at a distance x and time t can be obtained as (Stephen et. al 1998):

$$C(x,t) = k\sqrt{t}\{e^{\frac{-x^2}{4Dt}} - [\frac{x\sqrt{\pi}}{2\sqrt{Dt}} erfc(\frac{x}{2\sqrt{Dt}} erfc(\frac{x}{2\sqrt{Dt}})]\}. \quad (2\text{-}86)$$

2.13.4 Effect of concrete cover on service life of concrete components

Concrete cover is required to protect reinforcing bars from corrosion, to maintain adequate bond between the concrete and the reinforcing bars, and for ease of casting. In severe chloride environments the cover depth used for concrete structures should be selected for corrosion protection. The required minimum cover depth for prestressed concrete beams is normally less than that required for conventional reinforced concrete beams. According to the ACI 318-02 recommendations (ACI 1992), the minimum cover depth for precast/prestressed concrete beams should be at least equal to 38.1 mm (1.5 in).

In order to keep rebar and tendons away from chlorides an increase in concrete cover depth is essential. Thus, a deeper concrete cover may be necessary when a long service life period, such as more than 100 years, is set as a goal.

Some prestressed concrete bridges in coastal areas have been replaced due to heavy corrosion after only a few decades of use, and in some cases the cost of maintenance was more than the initial construction cost. When large cracks due to corrosion are observed, it means that steel corrosion is already so severe that even careful repair is no longer sufficient. The design lifetime of a structure based on concrete cover depth can be evaluated based on Fick's 2nd law equation as specified in Equation

(2-84) for a constant chloride environment or Equation (2-86) for a build-up chloride environment (Stephen et. al 1998).

2.14 Summary

In this chapter, the fundamental assumptions, criteria and procedures for the design and analysis of spliced precast/prestressed girder bridges were briefly complied, providing ample information that was used in this study. The major design criteria and additional considerations in structural analyses were presented to show the differences between conventional precast/prestressed concrete bridges and spliced girder bridges. The load patterns from different construction sequence methods and the corresponding prestress losses presented in this chapter were later used in the optimization and sensitivity studies presented in Chapter 4 and Chapter 5. Equivalent post-tensioning loads in non-prismatic sections were derived and setup in similar form to equivalent uniform load patterns in prismatic sections with additional point loads at the splice locations due to the non-prismatic section effects. In addition, the general concept and methods to preliminarily asses durability and life-cycle cost of concrete structures were reviewed are later integrated in the optimization studies presented in Chapter 4.

3 Design Optimization of Spliced Precast/Prestressed Girder Bridges

3.1 Introduction

This chapter presents the approach used for the structural optimization and sensitivity studies on Spliced Precast/Prestressed Girder Bridges. The formulation and approaches for single and multicriteria structural optimization are presented. The single-objective of cost minimization was chosen as the basic problem for the optimization studies. Multicriteria methods address situations where in addition to minimum cost, other criteria such as minimum post-tensioning, minimum concrete volume, and minimum weight should also be satisfied. The constraint approach was used to generate efficient solutions and compromise programming is used for selecting the best solution. Different levels of optimization, namely, system (or configuration) and component optimization were applied to SGB to determine prestress requirements and develop new optimal pier/negative sections. The implementation of the optimization process in a custom program in the Matlab environment is presented.

3.2 Structural Optimization

The conventional design process starts with some initial values for the design variables thus defining an initial design, which is then analyzed and checked against an accepted in the form of performance limits. If the allowable values are exceeded, then the design variables are adjusted and the process is repeated until the final design

satisfies the allowable limits. Other design criterions are then checked one by one until an acceptable design is obtained. This process usually yields conservative design results, but it is an expensive process. In addition, when the parameters in the problem change, the conventional process must be restarted and all calculations must be repeated. Clearly, this process is improved, in both outcome and time investment, as experience is obtained with the system being designed minimized the number of iterations since the values for the design variables that lead to favorable solution can be arrived at quicker, sometimes very early in the design process.

A computational optimal design process differs from the conventional one described above by taking into account all the design variables and criteria simultaneously and improving the design through automated iterations. The advantages of using optimization are that once the problem has been formulated and defined, it is easy to solve it for a variety of different conditions and requirements. Furthermore, changes to the design variables are directed towards the attainment of a specific performance measure through the help of mathematical algorithms.

Structural design optimization has been widely used for the design of steel, reinforced concrete, and prestressed concrete bridges. The objective of an optimal bridge design problem is to determine the structural system design variables that satisfy the behavior and constraints of the problem. Constraints can be assembled directly from bridge design code specifications, while the design problem behavior can be the cost of the bridge structure or other merit functions.

The standard mathematical form of an optimization problem is normally written as:

Objective function: Min $f(\boldsymbol{x})$

Subject to: $g_i(\boldsymbol{x}) \leq 0 \qquad i = 1 \text{ to } m$

$h_j(\boldsymbol{x}) = 0 \qquad j = 1 \text{ to } p$

$\boldsymbol{X}^L \leq \boldsymbol{x} \leq \boldsymbol{X}^U$

where $\boldsymbol{x}$ is the design variables vector, $\boldsymbol{X}^L$ and $\boldsymbol{X}^U$, are the lower and upper bound vectors for the design variables, $f(\boldsymbol{x})$ is the objective function, and $g_i(\boldsymbol{x})$ and $h_i(\boldsymbol{x})$ are the inequality and equality constraints, respectively.

Optimization problems can be classified as *unconstrained problems* and *constrained problems*. An unconstrained problem has no constraints restricting the problem while the constrained problems contained constraints that restrict the design. In a constrained problem, the problem needs to be transformed into unconstrained subproblems that can be solved as the basis of an iterative automated process.

Optimization problems can be classified as linear programming problems and nonlinear programming problems. When both the objective function and the constraints are linear functions of the design variables, the problem is known as a *linear programming problem* (LP). When either the objective function or the constraints are nonlinear function of the design variables, the problem is known as a *nonlinear programming problem* (NLP). *Quadratic programming* (QP) concerns the minimization or maximization of a quadratic objective function that is linearly constrained. The solutions from LP and QP problems are readily and reliably obtained while the solution

of NP problems require iterative procedures to establish a direction of the search at each major iteration.

The formulation of an optimum design problem involves translating a descriptive statement of the problem into a well defined mathematical statement. The formulation of a structural optimization problem can be defined by the following steps (Arora 2004):

Step 1: Identification of the problem statement.

Step 2: Collection of data and information.

Step 3: Identification and definition of the design variables.

Step 4: Identification and definition of an objective function.

Step 5: Identification and definition of the design constraints.

3.2.1 Problem statement

The descriptive objective of the project needs to be identified by the designer or project owner. The problem statement describes the overall objectives of the project and the requirement criteria.

3.2.2 Data and information

The information of material cost, performance requirements, material properties, and other relevant information needs to be gathered before developing a mathematical formulation of the problem. Analysis design tools and their procedures must be identified at this stage.

3.2.3 Design variables

Design variables are those that describe the system design in mathematical terms. They are the variables in the problem that are allowed to vary or change in the design process. Design variables indicate all of the unknowns in the optimization problem. Optimization is the process of choosing values for the design variables that yield an optimum design. In order to maximize the efficiency of the computational algorithm, only key parameters that are important to the system design are chosen as design variables. The system design is defined once these variables are specified. Normally, design variables are independent of each other.

Design variables can be classified as discrete (or integer), continuous, or a mixed of both. *Discrete variable*s must have a value from a specified discrete set (integer values or just zero or one), while *continuous variables* can have any value from a continuum. *Mixed integer variables* problem can have both discrete and continuous design variables. In reality, design variables cannot be arbitrary due to manufacturing and fabrication limitations. In most structural design problems the discrete nature of the design variables tends to be disregarded due the expensive nature of the calculations needed to deal with them. Rather, the optimum solution is typically obtained for continuous variables and are then adjusted to the nearest available discrete value. This assumption has proven to be acceptable since continuous-variable optimal solutions always give conservative results while the discrete solutions normally lay in the boundary of continuous solutions.

3.2.4 Objective functions

There can be many feasible designs for a system, and clearly some are better than others. In order to compare different designs, an objective function is used as a criterion to measure the "goodness" or "efficiency" of the system. The *objective function* is a scalar value used as a merit criteria to obtain an optimal solution. A valid objective function must be influenced directly or indirectly by the design variables of the design problem; otherwise, it is not a meaningful objective function. The optimized design is the one that yields the best value for the objective function. The objective function can be maximized or minimized depending on the problem requirements. Possible objective functions for the design of spliced girder bridges are the minimum superstructure cost, the minimum amount of prestressing steel, the maximum girder spacing, the minimum concrete volume, the maximum feasible span length, and the minimum superstructure depth.

3.2.5 Constraints

Constraints are represented by function relations among the design variables. Constraints are typically classified as either equality, $h(x)$, or inequality, $g(x)$, constraints. Like the objective function, constraints can be linear or nonlinear. Typically, equality constraints are in the form of functions equal to zero while inequality constraints are functions that can have values less/more than or equal to zero.

Inequality constraints: $g_i(x) \leq 0$ (3-1)

Equality constraints: $h_j(x) = 0$ (3-2)

Two types of constraints were considered for the presented optimal bridge design studies. The first constraint is a function of serviceability and ultimate state design limits. The second type constraints are described in terms of practical design limitations such as the available girder depth, practical girder spacing, and maximum number of pre-tensioning strands per row in the prestressed concrete girder.

3.3 Optimization approach

Classical structural optimization combines techniques from different disciplines including computer aided design, structural finite element analyses, structural sensitivity analyses, and mathematical algorithms. The detail of each technique is described as follows:

3.3.1 Computer aided design

Computer aided design refers to the computerized tools used in the design optimization process for pre- and post-processing purposes. In this study, each bridge girder was modeled as a beam line and divided into finite elements. The element length of the beam was discretized into small elements to cover all critical locations, i.e., the midspan of middle segment, the splice location, and the midspan of the end segments. Then later, the internal forces, displacements, and stresses were obtained at these locations. The modeling and output retrieval was achieved through a custom frame analysis program written in the Matlab environment.

3.3.2 Finite element analyses

The finite element method is the most widely used form of computer-based engineering analysis. It is a numerical procedure for analyzing structures that are too complex to be solved efficiently of satisfactorily by analytical methods. Finite element methods are used to perform analysis in order to obtain the responses (i.e., internal forces and deflections) caused by applied loads. Finite element analyses are normally used in structural optimization to evaluate the structural responses required by the objective and constraint functions, and also by the variable sensitivity analyses.

3.3.3 Sensitivities analyses

Sensitivity analyses provide gradient information on the objective and constraint functions with respect to the design variables for formulating the optimization problem. Sensitivity analyses allow finding the effect on the objective function if the design variable values are changed.

Two types of techniques, numerical and analytical, can be used to calculate structural sensitivity derivatives for structures [Adelman and Haftka, 1986]. Numerical techniques use finite different methods, which are straightforward to determine since derivatives are calculated by finite difference approximations. The accuracy of the derivatives obtained from this technique depends on the perturbation step size for the finite difference method. Analytical techniques include the direct differentiation method and adjoint variable methods. Analytical techniques are suitable for applications that require high computational efforts.

3.3.4 Mathematical algorithm

The selection of changes to the design variables such that they lead to an improvement in the objective design function is controlled by some form of a mathematical algorithm. Mathematical algorithms for solving constrained optimization problem, are broadly classified as direct methods and transformation methods (Arora and Belegundu, 1984 and 1985). Transformation methods include the barrier (interior) and penalty (exterior) function methods as well as the augmented Lagrangian or multiplier methods. Transformation methods were developed to solve constrained optimization problems by transforming them into a sequence of unconstrained problems whose collective solution converges to the solution of the original problem. The concept of transformation methods is to construct a transformed function by adding a *penalty* term for the constraints violations to the objective function. Transformation methods are not widely used due to their limitation inherited from the transformation functions, which have to be assumed. Direct methods were developed to solve the original constrained optimization problem directly. The direction vector $d^{(k)}$ is calculated using the function values and their gradients at point $X^{(k)}$. The step size calculation needs only the function values. Different methods can be generated depending on how the direction d and step size are calculated. Many algorithms such as the gradient projection method, the method of feasible directions, the generalized reduced gradient method, and the constrained steepest descent method have been developed and successfully used for engineering design problems. Compared to other methods, the constrained steepest descent (CSD) method is one of the most commonly used since it is robust and effective for solving nonlinear constrained optimization problems (Arora 1989).

3.4 Optimization Algorithm Types

In this section, three classical different optimization algorithm types, which include gradient based algorithm, the direct search algorithm, and the branch and bound combinatorial search algorithm, are briefly explained. Later, optimal results obtained from these methods are compared and the advantages and disadvantages of using these methods, i.e. computation time, types of design variables, and types of constraints, are discussed to provide the basis for the algorithm selection in this study.

Gradient based algorithms rely on the gradients derived from the objective and constraint functions and can handle only continuous design variables. The *direct* search algorithm is a global optimization algorithm that does not require derivative information of the objective function or constraints. The *branch and bound* algorithm is a combinatorial search approach that can handle both continuous and integer variables also without the need of gradient information of the objective or constraint functions. Details for each algorithm used in this study are presented in the following section:

3.4.1 Gradient based algorithms

Gradient based algorithms are commonly used for nonlinear, constrained, continuous optimization problem. The algorithm is a sequential quadratic programming approach. In the optimization of spliced girder bridges the objective functions and constraints are nonlinear functions of the design variables. Therefore, the CSD method using a gradient based algorithm was used. The four steps in the CSD method are as follows:

a) Linearize the objective and constraint functions about the current design estimate,

b) Define the subproblem formulation by the linearized objective and constraint functions to determine a *search direction*,

c) Solve the subproblem to obtain a search direction, and

d) Calculate a *step size* to minimize the *descent function* in the search direction.

Constrained steepest gradient-based algorithms rely on the gradients derived by linearizing the objective and constraint functions with respect to the design variables. Derivatives of the objective and constraints functions are used to construct an approximate problem by redefining them through Taylor series expansions. The derivatives of the obtained linear Taylor series can be numerically evaluated by finite difference approaches. For example, the forward difference technique is commonly used to evaluate the numerical differentiation of a multi-variable function *f(x)* with respect to variable x_i, which is defined as:

$$\frac{\partial f}{\partial x_i} = \frac{f(x_1, x_i + \Delta x_i, ..., x_n) - f(x_1, ..., x_i, ...x_n)}{\Delta x_i}, \tag{3-3}$$

where Δx_i is a small perturbation in the variable x_i. The accuracy of function gradients depend on the selection of the perturbation Δx_i.

The search direction is determined by a subproblem based on the linearized objective and constraint functions of the current design. The descent function plays an important role in constrained steepest descent (CSD) methods since it is used to monitor the progress of the algorithm towards an optimum point and is used by the optimization algorithm to determine an appropriate step size. The basic concept is to compute a step

size along the search direction such that the descent function is reduced. Figure 3-1 illustrates the steps of constrained steepest descent function for a gradient-based optimization algorithm.

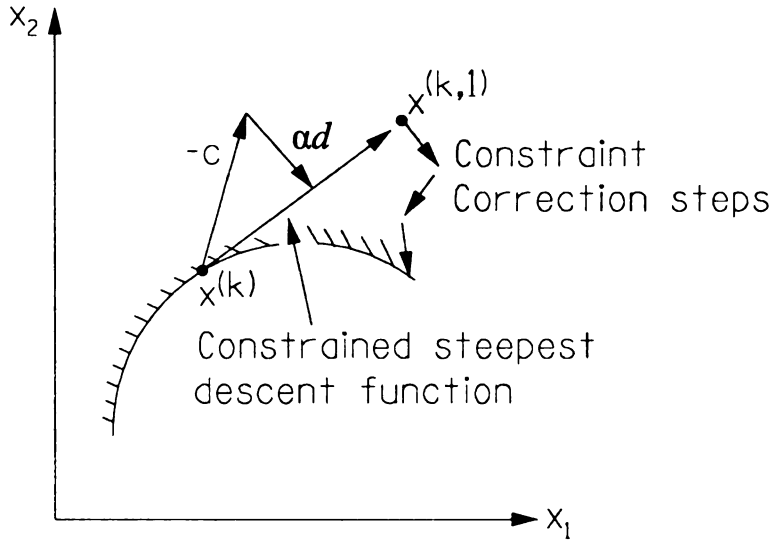

Figure 3-1 *Steps of constrained steepest descent gradient method*

Pshenichny's descent function (Arora, 1989, 1997) was used as the descent function for the CSD method. The steepest descent function used the function gradient vector (Equation 3-4) at each point to determine the search direction for each iteration. Figure 3-2 schematically illustrates the steepest descent function directions. At any point x where the gradient vector is nonzero, a negative gradient, $-\nabla f(x)$, will point "downhill" towards lower values of the objective function *f(x)*. Generally, the negative gradient is locally a direction of steepest descent as the objective function decreases more rapidly along this direction than along any other path.

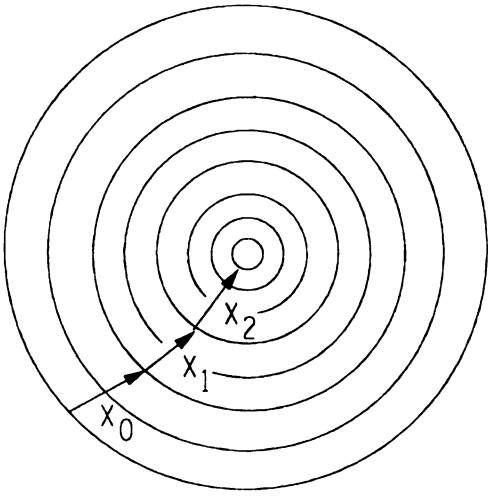

Figure 3-2 *Steepest descent function direction*

The steepest descent method starts from an initial guess x_o and successive approximate solutions are given by:

$$X^{(k+1)} = X^{(k)} + \alpha_k \nabla f(X^{(k)}) = X^{(k)} + \alpha_k d^{(k)} \quad , \qquad (3\text{-}4)$$

where the superscript k represents the iteration number (k = 0, 1, 2,...); $X^{(k)}$ is the design variables vector in the k^{th} iteration; $d^{(k)}$ is the search direction calculated using function values and their gradients; $X^{(k+1)}$ is the design estimate in the (k+1th) iteration. The step size line search parameter (α_k) determines how far to go in the chosen direction and is given as follows:

$$\alpha_k = \frac{g_k^T g_k}{g_k^T H_k g_k} \qquad (3\text{-}5)$$

where g_k is the gradient and H_k is the Hessian matrix of the objective function (Arora 1989)

The *gradient vector* of objective function is used to compute the search direction as shown in equation (3-6). It is composed by the partial derivatives of the objective function with respect to each of the independent variables as follows:

$$\nabla f(x) \equiv g_k(x) \equiv \begin{bmatrix} \frac{\partial f}{\partial x_1} \\ \frac{\partial f}{\partial x_2} \\ \vdots \\ \frac{\partial f}{\partial x_n} \end{bmatrix}. \tag{3-6}$$

The *Hessian matrix (H)* represents the second-order derivatives of the objective function with respect to the design variables. The Hessian matrix is also used to calculate the search direction as shown in equation (3-7) and also used to determine the optimal condition of the optimal point as shown later in equation (3-10). The Hessian matrix of f is a square and symmetric matrix of the second derivatives of objective function $f(x)$ and is given as follows:

$$H_k \equiv \begin{bmatrix} \frac{\partial^2 f}{\partial x_1^2} & \cdots & \frac{\partial^2 f}{\partial x_i \partial x_n} \\ \vdots & \cdots & \vdots \\ \frac{\partial^2 f}{\partial x_n \partial x_1} & \cdots & \frac{\partial^2 f}{\partial x_n^2} \end{bmatrix}. \tag{3-7}$$

The concept behind this approach is to compute a step size along the search direction $d^{(k)}$ such that the descent function is reduced at each iteration of the algorithm. The step size direction is a line, or one-dimensional, search. For constrained problems it is preferred to determine the step size by using an inexact line search since it is more efficient. However, this method involves a sequence of major iterations. Each iteration

requires the solution of linearly constrained subproblem where the nonlinearities are confined to the objective function. A design point is chosen to initiate the iterative process. The iteration process is continued until a final design point is reached; that is, when there are no further changes in the value of the objective function.

The descent function used to solve constrained optimization problems requires a searching direction towards the optimum design. A searching direction is established by solving a subproblem. Quadratic programming (QP) is chosen to determine the searching direction due to its high efficiency and quadratic convergence rate. The *sequential quadratic programming* subproblem utilizes a Hessian matrix constructed by a quadratic objective function and linear constrains, which are defined as (Arora 1989):

$$f = \frac{1}{2} d^T H_k d + g_k^T d; \tag{3-8}$$

where g_k is the gradient; d is search direction; and H_k is the Hessian of the objective function.

In large-scale optimization problems it is difficult to calculate the Hessian matrix. *Quasi-Newton Methods* have been developed to approximate the Hessian matrix. The hessian matrix is updated by using design changes and the gradient vector of the previous iteration. The modified BFGS (Broyden-Fletcher-Goldfarb-Shanno) (Powell 1978) method was thus implemented to approximate the Hessian matrix.

Perturbation vectors are used to determine a local optimum point as shown in equation (3-9) and (3-10) and are defined as: $\partial x \equiv x - x_O$ and $\partial f \equiv f(x) - f(x_O)$. As x is to be considered as a local minimum, it must satisfy two optimality conditions termed: the *first–order necessary condition* and the *second-order sufficiency*. The first-order

necessary condition is attained when $f(x)$ has a minimum value f_* at x_* such that any perturbations in x must result in higher value of f by definition of x_* to first order. Equation (3-9) represents the first-order necessary condition.

$$\partial f_* = \nabla f(x_*)\partial x_* \geq 0. \tag{3-9}$$

If $f(x), x \in X \subset \Re^n$, has a local minimum at an interior point x_* of the set X and if $f(x)$ is continuously differentiable at x_*, then $\nabla f(x_*) = 0^T$. This result is a necessary condition because it may also be true at points that are not local minima i.e., the gradient will be zero at a local maximum and at a saddlepoint. All points at which the gradient is zero are called *stationary points* and the necessary condition is called the *stationarity condition.* The second-order sufficiency information as shown in Equation (3-10) helps make a more firm conclusion of attaining a minimum/maximum condition since the first-order local derivative gives only useful information but it is not conclusive.

$$\partial f_+ = \frac{1}{2}\partial x^T H(x_+)\partial x. \geq 0 \tag{3-10}$$

The sign of ∂f_+ depends on the sign of the differential quadratic form $\partial x^T H(x_+)\partial x$. If this quadratic form (Equation 3-10) is strictly positive for all $\partial x \neq 0$, then x_+ is definitely a local minimum. If the Hessian matrix of $f(x)$ is positive-definite at a stationary point x_+, then x_+ is a local minimum.

An algorithm is considered to be convergent when it reaches a local minimum point. An algorithm is considered as globally convergent when it converges from any arbitrary starting initial design. To ensure that the optimized solution does not correspond to a local minimum the optimization procedure should be performed more than one time by changing the starting design point. If results still yield the same answer

irrespective of the starting design point, then the result can be considered as non-local optimum.

The gradient based algorithm normally takes less computation time than other algorithms since it uses the steepest descent function, which decreases more rapidly along steepest direction and will point "downhill" towards lower values of the objective function, for a search direction for each iteration. The disadvantage of using this algorithm is that it is limited to problems with continuous design variables and thus cannot handle integer or mixed integer variable problems. In addition, it requires derivatives of the objective and constraints functions to construct the optimization problem.

3.4.2 Direct search algorithms

Direct search algorithm methods do not require derivatives of the objective or constraints functions. These methods also do not depend on the starting point because the first point is arbitrary selected, typically at the center of the design space. The method starts by sampling the center of design space, and then the algorithm begins to subdivide the design space into smaller rectangles. The algorithm iteratively continues this process, selecting and subdividing those rectangles that have the highest likelihood of producing an objective function value lower than the current lowest point. The direct search algorithm is pure evaluation and thus its design variables can be discrete or continuous variables.

An algorithm based on the above concept is the DIRECT search algorithm by Jones (1994). It combines global and local searching. For example, small rectangles with better sampled points at their centers are likely to be further subdivided (local search)

and larger rectangles have a greater likelihood of being further subdivided (global search).

Direct search algorithms stop when the number of iterations performed by the algorithm reaches the value of maximum iterations, when the total number of objective function evaluations performed by the algorithm reaches the value of maximum function evaluations, or when the change in the objective function from one point to next point is less than a given tolerance.

The greatest advantage of direct search algorithms is the combination of global and local searching. A distinct advantage over other optimization algorithms is that it does not require finite difference step size and convergence tolerances. In addition, no staring point is specifically required since the first point is always at the center of the design space.

Direct search algorithms also have few disadvantages, e.g., they cannot work with equality constraints, they cannot terminate before the maximum number of function evaluations and/or iteration have been exceeded, and they need bounds on the design space in order to know how to divide the rectangles. The optimal result of this algorithm is improved by a semi-directed random search; consequently, it is computationally more compared to the gradient based algorithms.

3.4.3 Branch and bound combinatorial search algorithms

Branch and bound algorithms are based on exhaustive searches. The operation of combinatorial search algorithms can be visualized with search trees. The search tree has member group levels corresponding to the numbers of design variables. Each member

group can be expanded into nodes. In the search tree for an exhaustive search a number of branches emanates from each node number.

The branch and bound search begins by fixing the value of each member group at a time and treating other groups as continuous variables to find their optimal values. The lower bound of each group is obtained and the lowest bound for all groups is determined. The last selection of the lowest bound for all groups represents a discrete design since it has a lower value than the previous candidate in the groups.

The branch and bound method eliminates many of the design variables through this exhaustive search. A nonlinear programming algorithm is executed to perform the continuous optimization to establish the lower bounds prior to determining discrete solutions.

The branch and bound method has been used successfully to deal with discrete and continuous design variable problems. However, for problems with a large number of design variables, the number of subproblems (nodes) becomes large. Therefore, the branch and bound method is not suitable for problems with many design variables since they could lead to very expensive computation. In addition, branch and bound methods guarantee to find the global optimum only if the problem is linear or convex.

3.4.4 Comparison of optimal results

A single-span spliced girder bridge built through single-stage post-tensioning with a total span length of 42.67 m (140 feet) was used as a case study to compare the optimal results from different optimization algorithm types. Three different algorithm methods, which included a gradient based algorithm (Matlab - *fmincon* function) (Mathwork 2004), a direct search method (DIRECT) (Jones 1994), and a branch and

bound algorithm (OPTIMUS software) (STI Technologies, Inc. 2005), were used to compare their optimal results.

Table 3-1 shows the comparison of optimum design variable values for each of the optimization algorithm types. Preliminary results for the design variables obtained from the sequential quadratic programming algorithm (MATLAB-*fmincon* function) are continuous numbers, therefore some design variables need to be rounded off. However, the design variables obtained from the DIRECT and OPTIMUS algorithms are a mixed set of continuous and integer numbers. It can be seen that the objective value from *fmincon* gave a lower objective function value than the DIRECT and the OPTIMUS algorithms since all design variables are continuous. DIRECT is considered both a global and local optimization algorithm and thus it led to a lower objective value than the branch and bound method which depends only on an exhaustive search and does not guarantee the attainment of a global optimum.

In order to improve the results from DIRECT and OPTIMUS closer to the *fmincon* solution, the number of iterations or maximum number of evaluations used in the algorithms should be increased. This could significantly increase the computation time compared to the *fmincon* method (days VS hours).

Table 3-1 *Comparison of optimization versus algorithm performance*

Design variables	*fmincon* Sequential Quadratic prog.	*fmincon* Sequential Quadratic prog.	DIRECT Global optimization	OPTIMUS mixed integer continous nonlinear programming
S	**11.198**	**11.198**	**11.182**	**11.119**
npr_{11}	7.95	8	12	11
npr_{21}	7.95	8	3	2
npr_{31}	2	2	2	1
npr_{41}	2	2	2	2
$npr_{11}+npr_{21}+npr_{31}+npr_{41}$	**19.9**	**20**	**19**	**16**
npr_{12}	20.1	20	13	10
npr_{22}	4.1	4	8	8
npr_{32}	0	0	1	0
npr_{42}	0	0	0	0
$npr_{12}+npr_{22}+npr_{32}+npr_{42}$	**24.1**	**24**	**22**	**18**
n_{po}	**59.17**	**59**	**63**	**66**
y_a	38.47	38.47	38.69	39.83
y_b	10	10	10.09	10
n_{prtl}	4	4	4	3
n_{dl}	2	2	2	2
pra	**0.25**	**0.25**	**0.25**	**0.25**
f(x)	2.748e6	2.748e6	2.8589e6	2.86353e6
Constraint Satisfied	OK	exceed 10 psi	OK	OK

When comparing results from the different algorithms, maximum beam spacing, splice location, and the number of strands can be seen to be within the same range. Since the objective of the present research was to understand the response and behavior of SGB and to develop design charts for preliminary design, the use of nonlinear continuous programming (*fmincon* in the MATLAB) can be considered adequate and was thus used in this study. In addition, if designers were to use design charts developed through optimization they would have to interpolate and interpret their solution from the presented curves. Therefore, there is no guarantee that they will choose the exact

solutions obtained from the optimization solution. Nonlinear continuous programming (*fmincon* function in MATLAB) was thus selected for this study to minimize computation effort.

3.5 Multicriteria Optimization

Normally there can be several design solutions that satisfy all requirements of safety and serviceability and a number of specified merit criteria imposed by a design code. Thus, the designer needs to make a difficult decision in selecting the best design among the possible alternative solutions that adequately satisfy all the governing criteria. The combination of single objective functions is considered as a form of multicriteria optimization. Multicriteria optimization considers two, or more objective functions simultaneously, and these functions may have conflicts. Multicriteria optimization achieves a compromise between conflicting objectives and represents more rational solutions than those obtained by optimizing individual objective functions (Arora 2004). The resulting solution is expected to be feasible, efficient, and non-dominant with regards to all criteria and should ensure the best compromise between all competing objective functions.

3.5.1 Mathematical formulation

The multicriteria optimization problem can be formulated as follows:

Objective function: $\text{Min } F_i(\boldsymbol{x}) = (f_1(x), f_2(x), \ldots, f_j(x))$

Such that: $f_j(\boldsymbol{x}) \leq \varepsilon_j \qquad j = 1, 2, \ldots, m$

Subject to: $g_k(\boldsymbol{x}) \leq 0 \qquad k = 1 \text{ to } n$

$$h_l(\mathbf{x}) = 0 \qquad l = 1 \text{ to } p;$$

where m is the number of objective functions, n is the number of inequality constraints, p is the number of equality constraints, $F_i(\mathbf{x})$ is the multicriteria objective functions and has m-dimensional vector of objective functions, $f_j(\mathbf{x})$ is the single objective functions, and $g_k(\mathbf{x})$ and $h_l(\mathbf{x})$ are the equality and inequality constraints, respectively.

When several objective functions are considered at the same time, many optimal solutions can be obtained. For example, Figure 3-3 represents optimal design variables (x_i) for two objective function f_1 and f_2. The feasible design space (S) is defined as a collection of all the feasible design points as shown in Equation 3-11. The inequality constraint g_1 and g_2 are the constraints that restricted the design for both objective functions.

$$S = \{x \mid h_i(x) \le 0;\ i = 1 \text{to } p;\ \text{and}\ \ g_i(x) \le 0;\ i = 1 \text{to } n\}; \tag{3-11}$$

where $h_i(x)$ is equality constraints and $g_i(x)$ is the inequality constraints; and x_i is design variables

In Figure 3-3, the minimization of objective function f_1 cannot yield the minimization of objective function f_2 and vice versa, thus the designer has to choose which objective function should be used as the main criterion in a multi-criteria optimization consideration.

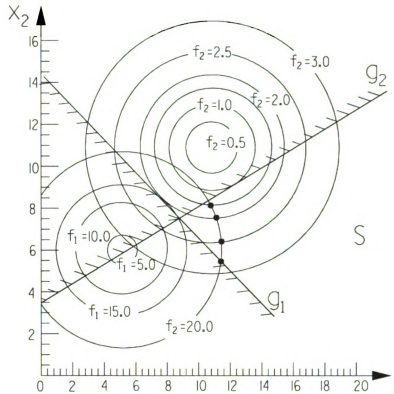

Figure 3-3 *Graphical representation of a two-objective optimization problem*

3.5.2 ε-constraint approach

Multicriteria problems are commonly solved by either the weighted objective approach or *ε-constraint method,* also known as the *trade-off approach*. The *ε-constraint method* has gained wide acceptance as compared to the weighted objective approach because of its practicality and rationality (Lounis and Chon 1993).

The *weighted objective approach* can be formulated as follows:

$$\min\ f(x) = w_1 c_1(x) + w_2 c_2(x) \tag{3-12}$$

where w_i is the weight and $c_i(x)$ is the single objective functions. The weights in the weighted objective approach are rarely known precisely, so prefered values are adjusted gradually until they become more evident. This approach is subjective and can mislead the optimum results. Thus, the designer should trace the effect of these

subjective preferences on the optimal solution obtained after solving the problem (Papalambros and Wilde 2000). The weighted objective approach was not used in this study since the weight factors for each of the single-objective functions are subjective, unlike the *ε-constraint* approach which treats all single-objective functions equally.

The *ε-constraint method* consists of transforming the multi-objective optimization problem into a single scalar-primary objective optimization problem. All secondary objectives are transformed into constraints bound by some allowable level ε_i and are added into the transformed single-objective optimization problem. The most important objective function is chosen as a primary objective and the other objectives are then considered as secondary objectives. After the multi-objective optimization problem is transformed into an equivalent single-objective optimization by the *ε-constraint* approach, each single objective can be solved by the single-objective optimization approach stated in section 3.4.1.

Generally, there is no single optimal solution that simultaneously yields a minimum value for all single-objective functions in a multi-objective problem. The concept of Pareto optimum, which deals with non-dominated and non-inferior solutions, (Carmichael 1980) is widely used as a solution approach to multi-objective optimization problems.

A subset of the Pareto optima is generated by the ε-constraint approach, which is based on the adoption of one criterion as a scalar objective function and the transformation of other criteria into constraints bound by some predetermined constants ε_i. Predetermined constant bounds are determined from the minimum values of each objective function. The values of ε_i are then selected between the minimum and

maximum ranges of the predetermined constraint ε_i. Each objective function thus yields a set of an optimal design variables x_j* in which $f_i(x_j$*) is a minimum. Defining $f_i(x_j$*) as the lower bound and $f_i(x_i$*) as the upper bound on ε_i , or:

$$f_i(x_j^*) \leq \varepsilon_i \leq f_i(x_i^*). \qquad (3\text{-}13)$$

The values of ε_i are then varied to generate the entire pareto optimal set. A vector x* is considered a Pareto optimum if there is no feasible solution x that may yield a decrease of some objective function without causing a simultaneous increase of at least another objective function.

3.5.3 Compromised programming

Once a subset of Pareto optima has been generated the designer has to make a decision to select the best solution from the subset. The technique of compromised programming (Lounis and Cohn 1995) defines the best solution as the minimum distance from the set of non-dominant solutions to the ideal solution. A solution to this multicriteria optimization problem is achieved by the *"Minimax and Minimum Euclidian Distances Method"* (Duckstein 1984). Euclidian distances are used as a criterion for comparison in compromised programming and can lead to practical approaches for decision making in the presence of multiple and conflicting criteria. This approach has gained acceptance because it is both practical and rational (Lounis and Cohn 1993 and 1995).

The "minimax" criterion is implemented by minimizing the normalized deviation from the ideal solution f_{min} measured by the family of distance metrics L_p. The value of

L_p, indicates how close the solution is to the ideal solution. The satisfying solution can be determined by selecting the minimum normalized deviation (L_p) between the minimum Euclidean distance (p = 2) and the minimum largest deviation (p = ∞), or "*Minimax Criterion*"

The *minimum Euclidean distance* (p = 2) is determined by normalizing minimum distance from the set of non-dominant solutions to the ideal solution and is defined as follows:

$$\min\ L_2(x) = \min[\sum_{i=1}^{m} | \frac{f_i(x) - \min f_i(x)}{\max f_i(x) - \min f_i(x)} |^2]^{1/2}. \qquad (3\text{-}14)$$

The *minimum largest deviation* of the distance from the set of non-dominant solutions to the ideal solution is determined as follows:

$$\min\ L_\infty(x) = \min \max \left| \frac{f_i(x) - \min f_i(x)}{\max f_i(x) - \min f_i(x)} \right|. \qquad (3\text{-}15)$$

3.6 Structural Optimization of Spliced Precast/Prestressed Girder bridges

The design of spliced girder bridges depends on several parameters that significantly influence performance and cost. The most relevant are time dependent effects, splicing locations, construction sequence, girder segment geometries, number of beams, and the number and profiles of pre-tensioned and post-tensioned reinforcement. Normally most design variables are determined based on the designer's judgment through a trial and error process. Consequently there is no guarantee of obtaining the

most economical design, which requires more time and effort to explore, and which typical projects usually cannot afford.

Optimization for the design of spliced precast/prestress girder bridges were implemented to make the design more efficient and to eliminate the trial and error approach and to provide a systematic approach to arrive at appropriate design variable solutions, significant cost savings, performance improvements and ease of design by providing guidance and insight into optimal solutions.

Bridge systems may be associated with three levels of optimization: (1) components, (2) transverse and longitudinal configurations, and (3) complete structural systems. Only component and configuration optimization were considered in this work for the design optimization of spliced girder bridges.

3.6.1 Component optimization

Component optimization deals with the study of optimal dimensioning and section sizing of prestressed concrete girders. Component optimization for prestressed concrete girders has broadly been used in research efforts sponsored by state highway agencies for developing standard sections.

Presently, precast/prestressed concrete girders are being used extensively in continuous multi-span bridges in which continuous segments over the pier (pier segments or negative segments) are custom-designed to carry the high negative bending moment and high shear demands. Consequently, deep sections using haunches are typically used. Different haunch depths were considered to assess the sensitivity of the structural system to the pier segment flexural stiffness. These analyses were conducted by using frame analyses that included construction staging and time-dependent effects.

A component optimization process was performed to obtain the dimensions of optimal negative sections for two-span continuous systems. This process was coupled with the configuration optimization problem in order to obtain the best geometry solution for a given span length, beam spacing, and splice locations with the most efficient girder at the pier location.

Four methods to increase the section depth over the pier section were considered in this study. The main goal was to assess the cost efficiency of different methods used to obtain pier segments from standard sections. The study assessed optimal designs for the following cases:

a) Use of existing standard positive sections with an additional concrete block (soffit) attached to the underside of the beam (*Figure 3-4a*).

b) A new optimal prismatic section to be used in both positive and negative moment regions (*Figure 3-4b*).

c) A new optimal negative section with variable web (*Figure 3-4c*).

d) A new optimal negative section with variable soffit and constant web (*Figure 3-4d*).

3.6.2 Configuration optimization

Configuration optimization includes the effect of number of spans, pier locations, number of girders (beam spacing), and pre-tensioning and post-tensioning requirements (number of strands and layout). In addition, configuration optimization can also include the substructure. Since the number of supports is commonly reduced for SGB, the total cost of the system construction is anticipated to be reduced.

Structural optimization techniques was used to develop optimal configuration and sectional girder requirements for spliced girder bridges to improve understanding of system behavior, design variable sensitivity, and serve as a guide to produce design aids. Design aids can depict the relations between girder shape, girder spacing, pre-tensioning and post-tensioning requirements (including profiles), splicing locations, pier segment geometries, and initial and final concrete compressive strengths. It is thought that bridge engineers would find benefits from the presented optimization results since they provide information on system performance as a function of multiple design variables and their collection in the form of design charts can also help expedite the design process.

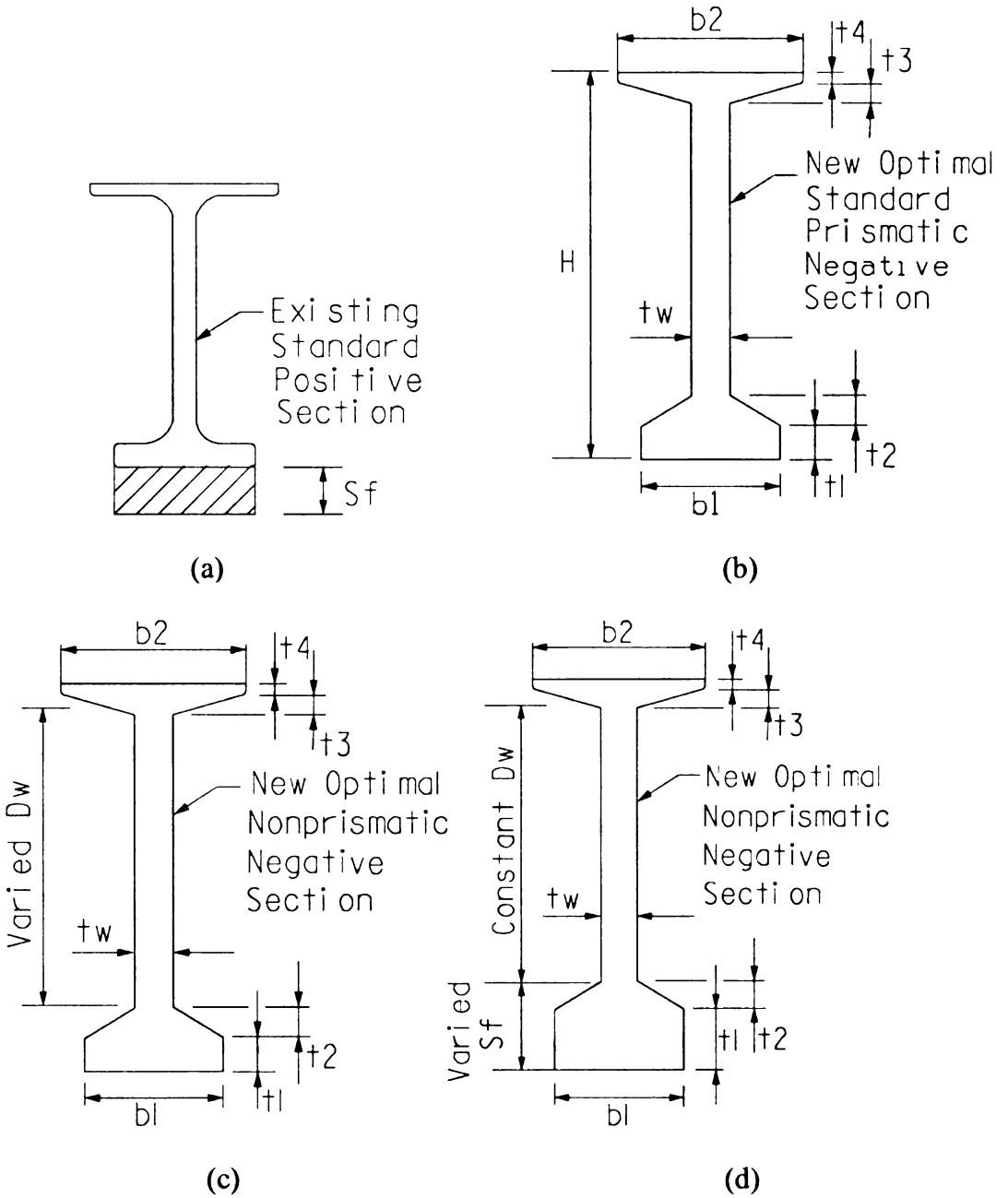

Figure 3-4 *Negative Segment Alternatives: (a) existing standard girder with attached soffit (b) new optimal standard prismatic girder (c) new optimal standard non-prismatic girder with variable web depth (d) new optimal standard non-prismatic girder with variable soffit*

3.6.3 Single objective optimization of spliced girder bridges

The single objective functions that were adopted as merit criteria for the optimal design of longitudinally spliced precast/prestressed girder bridges are listed below:

a) Minimum superstructure construction cost

This objective can be considered as the most realistic objective in bridge design since the superstructure cost represents about 70% of the total structure cost (Lounis 1993). A reliable construction cost is not easy to define because it often varies with time and location. However, the assumed unit costs (see Section 4.5) can be considered adequate for the comparison purposes of this study.

b) Minimum post-tensioning requirements

The post-tensioning strand cost is considered higher than the pre-tensioning strand cost since it involves the operation cost at the site as well as the cost of anchorage hardware. Thus, the goal of this objective function is to use the minimum number of post-tensioning which will lead to the maximum number of pre-tensioning strands.

c) Minimum pre-tensioning requirements

Normally, pre-tensioning strand cost is included as part of the prestressed concrete beam. Thus there is no separate cost between the beam and the pre-tensioning cost. However, this objective was included to assess the effect of minimizing the numbers of pre-tensioning strands for an achievable span length.

d) Minimum girder concrete volume

This objective was used for developing non-standard pier segments for two-span continuous spliced girder bridges since no cost data for the newly proposed girders is available. This objective is equivalent to minimizing superstructure weight.

3.7 Multicriteria Optimization of Spliced Girder Bridges

A common design criterion for spliced girder bridge design is the minimization of total superstructure cost. However, in some situations, other criteria, such as minimization of post-tensioning requirements, minimization of concrete volume, minimization of superstructure depth, maximization of span length, and reduction on the number of piers may be of interest. When the combination of single-objective optimization functions is considered, multicriteria optimization can be used to model a compromising problem to determine an optimal solution. The proposed multi-objective function was the minimization of cost since it is the first practical objective that designer and owner will consider.

The economics multicriteria objective function $F_1(x)$ considered the minimization of superstructure construction cost, the minimization of concrete volume, and the minimization of pre-tensioning and post-tensioning requirements. $F_1(x)$ can then be defined by the combination of the following single-objective functions:

$f_1(x)$ = Min. superstructure cost = $n_g C_g + C_c V_c + A_{ps} C_{po} + t_p C_t + m_r C_s + C_f A_f$

$f_2(x)$ = Min. concrete volume = V_c

$f_3(x)$ = Min. post-tensioning strands = A_{ps}

$f_4(x)$ = Min. pre-tensioning strands = A_{pre}

where n_g = number of girders; A_{ps} = number of post-tensioning strands; A_{ps} = number of pre-tensioning strands; t_p = number of temporay supports; m_r = mass of non-prestressed steel; V_c = volume of concrete; A_f = surface area of slab formwork; C_c = cost of concrete; C_p = cost of prestressing; C_{po} = cost of post-tensioning; C_t = cost of temporary support; C_g = erection cost for girders (including cost of concrete and prestressing steel); C_s = cost of non-prestressing; and C_f= cost of slab forming.

3.8 Implementation

The single- and multi-objective optimization of spliced girder bridges were implemented in a custom automated program written in Matlab (MathWorks 2002). Matlab is widely used in engineering and mathematics applications due to its robust operation and useful built-in predefined program code, which allows the user to easily import and export data from external programs. Objective functions and constraints were evaluated in conjunction with the mathematical optimization algorithms within Matlab.

A flow chart for the implemented optimization approach is shown in Figure 3-5. Custom computer aided design algorithms were used as preprocessing to discretize the beam line into finite elements. Each beam line was divided into finite elements of size between 305 mm (1 ft) and 1525 mm (5 ft) to cover all critical locations, i.e., the midspan of middle segment, the splice location, the midspan of the end segments.

Sensitivity analysis is used to provide gradient information on the objective and constraint functions with respect to the design variables to determine the effect on the objective function if the design variable values are changed. The sensitivity analyses were carried out through the analytical approach in a custom routine implemented in Matlab.

Structural analyses of the SGB structure were based on 2-D elastic analyses including the effect of non-prismatic section properties along the span, time-dependent material behavior, and staged construction. A custom program using the stiffness method of analysis was used. Each span segment was divided into multiple elements to obtain stresses, internal forces and deflection results at several locations along the span. Section properties of non-prismatic elements were taken as the average from those at the end nodes for a given element. Time dependent losses were determined based on the AASHTO-LRFD bridge design specifications (AASHTO 2003). Each construction method was analyzed separately and the maximum achievable span length for each construction method was compared to determine their efficiency.

In the mathematical programming, the initial values for the design variables used were predefined within upper and lower bound limits. The search direction and a step size toward the optimal solution were determined using built-in Matlab functions and the

constrained steepest descent method. The system geometry was then updated and provided as input for the next analysis until the objective function value converged to a unique solution and the optimality conditions are satisfied.

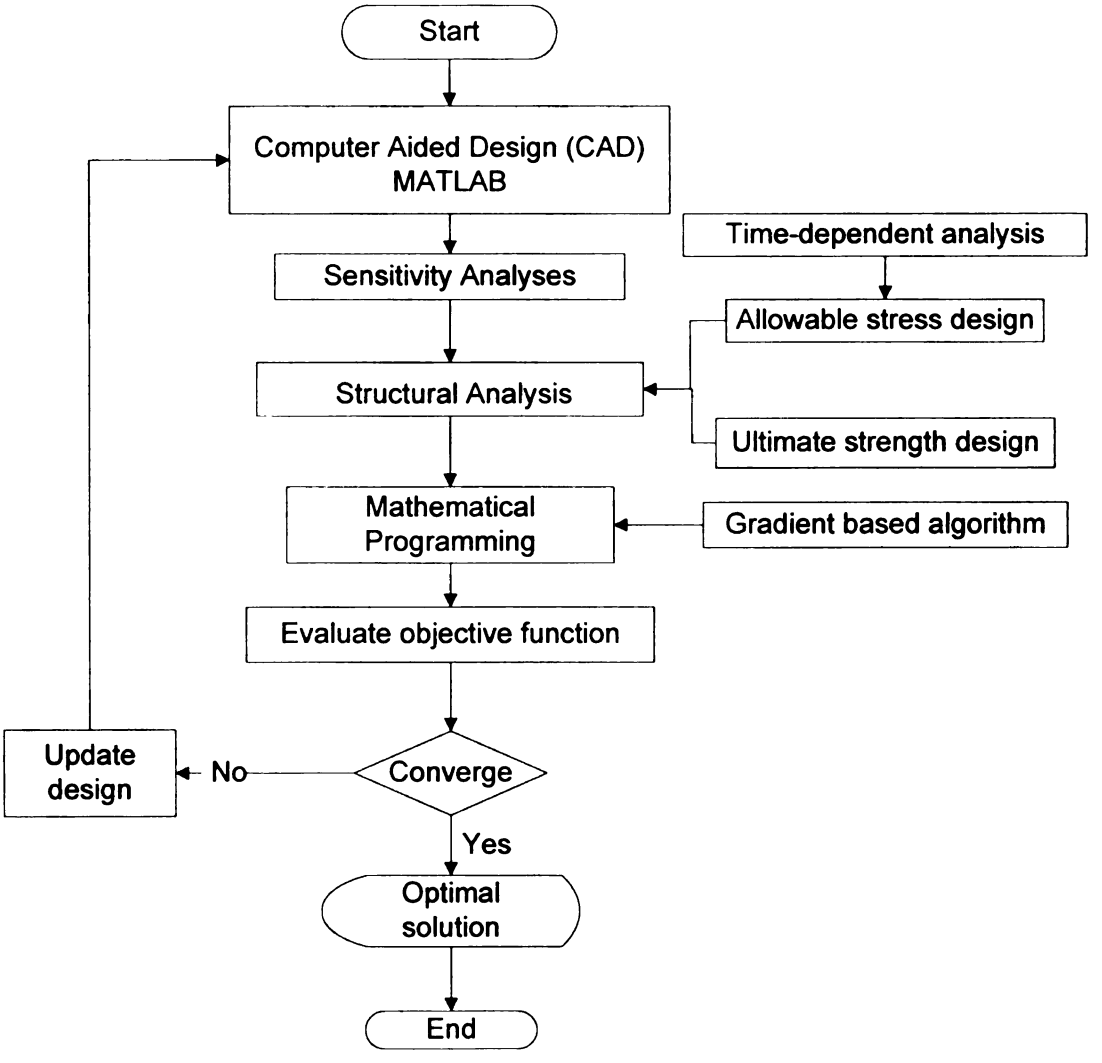

Figure 3-5 *Flow chart of computer program for optimization of spliced precast/prestressed girder bridge systems.*

3.9 Summary

This chapter presented an overview of the theory and methods used in this work taken for single-objective and multicriteria optimization studies on spliced prestressed concrete girder bridges. The objective functions and constraints of spliced girder bridges are nonlinear functions of the design variables. Therefore, the constrained steepest descent method using a gradient based algorithm was selected since it is robust and effective for solving nonlinear constrained optimization problems (Arora 1989). For the multicriteria optimization, the constraint approach was used to generate a set of pareto optima with non-dominated solutions and compromise programming was utilized for selecting the best solution. These approaches were implemented in the Matlab environment by combining time-dependent and construction staging frame analyses with built-in Matlab optimization functions in a custom automated program.

4 Optimum System Designs of Single-span Spliced Precast/Prestressed Bridges

4.1 Introduction

Single-Span Spliced Precast/Prestressed Girder Bridges (SSGB) are of interest to bridge engineers because they can significantly increase the spanning capabilities of conventional prestressed concrete bridges. Consequently, this system is favored when limitation on pier placement exists. Currently, only custom deep beam cross-sections are used for SSGB since they can span much longer than typical standard beams. The objective here is to explore the benefits of using *standard* precast/prestressed concrete girder sections in SSGB construction since their fabrication and erection cost can be much lower than for custom girders.

In order to obtain efficient optimal solutions of SSGB and to eliminate trial and error design iterations, structural optimization can be utilized in the design and analysis process. Single objective functions as well as multi-criteria objective functions are used to determine the optimal results of design requirements in the optimization process. The single objective optimization functions used in this study were the minimization of superstructure cost, the minimization of post-tensioning strands, and the minimization of pre-tensioning strands. A multi-criteria optimization approach combines these single objective functions to obtain compromise solutions to all these individual design objectives.

Results from optimization studies were used to develop design aids for SSGB. These results were for both single and multiple objective optimization problems. The maximum achievable span length for different beam types at different beam spacing and splice locations was obtained from the optimizied design. Three types of construction sequence methods were explored to evaluate the influence of construction sequence on the maximum achievable span length as well as on prestresing requirements.

Finally, the effect of clear cover on prestressing strands and on reinforcement in the deck were investigated to asses the service life of SSGB. This additional design requirement was then used to determine the life-cycle-cost of SSGB.

4.2 Problem Statement

A three-lane single-span spliced girder bridge with a total width of 18.59 m (61 ft), as shown in Figure 4-1, and a span length *(L)*consisting of three segments, as illustrated in Figure 4-2, was used in this study. The end segments were assumed to be equal. The splice location, which is the ratio of the end segment length (L_1) to the total span length (L), was used to define the mid-segment and end-segment length. The cast-in-place concrete slab thickness was assumed to be 216 mm (8.5"). The beam spacing varied from 1.8 m (6 ft) to 2.7 m (9 ft). Bulb-tee beams, AASHTO beams, and box beams were investigated. The material properties are given in more detail in the design parameter session (Section 4.3).

The design study was conducted using the simplified design method of the AASHTO-LRFD Bridge Design Specifications (AASHTO 2003) and the recommendations from the NCHRP 12-57 study (Castrodale and White 2004). Service limit states and ultimate limit states were considered in the design.

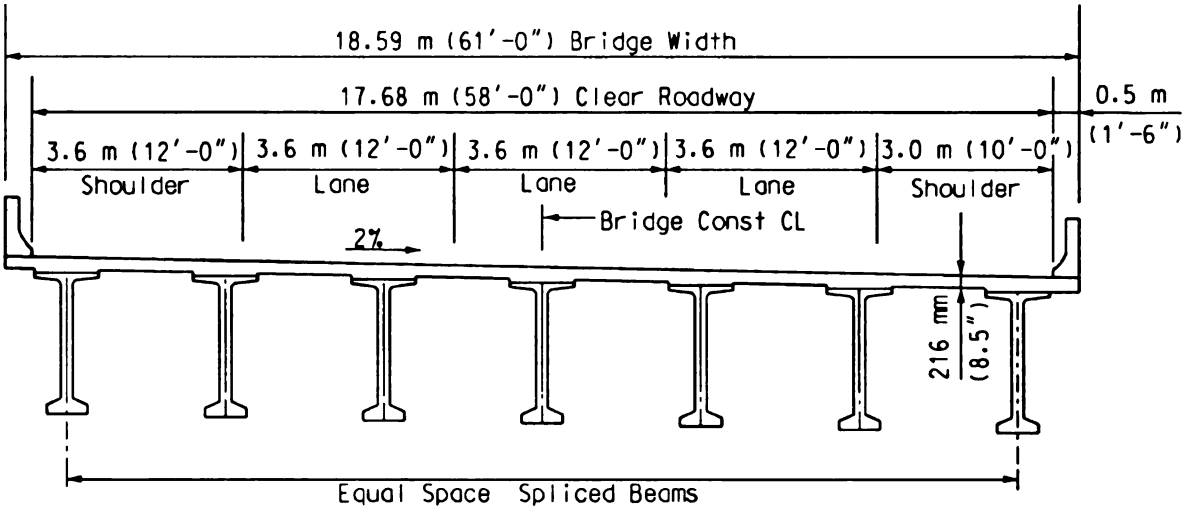

Figure 4-1 *Bridge cross-section of prototype bridge*

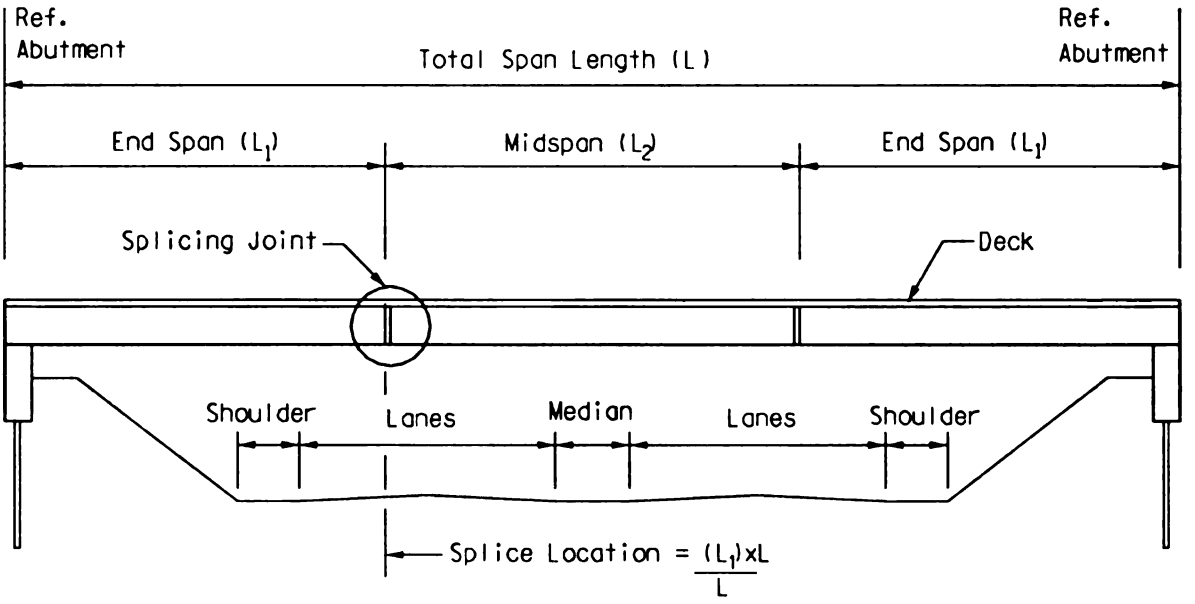

Figure 4-2 *Three-segment single-span spliced precast/prestressed bridge*

4.3 Design Parameters

Values that remain fixed in the optimization process are considered design parameters. These parameters have a significant role in defining the problem and they consequently significantly influence the resulting value for the design variables.

The main geometry design parameters include beam spacing *(S)*; total span length *(L)*; splice location *(pra)*; and the girder sectional properties (for AASHTO I-beams, PCI Bulb-tee beams, and Box-beams). The sectional properties include A_g = beam area, S_b = bottom sectional modulus, and S_t = top sectional modulus. Beam spacing was varied from S = 1.8 m (6 ft) to 2.7 m (9 ft) with 305 mm (1 ft) increments. The splice location *(pra)* was defined as the ratio of the end span length (L_1) over the total span length (*L*). Three splice locations were investigated, namely 0.20*L*, 0.25*L*, and *0.30L*. Optimization algorithms were then used to obtain optimal SSGB solutions for each span length. The objective functions used in the optimization of SSGB to determine the optimal solution were minimum construction cost, minimum post-tensioning, and minimum pre-tensioning, respectively. The maximum achievable span length *(L)* was determined by increasing the total span length to the point where it yielded an infeasible solution. The problem formulation for the optimization of SSGB is given in detail in Section 4.5.

Concrete properties for the girders, deck and splice joints are summarized in Table 4-1. The pre-tensioning and post-tensioning strands were taken to be 15.24 mm (0.6 in.) diameter and to be made from low-relaxation steel, with properties as given in the AASHTO LRFD specifications (AASHTO 2003).

Table 4-1 *Assumed material properties*

Girder Concrete	Deck & Splice Concrete	Pretensioning Strands	Post-Tensioning Strands
SI Units			
f'_c = 44.8 MPa	f'_{cd} = 31.0 MPa	A_{ps} = 140 mm^2	A_{ps} = 140 mm^2
f'_{ci} = 34.5 MPa	f'_{cdi} = 24.1 MPa	f_{pu} = 1862 MPa	f_{pu} = 1862 MPa
E_c = 33.7 MPa	E_{cd} = 28.0 MPa	f_{py} = 1675 MPa	f_{py} = 1675 MPa
E_{ci} = 29.6 MPa	E_{cdi} = 24.7 MPa	f_{po} = 1396 MPa	f_{pj} = 1508 MPa
		E_p = 196502 MPa	E_p = 196502 MPa
US Units			
f'_c = 6500 psi	f'_{cd} = 4500 psi	A_{ps} = 0.217 in.^{2}	A_{ps} = 0.217 in.^{2}
f'_{ci} = 5000 psi	f'_{cdi} = 3500 psi	f_{pu} = 270 ksi	f_{pu} = 270 ksi
E_c = 4888 ksi	E_{cd} = 4067 ksi	f_{py} = 243 ksi	f_{py} = 243 ksi
E_{ci} = 4287 ksi	E_{cdi} = 3587 ksi	f_{po} = 202.5 ksi	f_{pj} = 218.7 ksi
		E_p = 28500 ksi	E_p = 28500 ksi

In this study, typical standard girder shapes used in SSGB were investigated, which included AASHTO I-Beams, Box-Beams, and PCI-beams. Only deep beam shapes were investigated since shallow section would not benefit from the effects of post-tensioning. Thus, only AASHTO Types III through VI was investigated. The depth of box beams depends on the fabricator's production capability. In the state of Michigan, the maximum box beam depth used for conventional precast/prestressed concrete bridge girders is 1220 mm x 1370 mm (48" x 54"). Three different size of box beams, which include 1067 mm x 1220 mm (42"x 48"), 1220 mm x 1220 mm (48"x 48"), and 1524 mm x 1370 mm (54"x 48"), were investigated in the study. Two PCI bulb-tee girders, namely the PCI-BT 72 and PCI-BT 96, were also used in the study.

4.4 Analysis of Spliced Precast/Prestressed Girder Bridges

Analysis of the spliced girder bridge structure was based on a 2-D elastic frame analysis including the effects of time-dependent material behavior and staged construction. A custom frame analysis program using the stiffness method was used. Each span segment was divided into multiple elements to obtain stresses, internal forces and deflection results at the member ends. The beam-line model was subjected to the demands of an interior girder according to the load distribution factors given in the AASHTO-LRFD Specifications (AASHTO 2003). Interior girders were used in the analysis since their demands usually control the superstructure design. In addition, usually all beams are designed as interior beams to allow for future bridge widening.

Stressing losses were computed using the simplified AASHTO-LRFD (AASHTO 2003) method with consideration of the effects of combined pre-tensioning and post-tensioning on the girder segments, as recommended by a recent NCHRP study on spliced girder bridge design (Castrodale and White 2004). Design lifetime of the spliced girder bridge system was taken to be 75 years after all prestress losses have occurred. The section design was performed using a custom program coded in MATLAB (Mathworks 2002), which enforced compliance with service limit states as stated in Section 4.5.

The analysis program was verified by comparing its results to those from a Single-Span SGB Design Example (Example 1) from the NCHRP 517 report (Castrodale and White 2004). The design example uses the modified 2.4 meter (96 in.) PCI bulb-tee with a beam spacing of 2.7 m (9 ft) for a span length of 59.7 m (196 ft). Single-staged post-tensioning applied after pouring the deck was used as the constructor process for

the study example. All moment demands at each stage and stresses at the top and bottom of the beam, and at the top of the deck, for all critical construction stages and load combinations were checked along the length of the span. The only difference between the analysis from this study and the NCHRP 517 example was the post-tensioning profile. The NCHRP example assumes straight line segments that approximate a parabolic curve, whereas the developed analysis tool for this study uses an actual continuous parabolic curve (see Section 2.5.3c). The final output results were found to be within 5% of the NCHRP 517 results.

4.5 Optimum Design of Single-Span Spliced Girder Bridges

Three different construction sequence methods were investigated in this study to determine their effect on the design of single-span spliced girder bridges. The optimization formulation of each construction sequence method is described in detail in the following subsections.

4.5.1 Single-stage post-tensioning after pouring deck (Method 1)

In this method, the precast/prestressed beams are first installed on temporary supports at the site. Spliced joints and diaphragms are then poured and cured. The deck is added once the spliced and diaphragms have developed enough strength to resist partial load. After the deck develops enough concrete strength, full longitudinal post-tensioning is applied to connect all segments. The temporary supports are removed once the deck develops enough strength to achieve composite action with the beams. The optimization problem for this construction stage can be formulated in the following sections.

a) Design variables

The design variables for the optimization problem are those defining the amount and layout of the pre-tensioning and post-tensioning strands in the girders as described in Figure 4-3. The design variables for the SSGB problem are illustrated in Figure 4-3 and include:

npr_{1i} = number of bottom pre-tensioning strands on end segments at i^{th} row (e.g., npr_{11} represents the number of bottom pre-tensioning strands on the end-segment at the 1st bottom row of the girder);

npr_{2i} = number of bottom pre-tensioning strands on mid-span segments at i^{th} row;

$nprt_1$ = number of top pre-tensioning strands on end-segments;

$nprt_2$ = number of top pre-tensioning strands on mid-segment;

npo = total number of post-tensioning strands on beam;

y_a = vertical distance from the bottom extreme fiber to the net centroid of the post-tensioned duct at the end-segments;

y_{bb} = vertical distance from the bottom extreme fiber to the net centroid of the post-tensioned duct at the mid-segment.

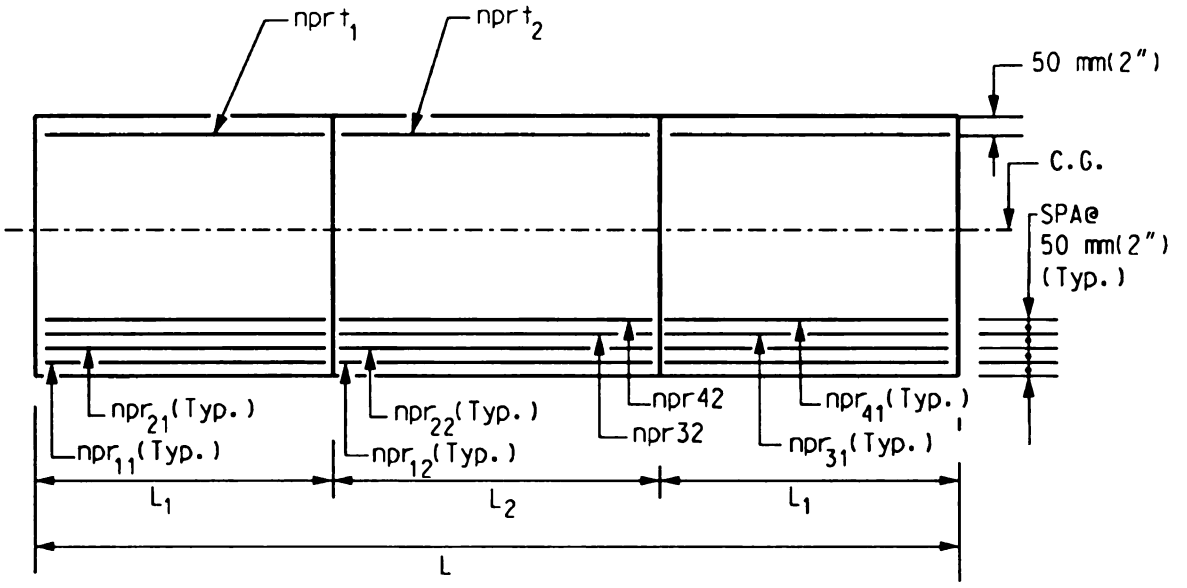

(a) Pre-tensionning requirement

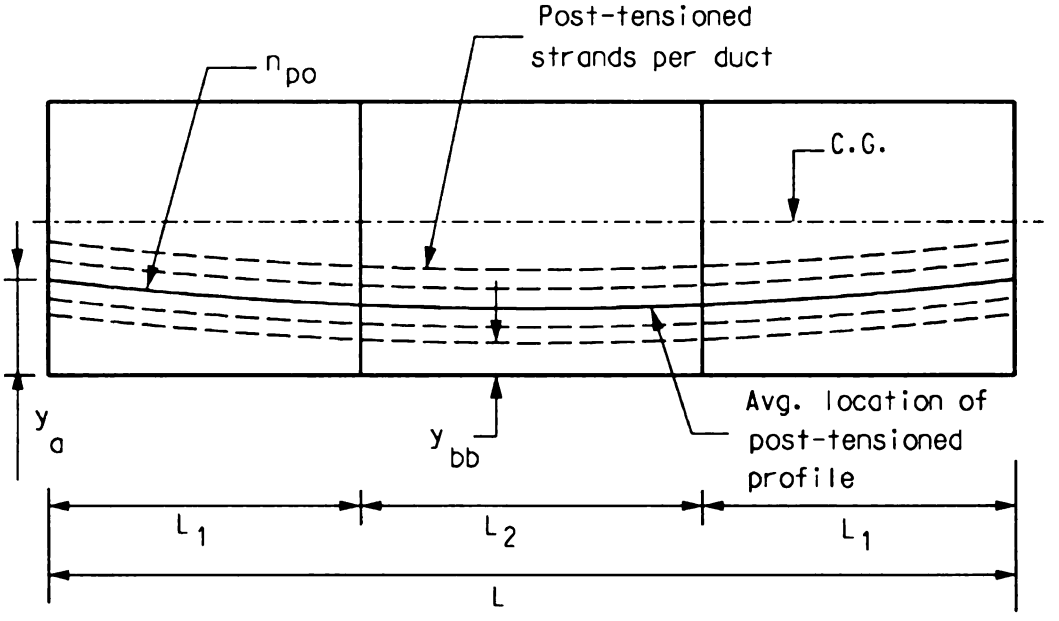

(b) Post-tensioning requirement

Figure 4-3. *Variables for the design optimization of spliced girder bridges*

These, and the remaining design variables, are noted in Figure 4-3. Variables y_a and y_{bb} are not direct design variables (i.e., not part of the objective function); however, they have an influence on other design variables and should be included as design

variables. For example, when distances y_a and y_{bb} change the required numbers of post-tensioned strands and numbers of pre-tensioned strands will be different due to their coupled relationships.

Each pre-tensioning strand was layer taken to be located 50 mm (2 in.) apart, including the distance of the first row of strands to the beam bottom/top. The post-tensioning tendon was assumed to follow a quadratic parabolic profile. Normally, post-tensioning strands require several ducts. In order to avoid having several duct profiles as design variables, an *effective* post-tensioning profile was used to represent a group of ducts. Thus, every post-tensioning duct in the spliced girder section was assumed to have the same post-tensioning profile. The distance between individual post-tensioning ducts was assumed to be uniform at 152 mm (6 in.) apart. The lowest point of the post-tensioning profile on the bottom row at the middle section was one of the design variables, y_{bb}, and it was assumed to be at least 152 mm (6 in.) from the extreme bottom fiber. The effective post-tensioning profile location was determined by the summation of the vertical distances measured from the extreme bottom fiber to the centroid of each duct and divided by numbers of the ducts at that location.

b) Objective function

Typically, there can be several design solutions that satisfy all requirements of safety and serviceability imposed by a design code and a number of specified merit criteria. A common design criterion in bridge design is the minimization of superstructure construction cost (Cohn and Lounis 1994; Lounis and Cohn 1996; Lounis et. al 1997). For this study, the objective function was the minimization of superstructure

construction cost, which is defined in Equation (4-1). Details of each material component objective function cost are specified in Table 4-2.

$$f(x_i) = C_{PS} + C_{PT} + C_{CD} + C_{TS} + C_B + C_R, \quad (4\text{-}1)$$

where C_{PS} is defined as the pre-tensioning cost; C_{PT} is defined as the post-tensioning cost; C_{CD} is defined as the concrete deck cost; C_{TS} is defined as the temporary support cost; and C_B is defined as the beam cost.

A recent NCHRP project report on spliced girder bridges (Castrodale and White 2004) collected cost data for a sampling of projects around the US. However, detailed construction cost information for post-tensioned spliced girder bridges was difficult to obtain since most states only track cost data on a project basis. In addition, the research team found great variations in costs between regions, methods of project delivery, and local consulting practices. As a result, it was difficult to assign meaningful cost parameters that are generally relevant.

Since it was difficult to determine realistic cost values to use in the proposed cost minimization objective function, cost estimates were based on values used for conventional prestressed girders with supplemental costs for temporary supports and post-tensioning. While this type of incremental approach is rarely valid (Castrodale and White 2004), it was considered adequate for the comparative study of standard beam sections being dealt with in the present study. The assumed unit materials cost are summarized in Table 4-3.

Table 4-2 *Components of objective function*

Material	Component Cost
Pre-tensioning, C_{PS}	$C_p \cdot N_g \cdot [(npr_{i1} + nprt_1) \cdot L_1 \cdot 2 + \cdot (npr_{i2} + nprt_2) \cdot$
Post-tensioning, C_{PT}	$C_{po} \cdot N_g \cdot n_{po} \cdot (L_1 \cdot 2 + L_2)$
Beam, C_B	$C_b \cdot N_g \cdot (L_1 \cdot 2 + L_2)$
Concrete, C_{CD}	$C_c \cdot L \cdot W \cdot t_s$
Reinforcement, C_R	$C_r \cdot W \cdot (L_1 \cdot 2 + L_2) \cdot W_{st}$
Temp support, C_{TS}	$C_{ts} \cdot N_g \cdot 2$

c) Design constraints

The optimization constraints for the SSGB optimization problem were the service and strength limit states specified in the AASHTO-LRFD Bridge Design Specifications (AASHTO 2003) and the recommendations from NCHRP Report 517 (Castrodale and White 2004). Constraints for the service limit state were defined in terms of flexural stress limits on the girder and deck. For flexure, service limit state requirements govern the required prestressed force. Constraints for the strength limit state included checks on moment and shear capacities. The ductility requirement was satisfied by ensuring that the relative neutral axis depth at the ultimate limit state c/d_e was less than 0.42 (AASHTO 2003).

Stresses from applied (external) loads were computed from the bending moment demands for composite and non-composite section properties, as appropriate. Stresses

were evaluated separately for each critical construction stage. The stress limits for each construction sequence method are different since they depend on the material properties at that stage as well as the loading conditions (i.e., full service load, partial service load without live load, and partial service load with live load). For example, when the pre-tensioning strands are applied to the girder, the girder still has not developed enough strength; therefore, the concrete's initial compressive strength is used for their stress limit. On the other hand, when the deck is applied to the bridge, the girder concrete has already developed its final compressive strength; therefore the final concrete compressive strength is used for the limit state.

Table 4-3 *Assumed unit cost of materials*

Component Item	Unit Cost
SI Units	
Cost of Concrete (C_c)	176 \$/m^3
Cost of Pre-Tensioning (C_p)	50 \$/strand-m
Cost of Post-Tensioning (C_{po})	100 \$/strand-m
Cost of Temporary Support (C_{temp})	1000 \$/beam
Cost of PCI-BT 96 (C_b)	900 \$/m
Cost of I-Beam: Type IV (C_b)	420 \$/m
Cost of Epoxy Reinforcement (C_r)	2 \$/kg
US Units	
Cost of Concrete (C_c)	230 \$/yd^3
Cost of Pre-Tensioning (C_p)	15 \$/strand-ft
Cost of Post-Tensioning (C_{po})	30 \$/strand-ft
Cost of Temporary Support (C_{temp})	1000 \$/beam
Cost of PCI-BT 96 (C_b)	300 \$/ft
Cost of I-Beam: Type IV (C_b)	140 \$/ft

Flexural stresses for each critical construction stage as listed in Table 4-4 were checked against the allowable compression and tension stresses. The allowable concrete stress limits used are those prescribed by AASHTO LRFD (AASHTO 2003), which is summarized in Table 4-5. Three locations across the composite girder-deck section were checked along the span. Stresses on the bottom and top fiber of the girder and the top fiber of the deck were checked at each critical stage to guarantee that all stresses satisfied the constraints, i.e., they should be within the prescribed limits as listed in Table 4-5 .

Table 4-4 *Construction sequence for single-staged post-tensioning applied after pouring deck in spliced girder bridges*

Construction Stages	Time (days)	Action Description	Pre-tensioning Critical Stage	Post-tensioning Critical Stage
1	-	Stress pre-tensioning strands		
2	0	Cast girder segments		
3	1	Release pre-tensioning strands	X	
4	50	Erect girder segments		
5	60	Place deck and splice concrete	X	
6	75	Stress post-tensioning strands	X	X
7	100	Add barriers		X
8	140	Apply live load		
9	15000	Add future wearing surface		
10	27500	After all prestress losses	X	X

There are seven critical stage constraints for each location of the composite section. The formulation of the bottom girder stress constraints (*Constraints 1aa* to *7aa*) for each of the critical construction stages is outlined in the next sections. *Constraint 1aa* refers to

the stress at stage 1 at the bottom extreme fiber of the girder after pouring the deck. The nomenclature of *Constraint 1aa* is defined as follows: *1* defines stage 1, the first *a* defines the girder bottom extreme fiber, and the last *a* defines that the construction method is that of post-tensioning after pouring the deck. Similar constraint formulations were implemented for the girder top extreme fiber (*Constraints 1ba* to *7ba*) and the top deck stresses (*Constraints 1ca* to *7ca*). *Thus, Constraint 1ba* refers to the girder stress at stage 1 at the girder top extreme fiber after pouring the deck and *Constraint 1ca* refers to the stress at stage 1 at the top of the deck with post-tensioning after pouring the deck.

Table 4-5 *Allowable concrete stress limits for single-staged post-tensioning applied after pouring deck at each construction stage*

Construction Stages	Stress Type	Girder concrete	Deck concrete
1) Prestressing Strand Release	Compression	$0.6f'_{ci}$	
	Tension	-1.4 MPa (-200 psi)	
2) Deck /Splice Concrete	Compression	$0.6f'_c$	
	Tension	-1.4 MPa (-200 psi)	
3) Post-Tensioning	Compression	$0.6f'_c$	$0.6f'_{cd}$
	Tension	$-0.0914\sqrt{f'_c}$(MPa)	$-0.0914\sqrt{f'_{cd}}$ (MPa)
		$-0.24\sqrt{f'_c}$ (ksi)	$-0.24\sqrt{f'_{cd}}$ (ksi)
4) Final Condition (after losses)	Compression 1	$0.6\phi_w f'_c$	$0.6\phi_w f'_{cd}$
	Compression 2	$0.45f'_c$	$0.45f'_{cd}$
	Compression 3	$0.4f'_c$	$0.4f'_{cd}$
	Tension 1	$-0.0724\sqrt{f'_c}$ (MPa)	
		$-0.19\sqrt{f'_c}$ (ksi)	

Constraint 1aa: *Stress Check at Pre-tensioning Stage*

This construction stage considers the stresses due to the girder weight and the pre-tensioning force. At this stage only prestress losses due to relaxation at release and elastic shortening are deducted from the initial prestress stress of pre-tensioned strands. The girder bottom fiber compression stress constraint is then defined by:

$$\sigma_{1aa} = -\frac{M_g}{S_{bg}} + \frac{A_{ps} f_{pe1}}{A_g} - \frac{A_{ps} f_{pe1} e_p}{S_{bg}} \leq 0.6 f'_{ci}. \tag{4-2}$$

Constraint 2aa: *Stress Check at Placement of Deck and Splice Stage*

Constraint 2 applies to the concrete casting operation of the deck, deck haunch, and splice regions. The deck, haunch and splice are poured at this stage. Since the deck is still not hardened, non-composite sectional girder properties are used. Prestress losses for this stage include those from elastic shortening, creep, shrinkage, and steel relaxation. Girder stresses at the bottom fiber are thus given by:

$$\sigma_{2aa} = -\frac{M_g}{S_{bg}} - \frac{M_d}{S_{bg}} - \frac{M_h}{S_{bg}} - \frac{M_c}{S_{bg}} + \frac{A_{ps} f_{pe2}}{A_g} - \frac{A_{ps} f_{pe2}\ e_p}{S_{bg}} \leq 0.6 f'_c. \tag{4-3}$$

Constraint 3aa: *Stress Check at Post-Tensioning Stage*

This constraint applies to the longitudinal splicing of the pre-tensioned girders through a single post-tensioning operation. As previously presented, an equivalent tendon profile with a parabolic profile, obtained according to the uniform dead load, is assumed. At this stage, the deck is taken to be working compositely with the beam. Prestress losses at this stage include those from elastic shortening, creep, shrinkage, steel relaxation, and additional elastic shortening due to post-tensioning. The bottom fiber girder stress constraint is thus defined by:

$$\sigma_{3aa} = -\frac{M_g}{S_{bg}} - \frac{M_d}{S_{bg}} - \frac{M_h}{S_{bg}} - \frac{M_r}{S_{bc}} + \frac{A_{ps} f_{pe3}}{A_g} + \frac{A_{ps} f_{pe3} e_p}{S_{bg}} +$$

$$\frac{n_{po} a_{ps} f_{pof}}{A_c} + \frac{n_{po} a_{ps} f_{pof} e_e}{S_{bc}} \leq 0.6 f_c'. \qquad (4\text{-}4)$$

Constraint 4aa: *Compression Stress Check under Full Service Load*

This constraint applies to the service condition where the composite girders carry full live loads and superimposed dead loads in addition to the loads applied in previous stages. Compression stress limits under full service load are checked at this constraint. Prestress losses for this constraint include elastic shortening, creep, shrinkage, relaxation of steel, and additional elastic shortening due to post-tensioning. This constraint is defined by:

$$\sigma_{4aa} = -\frac{M_g}{S_{bg}} - \frac{M_d}{S_{bg}} - \frac{M_h}{S_{bg}} - \frac{M_r}{S_{bc}} - \frac{M_s}{S_{bc}} - \frac{M_{ll}}{S_{bc}} + \frac{A_{ps} f_{pe4}}{A_g} + \frac{A_{ps} f_{pe4} e_p}{S_{bg}} +$$

$$\frac{n_{po} a_{ps} f_{poff}}{A_c} + \frac{n_{po} a_{ps} f_{poff} e_e}{S_{bc}} \leq 0.6 f_c'. \qquad (4\text{-}5)$$

Constraint 5aa: *Tension Stress Check with Reduced Live Load*

The applied loads and prestress losses for this constraint are similar to those of *Constraint 4aa* with the exception of a 20 percent reduction in the live load. The objective is to check the tension limit state of the girder at the final stage as defined by:

$$\sigma_{5aa} = -\frac{M_g}{S_{bg}} - \frac{M_d}{S_{bg}} - \frac{M_h}{S_{bg}} - \frac{M_r}{S_{bc}} - \frac{M_s}{S_{bc}} - 0.8\frac{M_{ll}}{S_{bc}} + \frac{A_{ps} f_{pe4}}{A_g} + \frac{A_{ps} f_{pe4} e_p}{S_{bg}} +$$

$$\frac{n_{po}a_{ps}f_{poff}}{A_c}+\frac{n_{po}a_{ps}f_{poff}e_e}{S_{bc}} \le \text{ -0.0724}\sqrt{f'_c}\text{ (MPa) or -0.19}\sqrt{f'_c}\text{ (ksi).} \qquad (4\text{-}6)$$

Constraint 6aa: *Compression Stress Check without Live Load*

This constraint check considers all loads and prestress losses as in *Constraint 4aa* with the exception of live load. The compression limit state under these conditions is then checked according to:

$$\sigma_{6aa} = -\frac{M_g}{S_{bg}}-\frac{M_d}{S_{bg}}-\frac{M_h}{S_{bg}}-\frac{M_r}{S_{bc}}-\frac{M_s}{S_{bc}}+\frac{A_{ps}f_{pe_4}}{A_g}+\frac{A_{ps}f_{pe_4}e_p}{S_{bg}}+$$

$$\frac{n_{po}a_{ps}f_{poff}}{A_c}+\frac{n_{po}a_{ps}f_{poff}e_e}{S_{bc}} \le 0.45f'_c.$$

(4-7)

Constraint 7aa: *Stress Check at Compression for the Partial Service Load*

This critical stress check considers all of the loads of *Constraint 4aa* reduced by 50 percent except the live load. All the prestress losses considered for *Constraint 4aa* apply here also. The bottom fiber girder stress check is then defined by:

$$\sigma_{7aa} = 0.5\left(-\frac{M_g}{S_{bg}}-\frac{M_d}{S_{bg}}-\frac{M_h}{S_{bg}}-\frac{M_r}{S_{bc}}-\frac{M_s}{S_{bc}}+\frac{A_{ps}f_{pe_4}}{A_g}+\frac{A_{ps}f_{pe_4}e_p}{S_{bg}}\right)+$$

$$0.5\left(\frac{n_{po}a_{ps}f_{poff}}{A_c}+\frac{n_{po}a_{ps}f_{poff}e_e}{S_{bc}}\right)-\frac{M_{ll}}{S_{tc}} \le 0.4f'_c. \qquad (4\text{-}8)$$

d) Results and discussion

Use of single-span SGBs is commonly limited to specific medium to long-span bridge projects; therefore, custom girders with deep sections are typically used. The use

of standard prismatic precast/prestressed girder in SGBs would make the system more economical and, perhaps, more widely used. The efficiency of typical standard precast prestressed concrete beams were thus investigated in this study for SGBs applications. These standard sections were AASHTO I-beam Types III through Type VI, Michigan's DOT MI-1800 I-beam, PCI's PCI-BT 72 and PCI-BT 96 bulb-tee beams, and box beams of dimensions: 1067mm x 1220mm (42" x 48"), 1220mm x 1220mm (48" x 48"), and 1370mm x 1220mm (54" x 48"). The efficiency of the standard beams was determined by the achievable span length that satisfied all of the design constraints.

The maximum span length of conventional precast prestressed concrete girders is usually determined based on the initial concrete compressive strength (f'_{ci}) and the service concrete compressive strength (f'_c). These same concrete compressive strengths were chosen to be consistent with the analyses on SGBs. Maximum beam spacing was varied from 1.8 meters (6 ft) to 2.7 meters (9 ft) with 305 mm (1 ft) increments. Single-span conventional prestressed concrete beams were analyzed by increasing the span length using the commercial program CONSPAN (LEAP 2005) until they became infeasible while SGBs were analyzed by custom design code written in MATLAB (Mathwork 2002).

Comparison of maximum achievable span lengths and the percentage of span increase between conventional precast prestressed concrete girders and simply-supported SGBs for each beam type are summarized in Table 4-6 and Table 4-7. These results show that the splice location at $0.25(L)$ is the most efficient for single-span spliced girder bridges with equal end-segment lengths.

Based on the results, AASHTO Type III beams, which were the shallowest beam in the study, yielded the maximum percentage increase in span length compared with its maximum conventional simple span length. These results show that longitudinal splicing of precast beams is not only efficient for deep beam sections; standard prestressed beams with short to moderate depths, such as the AASHTO Type III, can also be longitudinally spliced to significantly extend their spanning capability.

Shallow girder sections have higher efficiency in percentage increase of the span length than deeper girder sections. When the depth of the AASHTO I-beam is increased, the percent increase of spliced girder span length is less than that of a shallower AASHTO I-beam. For example, spliced AASHTO Type VI beams have a percentage increase in span length that is smaller than for the AASHTO Type V, Type IV, and Type III beams, sequentially.

When the beam spacing is large, the percentage increase in the span length is higher than with tight beam spacing. This result indicates that longitudinal splicing is more efficient when large beam spacing is used. When the vertical underclearance is not an issue, using deeper beam sections with larger beam spacing can reduce the construction cost dramatically. Normally the cost of standard beam types, such as AASHTO Types III and IV, is not much different compared to the cost reduction of eliminating beams. This outcome concurs with the current practice of using spliced girder bridges to extend span length as well as to reduce the numbers of beams (larger beam spacing) in the bridge system.

Table 4-6 *Maximum span length of SGBs and conventional box-beams*

Beam Spacing	Max. Span Length (m) Conventional Girder	Spliced Girder L_1/L			Percent Increase (Spliced Girder)		
		0.2	0.25	0.3	0.2	0.25	0.3
SI Units							
1067mm X 1220mm							
2.1 m	30.2	39.3	41.8	41.5	30%	38%	37%
2.4 m	28.7	39.0	40.2	41.1	36%	40%	44%
2.7 m	28.0	38.1	39.0	39.6	36%	39%	41%
1220mm X 1220mm							
2.1 m	34.4	46.0	47.9	48.2	34%	39%	40%
2.4 m	33.8	45.4	46.3	46.9	34%	37%	39%
2.7 m	32.9	44.2	45.7	45.1	34%	39%	37%
1524mm X 1220mm							
2.1 m	41.1	50.6	52.4	52.1	23%	27%	27%
2.4 m	39.0	49.1	50.6	51.8	26%	30%	33%
2.7 m	38.4	48.8	49.1	51.2	27%	28%	33%

Beam Spacing	Max. Span Length (ft) Conventional Girder	Spliced Girder L_1/L			Percent Increase (Spliced Girder)		
		0.2	0.25	0.3	0.2	0.25	0.3
US Units							
Box-Beam 42"x48"							
7 ft	99	129	137	136	30%	38%	37%
8 ft	94	128	132	135	36%	40%	44%
9 ft	92	125	128	130	36%	39%	41%
Box-Beam 48"x48"							
7 ft	113	151	157	158	34%	39%	40%
8 ft	111	149	152	154	34%	37%	39%
9 ft	108	145	150	148	34%	39%	37%
Box-Beam 54"x48"							
7 ft	135	166	172	171	23%	27%	27%
8 ft	128	161	166	170	26%	30%	33%
9 ft	126	160	161	168	27%	28%	33%

Table 4-7 Maximum span length of SGBs and conventional I- and bulb-tee beams (SI Units)

Beam Spacing	Max. Span Length (m) Conventional Girder	Spliced Girder L_1/L			Percent Increase (Spliced Girder)		
		0.2	0.25	0.30	0.2	0.25	0.3
Metric Units							
AASHTO Type III							
1.8 m	25.9	37.5	41.1	39.9	45%	59%	54%
2.1 m	24.1	36.0	39.3	38.4	49%	63%	59%
2.4 m	22.9	34.7	37.5	36.6	52%	64%	60%
AASHTO Type IV							
2.1 m	30.5	42.4	45.7	45.1	39%	50%	48%
2.4 m	29.6	40.8	44.5	43.6	38%	51%	47%
2.7 m	29.0	39.9	43.0	42.1	38%	48%	45%
AASHTO Type V							
1.8 m	39.3	52.1	53.6	54.3	33%	36%	38%
2.1 m	37.5	50.9	52.4	52.1	36%	40%	39%
2.4 m	35.7	48.8	50.6	50.0	37%	42%	40%
AASHTO Type VI							
2.1 m	44.5	53.6	55.8	55.8	21%	25%	25%
2.4 m	41.8	52.4	55.5	54.9	26%	33%	31%
2.7 m	39.3	51.5	54.3	53.6	31%	38%	36%
MI-1800							
2.1 m	42.1	54.3	57.9	57.0	29%	38%	36%
2.4 m	40.2	52.1	57.3	55.5	30%	42%	38%
2.7 m	37.5	51.5	54.9	54.3	37%	46%	45%
		0.2	**0.223**	**0.25**	**0.2**	**0.223**	**0.25**
PCI-BT 96							
2.7 m	44.5	61.0	63.1	64.6	37%	42%	45%
3.0 m	42.1	60.4	61.6	64.0	43%	46%	52%
3.3 m	41.5	59.1	61.0	61.9	43%	47%	49%

Table 4-7 Maximum span length of SGBs and conventional I- and bulb-tee beams *(US Units - Cont.)*

Beam Spacing	Max. Span Length (ft) Conventional Girder	Spliced Girder L_1/L			Percent Increase (Spliced Girder)		
		0.2	0.25	0.3	0.2	0.25	0.3
English Units							
AASHTO Type III							
6 ft	85	123	135	131	45%	59%	54%
7 ft	79	118	129	126	49%	63%	59%
8 ft	75	114	123	120	52%	64%	60%
AASHTO Type IV							
7 ft	100	139	150	148	39%	50%	48%
8 ft	97	134	146	143	38%	51%	47%
9 ft	95	131	141	138	38%	48%	45%
AASHTO Type V							
6 ft	129	171	176	178	33%	36%	38%
7 ft	123	167	172	171	36%	40%	39%
8 ft	117	160	166	164	37%	42%	40%
AASHTO Type VI							
7 ft	146	176	183	183	21%	25%	25%
8 ft	137	172	182	180	26%	33%	31%
9 ft	129	169	178	176	31%	38%	36%
MI-1800							
7 ft	138	178	190	187	29%	38%	36%
8 ft	132	171	188	182	30%	42%	38%
9 ft	123	169	180	178	37%	46%	45%
		0.2	**0.223**	**0.25**	**0.2**	**0.223**	**0.25**
PCI-BT 96							
9 ft	146	200	207	212	37%	42%	45%
10 ft	138	198	202	210	43%	46%	52%
11 ft	136	194	200	203	43%	47%	49%

4.5.2 Single-stage post-tensioning before pouring deck (Method 2)

In this method, the precast/prestressed beams are first installed on temporary supports at the site. Then a full longitudinal post-tensioning is applied to connect all segments. Spliced joints and diaphragms are then poured and cured. The deck is added once the splice and diaphragms have developed enough strength to resist partial loads. Temporary supports are removed once the deck develops enough strength to achieve composite action with the beams. The optimization problem of this construction stage is formulated in the following sub-sections.

a) Design variables

Design variables for this construction sequence method are similar to single-stage post-tensioning applied after pouring the deck (see Section 4.5.1a). The only difference is that the post-tensioning operation is applied before the deck is cast.

b) Objective functions

The objective function in this construction sequence method is the same as for the case of single-stage post-tensioning applied after pouring the deck, namely the minimization of structural cost (see Section 4.5.1b).

c) Design constraints

Flexural stresses at each critical construction stage as listed in Table 4-8 were checked against the allowable compression and tension stresses. The allowable concrete stress limits used are those prescribed by the AASHTO-LRFD specifications (AASHTO 2003), which are summarized in Table 4-9. Three locations across the composite girder-deck section were checked along the span. The stresses on the bottom and top flexural

fibers of the girder and the top fiber on the deck were checked at each critical stage to guarantee that all stresses satisfied the constraints.

Table 4-8 *Construction sequence for single-staged post-tensioning applied before pouring deck in spliced girder bridges*

Construction Stages	Time (days)	Action Description	Pre-tensioning Critical Stage	Post-tensioning Critical Stage
1	-	Stress pre-tensioning strands		
2	0	Cast girder segments		
3	1	Release pre-tensioning strands	X	
4	50	Erect girder segments		
5	75	Stress post-tensioning strands	X	X
6	90	Place deck and splice concrete	X	X
7	120	Add barriers		X
8	140	Apply live load		
9	15000	Add future wearing surface		
10	27500	After all prestress losses	X	X

For this construction option there are eight critical stage constraints on each location of the composite section. Only the formulation of the girder bottom stress constraints (*Constraints 1ab* to *7ab*) for each critical construction stage of the service limit state are outlined in the next sections. *Constraint 1ab* is refers to the stress at stage 1 at the girder bottom extreme fiber before pouring the deck. The nomenclature of *Constraint 1ab* is defined as follows: *1* refers to the stress at stage 1, the first *a* is defined as at the extreme bottom fiber, and the second *b* is defined as post-tensioning before pouring the deck. Similar constraint formulations were implemented for the girder top fiber (*Constraint 1bb-7bb*) and the deck top stresses (*Constraint 1cb-7cb*). *Constraint 1bb* is the stress at

stage 1 at the girder top extreme fiber after pouring the deck. *Constraint 1cb* is the stress at stage 1 at the top of the deck.

Table 4-9 *Allowable concrete stress limits for single-staged post-tensioning applied before pouring deck at each construction stage*

Construction Stages	Stress Type	Girder concrete	Deck concrete
1) Prestressing Strand Release	Compression	$0.6f'_{ci}$	
	Tension	-1.4 MPa (-200 psi)	
2) Post-Tensioning	Compression	$0.6f'_c$	
	Tension	-1.4 MPa (-200 psi)	
3) Deck /Splice Concrete	Compression	$0.6f'_c$	
	Tension	-1.4 MPa (-200 psi)	
4) Live loads/superimposed loads	Compression	$0.6f'_c$	$0.6f'_{cd}$
	Tension	$-0.0914\sqrt{f'_c}$(MPa)	$-0.0914\sqrt{f'_{cd}}$ (MPa)
		$-0.24\sqrt{f'_c}$ (ksi)	$-0.24\sqrt{f'_{cd}}$ (ksi)
5) Final Condition (after losses)	Compression 1	$0.6\phi_w f'_c$	$0.6\phi_w f'_{cd}$
	Compression 2	$0.45f'_c$	$0.45f'_{cd}$
	Compression 3	$0.4f'_c$	$0.4f'_{cd}$
	Tension 1	$-0.0724\sqrt{f'_c}$ (MPa)	
		$-0.19\sqrt{f'_c}$ (ksi)	

***Constraint 1ab*:** *Stress Check at Pre-tensioning Stage*

This construction stage considers the stresses due to girder weight and the pre-tensioning force similar to the construction Method 1 (see Section 4.5.1c). At this stage only prestress losses due to relaxation at release and elastic shortening are deducted from the initial prestress stress of the pre-tensioned strands. The girder bottom stress constraint is then defined as:

$$\sigma_{1ab} = -\frac{M_g}{S_{bg}} + \frac{A_{ps} f_{pe1}}{A_g} - \frac{A_{ps} f_{pe1} e_p}{S_{bg}} \leq 0.6 f'_{ci}. \tag{4-9}$$

Constraint 2ab: *Stress Check at Post-Tensioning Stage*

Post-tensioning is applied prior to pouring the deck, thus only the non-composite girder section is used to resist additional loads due to post-tensioning forces. Prestress losses at this stage are those from elastic shortening, creep, shrinkage, and relaxation of the steel. The girder bottom stresses are given by:

$$\sigma_{2ab} = -\frac{M_g}{S_{bg}} + \frac{A_{ps} f_{pe2}}{A_g} + \frac{A_{ps} f_{pe2} e_p}{S_{bg}} + \frac{n_{po} a_{ps} f_{pof}}{A_g} +$$

$$\frac{n_{po} a_{ps} f_{pof} e_e}{S_{bg}} \leq 0.6 f_c'. \tag{4-10}$$

Constraint 3ab: *Stress Check at Placement of Deck and Splice Stage*

The deck, haunch and splice are poured at this stage after longitudinal post-tensioning in the previous stage. Since the deck has still not hardened, non-composite sectional girder properties are used to determine the stresses. Prestress losses for this stage include those from elastic shortening, creep, shrinkage, and steel relaxation. Bottom girder stresses are thus:

$$\sigma_{3ab} = -\frac{M_g}{S_{bg}} - \frac{M_d}{S_{bg}} - \frac{M_h}{S_{bg}} - \frac{M_c}{S_{bg}} + \frac{A_{ps} f_{pe3}}{A_g} - \frac{A_{ps} f_{pe3} e_p}{S_{bg}} +$$

$$\frac{n_{po} a_{ps} f_{pof}}{A_g} + \frac{n_{po} a_{ps} f_{pof} e_e}{S_{bg}} \leq 0.6 f_c'. \tag{4-11}$$

Constraint 4ab: *Compression Stress Check under Full Service Load*

Compression stress limits under full service load are checked under this constraint. Only forces from the applied superimposed dead loads, loads from the removal of temporary support, and live loads are resisted by the girder and deck composite section. The previous forces are still resisted by the non-composite girder section. Prestress losses for this constraint include elastic shortening, creep, shrinkage, relaxation of the steel, and additional elastic shortening due to post-tensioning. This stress constraint is thus defined by:

$$\sigma_{4ab} = -\frac{M_g}{S_{bg}} - \frac{M_d}{S_{bg}} - \frac{M_h}{S_{bg}} - \frac{M_r}{S_{bc}} - \frac{M_s}{S_{bc}} - \frac{M_{ll}}{S_{bc}} + \frac{A_{ps} f_{pe4}}{A_g} + \frac{A_{ps} f_{pe4} e_p}{S_{bg}} +$$

$$\frac{n_{po} a_{ps} f_{poff}}{A_g} + \frac{n_{po} a_{ps} f_{poff} e_e}{S_{bg}} \leq 0.6 f'_c. \qquad (4\text{-}12)$$

Constraint 5ab: *Tension Stress Check with Reduced Live Load*

The applied loads and prestress losses for this constraint are similar to *Constraint 4ab* except the live load is reduced by 20 percent in order to check the tension limit state of the girder at the final stage, as defined by:

$$\sigma_{5ab} = -\frac{M_g}{S_{bg}} - \frac{M_d}{S_{bg}} - \frac{M_h}{S_{bg}} - \frac{M_r}{S_{bc}} - \frac{M_s}{S_{bc}} - 0.8\frac{M_{ll}}{S_{bc}} + \frac{A_{ps} f_{pe4}}{A_g} + \frac{A_{ps} f_{pe4} e_p}{S_{bg}} +$$

$$\frac{n_{po} a_{ps} f_{poff}}{A_g} + \frac{n_{po} a_{ps} f_{poff} e_e}{S_{bg}} \geq -0.0724\sqrt{f'_c}\ \text{(MPa) or } -0.19\sqrt{f'_c}\ \text{(ksi)}. \qquad (4\text{-}13)$$

Constraint 6ab: *Compression Stress Check without Live Load*

This constraint considers all loads and prestress losses as in *Constraint 4ab* with the exception of the live load. The compression limit state under these conditions is then checked according to:

$$\sigma_{6ab} = -\frac{M_g}{S_{bg}} - \frac{M_d}{S_{bg}} - \frac{M_h}{S_{bg}} - \frac{M_r}{S_{bc}} - \frac{M_s}{S_{bc}} + \frac{A_{ps} f_{pe4}}{A_g} + \frac{A_{ps} f_{pe4} e_p}{S_{bg}} +$$

$$\frac{n_{po} a_{ps} f_{poff}}{A_g} + \frac{n_{po} a_{ps} f_{poff} e_e}{S_{bg}} \leq 0.45 f'_c. \qquad (4\text{-}14)$$

Constraint 7ab: *Stress Check at Compression for the Partial Service Load*

This critical stress check considers all of the loads of *Constraint 4ab* reduced by 50 percent except for the live load. All of the prestress losses considered for *Constraint 4ab* apply here also. The bottom girder stress check is then defined by:

$$\sigma_{7ab} = 0.5[-\frac{M_g}{S_{bg}} - \frac{M_d}{S_{bg}} - \frac{M_h}{S_{bg}} - \frac{M_r}{S_{bc}} - \frac{M_s}{S_{bc}} + \frac{A_{ps} f_{pe4}}{A_g} + \frac{A_{ps} f_{pe4} e_p}{S_{bg}} +$$

$$\frac{n_{po} a_{ps} f_{poff}}{A_g} + \frac{n_{po} a_{ps} f_{poff} e_e}{S_{bg}}] - \frac{M_{ll}}{S_{tc}} \leq 0.4 f'_c. \qquad (4\text{-}15)$$

d) Results and discussion

A single-span spliced girder bridge with a single-staged post-tensioning applied before pouring the deck was investigated in order to compare its maximum achievable span length with the construction sequences in Method 1 and Method 3. The same

standard beam sections used for Method 1 (see Section 4.5.1d) were used for these analyses.

The achievable span lengths when using this construction method are much shorter than when construction Method 1 is used. Post-tensioning was applied to the non composite section; therefore, there is little gain from post-tensioning besides making the segments continuous. When the three segments become one continuous piece, their flexural demands (which are used to determine the flexural stresses due to the deck load, haunch load, and construction load), increase dramatically due to the increase in span length.

According to the results, a single-span spliced girder bridge with a single-staged post-tensioning applied before pouring the deck is not an efficient construction sequence method as it hardly increases the maximum achievable span length when compared with conventional precast concrete girder use as simple spans. Thus, this construction sequence method is not recommended.

4.5.3 Multi-staged post-tensioning (Method 3)

In this method, the precast/prestressed beams are first installed on temporary supports at the site. Then the first stage of full longitudinal post-tensioning is applied to connect all segments. Spliced joints and diaphragms are then poured and allowed to cure. The deck is added once the spliced and diaphragms have developed enough strength to resist partial loads. After the deck develops enough concrete strength, the second stage of full longitudinal post-tensioning is applied to the continuous segment. The temporary supports are then removed. The optimization problem for this construction stage is formulated in the following.

a) Design variables

Design variables for this construction sequence method are again similar to construction Method 1 (see Section 4.5.1a). The only different design variables for this construction method are the number of post-tensioning strands, which are applied twice: first before pouring the deck and then after the deck is cast.

b) Objective functions

The objective function for this construction sequence method is similar to construction Method 1, which is the minimization of structural cost (see Section 4.5.1b).

c) Design constraints

Stresses at each critical construction stage as listed in

Table **4-10**, are checked against the allowable compression and tension stresses. The allowable concrete stress limits used are those prescribed by the AASHTO-LRFD specifications (AASHTO 2003), which are summarized in Table 4-11. There are 10 critical stage constraints on each location of the composite section. Only the formulation of the girder bottom stress constraints (*Constraints 1am-8am*) for each critical construction stage of service limit state are outlined in the next sections. Similar constraint formulations were formulated and implemented for the stresses at the girder top fiber (*Constraints 1bm-8bmb*) and deck top (*Constraints 1cm-8cm*).

Constraint 1am: *Stress Check at Pre-Tensioning Stage*

Girder loads and pre-tensioning forces for this stage are applied at the same time as for the construction Method 1. Therefore, their girder bottom stress constraint

equation, girder top stress equation, and deck top stress equation are equal to *Constraint 1aa*, *Constraint 1ba,* and *Constraint 1ca*, respectively. This constraint expression is:

$$\sigma_{1am} = -\frac{M_g}{S_{bg}} + \frac{A_{ps} f_{pe1}}{A_g} - \frac{A_{ps} f_{pe1} e_p}{S_{bg}} \leq 0.6 f'_{ci}. \tag{4-16}$$

Table 4-10 *Construction sequence for multi-staged post-tensioning*

Construction Stages	Time (days)	Action Description	Pre-Tensioning Critical Stage	Post-Tensioning Critical Stage
1	-	Stress pre-tensioning strands		
2	0	Cast girder segments		
3	1	Release pre-tensioning strands	X	
4	50	Erect girder segments		
5	75	Stress 1st post-tensioning strands	X	X
6	90	Place deck and splice concrete	X	X
7	120	Stress 2nd post-tensioning strands	X	X
8	130	Add barriers		X
9	140	Apply live load		
10	15000	Add future wearing surface		
11	27500	Condition after all prestress losses	X	X

Constraint 2am: *Stress Check at First Post-Tensioning Stage*

Post-tensioning is applied prior to deck casting; thus, only the non-composite girder section is used to resist the additional loads due to post-tensioning. Prestress losses at this stage are those from elastic shortening, creep, shrinkage, and relaxation of the steel. The bottom stresses are given by:

$$\sigma_{2am} = -\frac{M_g}{S_{bg}} + \frac{A_{ps} f_{pe2}}{A_g} + \frac{A_{ps} f_{pe2} e_p}{S_{bg}} + \frac{n_{po} a_{ps} f_{pof}}{A_g} +$$

$$\frac{n_{po} a_{ps} f_{pof} e_e}{S_{bg}} \le 0.6 f_c'. \qquad (4\text{-}17)$$

Table 4-11 *Allowable concrete stress limits for multi-staged post-tensioning at each construction stage*

Construction Stages	Stress Type	Girder concrete	Deck concrete
1) Prestressing Strand Release	Compression	$0.6f'_{ci}$	
	Tension	-1.4 MPa (-200 psi)	
2) First Post-Tensioning	Compression	$0.6f'_c$	
	Tension	-1.4 MPa (-200 psi)	
3) Deck /Splice Concrete	Compression	$0.6f'_c$	
	Tension	-1.4 MPa (-200 psi)	
4) Second Post-Tensioning	Compression	$0.6f'_c$	$0.6f'_{cd}$
	Tension	$-0.0914\sqrt{f'_c}$(MPa)	$-0.0914\sqrt{f'_{cd}}$ (MPa)
		$-0.24\sqrt{f'_c}$ (ksi)	$0.24\sqrt{f'_{cd}}$ (ksi)
5) Final Condition (after losses)	Compression 1	$0.6\phi_w f'_c$	$0.6\phi_w f'_{cd}$
	Compression 2	$0.45f'_c$	$0.45f'_{cd}$
	Compression 3	$0.4f'_c$	$0.4f'_{cd}$
	Tension 1	$-0.0724\sqrt{f'_c}$ (MPa)	
		$-0.19\sqrt{f'_c}$ (ksi)	

Constraint 3am: *Stress Check at Placement of Deck and Splice Stage*

The deck, haunch and splice are poured at this stage after longitudinal post-tensioning in the second stage. Prestress losses for this stage include those from elastic shortening, creep, shrinkage, and steel relaxation. Bottom girder stresses are limited given by:

$$\sigma_{am} = -\frac{M_g}{S_{bg}} - \frac{M_d}{S_{bg}} - \frac{M_h}{S_{bg}} - \frac{M_c}{S_{bg}} + \frac{A_{ps} f_{pe3}}{A_g} - \frac{A_{ps} f_{pe3} e_p}{S_{bg}} +$$

$$\frac{n_{po1} a_{ps} f_{pof}}{A_g} + \frac{n_{po1} a_{ps} f_{pof} e_e}{S_{bg}} \leq 0.6 f_c'. \tag{4-18}$$

Constraint 4am: *Stress Check at Second Post-Tensioning Stage*

The second post-tensioning operation is conducted after casting of the deck. Thus, the composite girder section is used to resist the additional loads from the post-tensioning forces. Only the forces from the second post-tensioning event are resisted by the composite section of girder and deck. The previous forces are still resisted by the non-composite section. Prestress losses for this constraint include elastic shortening, creep, shrinkage, relaxation of the steel, and additional elastic shortening due to post-tensioning. The bottom girder compression stress constraint is then defined by:

$$\sigma_{4am} = -\frac{M_g}{S_{bg}} - \frac{M_d}{S_{bg}} - \frac{M_h}{S_{bg}} + \frac{A_{ps} f_{pe4}}{A_g} + \frac{A_{ps} f_{pe4} e_p}{S_{bg}} +$$

$$\frac{n_{po1} a_{ps} f_{poff}}{A_g} + \frac{n_{po1} a_{ps} f_{poff} e_e}{S_{bg}} + \frac{n_{po2} a_{ps} f_{pof}}{A_c} +$$

$$\frac{n_{po2} a_{ps} f_{pof} e_e}{S_{bc}} \leq 0.6 f_c'. \tag{4-19}$$

Constraint 5am: *Compression Stress Check under Full Service Load*

Compression stress limits under full service load are checked at this constraint. Only forces from the applied superimposed dead loads, removal of temporary supports, and live loads are resisted by the girder and deck composite section. Forces prior to these are still resisted by the non-composite section. Prestress losses for this constraint include elastic shortening, creep, shrinkage, steel relaxation, and additional elastic shortening due to post-tensioning. The bottom girder stress constraint is then defined as:

$$\sigma_{5am} = -\frac{M_g}{S_{bg}} - \frac{M_d}{S_{bg}} - \frac{M_h}{S_{bg}} - \frac{M_r}{S_{bc}} - \frac{M_s}{S_{bc}} - \frac{M_{ll}}{S_{bc}} + \frac{A_{ps} f_{pe4}}{A_g} + \frac{A_{ps} f_{pe4} e_p}{S_{bg}} +$$

$$\frac{n_{po1} a_{ps} f_{poff}}{A_g} + \frac{n_{po1} a_{ps} f_{poff} e_e}{S_{bg}} + \frac{n_{po2} a_{ps} f_{poff}}{A_c} +$$

$$\frac{n_{po2} a_{ps} f_{poff} e_e}{S_{bc}} \leq 0.6 f'_c. \qquad (4\text{-}20)$$

Constraint 6am: *Tension Stress Check with Reduced Live Load*

The applied loads and prestress losses for this constraint are similar to *Constraint 4am* except that the live load is reduced by 20 percent in order to check the tension limit state of the girder at the final stage as defined by:

$$\sigma_{6am} = -\frac{M_g}{S_{bg}} - \frac{M_d}{S_{bg}} - \frac{M_h}{S_{bg}} - \frac{M_r}{S_{bc}} - \frac{M_s}{S_{bc}} - 0.8\frac{M_{ll}}{S_{bc}} + \frac{A_{ps}f_{pe4}}{A_g} +$$

$$\frac{A_{ps}f_{pe4}e_p}{S_{bg}} + \frac{n_{po1}a_{ps}f_{poff}}{A_g} + \frac{n_{po1}a_{ps}f_{poff}e_e}{S_{bg}} +$$

$$\frac{n_{po2}a_{ps}f_{poff}}{A_c} + \frac{n_{po2}a_{ps}f_{poff}e_e}{S_{bc}} \geq -0.0724\sqrt{f'_c}\ \text{(MPa) or } -0.19\sqrt{f'_c}\ \text{(ksi).} \quad (4\text{-}21)$$

Constraint 7am: *Compression Stress Check without Live Load*

This constraint check considers all loads and prestress losses as in *Constraint 4am* with the exception of live load. The compression limit state under these conditions is then checked according to:

$$\sigma_{7am} = -\frac{M_g}{S_{bg}} - \frac{M_d}{S_{bg}} - \frac{M_h}{S_{bg}} - \frac{M_r}{S_{bc}} - \frac{M_s}{S_{bc}} + \frac{A_{ps}f_{pe4}}{A_g} + \frac{A_{ps}f_{pe4}e_p}{S_{bg}} +$$

$$\frac{n_{po1}a_{ps}f_{poff}}{A_g} + \frac{n_{po1}a_{ps}f_{poff}e_e}{S_{bg}} + \frac{n_{po2}a_{ps}f_{poff}}{A_c} +$$

$$\frac{n_{po2}a_{ps}f_{poff}e_e}{S_{bc}} \leq 0.45f'_c. \quad (4\text{-}22)$$

***Constraint* 8am:** *Stress Check at Compression for Partial Service Load*

This critical stress check considers all of the loads of *Constraint 4am* reduced by 50 percent except for the live load. All the prestress losses considered for *Constraint 4am* apply here also. The girder bottom stress check is then defined by:

$$\sigma_{8am} = 0.5[-\frac{M_g}{S_{bg}} - \frac{M_d}{S_{bg}} - \frac{M_h}{S_{bg}} - \frac{M_r}{S_{bc}} - \frac{M_s}{S_{bc}} + \frac{A_{ps} f_{pe4}}{A_g} + \frac{A_{ps} f_{pe4} e_p}{S_{bg}} +$$

$$\frac{n_{po1} a_{ps} f_{poff}}{A_g} + \frac{n_{po1} a_{ps} f_{poff} e_e}{S_{bg}} + \frac{n_{po2} a_{ps} f_{poff}}{A_c} +$$

$$\frac{n_{po2} a_{ps} f_{poff} e_e}{S_{bc}}] - \frac{M_{ll}}{S_{tc}} \leq 0.4 f'_c. \qquad (4\text{-}23)$$

d) Results and discussion

A single-span spliced girder bridge with multi-staged post-tensioning applied before deck casting was investigated to determine the efficiency of this construction method. These analyses used standard AASHTO I-beams Type III through Type VI.

The results of maximum achievable span lengths for this construction method were found to be between those achieved for the methods of single-stage post-tensioning applied before deck (Method 1) and after deck (Method 2) casting. The reason for the reduced span lengths, compared to construction Method 1, was that the first post-tensioning event was applied to the noncomposite section; thus little benefit is obtained from it at this stage besides making the segments continuous. The second post-tensioning event helps increase the span length because it is applied after the section becomes composite (girder/deck). The deck is cast after the first post-tensioning event; therefore, large moment and flexural stress demands are to be anticipated. Although additional compression stresses were gained through the second post-tensioning operator to aid resisting more flexural loads, the beam can not span as long as when built using

construction Method 1. This is due to stress constraints at the deck casting stage, which control the design of the multi-post-tensioning construction sequence.

According to the results, construction of single-span spliced girder bridges with multi-staged post-tensioning is recommended when future deck replacement is anticipated. By using this method, the beam would not be overstressed once the existing deck is removed. Additionally, this construction method can allowed for longer spans than those achievable through a single-stage post-tensioning operation before deck casting. The disadvantage of this construction method is the cost of the second post-tensioning operation since it requires the contractor to revisit the site once the deck is poured. Also, the backwall cannot be cast until the second post-tensioning operation is finished; thus increasing construction time.

Based on the results for the three construction sequence methods considered in this study, a single-span spliced girder bridge with a single-staged post-tensioning applied after deck pouring is the most efficient construction sequence method since this method provides the longest maximum achievable span length over other construction sequence methods. However, other construction sequence methods were investigated since they may be considered during the design phrase. For example, in areas where future deck replacement is anticipated, a multi-staged construction sequence method may be the best suitable.

4.6 Multicriteria Optimum Design of Single-Span Spliced Girder Bridges

A three-lane single-span PCI-BT 96 spliced girder bridge with single-stage post-tensioned applied after deck casting was chosen herein as a prototype structure to

demonstrate how multicriteria optimization can be applied for a spliced girder bridge. A SSGB with a total width of 18.5 m (61 ft) and maximum beam spacing of 2.7 m (9 ft) was used in this study. The span length is 56.4 m (185 ft) and the system is to use three longitudinally spliced segments with equal length end-segments. The splice location, which is a ratio of the end-segment length (L_1) to the total span length (L), was part of the design variables to determine the most efficient splice location. The girders are to use high-strength concrete with a final compressive strength of 62 MPa (9 ksi) and an initial compressive strength of 34.5 MPa (5 ksi).

4.6.1 Multicriteria objective functions

The selection of the best bridge system may be based on one or more merit criteria, thus the selection of an optimal bridge system may be modeled as a multicriteria objective function. Multicriteria optimization techniques are approaches that couple the processes of design and decision making. A multicriteria objective function is composed of a set of different single objective functions. $F_1(x)$ is an economics multicriteria optimization which can be defined by the following combination: a minimum superstructure cost $f_1(x)$, a minimum number of pre-tensioned strands $f_2(x)$, and a minimum number of post-tensioned strands $f_3(x)$. These objective functions can be defined as follows:

$$F_1(x)_{min} = Economics\ multicriteria$$

$$= [f_1(x)_{min}\ f_2(x)_{min} f_3(x)_{min}] \tag{4-24}$$

$$f_1(x) = Min.\ superstructure\ cost$$

$$= C_{PS} + C_{PT} + C_{CD} + C_{TS} + C_B + C_R \tag{4-25}$$

$f_2(x)$ = *Min. number of pre-tensioning strands*

$$= npr_{11} + npr_{21} + npr_{31} + npr_{41} + npr_{12} + npr_{22} + npr_{32} + npr_{42} + nprt_1 + nprt_2 \quad (4\text{-}26)$$

$f_3(x)$ = Min. number of post-tensioning strands = npo. (4-27)

Each single objective function was formulated separately to determine its optimal design solution. Details of minimum superstructure cost for the objective function in Equation (4-25) were presented earlier in Table 4-2.

4.6.2 Comparison results of single-objective optimizations

Optimal design variable solutions for each of the single objective function were obtained and the results are summarized in Table 4-12. Detailed design variable notations were specified in Section 4.5.1a and are not repeated here.

The most efficient splice location *(pra)* for all of the single objective functions yielded the same result: 0.25(L). As expected, the minimization of the number of post-tensioning strands (function f_3) yields the maximum number of pre-tensioning strands. Conversely, the minimization of pre-tensioning strands (function f_2) yields the maximum number of post-tensioning strands. Minimization of construction cost yielded the same post-tensioning requirements as that from the minimization of post-tensioned strands (thirty seven strands). However, it should be noted that this objective function (minimum construction cost) required less number of pre-tensioning strands than found from the minimization of pre-tensioning strands (function f_e), and a greater number of pre-tensioning strands than found when minimizing the number of post-tensioning strands (function f_e).

Table 4-12 *Optimization results for each objective function*

Design Variables	L = 56.4 m (185 ft)		
	$f_1(x)$ Min Const cost	$f_2(x)$ min npr_{ii}	$f_3(x)$ min *npo*
npr_{11}	8	2	7
npr_{21}	0	0	6
npr_{31}	0	0	5
npr_{41}	0	0	1
npr_{12}	8	10	8
npr_{22}	8	0	8
npr_{32}	8	0	8
npr_{42}	2	0	2
npo	37	61	37
y_a	406 mm (16")	965 mm (38")	965 mm (38")
y_{bb}	178 mm (7")	178 mm (7")	178 mm (7")
npt_1	2	2	4
npt_2	6	2	6
pra	0.25	0.25	0.25
Objective	$6,181,501	16	37
npr_{ii} (total)	43	16	57
Construction cost	$6,181,501	$8,00,1793	$6,568,841

The discussion of results above shows that the optimal solutions for the objective functions considered can be very different, especially when they contradict each other. Thus, multicriteria optimization should be used to obtain compromised solutions with the same given parameters (span length, beam spacing, and splice locations).

4.6.3 Pareto optima results and discussion

When all objective criteria are not equally important, or when there exist conflicting criteria, vector optimization is used to select the preferred solution in a more

rational way. Multicriteria optimization techniques are used to generate a set of pareto optima that are non-dominant solutions.

After obtaining solutions of each single objective function the range of minimum and maximum values were identified. The numbers of total pre-tensioning strands were thus varied from 16 to 57 strands while the numbers of post-tensioning strands were varied from 37 to 61, as shown in Table 4-12.

Pareto optima sets were generated by the constraint approach, which is based on the adoption of one criterion as a scalar primary objective function and the transformation of other objective criteria into constraints bounded by some predetermined constants. These scalar constraints are altered from the range of minimum to maximum values, and the subset of pareto optima is generated.

As previously stated, the multicriteria objective herein (Equation 4-24) is composed of three single objective functions. The combinations of single objective functions were selected as pairs to determine the pareto optima set. There were four pairs of objective functions selected in this study. Each pair of objective functions had one primary objective function and the other objective functions were set as constraints.

The constraints were divided into arbitrary intervals. As the interval range decreases, the accuracy of results is closer to the real compromised results. Since it is impossible to generate the entire pareto optima set, a subset of the pareto optima represented by six solutions was generated. Therefore, the predetermined constant constraints in this study were divided into five intervals.

1. The first pair of objective functions was to set a minimum total number of pre-tensioning strands as the main objective function while varying the total number of post-tensioning strands as constraints.
2. The second pair of objective functions was such that the minimization of the total number of post-tensioning strands was the main objective function while the varying number of total pre-tensioning strands was a constraint.
3. The third pair of objective functions was to set minimum superstructure construction cost as the main objective function while the numbers of total pre-tensioning strands were set as a constraint.
4. The fourth pair of objective functions was such that number of total pre-tensioning strands was the main objective function to be minimized while minimum superstructure construction cost was set as a constraint.

Subsets of pareto optima were thus generated for the different objective function pairs. The selection of the best solution from these subsets was decided based on compromising programming. The criterion used in compromising programming is the minimization of the normalized deviation from the ideal solution f_{min} measured by the family of distance metrics L_p .The value of L_p indicates how close the solution is to the ideal solution. The satisfying solution can be determined by selecting the minimum normalized deviation (L_p) between the minimum euclidean distance (p = 2) and the minimum largest deviation (p = ∞). This approach is also called the "Minimax Criterion" and is formulated by:

$$\min L_p(x) = \min_{x\in\Omega}[\sum_{i=1}^{m} | \frac{f_i(x) - \min f_i(x)}{\max f_i(x) - \min f_i(x)} | p]^{1/p} \quad ; (1 \le p \le \infty) \ . \qquad (4\text{-}28)$$

The first set of pareto results having the number of pre-tensioning strands as the main objective function to be minimized and the number of post-tensioning strands as a constraint are given in Table 4-13. The Euclidian distance and maximum distance of these pareto sets are best at $L_2(x)$ = 0.50 and $L_\infty(x)$ = 0.37, respectively, which are the minimum numbers of those values. These values correspond to Solution # 3 (see bold values in Table 4-13) where *npo* = 45 and npr_{ii} = 30.

Results for the second pareto set having number of post-tensioning strands as an objective and numbers of pre-tensioning strands as constraints are given in Table 4-14. The Euclidian distance and maximum distance of these pareto sets are best at $L_2(x)$ = 0.51 and $L_\infty(x)$ = 0.39, respectively (see bold values in Table 4-14). These values correspond to Solution # 3 where *npo* = 45 and npr_{ii} = 32.

Table 4-13 *Pareto set of npr_{ii} as objective and npo as constraint (case 1)*

Solution	Constraints $f_3(x)$ min npo	Objective function $f_2(x)$ min npr_{ii}	(f_3-minf_3) df_1,max	(f_2-minf_2) df_2,max	$L_\alpha(x)$ Maximum distance	$L_2(x)$ Euclidian distance
1	37	57	0.00	1.00	1.00	1.00
2	42	37	0.20	0.52	0.52	0.55
3	**45**	**30**	0.37	0.34	**0.37**	**0.50**
4	51	23	0.59	0.16	0.59	0.61
5	56	20	0.80	0.09	0.80	0.81
6	61	16	1.00	0.00	1.00	1.00

Table 4-14 *Pareto set of npo as objective and npr_{ii} as constraint (case 2)*

Solution	Constraints $f_2(x)$ min npr_{ii}	Objective function $f_3(x)$ min npo	(f_2-minf_2) df_2,max	(f_3-minf_3) df_3,max	$L_\alpha(x)$ Maximum distance	$L_2(x)$ Euclidian distance
1	16	61	0.00	1.00	1.00	1.00
2	24	50	0.20	0.55	0.55	0.58
3	**32**	**45**	0.39	0.32	**0.39**	**0.51**
4	40	39	0.59	0.07	0.59	0.59
5	48	37	0.78	0.00	0.78	0.78
6	57	37	1.00	0.00	1.00	1.00

Third pareto set results having minimum construction cost as an objective and numbers of pre-tensioning strands as constraints are given in

Table **4-15**. The Euclidian distance and the maximum distance of these pareto sets are minimum at $L_2(x) = 0.57$ and $L_\infty(x) = 0.41$, respectively (see bold values in Table 4-15). These values correspond to Solution # 3 where minimum construction cost = \$6,932,341 and $npr_{ii} = 27$.

Table 4-15 *Pareto set of min construction cost as objective and npr_{ii} as constraint(case 3)*

Solution	Constraints $f_2(x)$ min npr_{ii}	Objective function $f_1(x)$ min cost	(f_2-minf_2) df_2,max	(f_1-minf_1) df_1,max	$L_\alpha(x)$ Maximum distance	$L_2(x)$ Euclidian distance
1	16	\$8,001,793	0.00	1.00	1.00	1.00
2	22	\$7,209,841	0.20	0.56	0.56	0.60
3	**27**	**\$6,920,341**	0.40	0.41	**0.41**	**0.57**
4	32	\$6,682,591	0.60	0.28	0.60	0.66
5	38	\$6,32,1841	0.80	0.08	0.80	0.80
6	43	\$6,181,501	1.00	0.00	1.00	1.00

Results from the fourth pareto set having the minimization of pre-tensioning strands as an objective and minimum construction cost as a constraint are listed in Table 4-16. The Euclidian distance and maximum distance of these pareto sets are minimum at $L_2(x)$ = 0.54 and $L_\infty(x)$ = 0.40, respectively (see bold numbers in Table 4-16). These values correspond to Solution # 3 where minimum construction cost = $6,909,618 and npr_{ii} = 26.

Table 4-16 *Pareto set of min npr_{ii} as objective and min construction cost as constraint (case 4)*

Solution	Constraints $f_1(x)$ min cost	Objective function $f_2(x)$ min npr_{ii}	(f_1-minf_1) df_1,max	(f_2-minf_2) df_2,max	$L_\alpha(x)$ Maximum distance	$L_2(x)$ Euclidian distance
1	$6,181,501	43	0.00	1.00	1.00	1.00
2	$6,545,560	34	0.20	0.67	0.67	0.70
3	**$6,909,618**	**26**	0.40	0.36	**0.40**	**0.54**
4	$7,273,676	21	0.60	0.17	0.60	0.62
5	$7,637,735	20	0.80	0.13	0.80	0.81
6	$8,001,793	16	1.00	0.00	1.00	1.00

Results for the second pareto optima subset represented by six solutions is illustrated in Figure 4-4 while Figure 4-5 illustrates the results for the third pareto optima set. Figure 4-4 shows the relationship of pre-tensioning strands and post-tensioning requirements when one of them is the main objective function and the other is transformed to be a predetermined constant constraint and vice versa.

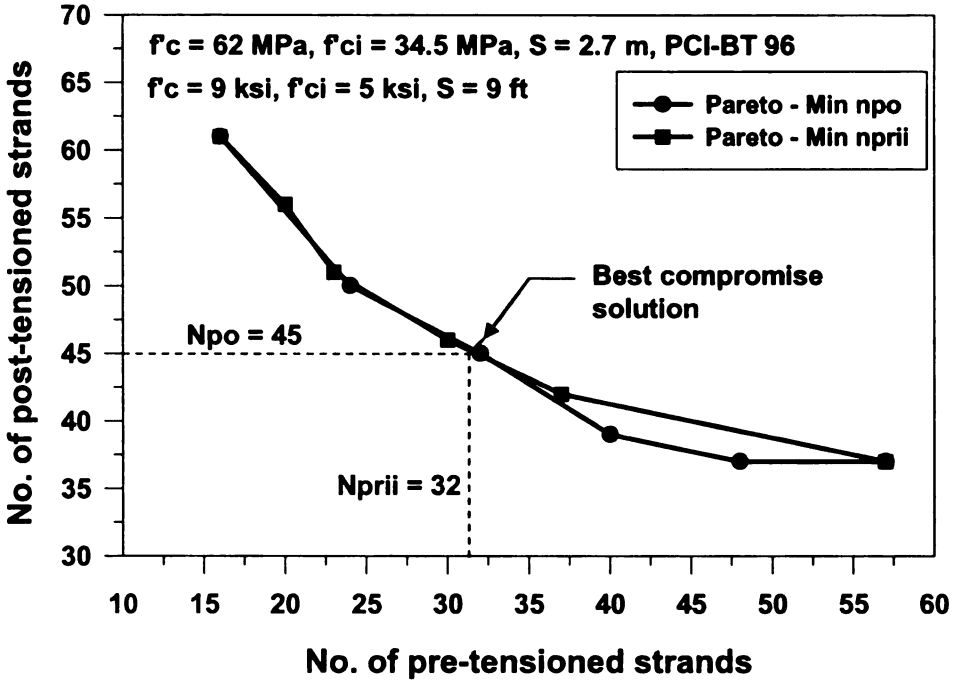

Figure 4-4. *Pareto set of pre-tensioned strand and post-tensioned strands*

The same approach was applied for Figure 4-5, which shows the relationship of pre-tensioning strand requirements and superstructure construction cost. The best compromise solution of these objective functions is indicated by the dashed line in these figures and also in bold font in Table 4-13 to Table 4-16.

Once the best compromise solution is obtained, the design variables that correspond to this can be determined directly from the optimization outputs. These design variables are illustrated in Table 4-17. Optimal solutions for the multicriteria optimization problem are as shown in Figure 4-4 (npo = 45 and npr_{ii} = 32). This optimal solution also yields the minimum superstructure construction cost.

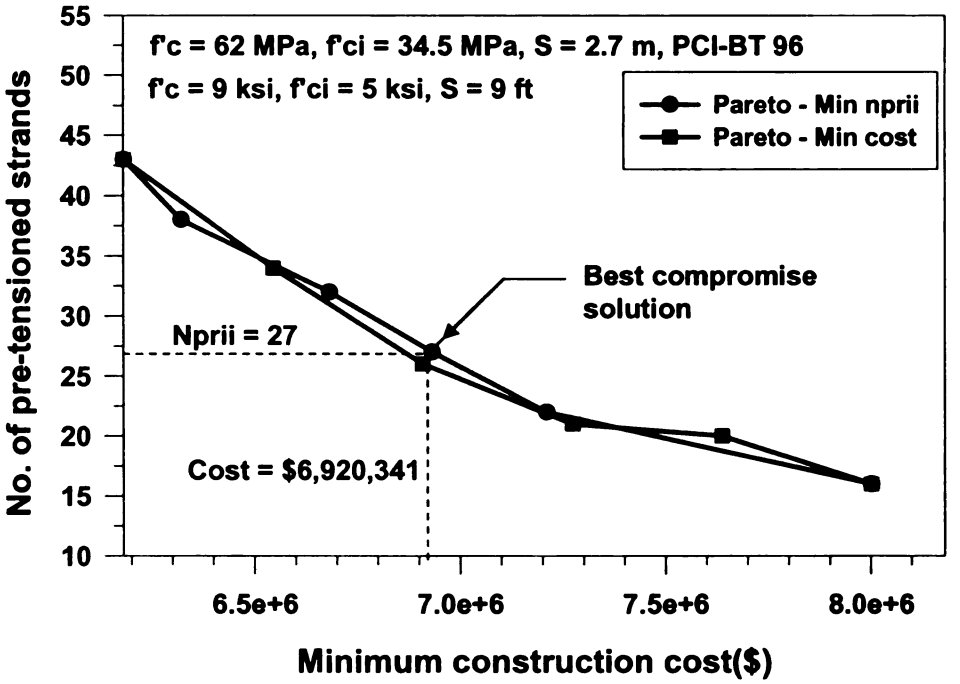

Figure 4-5. *Pareto set of pre-tensioned strand and minimum superstructure construction cost*

It can be noted that the design variable values for the optimal solution are between the minimum and maximum range obtained in Section 4.6.2. Our multicriteria optimal solution through compromising programming is non-dominated with regard to all criteria, which ensures the best compromise between all of them.

Table 4-17 *Design variables of best solutions of each pareto set*

	1st Pair	2nd Pair	3rd Pair	4th Pair
Main objective	**Min npr_{ii}**	**Min *npo***	**Min cost**	**Min npr_{ii}**
Constant Constraint	***npo***	**npr_{ii}**	**npr_{ii}**	**Cost**
npr_{11}	3	4	2	2
npr_{21}	0	0	0	0
npr_{31}	0	0	0	0
npr_{41}	0	0	0	0
npr_{12}	8	8	7	7
npr_{22}	7	7	6	6
npr_{32}	5	5	5	5
npr_{42}	1	1	1	1
npo	46	45	48	48
y_a	406 mm (16")	406 mm (16")	406 mm (16")	483 mm (16")
y_{bb}	178 mm (7")	178 mm (7")	178 mm (7")	178 mm (7")
npt_1	2	2	2	2
npt_2	4	4	4	4
npr_{ii}	30	32	27	26
Min const cost	$6,766,113	$6,699,649	$6,869,535	$6,909,622

4.7 Parametric Studies

4.7.1 Assumption and procedure for parametric studies

The goal of the study was to compare the effectiveness of several design options for extending the span range of longitudinally spliced precast/prestressed concrete girders. Parametric studies were done by considering both material and geometry of the structure to determine the maximum achievable span length.

A single-span spliced precast/prestressed girder bridge comprised of three segments, with single-stage post-tensioning applied after pouring the deck and a

composite deck was selected for the comparative design study. The PCI-BT 96 girder, with a spacing of 2.7 m (9 ft) and with a splice location at 0.25 of the total span length, was used in this study. The spliced location at 0.25 of the total span length was chosen since it was shown to be the most efficient splice location in the system optimization studies (see Section 4.6.2).

The base design of this study represents a typical design with normal weight concrete 2403 kg/m^3 (150 lb/ft^3) for both deck and girder. The concrete compressive strength for the girder at the final condition was taken as f_c' = 44.8 MPa (6.5 ksi) and that at the initial state taken as f_{ci}' = 34.5 ksi (5 ksi). The concrete compressive strength of deck at the final age was f_{cd}' = 31 Mpa (4.5 ksi). Pre-tensioned strands and post-tensioned strands are designed based on 15.24 mm (0.6 in.) diameter. A single-stage post-tensioning construction method was used in this comparative study since it was shown to yield a longer span than any other of the investigated construction sequences (see Section 4.5.1).

4.7.2 Material parametric studies for PCI-BT 96 beams

Maximum spans were determined for the single-span spliced girder bridge using the selected material design variations for a comparative design study. Calculations were performed using a custom program written in the MATLAB environment and included the minimization of superstructure cost as the main objective in the design optimization process.

Four major design variations on the base design were considered for the PCI-BT 96 spliced girder system. The variations ranged from examining the effect of concrete compressive strength to modifying the unit weight of concrete for the girder and deck. Following are the alternative designs that were developed through this study.

a) High strength concrete girders

The final high-strength concrete compressive strength (f_c') of precast girder was varied from 44.8 to 82.7 MPa (6.5 to 12 ksi) in increments of 3.5 MPa (0.5 ksi), while the concrete compressive strength at release (f_{ci}') of the precast girder was increased by $0.8f_c'$. The concrete compressive strength of deck at the final age was f'_{cd} = 31 Mpa (4.5 ksi). Normal weight concrete for both girder and deck was assumed. Table 4-18 losts the percentage increase of PCI-BT 96 span length when the strength of concrete is increased in 3.5 MPa (0.5 ksi) increments.

b) Lightweight concrete girders

The effect of reduced weight of the concrete in the girders was investigated by varying its unit weight from 1602 to 2402 Kg/m^3 (100 to 150 lb/ft^3) in increments of 160 Kg/m^3 (10 lb/ft^3). The strength of the concrete girder remained unchanged from the base design. Thus, this option simply reduces the weight of the girders. Table 4-19 lists the percentage increase for the PCI-BT 96 spliced span length when the unit weight of concrete for the girders is decreased in 160 Kg/m^3 (10 lb/ft^3) increments.

Table 4-18 *Effect of girder concrete strength on spanning increase of PCI-BT 96*

Case	Description	w_c kg/m^3 (pcf)	w_{cd} kg/m^3 (pcf)	f'_c MPa (ksi)	f'_{ci} MPa (ksi)	f'_{cd} MPa (ksi)	Max. span m (ft)	Span Increase m (ft)	% increase
1fc	Base design	2402	2402	**44.8**	**35.9**	31.0	64	0	0%
		(150)	(150)	**(6.5)**	**(5.2)**	(4.5)	(210)	(0)	0%
2fc	Increased f'_c	2402	2402	**48.3**	**38.6**	31.0	64.3	0.3	0.5%
		(150)	(150)	**(7.0)**	**(5.6)**	(4.5)	(211)	1	0.5%
3fc	Increased f'_c	2402	2402	**51.7**	**41.3**	31.0	64.6	0.6	0.95 %
		(150)	(150)	**(7.5)**	**(6)**	(4.5)	(212)	2	0.95 %
4fc	Increased f'_c	2402	2402	**55.2**	**44.1**	31.0	64.8	0.7	1.1%
		(150)	(150)	**(8.0)**	**(6.4)**	(4.5)	(212.5)	2.5	1.1%
5fc	Increased f'_c	2402	2402	**58.6**	**49.6**	31.0	64.9	0.9	1.4%
		(150)	(150)	**(8.5)**	**(55.2)**	(4.5)	(213)	3	1.4%
6fc	Increased f'_c	2402	2402	**62.1**	**55.2**	31.0	65.1	1.0	1.7%
		(150)	(150)	**(9.0)**	**(8)**	(4.5)	(213.5)	3.5	1.7%
7fc	Increased f'_c	2402	2402	**65.5**	**60.7**	31.0	65.2	1.2	1.9%
		(150)	(150)	**(9.5)**	**(8.8)**	(4.5)	(214)	4	1.9%
8fc	Increased f'_c	2402	2402	**68.9**	**66.2**	31.0	65.4	1.3	2.1%
		(150)	(150)	**(10.0)**	**(9.6)**	(4.5)	(215)	4.5	2.1%

Table 4-19 *Effect of girder concrete weight on spanning increase of PCI-BT 96*

Case	Description	w_c kg/m^3 (pcf)	w_{cd} kg/m^3 (pcf)	f'_c MPa (ksi)	f'_{ci} MPa (ksi)	f'_{cd} MPa (ksi)	Max. span m (ft)	Span Increase m (ft)	Percent increase
1wc	Base design	2402	2402	44.8	34.5	31.0	64	0	0%
		(150)	(150)	(6.5)	(5)	(4.5)	(210)	(0)	(0%)
2wc	Reduced w_c	**2243**	2402	44.8	34.5	31.0	65.2	1.2	2%
		(140)	(150)	(6.5)	(5)	(4.5)	(214)	(4)	(2%
3wc	Reduced w_c	**2082**	2402	44.8	34.5	31.0	65.8	1.8	2.8%
		(130)	(150)	(6.5)	(5)	(4.5)	(216)	(6)	(2.8%
4wc	Reduced w_c	**1922**	2402	44.8	34.5	31.0	66.8	2.7	4.2%
		(120)	(150)	(6.5)	(5)	(4.5)	(219)	(9)	(4.2%)
5wc	Reduced w_c	**1762**	2402	44.8	34.5	31.0	67.4	3.3	5.2%
		(110)	(150)	(6.5)	(5)	(4.5)	(221)	(11)	(5.2%)
6wc	Reduced w_c	**1602**	2402	44.8	34.5	31.0	68.3	4.2	6.7%
		(100)	(150)	(6.5)	(5)	(4.5)	(224)	(14)	(6.7%)

c) Lightweight concrete deck

The effect of reduced concrete deck weight was investigated by varying the concrete unit weight from 1602 to 2402 Kg/m^3 (100 to 150 lb/ft^3) in increments of 160 Kg/m^3 (10 lb/ft^3). The concrete strength for the deck remained unchanged from the base design. Thus, this option only reduces the weight of the deck placed on the bridge. Table 4-20 gives the percentage increase of PCI-BT 96 span length when the unit weight of concrete in the deck is decreased in 160 Kg/m^3 (10 lb/ft^3) increments.

Table 4-20 *Effect of lightweight concrete deck on spanning increase of PCI-BT 96 bridge*

Case	Description	w_c kg/m^3 (pcf)	w_{cd} kg/m^3 (pcf)	f'_c MPa (ksi)	f'_{ci} MPa (ksi)	f'_{cd} MPa (ksi)	Max. span m (ft)	Span Increase m (ft)	Percent increase
1wcd	Base design	2402	2402	44.8	34.5	31.0	64	0	0%
		(150)	(150)	(6.5)	(5)	(4.5)	(210)	(0)	(0%)
2wcd	Decreased w_{cd}	2402	**2243**	44.8	34.5	31.0	64.9	0.9	1.4%
		(150)	**(140)**	(6.5)	(5)	(4.5)	(213)	(3)	(1.4%)
3wcd	Decreased w_{cd}	2402	**2082**	44.8	34.5	31.0	65.5	1.5	2.4%
		(150)	**(130)**	(6.5)	(5)	(4.5)	(215)	(5)	(2.4%)
4wc	Decreased w_{cd}	2402	**1922**	44.8	34.5	31.0	65.9	1.8	2.9%
		(150)	**(120)**	(6.5)	(5)	(4.5)	(216)	(6)	(2.9%)
5wcd	Decreased w_{cd}	2402	**1762**	44.8	34.5	31.0	66.8	2.7	4.3%
		(150)	**(110)**	(6.5)	(5)	(4.5)	(219)	(9)	(4.3%)
6wcd	Decreased w_{cd}	2402	**1602**	44.8	34.5	31.0	67.1	3.0	4.8%
		(150)	**(100)**	(6.5)	(5)	(4.5)	(220)	(10)	(4.8%)

d) Lightweight concrete beam and deck

The effect of reduced weight in both girders and deck was investigated by considering concrete with unit weights varying from 1602 to 2402 Kg/m^3 (100 to 150 lb/ft^3). The strength of the concrete for both girder and deck remained unchanged from the base design. Therefore, this option only reduces the weight of the girder and deck placed on the bridge. Table 4-21 gives the percentage increase of PCI-BT 96 span length when the unit weight of the deck concrete (w_{cd}) and the unit weight of the girder concrete (w_c) is decreased in 160 Kg/m^3 (10 lb/ft^3) increments.

Table 4-21 *Span increase of lightweight concrete girder PCI-BT 96 and lightweight deck*

Case	Description	w_c kg/m^3 (pcf)	w_{cd} kg/m^3 (pcf)	f'_c MPa (ksi)	f'_{ci} MPa (ksi)	f'_{cd} MPa (ksi)	Max. span m (ft)	Span Increase m (ft)	Percent increase
1w	Base design	2402	2402	44.8	34.5	31.0	64.0	0	0%
		(150)	(150)	(6.5)	(5)	(4.5)	(210)	(0)	0%
2w	Decreased	**2243**	**2243**	44.8	34.5	31.0	65.5	1.5	2.4%
	w_c & w_{cd}								
		(140)	**(140)**	(6.5)	(5)	(4.5)	(215)	(5)	2.4%
3w	Decreased	**2082**	**2082**	44.8	34.5	31.0	67.0	3	4.8 %
	w_c & w_{cd}								
		(130)	**(130)**	(6.5)	(5)	(4.5)	(220)	(10)	4.8 %
4w	Decreased	**1922**	**1922**	44.8	34.5	31.0	68.3	4.3	6.7%
	w_c & w_{cd}								
		(120)	**(120)**	(6.5)	(5)	(4.5)	(224)	(14)	6.7%
5w	Decreased	**1762**	**1762**	44.8	34.5	31.0	70.1	6.1	9.5%
	w_c & w_{cd}								
		(110)	**(110)**	(6.5)	(5)	(4.5)	(230)	(20)	9.5%
6w	Decreased	**1602**	**1602**	44.8	34.5	31.0	71.3	7.3	11.4%
	w_c & w_{cd}								
		(100)	**(100)**	(6.5)	(5)	(4.5)	(234)	(24)	11.4%

e) Discussion of material parametric studies

The design results for all cases are listed in Table 4-18 to Table 4-21, which include maximum span lengths, span length increase, and the percentage increase in maximum span compared to the base design. The effect of girder concrete compressive strength with achievable span length is illustrated in Figure 4-6. The base design for the PCI-BT 96 girder yielded a maximum span of 64 m (210 ft), see Table 4-20 at the base design row. Increasing the concrete strength of the PCI BT-96 girders, yields a 1.5 percentage increase in span length, which is a minimal increase compared with the cost increase associated with a higher strength concrete. The high-strength concrete girder has increased the span length from 64 m (210 ft) to 65.4 m (214.5 ft). Since the design of

spliced girder bridge is normally not governed by stresses at the release stage, increasing the girder concrete compressive strength would not be effective.

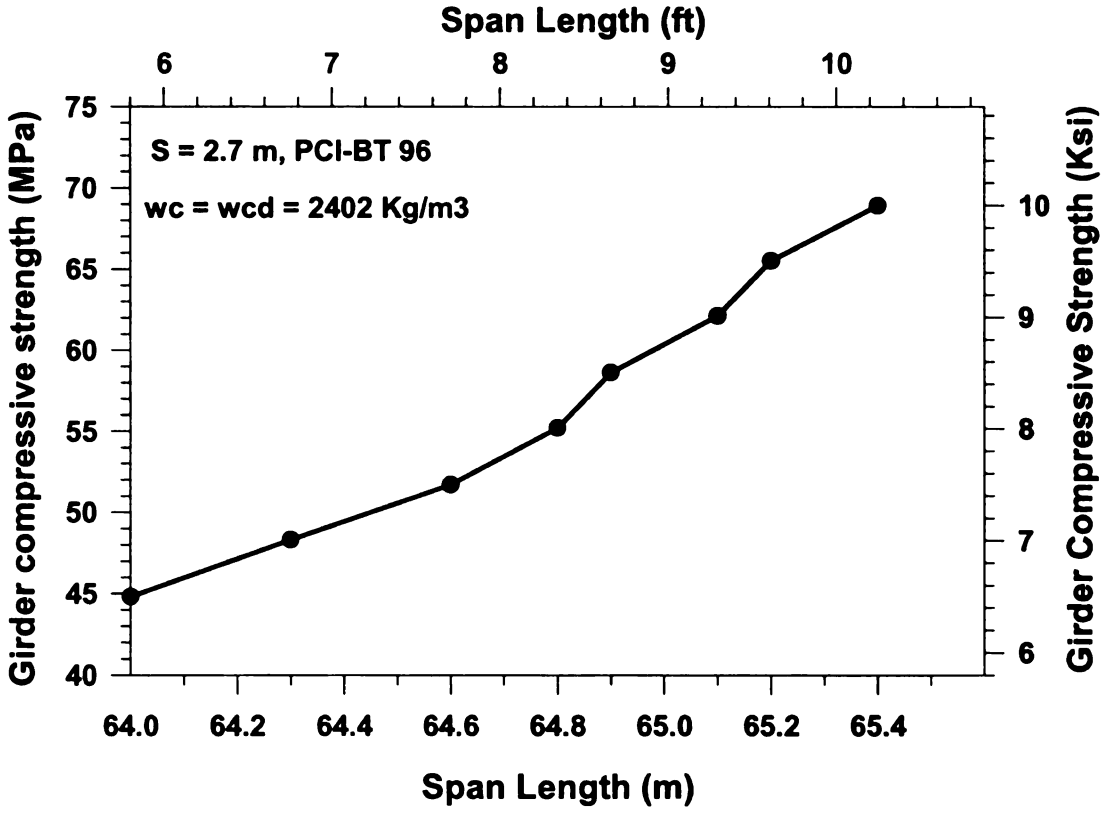

Figure 4-6 *Effect of girder concrete compressive strength on span length*

The effect of lightweight girder concrete on span length is illustrated in Figure 4-7. The use of lightweight concrete on the girders is shown to increase the system span length from 64 m (210 ft) to 68.3 m (224 ft) and provided an increase of 6.7 percent in span length when the girder unit weight was reduced by 801 kg/m^3 (50 lb/ft^3).

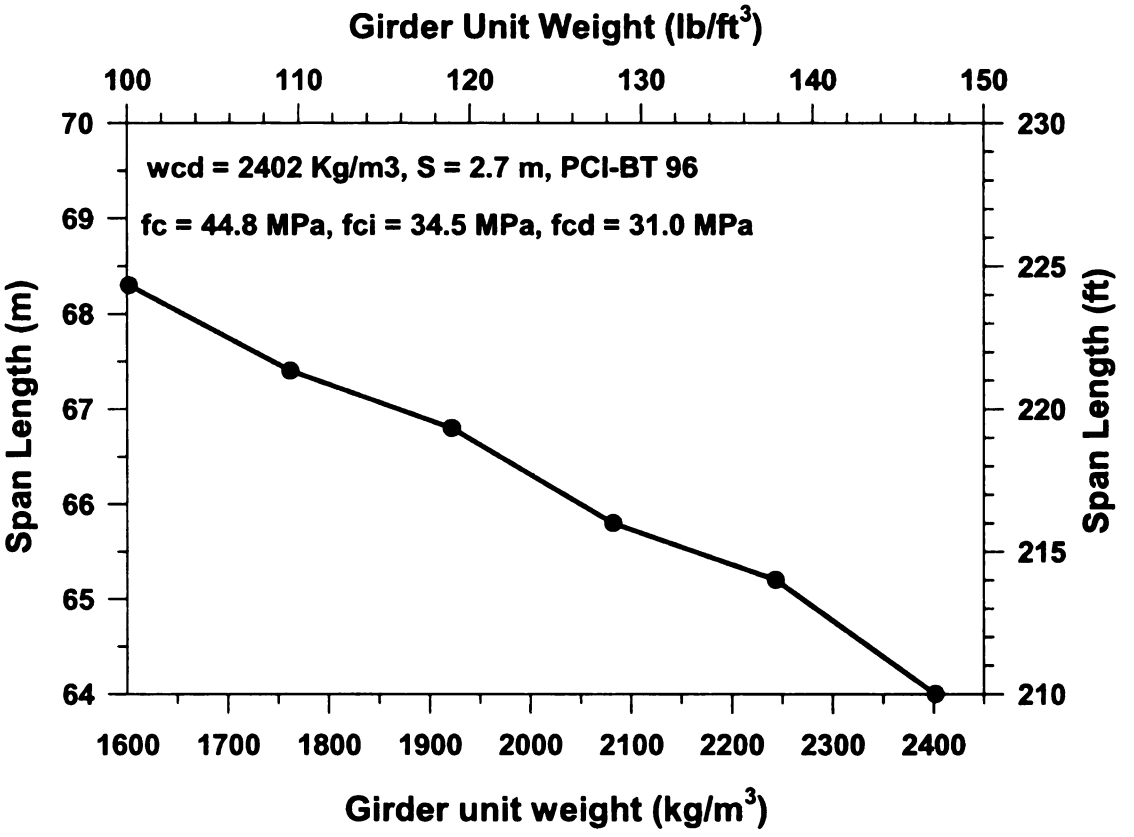

Figure 4-7 *Effect of girder unit weight on span length*

Figure 4-8 illustrates the effect of utilizing lightweight concrete for the deck on the system span length. The lightweight concrete deck is shown to increase the span length from 64 m (210 ft) to 67.1 m (220 ft) and provides an increase of 4.8 percent in span length when the deck unit weight was reduced by 801 kg/m^3 (50 lb/ft^3). Although this option may not increase the span as long as when using lightweight concrete for the girders, the use of lightweight concrete in the deck generates less design issues of concern than lightweight concrete in the girders. When lightweight concrete is used in prestressed girders, different design issues need to be carefully considered, especially for the prestress losses. Thus, the use of lightweight concrete on the deck only may be a good option for increasing span length.

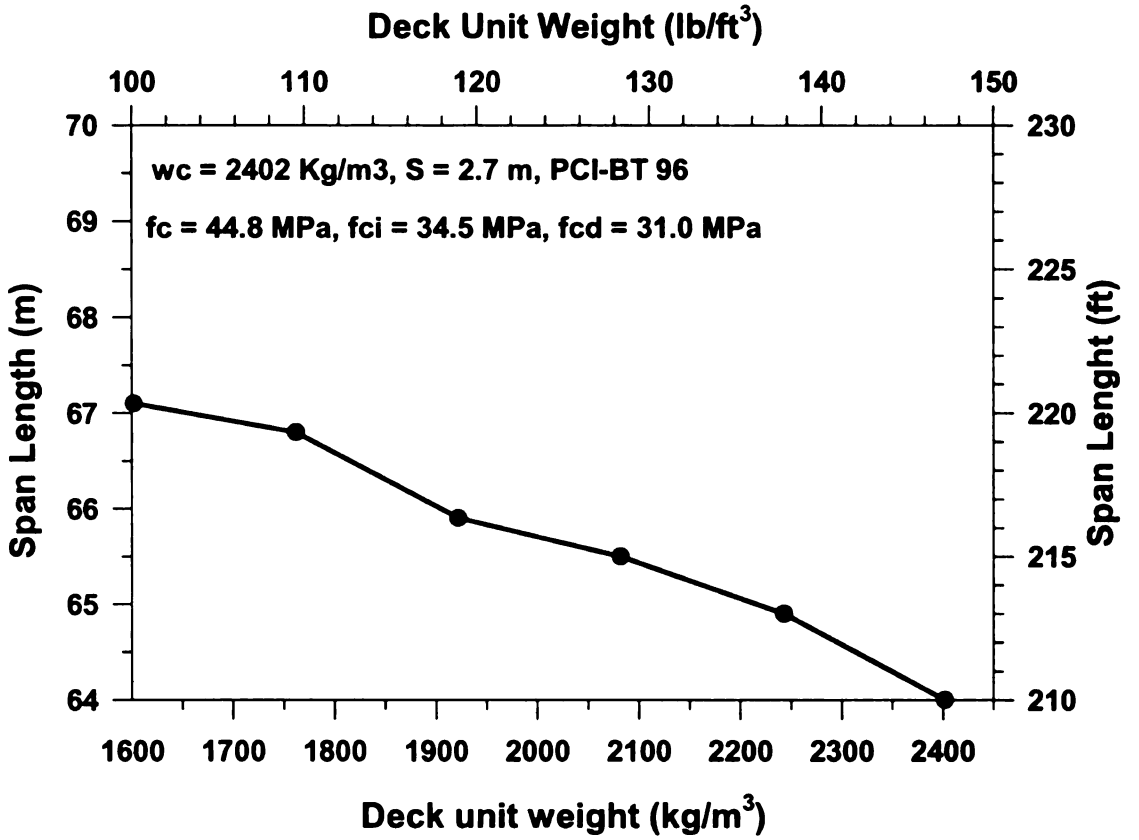

Figure 4-8 *Effect of deck unit weight on span length*

The maximum span length increase was obtained when using a combination of lightweight concrete for both girders and deck. Figure 4-9 shows the effect of utilizing lightweight concrete for the girders and the deck and its influence on span length. The use of lightweight concrete is shown to increase span length from 64 m (210 ft) to 71.3 m (234 ft) and thus provide an increase of 11.4 percent in span length when both the girder and deck concrete unit weight was reduced by 801 kg/m^3 (50 lb/ft^3).

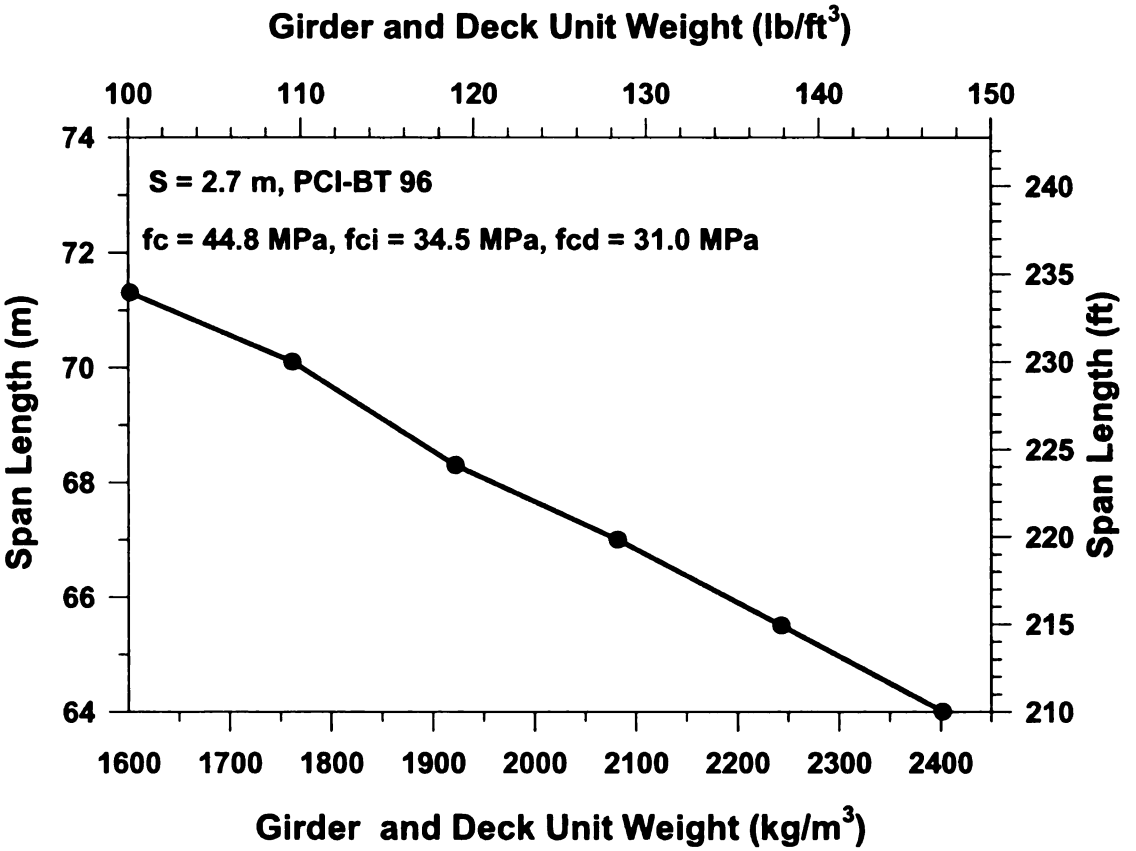

Figure 4-9 *Effect of girder and deck unit weight on span length*

The utilization of lightweight concrete for the beam, deck, or both provides an increase of maximum span because of the 160-801 kg/m^3 (10-50 lb/ft^3) reduction in concrete unit weight. The combination of options for increasing span ranges may be significantly different from the effect of individual options.

Analyses results were compared to give an indication of the effectiveness of each design option for increasing the maximum span. Results from this study should be considered as an indication of trends. In some cases, where girder section type, girder spacing, splice locations, and other conditions are changed, the effect of different alternatives may vary. Thus, the results from these comparisons must be considered as specific cases.

4.7.3 Parametric studies on girder types

Different girder types with equal or nearly equal heights were considered in this study to evaluate their maximum achievable span lengths. The girders under consideration were the MI-1800 I-beam (Michigan DOT), AASHTO's Type VI beam, and PCI's BT-72 beam. The maximum span length for each girder type with a beam spacing of 2.4 m (8 ft) was obtained for the base design (i.e. unspliced simple span) and four design variations. Non-composite section properties and general girder dimensions are given in Table 4-22.

Table 4-22 *Non-composite section properties of 1.8 m (6 ft) high girders*

Girder Type	H m (in.)	Y_{bg} m (in.)	A m^2 ($in.^2$)	I m^4 ($in.^4$)	t_w m (in.)	W_b m (in.)	W_t m (in.)
PCI-72	1.829 (72)	0.930 (36.60)	0.495 (767)	227 (545,857)	0.152 (6)	0.660 (26.00)	1.067 (42.00)
MI-1800	1.829 (72)	0.844 (33.23)	0.565 (875)	260 (624,700)	0.152 (6)	0.902 (35.50)	1.200 (47.25)
AASHTO Type VI	1.829 (72)	0.924 (36.38)	0.700 (1085	305 (733,319)	0.203 (8)	0.711 (28.00)	1.067 (42.00)

The base design is based on normal weight concrete 801 kg/m^3 (150 lb/ft^3) in both the girders and in the deck. The girder concrete compressive strength at release is taken as 34.5 MPa (5 ksi) and the girder concrete compressive strength at final

conditions is taken as 44.8 MPa (6.5 ksi). The parameters changed in the four design variations were:

a) High strength concrete girder $f_c' = 68.9$ MPa (10 ksi) and $f'_{ci} = 55.2$ MPa (8 ksi),

b) Lightweight concrete deck at 1922 kg/m^3 (120 lb/ft^3),

c) Lightweight concrete girders at 1922 kg/m^3 (120 lb/ft^3),

d) Lightweight concrete girders and deck at 1922 kg/m^3 (120 lb/ft^3).

The increase in maximum span length for the four design variations over the base design for each girder type indicates a different effect for the different girder types. The MI-1800 girder is the most efficient section compared with other beam types of equal depth. Even though the MI-1800 I-beam cross-section area is smaller than that of the AASHTO Type IV, it was shown to span longer for all design cases. This is due to its large top and bottom flange width, which allows it to contain more pre-tensioned strands on each row and thus have increase efficiency over the AASHTO Type IV and PCI-BT 72 girders.

Comparison of *base designs* for different girder types indicates that the MI-1800 I-beams and the AASTHO Type VI girder achieve the largest and equal maximum span length of 54.9 m (180 feet), while PCI-72 achieves a smaller maximum span of 50.9 m (167 feet). These base maximum span lengths are used as comparison with the maximum span length of design variation cases in Section 4.7.2.

The lightweight concrete MI-1800 girder with a lightweight concrete deck had the greatest maximum span length for all design variation cases. This design increased the achievable span length from 54.9 m (180 feet) of the base design to 60.7 m (199

feet), which is approximately an 11% increase. Use of lightweight concrete for both girders and deck is the most efficient way to increase span length for all design options, leading to improvements in maximum span length in the range of 7-11%.

Using either lightweight concrete girders or a lightweight concrete deck gives the same percentage increase of maximum span length for the PCI BT-72 and The MI-1800 girders. However, use of lightweight concrete has a lesser effect on the maximum span length of the AASHTO Type VI beams.

4.8 Life-cycle Analysis and Optimum Design of Single-span SGBs

The aim of this section is to include the durability considerations, as it relates to life-cycle cost, in the optimal design of longitudinally spliced girder bridges attacked by chloride and describe the importance of durability considerations in extending their life span from the design stage. Several methods to lengthen the service life of concrete structures exist, which include using sealers, use of concrete admixtures, using coatings, and increasing concrete clear cover. However, only parametric studies on the use of increased concrete clear cover of the slab and precast/prestressed concrete girder were considered since this approach must be defined during the design process, unlike other parameters that can be applied later once the structure is constructed.

4.8.1 Effect of concrete clear cover on chloride concentration

A single-span AASHTO Type III spliced girder bridge with an overall span of 36.3 m (119 ft) having a splice location at 0.25 of total span length was considered to investigate the effect of concrete cover depth on the service life of the structure. The

bridge has a width of 18.6 m (61 ft) and a beam spacing of 2.1 m (7 ft). In this study, the bridge was assumed to be located in a splash zone with a constant chloride concentration (Anna et al. 1993 and Stephen et al. 1998). The initial chloride concentration (C_o) in both cold and warm climates was assumed to be 19 kg/m^3 (1.19 lb/ft^3) (Stephen et al. 1998). This number was selected to represent a severe chloride environment (Stephen et al. 1998). Therefore, the design service life of this structure may be very short compared to a prestressed concrete bridge in a typical environment.

Chloride concentrations vary based on climate conditions (Dhir et al. 1991). The diffusion coefficient of concrete was assumed to be 0.0293 and 0.0728 for cold and warm areas, respectively (Stephen et al. 1998). Chloride concentrations for different concrete clear covers at time t were determined from Equation (4-29); where C_O is chloride concentration at the surface; *erf* is the error function; x is the distance from the concrete surface to the steel surface; D_c is the diffusion coefficient, t is the considered time. Chloride concentrations for different concrete clear covers for different climates are shown in Figure 4-10 for warm weather and Figure 4-11 for cold weather.

$$C(x,t) = C_O(1 - erf\frac{x}{2\sqrt{D_c t}}) \tag{4-29}$$

The effect of chloride concentration on the service life of the structure in warm and cold weather is shown in Figure 4-10 and Figure 4-11, respectively. These figures contain the results of different clear cover values as well as the allowable threshold used in the United States and Asian Regions (Stephen et al. 1998).

Service lifetime of a structure depends on the chloride threshold (Stephen et al. 1998). Normally, in cold areas of the United States, the chloride threshold is set at 0.7

kg/m^3 (0.04 lb/ft^3) while in warmer climates found in Asian countries the chloride threshold is set at 1.2 kg/m^3 (0.07 lb/ft^3). The service lifetime of each climate structure can thus be determined directly from Figure 4-10 and Figure 4-11. The service lifetimes per concrete clear cover distance are listed in Table 4-23.

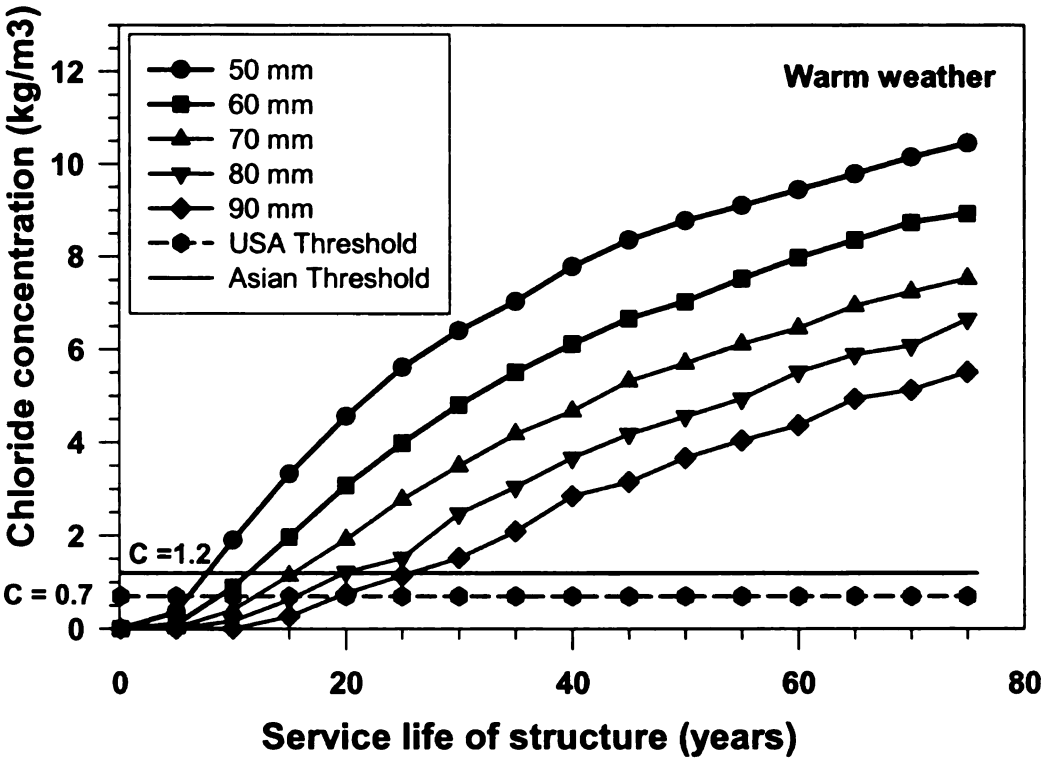

Figure 4-10 *Effect of concrete cover on the service life of structures (Warm Area)*

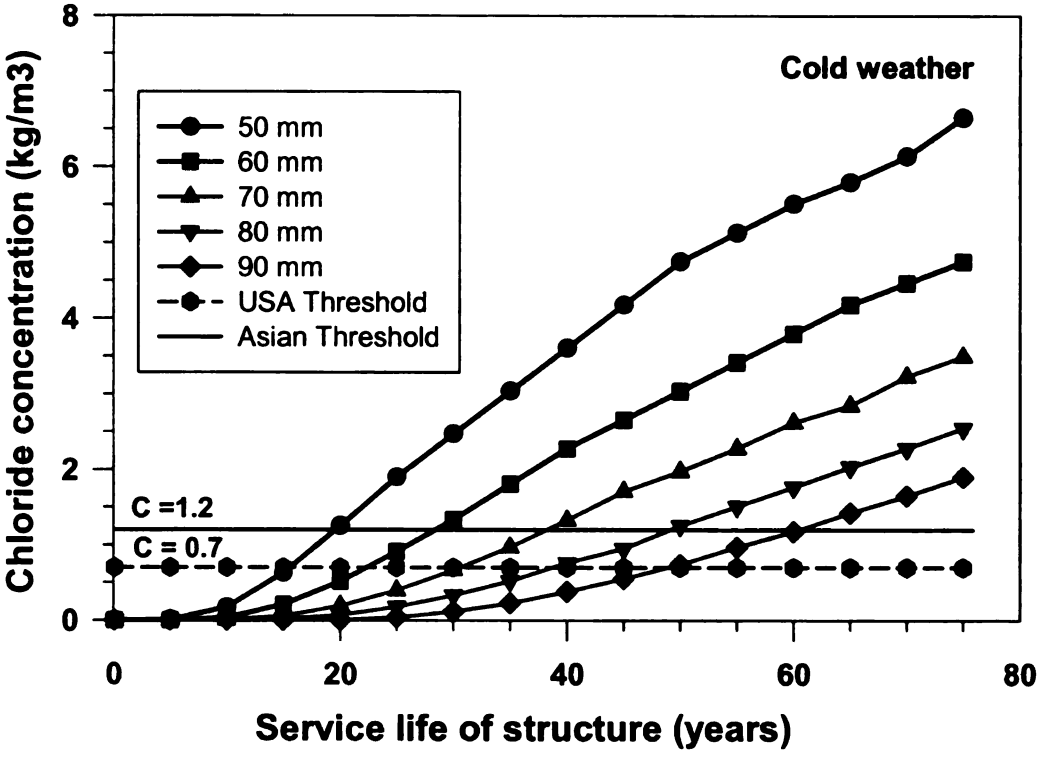

Figure 4-11 *Effect of concrete cover on the service life of structures (Cold Area)*

Table 4-23 *Service life time versus concrete cover in cold and warm areas*

Concrete Cover (mm)	Design Life (yrs)			
	Cold Area Threshold		Warm Area Threshold	
	0.7 kg/m^3 (0.04 lb/ft^3)	1.2 kg/m^3 (0.07 lb/ft^3)	0.7 kg/m^3 (0.04 lb/ft^3)	1.2 kg/m^3 (0.07 lb/ft^3)
50 (1.97")	13	16	5	7
60 (2.36")	19	23	8	10
70 (2.76")	26	33	10	14
80 (3.15")	40	48	16	19
90 (3.54")	48	63	20	25

The service lifetime of a structure located in a warm area is shown to be less than one-half that of a structure built in a cold area. In a low-temperature environment, the chloride diffusion rate decreases, therefore the service life of a structure is increased. In a warm environment, the chloride diffusion rate is increased, thereby decreasing the structure's service life. Temperature and surface characteristic normally yield considerable different results in the service life of a structure.

From Table 4-23 it can be seen that the service life of the structure can been increased by almost two and three times when the concrete cover is increased from 50 mm (2 in.) to 70 mm (2.76 in.) and 80 mm (3.15 in.), respectively.

4.8.2 Effect of concrete cover on initial cost

Conventional prestressed concrete beam designs were conducted to evaluate the service limit state and the strength limit state of the girder with different concrete covers. The initial construction cost of the girders and the deck were considered as the superstructure cost. The initial construction cost is determined based on the strength and serviceability design requirements. General bridge data used for the life-cycle-cost analyses is listed in Table 4-24.

Normally, the initial construction cost of any type of prestressed concrete girder is paid per meter, or foot, length and does not depend on the numbers of prestressing strands in the section. Therefore, it is unclear as to how much the initial construction cost would be increased by increasing the concrete cover depth. However, when the requirement of prestressing strands is too high such that they can not be fitted in the beam, a deeper standard beam may be needed. In this latter case, the initial construction cost would increase. Since precast/prestressed concrete beams are normally cast in

standard sections and paid for per linear length irrespective of the contentent, the initial beam cost can be considered unique to each beam type. This differs greatly from the use of reinforced concrete beams where the beam depth can be changed arbitrarily depending on the design requirements.

Table 4-24 *General bridge data information used in life-cycle-cost analyses*

General Parameter	Unit cost/Data
Bridge Width	18.6 m (61 ft)
Bridge length	36.3 m (119 ft)
No. of Beams	8
Slab thickness w/o cover	152 mm (6 in.)
Approx. reinforcement	96 Kg/m^3 (6 lb/ft^3)
Lifetime estimate prior to replacement	90 Years
Superstructure concrete deck	1,589 \$/m^3 (45 \$/ft^3)
Epoxy Steel Reinforcement	2.2 \$/kg (1 \$/lb)
AASHTO Type III 915mm (3 ft)	400 \$/m (122 \$/ft)
Deep Concrete Overlay 100mm (4 in.)	183 \$/m^2 (17 \$/ft^2)
Shallow Concrete Overlay 38mm (1.5 m.)	162 \$/m^2 (15 \$/ft^2)
Pre-tensioned strand cost	53 \$/m (16 \$/ft)
Post-tensioned strand cost	108 \$/m (33 \$/ft)

Parametric studies were thus conducted by varying the concrete clear cover on standard precast/prestressed beams. From the analyses results in Section 4.8 (Table 4-25), AASHTO Type III beams can be used in single-span spliced systems for span lengths up to 25900 mm (84.9 ft) with a beam spacing of 2100 mm (7 ft) and concrete cover not exceeding 65 mm (2.5 in.). When the concrete cover exceeds 65 mm (2.5 in.), a deeper beam, such as an AASHTO Type IV, needs to be used. Figure 4-12 illustrates the effect of concrete cover on initial cost in cold weather climates. Table 4-25 illustrates parametric studies of initial superstructure cost, maintenance cost, and life-cycle cost versus concrete clear cover.

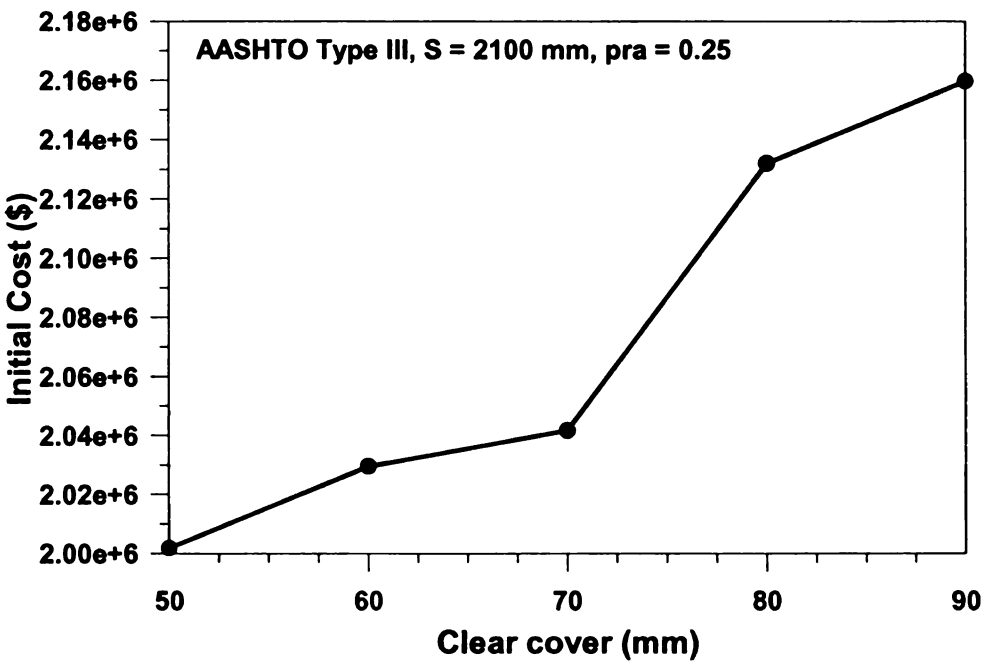

Figure 4-12 *Effect of concrete clear cover on initial construction cost (Cold Area)*

Table 4-25 *Studies on effect of concrete cover on superstructure cost*

Concrete Clear Cover (in.)	**1.97**	**2.36**	**2.76**	**3.15**	**3.54**
Clear Cover (in.)	1.97	2.36	2.76	3.15	3.54
Clear Cover Difference (in.)	0	0.39	0.79	1.18	1.57
Deck Area(ft^2)	7259	7259	7259	7259	7259
Total Beam length (ft)	952	952	952	952	952
New slab thickness (in.)	8.0	8.4	8.8	9.1	9.5
Deck concrete volume (ft^3)	4820	5058	5297	5535	5773
Reinforcement steel (lb.)	28922	30351	31780	33208	34637
AASHTO Beam Type	III	III	III	III	III
No. of pre-tensioned strands	27	26	26	27	26
No. of post-tensioned strands	39	40	40	42	43
Initial Cost					
Initial Deck Cost	$245,834	$257,980	$270,126	$282,272	$294,418
Initial Beam Cost	$1,755,908	$1,771,525	$1,771,525	$1,849,609	$1,865,225
Total Initial superstructure cost	**$2,001,742**	**$2,029,505**	**$2,041,651**	**$2,131,881**	**$2,159,644**
Maintenance and repair cost (Cold Area)					
Superstructure service life (yrs)	16	23	33	48	63
No. of Deep Overlay	2	2	1	1	0
No. of Shallow Overlay	3	2	2	1	1
Deep Concrete Cost Overlay per time	$123,403	$123,403	$123,403	$123,403	$123,403
Shallow Concrete Overlay Cost per time	$108,885	$108,885	$108,885	$108,885	$108,885
Deep Concrete Overlay Cost	$246,806	$246,806	$123,403	$123,403	$0
Shallow Concrete Overlay Cost	$326,655	$217,770	$217,770	$108,885	$155,550
Total Maintenance and Repair Cost	**$573,461**	**$464,576**	**$341,173**	**$232,288**	**$155,550**
Life-Cycle-Cost	**$2,575,203**	**$2,494,081**	**$2,382,824**	**$2,364,169**	**$2,315,194**
Percent increased from the intial cost	**29%**	**23%**	**17%**	**11%**	**7%**

4.8.3 Effect of concrete clear cover on life-cycle cost of single-span spliced girder bridges

The life-cycle-cost per year of a bridge structure can be determined by dividing the total life-cycle-cost by the design life-span (years). The life-cycle cost per year can then be used to compare the design alternatives of structures with different concrete cover depths. The life-cycle-cost also includes total maintenance cost during the service life time of structure. The maintenance cost is estimated for the numbers of times that need to have superstructure repair (i.e., shallow overlay, deep overlay, or deck replacement). The cost of different repaired task can be estimated from the unit cost database developed by state DOTs. Typically, maintenance cost is 0.5 to 1.2 times initial cost and the removal cost is extremely great (Yoshiki et al. 2001). Figure 4-13 and Figure 4-14 shows the relation of clear cover with maintenance and repair cost, and life-cycle-cost, respectively.

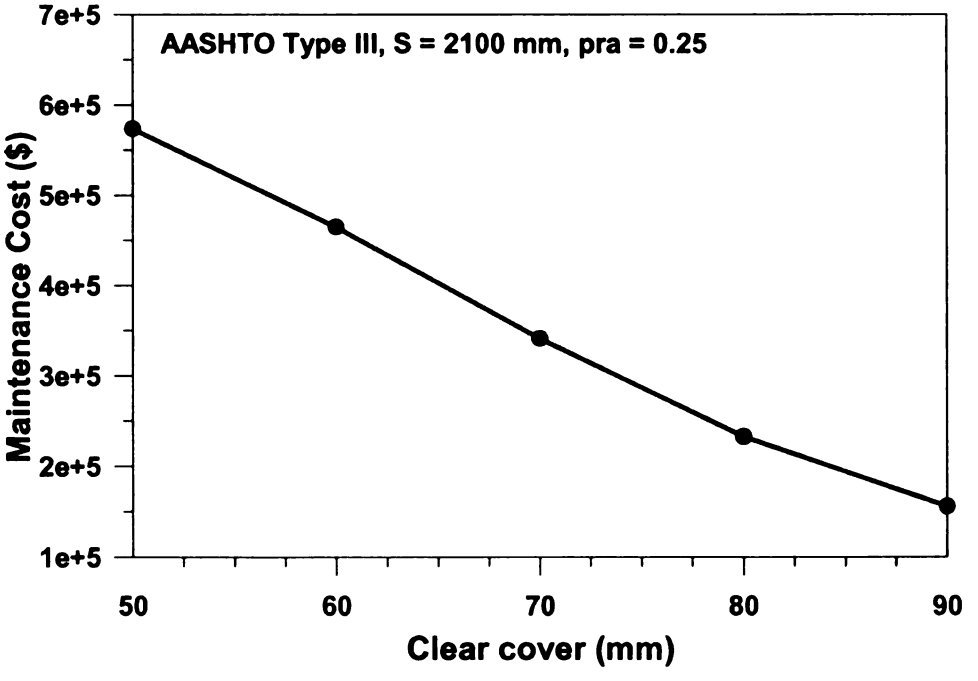

Figure 4-13 *Maintenance and repair cost versus concrete cover (Cold Area)*

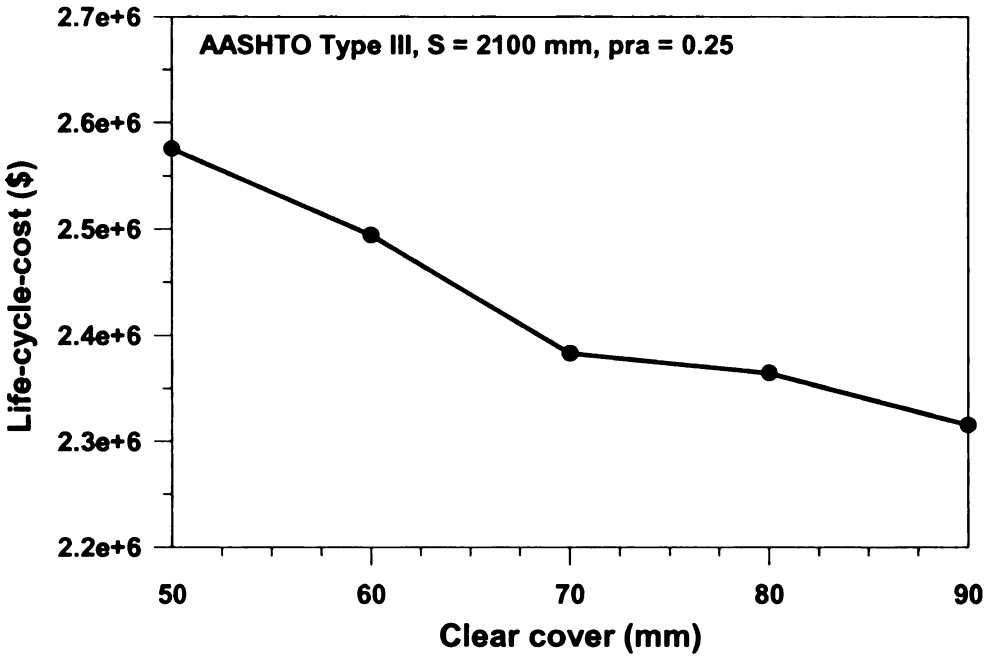

Figure 4-14 Life-cycle-cost versus concrete clear cover (Cold Area)

4.8.4 Comparison of life-cycle cost with initial strength-based design cost

Initial cost is governed by strength requirements, while life-cycle-cost incorporates all costs that could occur during the lifetime of the structure. In the previous study (Section 4.8.3), it was shown that for a structure in a cold area with 50 mm (2 in.) clear cover the life-cycle-cost can be 143% of the initial cost. On the other hand, if the clear cover is increased to 85 mm (3.35 in.) the service life of the structure will increase to 80 years. In this case, no additional cost needs to be added to the life-cycle-cost value. Figure 4-15 illustrates a comparison of initial, life-cycle, and maintenance cost as a function of concrete cover depth.

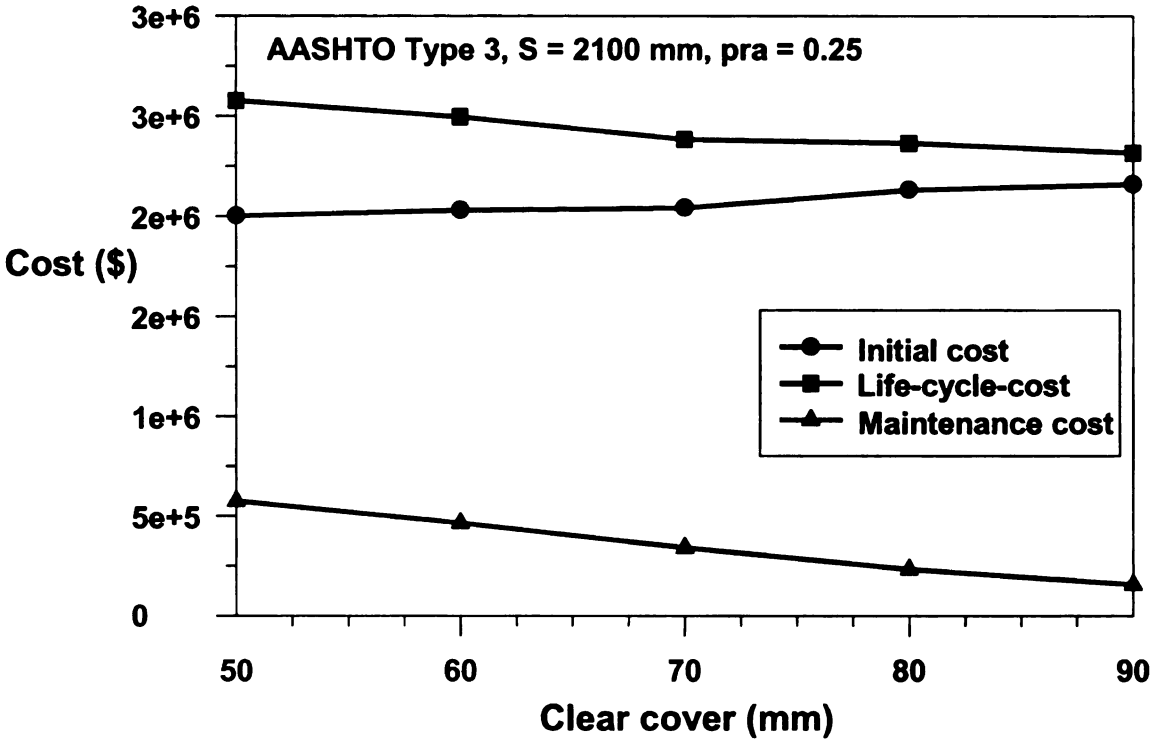

Figure 4-15 *Comparison of initial, maintenance and life-cycle-cost versus concrete clear cover*

4.8.5 Discussion of life-cycle-cost of spliced girder bridges

The diffusion coefficient for precast concrete components is normally much smaller than in conventional concrete components due to the small water/cement ratio and the high strength of the concrete used in precast/prestressed construction. Therefore, deterioration of precast/prestressed concrete bridges is typically less than in other types of concrete bridges. The increase in concrete cover depth is not always beneficial in terms of serviceability since there is a chance of developing shrinkage cracks. Therefore, there must be a compromise between strength and serviceability requirements versus the life-cycle-cost of the structure. For example, when the clear concrete cover in the beam

is increased, the eccentricity of the prestressing strands with respect to the centroid of beam cross-section is reduced. Therefore, prestressed concrete beams would require more prestressing strands to balance the superposed loads.

Experience to date has shown that when epoxy coated rebar is used in addition to the added minimum concrete cover depth no major deterioration has been found. However, minor problems due to poor workmanship have been observed. For example, unintended reduction of cover depth usually causes the initiation of corrosion problems. Thus, even bridges designed according to code requirements may have unintended shallow cover depths. Quality control of cover depth is therefore very important.

While providing proper concrete cover can reduce the rate of corrosion of the reinforcing steel, additional measures must be taken to ensure adequate and efficient protection in harsh environments. Such measures include the use of corrosion resistance concrete (CRC), the use of epoxy-coated reinforcement (ECR), the use of low water to cementitious material ratios, the use of surface coating, and the use of silica fume or fly ash to reduce the permeability of chloride ions in concrete.

Because the maintenance cost of existing structures is expected to continue increasing in the future, reasonable and effective maintenance measures must be developed. To achieve this goal, not only do technologies for the maintenance of existing structures need to be improved, but it is also necessary for design methods of newly constructed structures to take into account future maintenance as part of the life-cycle-cost.

When the life-cycle cost is included during the design phase, the initial cost of a new bridge could be higher than that of an existing bridge, but its maintenance cost

should be much less. This is due to the consideration of life-cycle-cost analysis during the design stage. Life-cycle-cost analysis includes the maintenance cost, the initial construction cost and the repair cost during service life the structure.

4.9 Effects of Erection Time Delay on Prestress Losses

The objective of this study was to investigate the variation of prestress losses due to the delay of the spliced girder segments erection. This situation can happen when the segments were fabricated and they sit in the yard for a long time prior to being transported to the construction site. The delay in erection could affect the time-dependent losses such as those due to creep and shrinkage.

A single-span spliced precast/prestressed girder bridge comprised of three segments, with single-stage post-tensioning applied after deck casting and a composite deck was selected for the comparative design study between the reference construction sequence proposed and a simulated construction sequence with delay. The PCI-BT 96 girder, with a spacing of 2.7 m (9 ft) and a splice location at 0.25 of the total span length, was used for the study.

Normally spliced segments are transported to the site and erected within 50 days after the pre-tensioned strands are released. For a single-stage post-tensioning construction method, the deck would thus be typically cast at day 60 and post-tensioning would likely be applied at day 75. To simulate delays in construction the girder segments were assumed to be transported to the site a month later than normal. The effect on prestress losses at each critical construction stage for the reference and delayed construction sequence are given in Table 4-26. The notations of each prestress loss components were described in Chapter 2.

Table 4-26 *Comparison of prestress losses at critical construction stage*

Pre-tensioning strands (Δf_{PRET})			
Critical construction stage	**Components of prestress loss**	**Normal Construction**	**Delay Construction**
Release of pre-tensioned strands	$\Delta f_{PES1} + \Delta f_{PR1}$	*87.1 MPa (12.63 ksi)*	*87.1 MPa (12.63 ksi)*
Placement of deck and splice concrete	$\Delta f_{PES1} + k_{CR1}\Delta f_{PCR} + k_{SH1}\Delta f_{PSR} + \Delta f_{PR2}$	*209.9 MPa (30.45 ksi)*	*223.6 MPa (32.43 ksi)*
Stressing of post-tensioning tendons	$\Delta f_{PES1} + k_{CR2}\Delta f_{PCR} + k_{SH2}\Delta f_{PSR} + \Delta f_{PR2} + \Delta f_{PES2}$	*281.7 MPa (40.85 ksi)*	*292.5 MPa (42.43 ksi)*
Final conditions after losses	$\Delta f_{PES1} + \Delta f_{PCR} + \Delta f_{PSR} + \Delta f_{PR2} + \Delta f_{PES2}$	*367.0 MPa (53.23 ksi)*	*367.0 MPa (53.23 ksi)*
Post-tensioning strands (Δf_{PT})			
Critical construction stage	**Components of prestress loss**	**Normal Construction**	**Delay Construction**
Stressing of post-tensioning tendons	$\Delta f_{PF} + \Delta f_{PA} + \Delta f_{PES}$	*87.0 MPa (12.62 ksi)*	*87.0 MPa (12.62 ksi)*
Final conditions after losses	$\Delta f_{PF} + \Delta f_{PA} + \Delta f_{PES} + \Delta f_{PCR} + \Delta f_{PSR} + \Delta f_{PR2}$	*359.4 MPa (52.13 ksi)*	*359.4 MPa (52.13 ksi)*

Comparison of prestress losses for different construction sequence times indicates that the prestress losses at the final stage are the same since the creep and shrinkage prestress losses according to the simplified AASHTO method are calculated based on the final, service life time of the structure, which is assumed to be 75 years.

Only the time-dependent prestress losses during intermediate construction stages between the release of pre-tensioning strands (stage 3) and the final conditions stage after all prestress losses (stage 10) are different. The creep and shrinkage prestress losses

at intermediate construction stages were calculated by multiplying the final creep and shrinkage prestress losses with corresponding factors give reference or refer to a section in the dissertation where this is explained. These factors depend on the time at each critical stage.

When construction is delayed only the prestress losses from the pre-tensioning strands at the placement of deck and splice (stage 5) and at post-tensioning (stage 6) were different and found to increase by 13.8 MPa (2 ksi). The increase in the prestress losses is considered very small and not to affect by the optimal solutions. This results show that the optimal solutions based on the reference construction time sequence assumed in Table 4-4 can be used even when delays in girder placement could be anticipated.

4.10 Summary

In this chapter, configuration optimization was applied to single-span spliced girder bridges. A single objective function, namely the minimization of construction cost, was used to evaluate the efficiency of construction methods for this system. Single-stage post-tensioning applied after deck casting was found to be the most efficient construction method since it yields longer spans than other construction methods.

The maximum achievable span length of longitudinally spliced standard precast/prestressed concrete girders was determined based on the best construction sequence method. Single-span spliced girder bridges lead to spanning increases of 28-60%, over conventional single-segment prestressed concrete bridge solutions. The requirements of pre-tensioning and post-tensioning strands as well as their locations

along the bridge span length were obtained from optimization studies and are provided in the form of design aids in Chapter 6.

Material parametric studies were investigated to evaluate different options to increase the span length of single-span SGBs. The combination of lightweight concrete for both girders and deck provide the greatest span length increase.

Results from multi-criteria optimization yielded a compromise solution for different single objective functions and represents more rational solution than those obtained by optimizing individual objective functions. Multicriteria optimization should be used when decision making must be made for several merit criteria. The resulting solution is expected to be non-dominant with regards to all criteria and ensures the best compromise between all competing objective functions.

Life-cycle-cost analyses were conducted to determine the increased initial superstructure design cost when considering maintenance and repairs. The service lifetime of the structure was considered during the design process by varying the concrete cover depth to increase the durability of girder components. Results showed that with less than 25 mm (1 in.) increase in the clear cover of concrete, the service lifetime of single-span spliced girder bridges can be increased more than twofold.

OPTIMAL DESIGN AND PERFORMANCE OF LONGITUDINALLY SPLICED PRECAST/PRESTRESSED CONCRETE BRIDGES

VOLUME II

By

Pimpida Surakomol

A DISSERTATION

Submitted to
Michigan State University
in partial fulfillment of the requirements
for the degree of

DOCTOR OF PHILOSOPHY

Department of Civil and Environmental Engineering

2005

5 Optimum System Design of Two-Span Continuous Spliced Girder Bridges

5.1 Introduction

This chapter documents the optimization design studies on continuous two-span spliced precast/prestressed girder bridges (SGB). Single objective and multi-criteria optimization were performed and compared to evaluate the influence of design parameters on this continuous system. Results of optimal solutions were provided in terms of design aids. Example of design aid is provided in Chapter 6 and the complete design aids of spliced precast/prestressed concrete girder bridges can be obtained from the MSU-CE report (Surakomol and Burgueno 2005).

Currently, only custom designed pier girders are used in the deeper sections of pier segments in continuous spans. Thus, the benefits of using standard conventional precast/prestressed concrete girder sections as well as newly optimized standard pier sections for two-span continuous systems were studied.

Different construction methods for this system were explored to obtain the most efficient construction method. The maximum achievable span lengths for different beam types at different beam spacing and splice locations were obtained and the results were compared.

5.2 Problem Statement

A two-span spliced girder bridge with a total width of 18.6 m (61 ft) and a span length (L) consisting of three segments was used in this study as a prototype continuous bridge structure. The bridge cross-section is similar to the cross-section shown in Figure 4-1, and previously described in Section 4.2. The end segments were assumed to be equal. The splice location, which is the ratio of the end (or field/positive) segment length (L1) to the total span length (L), was used to define the mid (or pier/negative) segment and end-segment lengths. The pier segment can consist of a standard section (see Figure 5-1) or a non-prismatic section (see Figure **5-2**). The cast-in-place concrete slab thickness was assumed to be 213 mm (8.5 in.). The beam spacing was assumed to vary from 1.8 m (6 ft) to 2.7 m (9 ft). Standard AASHTO beams were investigated and new optimized non-prismatic beams were developed.

The design studies were conducted using the simplified design method of the AASHTO-LRFD Bridge Design Specifications (AASHTO 2003) and the recommendations from the NCHRP 517 study (Castrodale and White 2004). Service limit states and ultimate limit states were considered in the design. A complete overview of the design and analysis consideration for continuous spliced girder bridges has been given in Chapter 2.

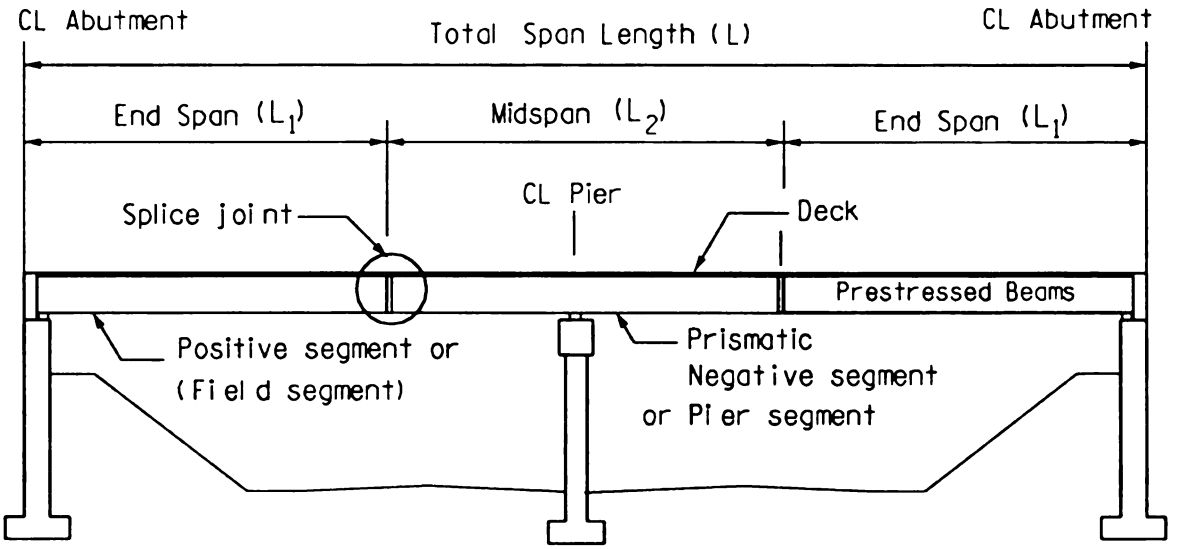

Figure 5-1 *Two-span spliced precast/prestressed bridge with prismatic pier segment*

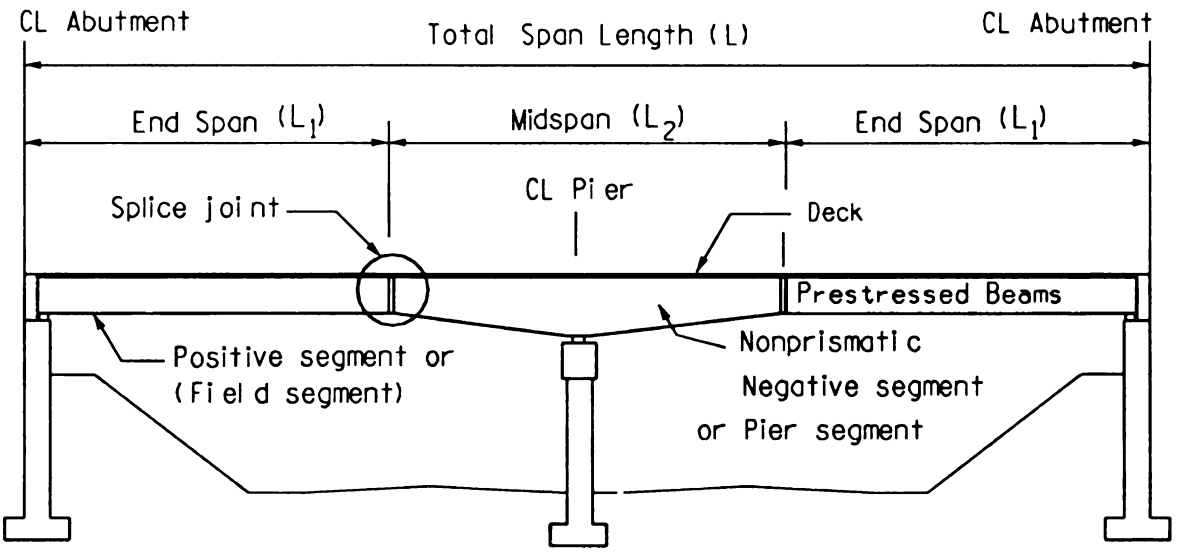

Figure 5-2 *Two-span spliced precast/prestressed bridge with non-prismatic pier segment*

5.3 Design Parameters

The main geometry design parameters for the prototype two-span SGB bridge system are similar to those used for the single-span SGB study (see Section 4.2 and Section 4.3). They are the beam spacing *(S)*, the total span length of each span *(L)*, the splice location *(pra)* and the standard sectional properties of the girders. Beam spacing was varied from S = 1.8 m (6 ft) to 2.7 m (9 ft) in 300 mm (1 ft) increments. The splice location *(pra)* is defined by the ratio of end segment (L_1) over the entire bridge span length L. Three splice locations were investigated, which were 0.35*(L)*, 0.375*(L)*, and *0.40(L)*. Concrete properties for the girders, deck and splice joints are summarized in Table 5-1. The pre-tensioning and post-tensioning strands are assumed to be 15.24 mm (0.6 in.) nominal diameter and made from low-relaxation steel.

5.4 Options to Negative Pier Segments in Continuous SGBs

Presently, precast/prestressed concrete girders are being used extensively in continuous-span bridges in which the pier, or negative, segments are custom-designed to carry the high negative-bending moment and high-shear demands. Consequently, deep sections using haunches are typically used. The availability and use of standard negative sections could reduce the cost of fabrication of pier segments; therefore, four different options to increase the section depth over the pier section were considered and studied. Girder dimensions for the four options considered are shown in Figure 5-3 through Figure 5-5 and were part of the design variables in sectional optimization studies detailed in Section 5.4.5.

Table 5-1 *Assumed material properties*

Girder Concrete	Deck & Splice Concrete	Pre-Tensioning Strands	Post-Tensioning Strands
SI units			
$f'_c = 44{,}816$ kN/m^2	$f'_{cd} = 31{,}026$ kN/m^2	$A_{ps} = 140$ mm^2	$A_{ps} = 140$ mm^2
$f'_{ci} = 34{,}474$ kN/m^2	$f'_{cdi} = 24{,}132$ kN/m^2	$f_{pu} = 1{,}861{,}585$ kN/m^2	$f_{pu} = 1{,}861{,}585$kN/m^2
$E_c = 33{,}702$ kN/m^2	$E_{cd} = 28{,}041$ kN/m^2	$f_{py} = 1{,}675{,}427$ kN/m^2	$f_{py} = 1{,}675{,}427$ kN/m^2
$E_{ci} = 29{,}558$ kN/m^2	$E_{cdi} = 24{,}732$ kN/m^2	$f_{po} = 1{,}396{,}189$ kN/m^2	$f_{pj} = 1{,}507{,}884$ kN/m^2
		$E_p = 196{,}500{,}660$ kN/m^2	$E_p = 196{,}500{,}660$ kN/m^2
US units			
$f'_c = 6{,}500$ psi	$f'_{cd} = 4{,}500$ psi	$A_{ps} = 0.217$ in.^{2}	$A_{ps} = 0.217$ in.^{2}
$f'_{ci} = 5{,}000$ psi	$f'_{cdi} = 3{,}500$ psi	$f_{pu} = 270$ ksi	$f_{pu} = 270$ ksi
$E_c = 4{,}888$ ksi	$E_{cd} = 4{,}067$ ksi	$f_{py} = 243$ ksi	$f_{py} = 243$ ksi
$E_{ci} = 4{,}287$ ksi	$E_{cdi} = 3{,}587$ ksi	$f_{po} = 202.5$ ksi	$f_{pj} = 218.7$ ksi
		$E_p = 28{,}500$ ksi	$E_p = 28{,}500$ ksi

The section optimization processes were coupled with the configuration optimization process to obtain optimal sectional geometry solutions at the pier locations. Different beam depths were considered to assess the sensitivity of the structural system to the pier segment stiffness. An overview on the options to negative pier segments considered in the study is given next.

5.4.1 Pier segment option 1: existing standard positive sections with soffit

The first method explores the use of available existing standard positive sections with an additional concrete block attached to the underside of the beam to make up the negative pier segment, as shown in Figure 5-3. The soffit tapers from a maximum on top of the pier to zero depth at the splice location to match the height of the standard positive segment.

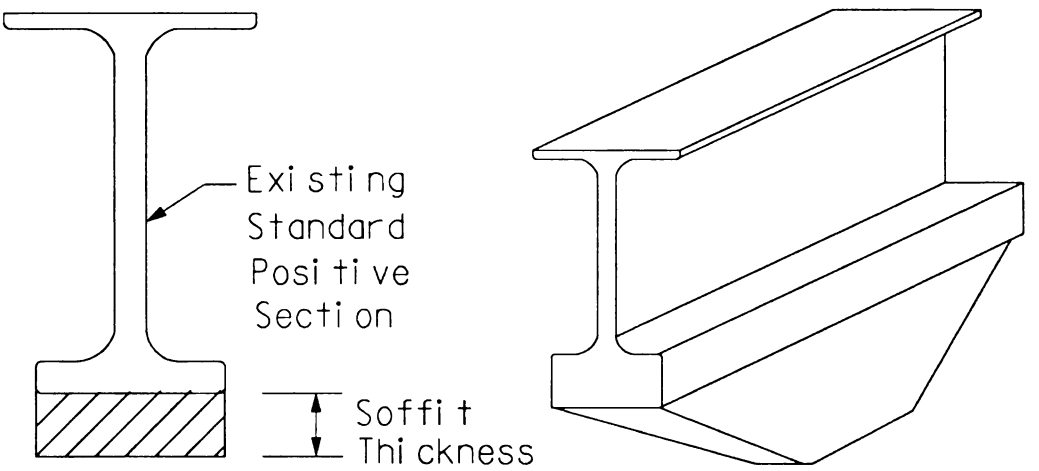

Figure 5-3 *Pier segment option 1: existing standard girder attached with soffit*

5.4.2 Pier segment option 2: new optimal non-prismatic section with variable web

A new optimal non-prismatic section was developed having a uniform flange thickness and a varied web height along the negative segment as shown in Figure 5-4. The web height increases linearly from the prismatic positive section to a maximum web height over the pier centerline. Due to the variable webs, this negative segment option is

lighter than solutions where the web is kept constant and the flange thickness is increased.

This new pier segment option was studied for optimal design for beam spacing of 1.8 m (6 ft), 2.1 m (7 ft) and 2.4 m (8 ft) and the span length was increased in increments of 3.0 m (10 ft), both given as parameters. The beam dimensions constituted the design variables in the component optimization and the upper and lower bounds to these dimensions were defined within practical ranges. The overall beam height over the pier was set not to exceed 1.5 times the total beam height of the prismatic section. This criterion was set based on current practice of custom designed pier segments. The dimension limits for the web and flanges were set to be in the range of available existing standard beam dimensions.

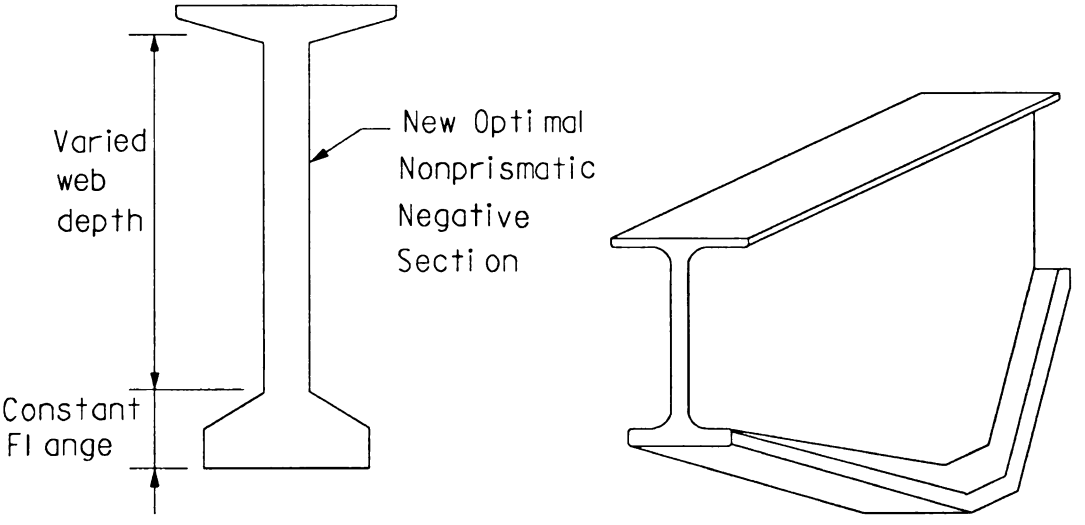

Figure 5-4 *Pier segment option 2*: n*ew optimal non-prismatic girder with variable web depth*

5.4.3 Pier segment option 3: new optimal non-prismatic section with constant web height

A new optimal non-prismatic section having a uniform web height and a varied bottom flange was also developed as an option for negative pier segments (see Figure 5-5). The bottom flange thickness increases linearly from the prismatic positive section to a maximum thickness at the pier centerline. This new section has a variable flange thickness and therefore its weight is heavier than other solutions where the bottom flange thickness is kept constant.

Beam dimensions were part of the component optimization process and the upper and lower bounds on these dimensions were defined within practical ranges. This new optimal girder was developed for a beam spacing of 1.8 m (6 ft), 2.1 m (7 ft), and 2.4 m (8 ft) and the span length was increased in the increments of 3.0 m (10 ft), both given as parameters.

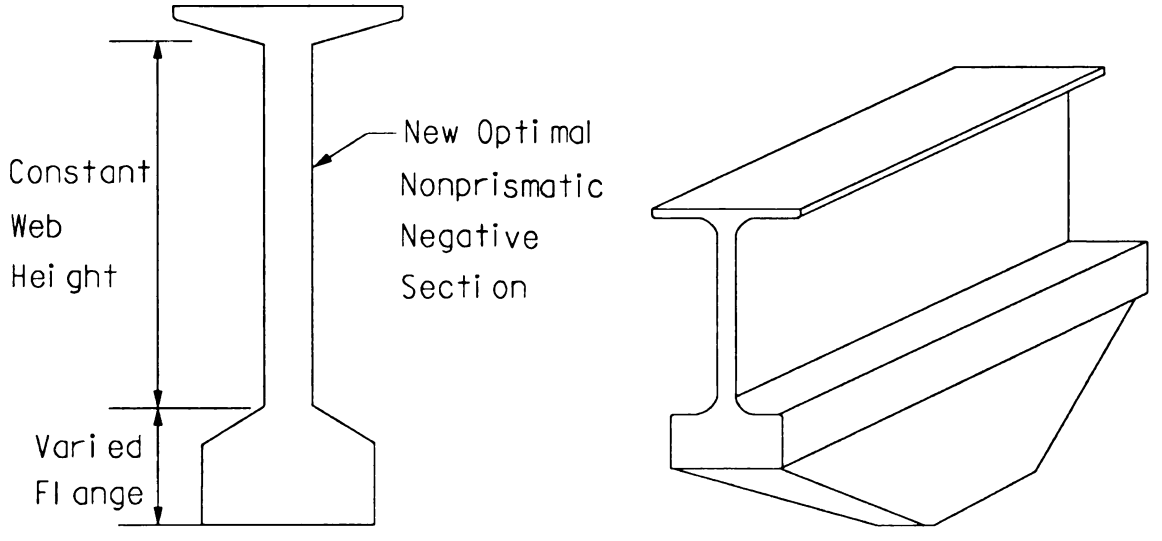

Figure 5-5 *Pier segment option 3*: n*ew optimal non-prismatic girder with variable bottom flange thickness*

5.4.4 Pier segment option 4: new optimal prismatic section for both positive and negative Segments

A new optimal *prismatic* section for use in both positive and negative segments was also developed as shown in Figure 5-6. This section is considered to be more cost-effective than having a girder of varied height since fabrication is less complicated.

This new optimal section option was developed for a beam spacing of 1.8 m (6 ft), 2.1 m (7 ft), and 2.4 m (8 ft) and the span length was increased in an increments of 3.0 m (10 ft) and given as a parameter. The overall height of the beam was developed by setting as upper bounds the results for the other pier segment options. Beam dimensions were also part of the component optimization process coupled with the system optimization.

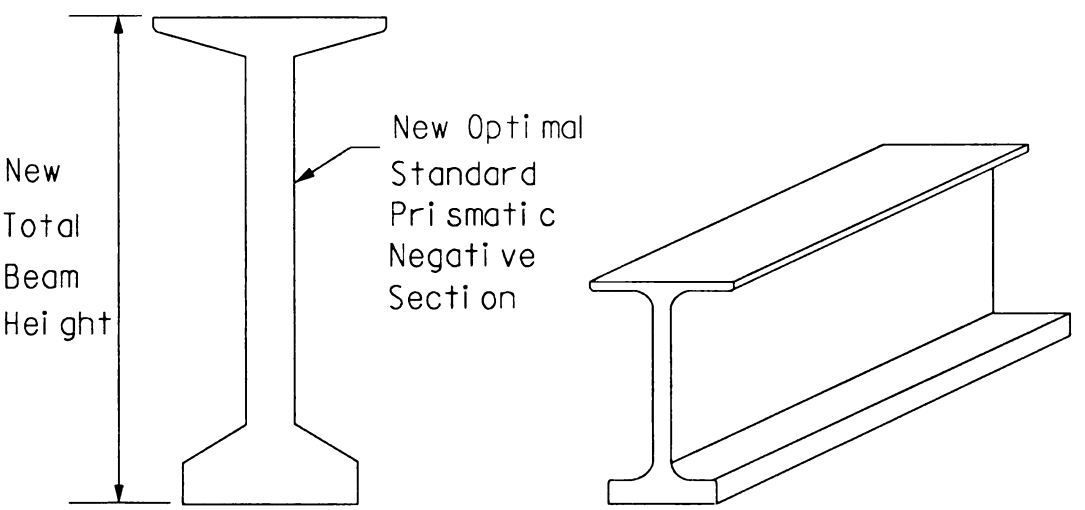

Figure 5-6 *Pier segment option 4: new optimal prismatic section for positive and negative segments*

5.4.5 Design variables for the development of pier segment options

Sectional optimization studies required the definition of design variables that define the beam dimensions. For the option using an existing standard positive segment with soffit, only one design variable is needed, namely the maximum soffit thickness (S_f) at the pier centerline (see Figure 5-7).

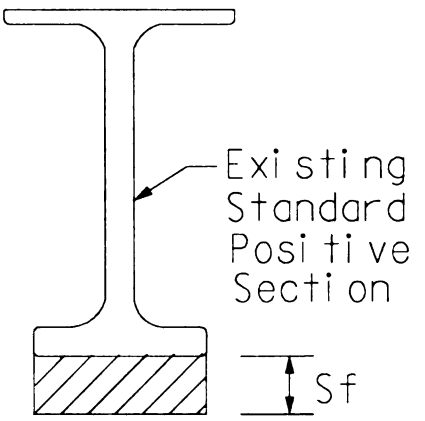

Figure 5-7 *Design variable for existing standard girder with soffit (pier segment option 1)*

The design variables for the new non-prismatic section with varied soffit thickness and constant web height are the bottom flange thicknesses (t_1 and t_2), the top flange thicknesses (t_3 and t_4), the bottom flange width (b_1), the top flange width (b_2), the web thickness (t_w), the web depth (D_w), and the soffit thickness (S_f) all defined at the pier centerline as shown in Figure 5-8.

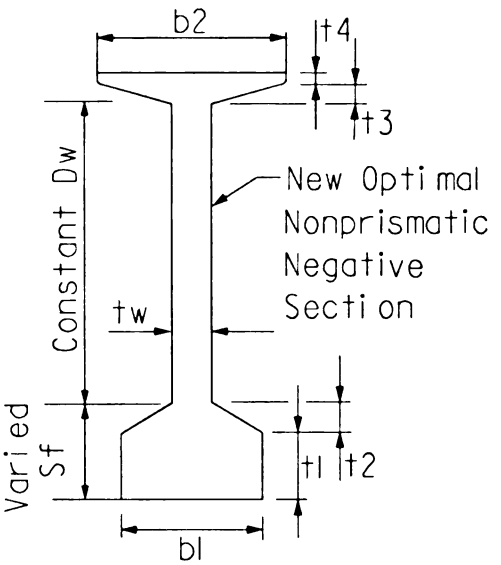

Figure 5-8 *Design variable for new non-prismatic section with constant web depth (pier segment option 2)*

Design variables for the new non-prismatic section with varied web height are the bottom flange thicknesses (t_1 and t_2), the top flange thicknesses (t_3 and t_4), the bottom flange width (b_1), the top flange width (b_2), the web thickness (t_w), and the web depth (D_w), all defined at the pier centerline as shown in Figure 5-9.

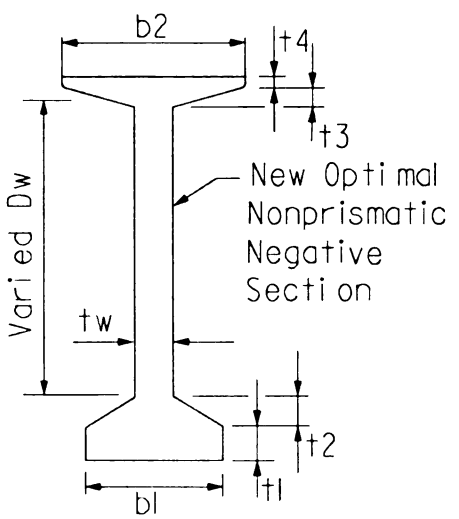

Figure 5-9 *Design variables for new non-prismatic section with varied web depth (pier segment option 3)*

The design variables of a new prismatic section for both positive and negative segments include the bottom flange thicknesses (t_1 and t_2), the top flange thicknesses (t_3 and t_4), the bottom flange width (b_1), the top flange width (b_2), the web thickness (t_w), and the web depth (D_w), all defined at the pier centerline as shown in Figure 5-10.

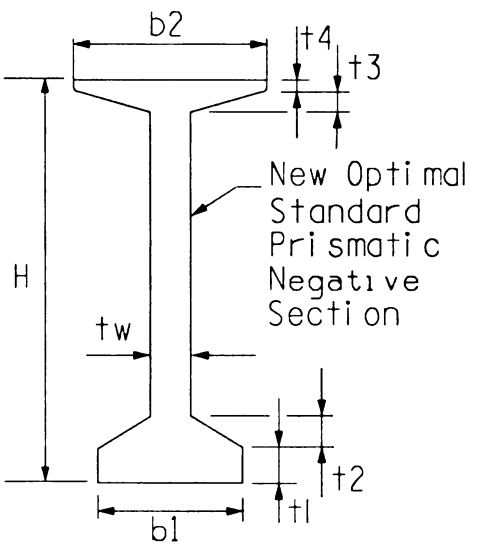

Figure 5-10 *Design variables for new prismatic section for both positive and negative segments (pier segment option 4)*

5.5 Analysis Continuous-Span Spliced Girder Bridges

The complete design and analysis considerations and procedures for continuous SGB are presented in Chapter 2 and are only briefly summarized in this section. The analysis for the two-span continuous spliced girder bridge systems was based on 2-D frame analyses including the effects of time-dependent material behavior and staged construction. A custom program using the stiffness method was used. Each span segment was divided into multiple elements to obtain stresses, internal forces and

deflection results at the member ends. The beam-line modeling concept was used to determine the demands of an interior girder according to the load distribution factors specified in the AASHTO-LRFD Specifications (AASHTO 2003). Interior girders were used in the analysis since their demands usually control the superstructure design. In addition, all beams are typically designed as interior beams to allow future bridge widening.

For all service limit states, analyses were performed using gross and uncracked section properties while moment and shear capacity calculations were used to evaluate the strength limit states. A two-span spliced girder bridge is statically indeterminate; therefore, secondary effects from prestressing as well as the effect temporary support removal were taken into account.

Prestress losses were computed using the simplified AASHTO-LRFD method (AASHTO 2003) with consideration of the effects of combined pre-tensioning and post-tensioning on the girder segments, as recommended by the recent NCHRP study on spliced girder bridge design (Castrodale and White 2004). The design lifetime of the spliced girder bridge system was assumed to be 75 years after all pre-stress losses had occurred. The analysis and section design was performed using a custom program coded in MATLAB (Mathworks 2004), which enforced compliance with service and strength limit states as defined in Section 5.6 and 5.7.

5.6 Optimum Design of Two-Span SGB by Single-Stage Post-Tensioning after Deck Casting

5.6.1 Design variables

The design optimization of two-span continuous SGB requires more variables that those considered for a single-span system (Chapter 4). Additional considerations include design variables associated with the sectional optimization options and the definition of additional variables to define the parabolic post-tensioning over the haunched negative segment. The design variables are a mixed set of integer and continuous geometric parameters defining the dimension and shape of the standard and non-prismatic precast/prestressed girder segments, the material layout, and the span arrangement of the bridge system. Only key design variables were thus considered in the design to maximize the efficiency of the computation algorithm.

The design variables for the sectional optimization problems described in Section 5.4.5 were combined with the additional design variables of prestress requirements and prestress locations along the span for each construction method. These later design variables are illustrated in Figure 5-11 and include: npr_{i1} = number of bottom pre-tensioned strands on end-segments at row i^{th} (for example, npr_{11} represents the number of bottom pre-tensioned strands on the end-segments at the 1^{st} bottom row of the girder); npr_{i2} = number of top pre-tensioned strands on the mid-span segments at row i^{th}; $nprt_1$ = number of top pre-tensioned strands on the end-segments; $nprt_2$ = number of bottom pre-tensioned strands on the mid-segment; npo_1 = total number of post-tensioned strands

in the girder for single-stage post-tensioning construction or a first stage post-tensioning operation for two-staged post-tensioning construction; y_a = vertical distance from the bottom extreme fiber of the girder to the net centroid of the equivalent post-tensioning duct at the end-segments; y_b = vertical distance from the neutral axis to the net centroid of the equivalent post-tensioning duct at the middle of the end segment; y_c = vertical distance from the girder composite neutral axis to the net centroid of the equivalent post-tensioning duct at the splice location; y_d = vertical distance from the girder composite neutral axis to the net centroid of the equivalent post-tensioning duct at the negative pier location.

The sign convention for y_a, y_b, y_c, and y_d is such that they are positive when measured down from the neutral axis. All of the above-mentioned design variables, are noted in Figure 5-11. Variables y_a, y_b, y_c, and y_d are not direct design variables (i.e., they are not part of the objective function). However, they have an influence on other design variables and were considered in the design as part of the equivalent post-tensioned loads.

The location of each pre-tensioned strand layer is taken to be 50 mm (2 in.) apart, including the distance of the first row of strands to the beam bottom and top. The post-tensioning tendons were assumed to follow quadratic parabolic profiles. Normally, post-tensioned strands require several ducts; however, only an *effective* post-tensioning profile was used to represent a group of ducts in order to simplify the optimization computation by minimizing the number of design variables. Figure 5-11a illustrates the

profile of this effective post-tensioning duct for the construction method of single-stage post-tensioning after deck casting. Figure 5-11b illustrates pre-tensioning requirements for both positive and negative segments.

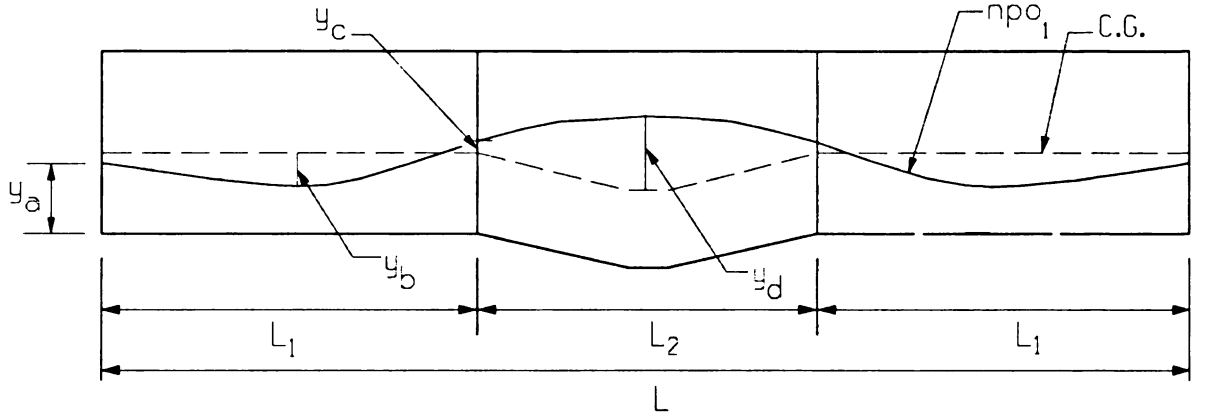

(a) Single-staged post-tensioning requirement

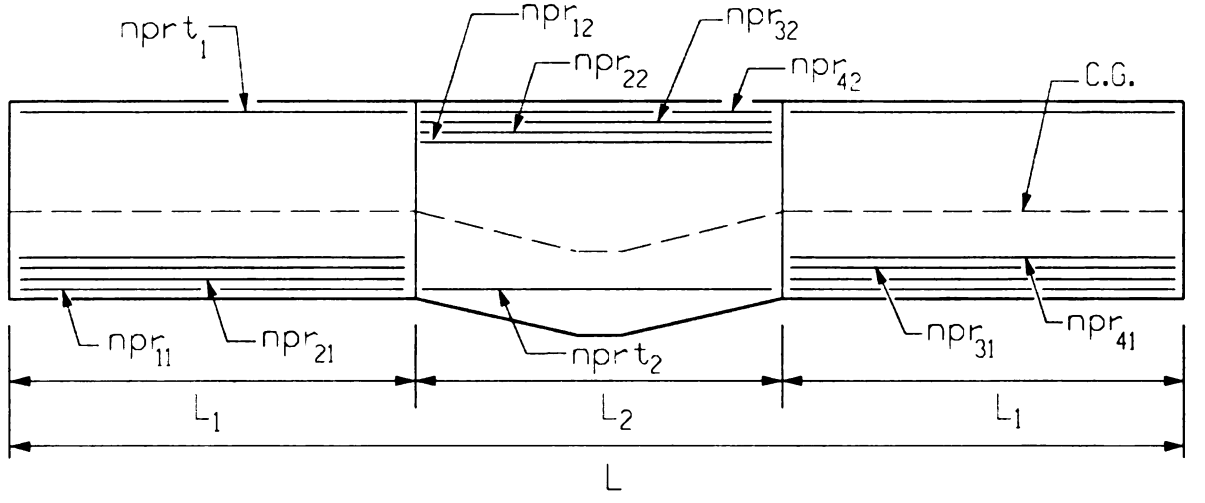

(b) Pre-tensioning requirement

Figure 5-11 *Variables for the design optimization of two-span continuous SGB built with single-staged post-tensioning after deck casting*

5.6.2 Objective functions

Design optimization procedures rely on an objective function to evaluate the "goodness" of a design and thus search for an improved solution that satisfies a set of constraints, in this case the requirements of safety and serviceability imposed by design codes and other merit criteria. A common design criterion in bridge design is the minimization of total superstructure cost. Superstructure cost is typically chosen since it commonly constitutes approximately 70% of the total bridge cost. The superstructure cost objective function is then defined as:

$$f(x_i) = C_{PS} + C_{PT} + C_{CD} + C_{TS} + C_B + C_R \tag{5-1}$$

Details for each of the terms in the above cost objective function (Equation 5-1) are specified in Table 5-2.

Table 5-2 *Components of objective function*

Component	Cost
Pre-Tensioning C_{PS}	$C_p \cdot N_g \cdot \left[(npr_{i1} + nprt_1) \cdot L_1 \cdot 2 + \cdot (npr_{i2} + nprt_2) \cdot L_2\right]$
Post-Tensioning C_{PT}	$C_{po} \cdot N_g \cdot n_{po} \cdot (L_1 \cdot 2 + L_2)$
Concrete C_{CD}	$C_c \cdot L \cdot W \cdot t_s$
Reinforcement C_R	$C_r \cdot W \cdot (L_1 \cdot 2 + L_2) \cdot W_{st}$
Beam C_B *(Standard beam)*	$C_b \cdot N_g \cdot (L_1 \cdot 2 + L_2)$
Beam C_B *(New optimal beam)*	$C_{bv} \cdot N_g \cdot CV$
Temp Support C_{TS}	$C_{ts} \cdot N_g \cdot 2$

Unit material costs for the two-span spliced girder bridge system were assumed to be similar to the unit material costs for single-span spliced girder bridge. These costs were described earlier in Section 4.5. Clearly, the costs of new prismatic and non-prismatic beam sections are expected to be different from standard beams. The cost of a standard pre-stressed concrete beam is defined as a cost per unit length. However, there is no clear guidance to estimate costs for new sections, whether prismatic or non-prismatic. Therefore, the cost of fabrication the non-standard beams in these studies was based on the concrete volume in each beam as specified in Table 5-3.

Table 5-3 *Concrete volume of new optimal beams*

Girder Section	Girder Concrete Volume Component
New Prismatic Beam	$CV = \frac{A_g}{144} \times (2 \times L_1 + L_2)$
New Non-prismatic Beam with Varied Web Depth	$CV = \frac{A_{g1}}{144} \times 2 \times L_1 + (\frac{(A_{g1} + A_{g2})}{144} \times 0.5 \times L_2)$
New Non-Prismatic Beam with Constant Web Depth	$CV = \frac{A_{g3}}{144} \times 2 \times L_1 + (\frac{(A_{g3} + A_{g4})}{144} \times 0.5 \times L_2)$

For the equations listed in Table 5-3: A_g is the area of the new prismatic beam; A_{g1} is the area of the new non-prismatic beam with varied web depth in the positive section; A_{g2} is the maximum area of a new non-prismatic beam with varied web depth over the pier location; A_{g3} is the area of a new non-prismatic beam with constant web depth in the positive section; A_{g4} is the maximum area of a new non-prismatic beam with constant web depth over the pier location.

5.6.3 Design constraints

Constraints for the optimization problem were the service and strength limit states specified in the AASHTO-LRFD Bridge Design Specifications (AASHTO 2003) and the recommendations from NCHRP Report 517 (Castrodale and White 2004). Constraints for the strength limit state included checks on moment and shear capacities. The ductility requirement was satisfied by ensuring that the relative neutral axis depth at the ultimate limit state, c/d_e, was less than 0.42 (AASHTO 2003).

Constraints for the service limit state were defined in terms of flexural stress limits on both the girder and deck. Stresses at each critical construction stage (see Table 5-4) were checked against the allowable compression and tension stresses recommended by the AASHTO-LRFD Specifications (AASHTO 2003), see Table 4-5. Three locations across the composite girder-deck section, namely, the girder bottom and top, and the top of the deck were checked along the span length of beam at each critical construction stage to guarantee that all stresses were within the prescribed limits. There are seven critical stage constraints on each location of the composite section as noted by the "X" symbols in Table 5-4.

The formulation for the bottom girder stress constraints (Constraints 1da to 7da) for each critical construction stage of the service limit state are outlined below. Similar expressions were defined and implemented for the top girder (Constraints 1ea to 7ea) and top deck (Constraints 1fa to 7fa) stresses. The constraint expressions described below illustrate the stress checks on the negative segment. Similar constraint formulations were defined and implemented for the positive segments.

Table 5-4 *Construction sequence for single-staged post-tensioning after deck casting*

Construction Stages	Time (days)	Action Description	Pre-Tensioning Critical Stage	Post-Tensioning Critical Stage
1	-	Stress pre-tensioning strands		
2	0	Cast girder segments		
3	1	Release pre-tensioning strands	X	
4	50	Erect girder segments		
5	60	Place deck and splice concrete	X	
6	75	Stress post-tensioning strands	X	X
7	100	Add barriers		X
8	140	Apply live load		
9	15000	Add future wearing surface		
10	27500	After all pre-stress losses	X	X

Constraint 1da: Compression Stress Check at Pre-Tensioning Stage

This construction stage considers the stresses due to the girder weight and the pre-tensioning force. The gross area of the negative girder section varies along the negative pier segment for the new non-prismatic sections and is uniform for the prismatic sections. At this stage, only prestress losses due to relaxation at release and elastic shortening were deducted from the initial prestress. Elastic shortening prestress loss was determined by using the average cross-sectional area of the negative segment (for non-prismatic elements) and this loss was assumed to be uniform along the entire negative segment. The actual stresses along the span were evaluated from their varied

girder gross sectional properties (A_{gn} and S_{bgn}) and eccentricity of the pre-tensioned strands (e_{pn}). The bottom girder compression stress constraint was then defined by:

$$\sigma_{1da} = -\frac{M_{gn}}{S_{bgn}} + \frac{A_{psn} f_{pe1n}}{A_{gn}} - \frac{A_{psn} f_{pe1n} e_{pn}}{S_{bgn}} \leq 0.6 f'_{ci}, \qquad (5\text{-}2)$$

where M_{gn} is the girder moment along the negative segment; A_{psn} is the total pre-tensioned area in the negative segment; f_{pe1n} is the effective prestress in the pre-tensioned strands after pre-tensioning; e_{pn} is the net eccentricity of pre-tensioning strands along the negative segment measured from the neutral axis of the section; S_{bgn} is the bottom section modulus along the negative segment; A_{gn} is the girder gross area along the negative segment; and σ_{b1n} is the girder bottom stress along the negative segment.

Constraint 2da: Compression Stress Check at Deck and Splice Placement Stage

Constraint 2da applies to the concrete casting of the deck, deck haunch, and splice regions. Non-composite sectional girder properties were used since the deck has not yet hardened. Prestress losses for this stage include those from elastic shortening, creep, shrinkage, and steel relaxation.

Creep losses due to pre-tensioning were determined by using the average girder gross section properties (relevant to non-prismatic elements). These average section properties include the average cross-section area, the average gross moment of intertia, and the average eccentricity of the pre-tensioned strands. This creep loss was assumed to

be uniform along the entire negative segment. Elastic shortening prestress losses were assumed to be the same as defined earlier on *Constraint 1da*. The actual stresses along the span were also evaluated from their varied girder sectional properties (A_{gn} and S_{bgn}) and eccentricity of the pre-tensioned strands (e_{pn}). Bottom girder compressive stresses were thus constrained by the following expression:

$$\sigma_{2da} = -\frac{M_{gn}}{S_{bgn}} - \frac{M_{dn}}{S_{bgn}} - \frac{M_{hn}}{S_{bgn}} - \frac{M_{cn}}{S_{bgn}} + \frac{A_{psn} f_{pe2n}}{A_{gn}} - \frac{A_{psn} f_{pe2n} e_{pn}}{S_{bgn}} \leq 0.6 f_c', \tag{5-3}$$

where M_{dn} is the deck moment along the negative segment; M_{hn} is the haunch moment along the negative segment; M_{cn} is the construction load moment along the negative segment; f_{pe2n} is the effective prestress in the pre-tensioned strands after placing the deck; and σ_{b2n} is the girder bottom stress along the negative segment.

Constraint 3da: Compression Stress Check at Post-Tensioning Stage

This constraint applies to the longitudinal splicing of the pre-tensioned girders through a single post-tensioning operation. A tendon profile composed of multiple quadratic parabolic curves was used to define the equivalent post-tensioning tendon location along the girders. Equivalent multi-uniform transverse loadings with nodal forces were used to represent the effect of post-tensioning forces. At this stage, the deck is assumed to be working compositely with the beam. Prestress losses at this stage include those from elastic shortening, creep, shrinkage, steel relaxation, and additional elastic shortening due to post-tensioning. Details of prestress loss calculations were

described in Section 2.11 and are not re-stated here. The bottom girder stress constraint is thus defined by:

$$\sigma_{3da} = -\frac{M_{gn}}{S_{bgn}} - \frac{M_{dn}}{S_{bgn}} - \frac{M_{hn}}{S_{bgn}} - \frac{M_{rn}}{S_{bcn}} + \frac{A_{psn} f_{pe3n}}{A_{gn}} + \frac{A_{psn} f_{pe3n} e_{pn}}{S_{bgn}} +$$

$$\frac{n_{po} a_{ps} f_{pof}}{A_{cn}} + \frac{M_{postn}}{S_{bcn}} - \frac{M_{\sec n}}{S_{bcn}} \le 0.6 f_c' . \qquad (5\text{-}4)$$

where M_{postn} is the primary moment due to post-tensioning; M_{sectn} is the secondary moment due to post-tensioning; M_{rn} is the moment due to temporary support removal; n_{po} is the total number of post-tensioned strands; a_{psn} is the total number of post-tensioning strands; f_{pof} is the effective prestress in the post-tensioned strands after post-tensioning; f_{pe3n} is the effective prestress in the pre-tensioned strands after post-tensioning; and σ_{b3n} is the girder bottom stress along negative segment.

Constraint 4da: Compression Stress Check Under Full Service Load

This constraint corresponds to the service condition where the composite girders carry full live loads and superimposed dead loads in addition to the loads applied in the previous stages. Prestress losses for this stage include elastic shortening, creep, shrinkage, steel relaxation, and additional elastic shortening due to post-tensioning. The compression stress limit under full service load is thus defined by:

$$\sigma_{4da} = -\frac{M_{gn}}{S_{bgn}} - \frac{M_{dn}}{S_{bgn}} - \frac{M_{hn}}{S_{bgn}} - \frac{M_{rn}}{S_{bcn}} - \frac{M_{sn}}{S_{bcn}} - \frac{M_{l\ln}}{S_{bcn}} + \frac{A_{psn} f_{pe4n}}{A_{gn}} +$$

$$\frac{A_{psn}f_{pe4n}e_{pn}}{S_{bgn}} + \frac{n_{po}a_{psn}f_{poff}}{A_{cn}} + \frac{M_{postn}}{S_{bcn}} - \frac{M_{\sec n}}{S_{bcn}} \qquad \leq 0.6f_c', \qquad (5\text{-}5)$$

where M_{lln} is the live load moment due to truck and lane loadings; f_{poff} is the effective prestress in the post-tensioned strands after applying the live load; f_{pe4n} is the effective prestress in the pre-tensioned strands after applying the live load; and σ_{b4n} is the girder bottom stress along the negative segment.

Constraint 5da: Tension Stress Check with Reduced Live Load

The applied loads and prestress losses for this constraint are similar to *Constraint 4da* except that the live load is reduced by 20 percent. The objective is to check the tension limit state of the girder at the final stage as defined by:

$$\sigma_{5da} = -\frac{M_{gn}}{S_{bgn}} - \frac{M_{dn}}{S_{bgn}} - \frac{M_{hn}}{S_{bgn}} - \frac{M_{rn}}{S_{bcn}} - \frac{M_{sn}}{S_{bcn}} - 0.8 \times \frac{M_{l\ln}}{S_{bcn}} + \frac{A_{psn}f_{pe4n}}{A_{gn}} +$$

$$\frac{A_{psn}f_{pe4n}e_{pn}}{S_{bgn}} \frac{n_{po}a_{psn}f_{poff}}{A_{cn}} + \frac{M_{post}}{S_{bcn}} - \frac{M_{\sec}}{S_{bcn}} \geq -0.0724\sqrt{f_c'} \qquad \text{(MPa)}$$

$$\geq -0.19\sqrt{f_c'} \text{ (ksi)} \qquad (5\text{-}6)$$

Constraint 6da: Compression Stress Check Without Live Load

This constraint considers all loads and prestress losses as defined for *Constraint 4da* with the exception of live load. The compression limit state under these conditions is then checked according to:

$$\sigma_{6da} = -\frac{M_{gn}}{S_{bgn}} - \frac{M_{dn}}{S_{bgn}} - \frac{M_{hn}}{S_{bgn}} - \frac{M_{rn}}{S_{bcn}} - \frac{M_{sn}}{S_{bcn}} + \frac{A_{psn}f_{pe4}}{A_{gn}} + \frac{A_{psn}f_{pe4n}e_{pn}}{S_{bgn}} +$$

$$\frac{n_{po}a_{psn}f_{poff}}{A_{cn}}+\frac{M_{post}}{S_{bcn}}-\frac{M_{\sec}}{S_{bcn}}\leq 0.45f_c'. \qquad (5\text{-}7)$$

Constraint 7da: Compression Stress Check for Partial Service Load

This critical stress check considers all of the loads of *Constraint 4da* reduced by 50 percent except the live load. All prestress losses considered for *Constraint 4da* apply here also. The bottom girder stress check is then defined by:

$$\sigma_{7da}=0.5\times[-\frac{M_{gn}}{S_{bgn}}-\frac{M_{dn}}{S_{bgn}}-\frac{M_{hn}}{S_{bgn}}-\frac{M_{rn}}{S_{bcn}}-\frac{M_{sn}}{S_{bcn}}+\frac{A_{psn}f_{pe4n}}{A_{gn}}+$$

$$\frac{A_{psn}f_{pe4n}e_{pn}}{S_{bgn}}\frac{n_{po}a_{psn}f_{poff}}{A_{cn}}+\frac{M_{post}}{S_{bcn}}-\frac{M_{\sec}}{S_{bcn}}]-\frac{M_{l\ln}}{S_{tcn}}\leq 0.4f_c' \qquad (5\text{-}8)$$

5.7 Optimum Design of Two-Span SGB by Multi-Staged Post-Tensioned Systems

The use of multi-staged post-tensioning where the non-composite girders are stressed for continuity prior to placement of the deck is commonly used in multi-span spliced girder bridges. Spliced girder bridges made continuous with multiple post-tensioning operations were investigated herein to determine the efficiency of the system in terms of construction cost as well as the resulting maximum achievable span length.

5.7.1 Design variables

The design variables for the multi-stage post-tensioning construction method are similar to those used for the single-stage post-tensioned application. An additional design variable in this construction method is the number of post-tensioning strands on the second post-tensioning operation (npo_2). Post-tensioning is applied twice - before and after casting the deck. Figure 5-12 shows the post-tensioning design variables for the multi-stage post-tensioning construction method. Pre-tensioning design variables for the two-stage post-tensioning method are the same as those used for the single-stage post-tensioning method as shown in Figure 5-11b.

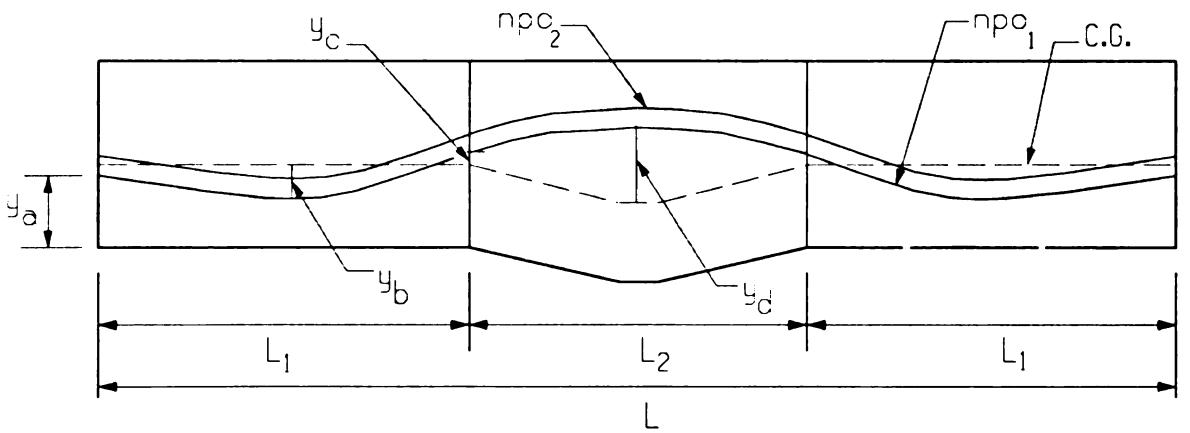

Figure 5-12 *Post-tensioning requirement variables for the design optimization of two-staged post-tensioning*

5.7.2 Objective function

The same objective function as that used for the single-stage post-tensioning construction method was used here, which was the minimization of structural cost. This was chosen in order to be able to compare the results from this section with those of Section 5.6.

5.7.3 Design Constraints

The optimization constraints used for this construction method include the service and strength limit states specified in the AASHTO-LRFD Bridge Design Specifications (AASHTO 2003) and the recommendations from NCHRP Report 517 (Castrodale and White 2004).

Constraints for the strength limit state included checks of moment and shear capacities and checks of the ductility requirement ($c/d_e < 0.42$) according to AASHTO-LRFD (AASHTO 2003). Constraints for the service limit state were defined in terms of flexural stress limits on both the girder and deck as outlined in Table 4-9. Stresses at each critical construction stage were checked against the allowable compression and tension stresses recommended by the AASHTO-LRFD Specifications (AASHTO 2003), see Table 5-5.

Table 5-5 *Construction sequence for multi-stage post-tensioning*

Construction Stages	Time (days)	Action Description	Pre-Tensioning Critical Stage	Post-Tensioning Critical Stage
1	-	Stress pre-tensioning strands		
2	0	Cast girder segments		
3	1	Release pre-tensioning strands	X	
4	50	Erect girder segments		
5	75	Stress 1st post-tensioning	X	X
6	90	Place deck and splice concrete	X	X
7	120	Stress 2nd post-tensioning	X	X
8	130	Add barriers		X
9	140	Apply live load		
10	15000	Add future wearing surface		
11	27500	After all pre-stress losses	X	X

There are ten critical stage constraints on each location of the composite section. Three locations across the composite girder-deck section, namely, the girder bottom and top, and the top of the deck were checked along the span length of beam at each critical construction stage to guarantee that all stresses were within the prescribed limits.

The formulation for the bottom girder stress constraints (*Constraints 1dm to 8dm*) for each critical construction stage of the service limit state are outlined below. Similar constraint formulations were defined and implemented for the stresses at the top of the girder (*Constraints 1em to 7em*) and at the top of the deck (*Constraints 1fm to 7fm*). The constraint expressions outlined below are the stress checks on the negative segment. Similar constraint formulations were defined and implemented for the positive segments.

Constraint 1dm: Compression Stress Check at Pre-Tensioning Stage.

The stresses at this stage are similar to *Constraint 1da* in Section 5.6, which include the girder weight and the pre-tensioning force. The section properties of the negative section vary along the negative pier segment for the non-prismatic sections and are clearly uniform for the prismatic sections.

Only prestress losses due to relaxation at release and elastic shortening were deducted from the initial prestress. Elastic shortening losses were assumed to be constant along the negative segment by using the average section properties of non-prismatic elements; whereas the actual stresses along the span were evaluated from their varied girder gross section properties (A_{gn} and S_{bgn}) and eccentricity of pre-tensioned strands (e_{pn}). The bottom girder compression stress constraint is thus expressed as follows:

$$\sigma_{1dm} = -\frac{M_{gn}}{S_{bgn}} + \frac{A_{psn} f_{pe1n}}{A_{gn}} - \frac{A_{psn} f_{pe1n} e_{pn}}{S_{bgn}} \leq 0.6 f'_{ci}. \qquad (5\text{-}9)$$

Constraint 2dm: Compression Stress Check at First Post-Tensioning Stage

For this construction method post-tensioning is applied prior to pouring the deck. Thus, only the non-composite girder section is used to resist additional loads due to post-tensioning forces. A tendon profile with multiple quadratic parabolic profiles was used to define the equivalent post-tensioning tendon location along the girders. Prestress losses for this stage include those from elastic shortening, creep, shrinkage, and steel relaxation.

Creep and elastic shortening losses on non-prismatic pier segments were determined by using the average girder gross section properties. These average section

properties include the average cross-sectional area, the average gross moment of intertia, and the average eccentricity of the pre-tensioned strands. These losses were assumed to be uniform along the negative segment. The actual stresses along the span were also evaluated from their varied girder sectional properties (A_{gn} and S_{bgn}) and eccentricity of pre-tensioned strands (e_{pn}). The bottom girder compressive stresses are thus constrained by the following expression:

$$\sigma_{2dm} = -\frac{M_{gn}}{S_{bgn}} + \frac{A_{psn} f_{pe2n}}{A_{gn}} + \frac{A_{psn} f_{pe2n} e_{pn}}{S_{bgn}} + \frac{n_{po1} a_{psn} f_{pof1}}{A_{gn}} -$$

$$\frac{M_{post1}}{S_{bgn}} - \frac{M_{sec1}}{S_{bgn}} \leq 0.6 f_c' , \qquad (5\text{-}10)$$

where M_{post1} is the primary moment due to first stage post-tensioning; M_{sec1} is the secondary moment due to first stage post-tensioning; n_{po1} is the total number of first stage post-tensioned strands; f_{pof1} is the effective pre-stress in the first post-tensioning strands after first post-tensioning; and σ_{b2n} is the girder bottom stress along the negative segment after first stage post-tensioning.

Constraint 3dm: Compression Stress Check at Deck and Splice Placement Stage

The deck, haunch and splice are poured at this stage after longitudinal post-tensioning in the second stage. These segments then become continuous along the span length. Prestress losses for this stage include those from elastic shortening, creep, shrinkage, and steel relaxation. The bottom girder stress constraint is thus defined by:

$$\sigma_{3dm} = -\frac{M_{gn}}{S_{bgn}} - \frac{M_{dn}}{S_{bgn}} - \frac{M_{hn}}{S_{bgn}} - \frac{M_{cn}}{S_{bgn}} + \frac{A_{psn} f_{pe3n}}{A_{gn}} - \frac{A_{psn} f_{pe3n} e_{pn}}{S_{bgn}}$$

$$\frac{n_{po1} a_{psn} f_{pof1}}{A_{gn}} + \frac{M_{post1}}{S_{bgn}} - \frac{M_{sec1}}{S_{bgn}} \leq 0.6 f_c', \tag{5-11}$$

where σ_{b3n} is the girder bottom stress along the negative segment after deck and splice placement.

Constraint 4dm: Compression Stress Check at Second Post-Tensioning Stage

A tendon profile defined by multiple quadratic parabolic curves, similar to the first post-tensioning, was also used to define the second equivalent post-tensioning tendon location along the girders. Second post-tensioning is applied after casting of the deck and splice, thus the composite girder section is used to resist additional loads due to post-tensioning forces. Only forces from the second post-tensioning operation are resisted by the composite section of the girder and deck. The previous forces are still resisted by the non-composite section. Prestress losses for this constraint include those from elastic shortening, creep, shrinkage, steel relaxation and additional elastic shortening due to post-tensioning. The bottom girder stress constraint is thus defined by:

$$\sigma_{4dm} = -\frac{M_{gn}}{S_{bgn}} - \frac{M_{dn}}{S_{bgn}} - \frac{M_{hn}}{S_{bgn}} + \frac{A_{psn} f_{pe4n}}{A_{gn}} + \frac{A_{psn} f_{pe4n} e_{pn}}{S_{bgn}} + \frac{M_{post2}}{S_{bcn}} + \frac{M_{sec2}}{S_{bcn}} +$$

$$\frac{n_{po1} a_{psn} f_{poff1}}{A_{gn}} + \frac{M_{post1}}{S_{bgn}} - \frac{M_{sec1}}{S_{bgn}} + \frac{n_{po2} a_{psn} f_{pof2}}{A_{cn}} \leq 0.6 f_c' \tag{5-12}$$

where M_{post2} is the primary moment due to second stage post-tensioning; M_{sec2} is the secondary moment due to second stage post-tensioning; n_{po2} is the total number of second stage post-tensioning strands; f_{poff1} is the effective prestress in the first post-tensioning strands after second post-tensioning; f_{pof2} is the effective prestress in the second post-tensioning strands after second post-tensioning; and σ_{b4n} is the girder bottom stress along the negative segment after second stage post-tensioning.

Constraint 5dm: Compression Stress Check under Full Service Load

Compression stress limits under full service load are checked at this constraint. Only forces from the applied superimposed dead loads, loads from the removal of temporary supports, and live loads are resisted by the composite section of girder and deck. The previous forces are still resisted by the non-composite section. Prestress losses for this constraint include elastic shortening, creep, shrinkage, steel relaxation, and additional elastic shortening due to post-tensioning. The compression stress limit under full service load is thus defined by:

$$\sigma_{5dm} = -\frac{M_{gn}}{S_{bgn}} - \frac{M_{dn}}{S_{bgn}} - \frac{M_{hn}}{S_{bgn}} - \frac{M_{rn}}{S_{bcn}} - \frac{M_{sn}}{S_{bcn}} - \frac{M_{l\ln}}{S_{bcn}} + \frac{A_{psn} f_{pe4n}}{A_{gn}} +$$

$$\frac{A_{psn} f_{pe4n} e_{pn}}{S_{bgn}} + \frac{n_{po1} a_{psn} f_{poff1}}{A_{gn}} + \frac{M_{post1}}{S_{bgn}} - \frac{M_{sec1}}{S_{bgn}} +$$

$$\frac{n_{po2} a_{psn} f_{poff2}}{A_{cn}} + \frac{M_{post2}}{S_{bcn}} - \frac{M_{sec2}}{S_{bcn}} \le 0.6 f'_c \qquad (5\text{-}13)$$

Constraint 6dm: Tension Stress Check with Reduced Live Load

The applied loads and prestress losses for this constraint are similar to those in *Constraint 4dm* except that the live load is reduced by 20 percent. The objective is to check the tension limit state of the girder at the final stage as defined by:

$$\sigma_{6dm} = -\frac{M_{gn}}{S_{bgn}} - \frac{M_{dn}}{S_{bgn}} - \frac{M_{hn}}{S_{bgn}} - \frac{M_{rn}}{S_{bcn}} - \frac{M_{sn}}{S_{bcn}} - 0.8 \times \frac{M_{l\ln}}{S_{bcn}} + \frac{A_{psn} f_{pe4n}}{A_{gn}} +$$

$$\frac{A_{psn} f_{pe4n} e_{pn}}{S_{bgn}} + \frac{n_{po1} a_{psn} f_{poff1}}{A_{gn}} + \frac{M_{post1}}{S_{bgn}} - \frac{M_{sec1}}{S_{bgn}} +$$

$$\frac{n_{po2} a_{psn} f_{poff2}}{A_{cn}} + \frac{M_{post2}}{S_{bcn}} - \frac{M_{sec2}}{S_{bcn}} \ge -0.0724\sqrt{f'_c} \text{ (MPa)}$$

$$\ge -0.19\sqrt{f'_c} \text{ (ksi)} \qquad (5\text{-}14)$$

Constraint 7dm: Compression Stress Check Without Live Load

This constraint considers all loads and prestress losses as defined for *Constraint 4dm* with the exception of live load. The compression limit state under these conditions is then checked according to:

$$\sigma_{7dm} = -\frac{M_{gn}}{S_{bgn}} - \frac{M_{dn}}{S_{bgn}} - \frac{M_{hn}}{S_{bgn}} - \frac{M_{rn}}{S_{bcn}} - \frac{M_{sn}}{S_{bcn}} + \frac{A_{psn} f_{pe4n}}{A_{gn}} + \frac{A_{psn} f_{pe4n} e_{pn}}{S_{bgn}} +$$

$$\frac{n_{po1} a_{psn} f_{poff1}}{A_{gn}} + \frac{M_{post1}}{S_{bgn}} - \frac{M_{sec1}}{S_{bgn}} +$$

$$\frac{n_{po2} a_{psn} f_{poff2}}{A_{cn}} + \frac{n_{po2} a_{psn} f_{poff2} e_{en}}{S_{bcn}} \leq 0.45 f'_c. \qquad (5\text{-}15)$$

Constraint 8dm: Compression Stress Check for Partial Service Load

This critical stress check considers all of the loads of *Constraint 4dm* reduced by 50 percent except the live load. All prestress losses considered for *Constraint 4dm* apply here also. The bottom girder stress check is then defined by:

$$\sigma_{8dm} = 0.5 \times [-\frac{M_{gn}}{S_{bgn}} - \frac{M_{dn}}{S_{bgn}} - \frac{M_{hn}}{S_{bgn}} - \frac{M_{rn}}{S_{bcn}} - \frac{M_{sn}}{S_{bcn}} + \frac{A_{psn} f_{pe4n}}{A_{gn}} + \frac{A_{psn} f_{pe4n} e_{pn}}{S_{bgn}} +$$

$$\frac{n_{po1} a_{psn} f_{poff1}}{A_{gn}} + \frac{M_{post1}}{S_{bgn}} - \frac{M_{sec}}{S_{bgn}} +$$

$$\frac{n_{po2} a_{psn} f_{poff2}}{A_{cn}} + \frac{M_{post2}}{S_{bcn}} - \frac{M_{sec2}}{S_{bcn}}] - \frac{M_{l\ln}}{S_{bcn}} \leq 0.4 f'_c. \qquad (5\text{-}16)$$

5.8 Results and Discussion

5.8.1 Prestress requirements for single- and multi-stage post-tensioning construction methods

An AASHTO Type IV standard beam was used to investigate the effect of construction sequence on two-span continuous spliced girder bridges. The objective

functions were based on the minimization of superstructure construction cost. Beam spacing at 1.8 m (6ft), 2.4 m (8ft), and 3.0 m (10 ft) were investigated for three splice locations: (0.35L, 0.375L, and 0.40L), where L is the total bridge span length of both spans.

Figure 5-13 through Figure 5-19 show the prestressing requirements for different span lengths. Single-stage post-tensioning and multi-stage post-tensioning results were plotted in the same graphs in order to compare the requirements and the maximum achievable span lengths.

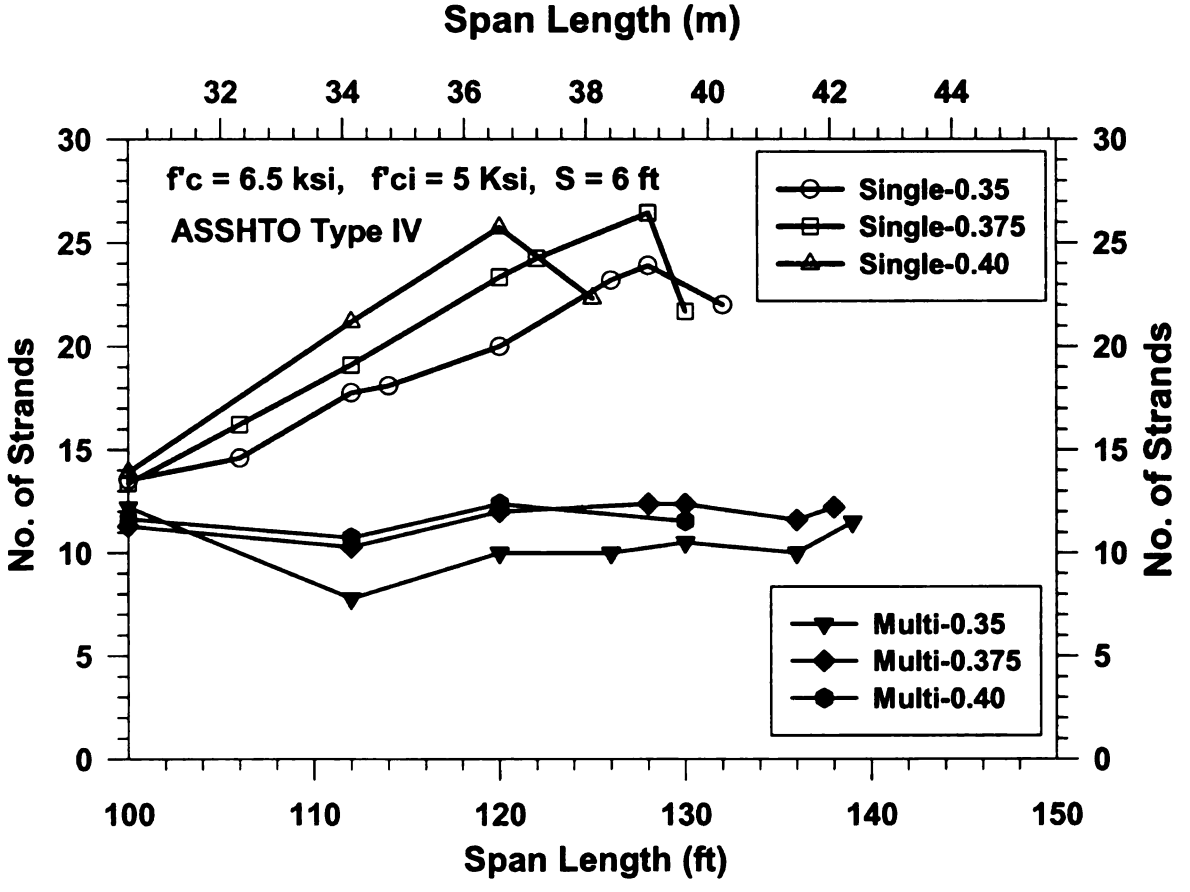

Figure 5-13 *Pre-tensioning requirements on positive segments for single- and multi-staged post-tensioning construction for S = 1.8 m (6ft)*

Based on the results shown in Figure 5-13, the splice location at 0.35 of the total span length is the most efficient splice location for both single- and multi-staged post-tensioning since it yields the maximum achievable span length in both cases. The results show that when multi-staged post-tensioning was used it yielded a longer span than when using a single-stage post-tensioning method. For example, at splice location of 0.35(L), the maximum achievable span length increased from 40.2 m (132 ft) to 42.4 m (139 ft) when employing a multi-stage construction method. This is about a 5% increase in span length.

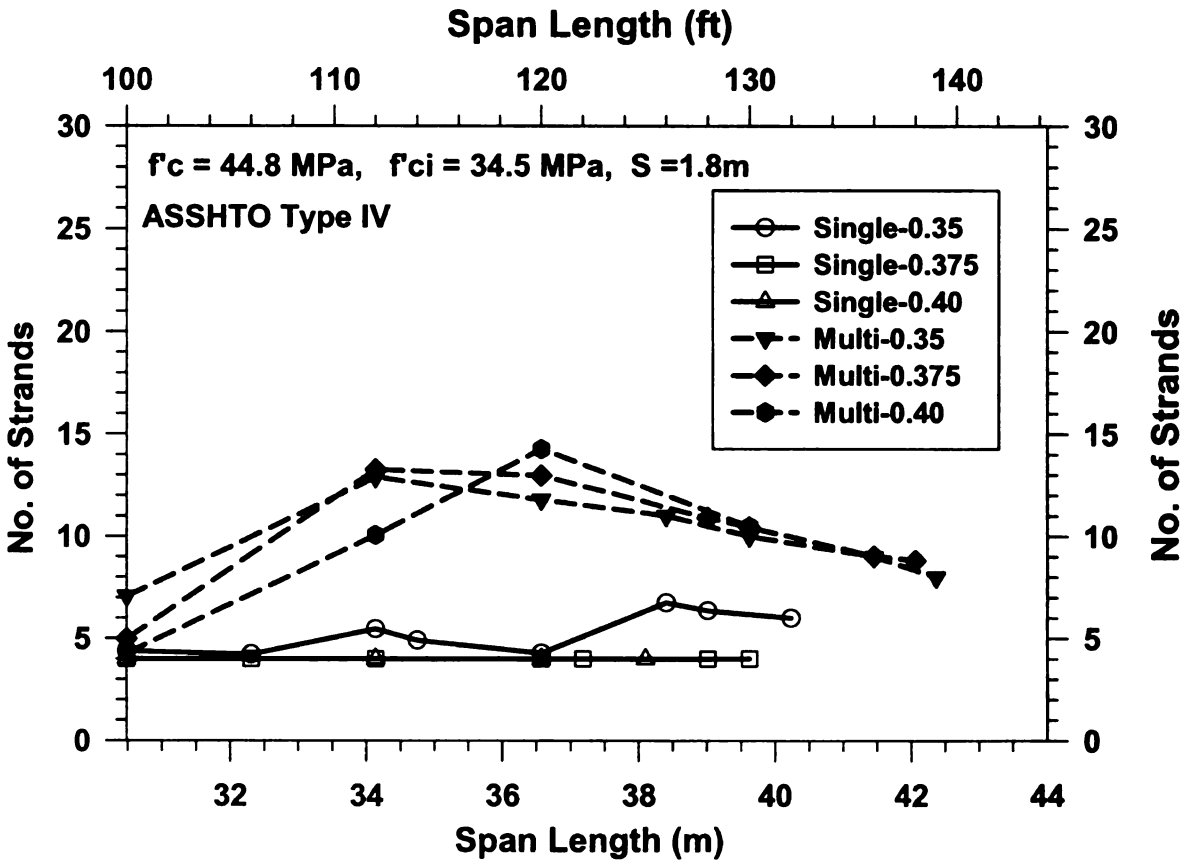

Figure 5-14 *Pre-tensioning requirements on the negative-segment of single- and multi-staged post-tensioning construction for S = 1.8 m (6 ft)*

The requirements of pre-tensioned strands for the AASHTO Type IV with a beam spacing of 1.8 m (6 ft) for the pier, or negative, segment are illustrated in Figure 5-14. It can be seen that pre-tensioned strand requirements at the positive segments for single-stage post-tensioning construction are higher than when using multi-stage post-tensioning; while the requirements of pre-tensioning strands at the pier segments for multi-stage post-tensioning construction are higher than those for a single-stage post-tensioning method. Requirements of pre-tensioned strands for a beam spacing of 2.4 m (8 ft) at the positive segments and at the negative segments are shown in Figure 5-15 and Figure 5-16, respectively. Figure 5-18 and Figure 5-21 provide the pre-stressing for a beam spacing of 3.0 m (10 ft). It can be seen that all of these graphs show the same result trends as interpreted above for a beam spacing of 1.8 m (6 ft).

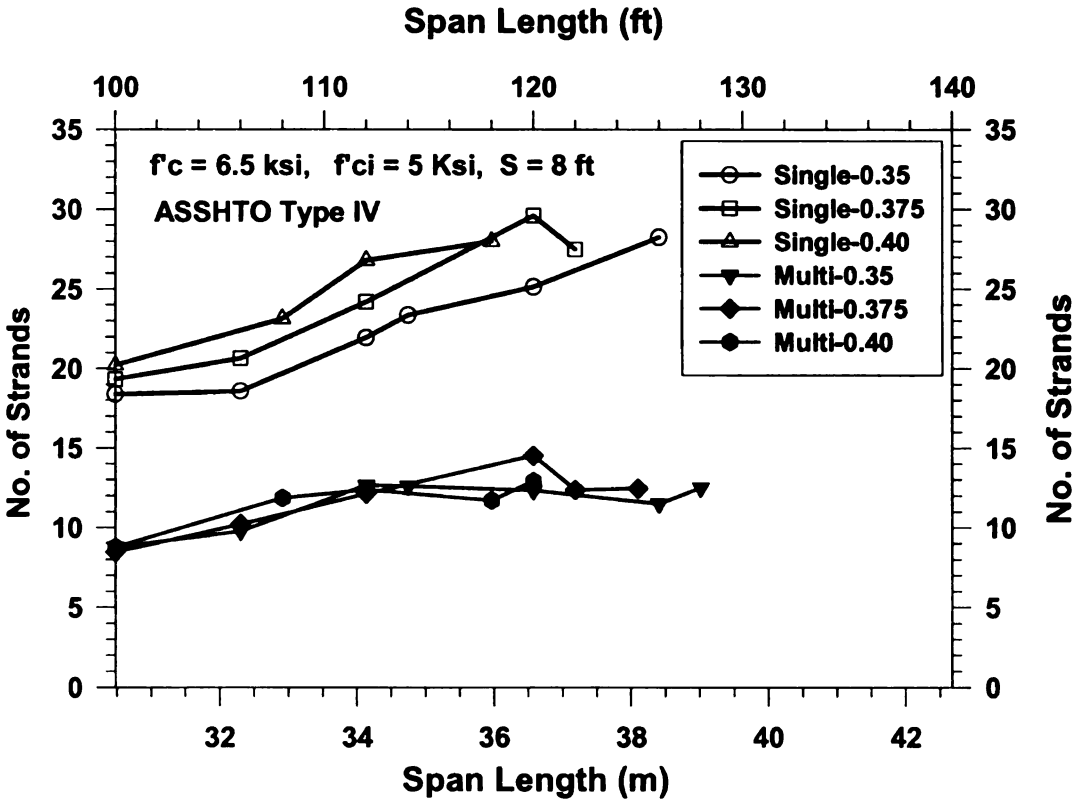

Figure 5-15 *Pre-tensioning requirements on positive segments of single- and multi-staged post-tensioning construction for S = 2.4 m (8 ft)*

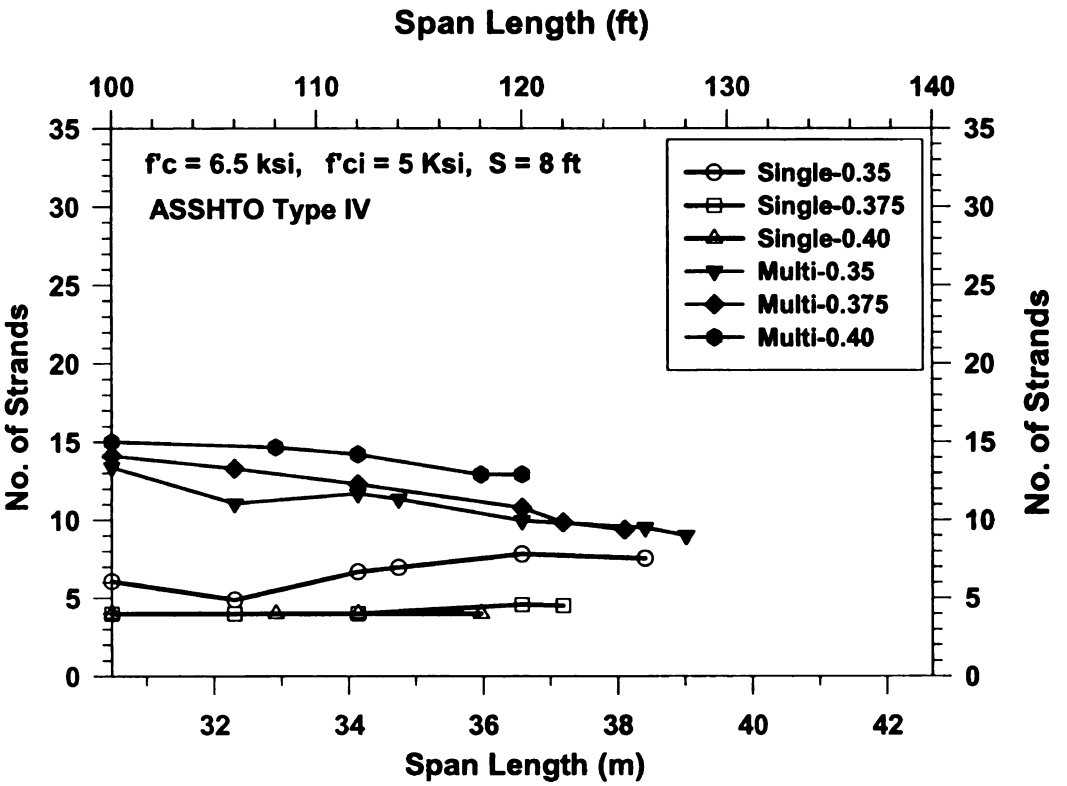

Figure 5-16 *Pre-tensioning requirements on negative segment of single- and multi-Staged Post-Tensioning Construction for S = 2.4 m (8 ft)*

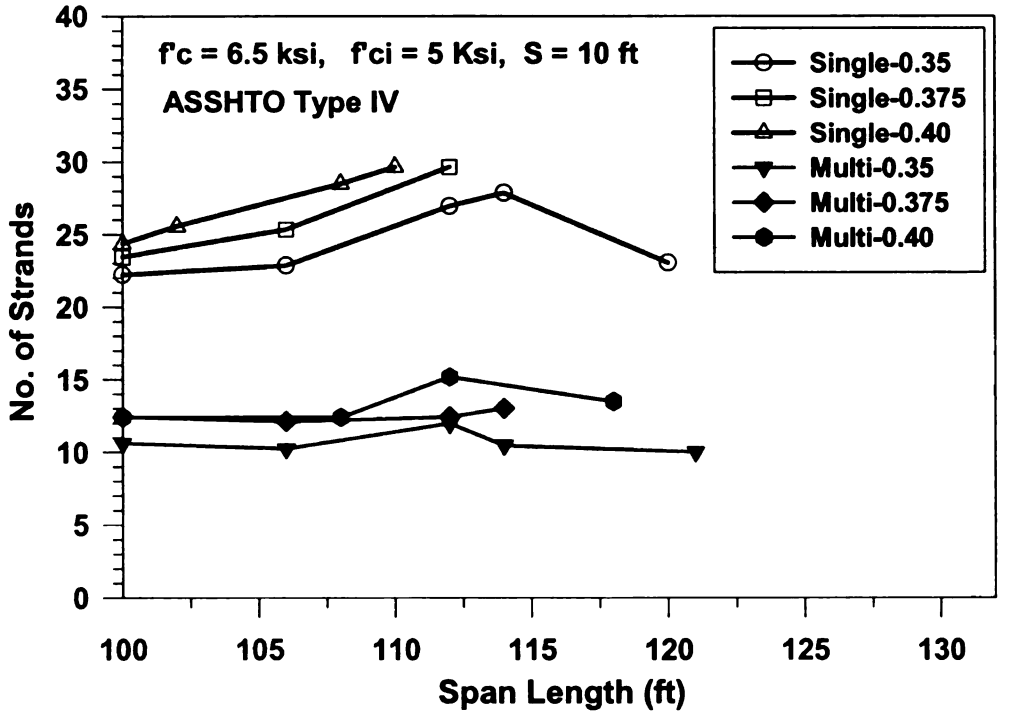

Figure 5-17 *Pre-tensioning requirements on positive segments of single- and multi-staged post-tensioning construction for S = 3.0 m (10 ft)*

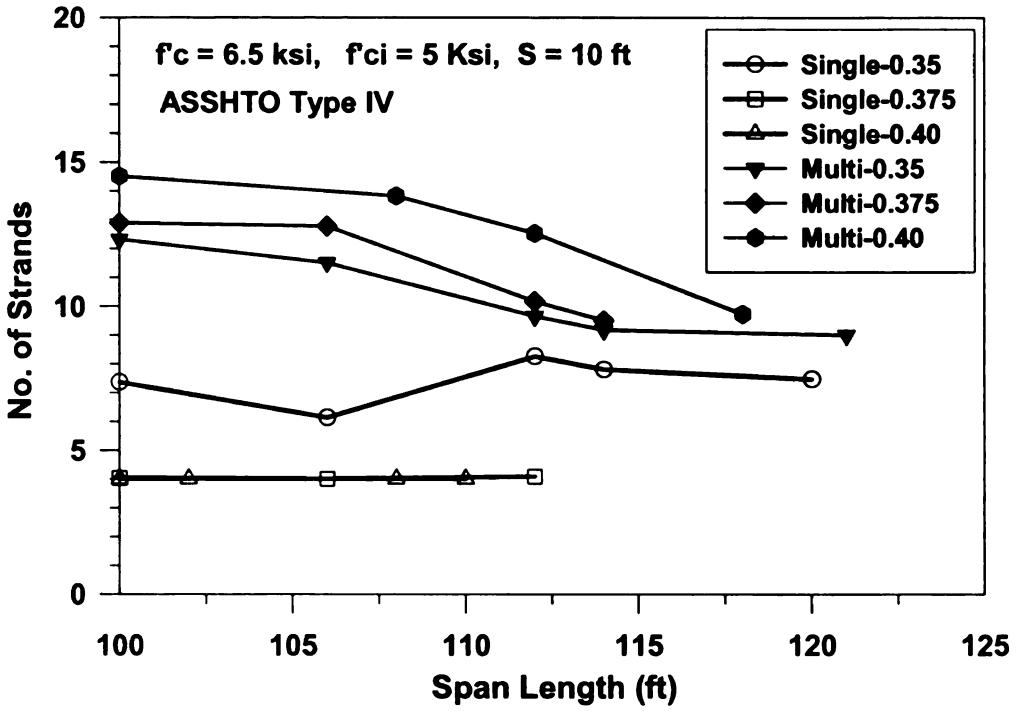

Figure 5-18 *Pre-tensioning requirements on negative segment of single- and multi-staged post-tensioning construction for S = 3.0 m (10 ft)*

Post-tensioning strand requirements for single-stage and multi-stage post-tensioning at 1.8 m (6 ft) beam spacing and different splice locations is illustrated in Figure 5-19. Requirements of post-tensioning strands for a beam spacing of 2.4 m (8 ft) and 3.0 m (10 ft) are also shown in Figure 5-20 and Figure 5-21, respectively.

The results in Figure 5-19 through Figure 5-21 show that more post-tensioning strands are required when a multi-stage post-tensioning construction method was used. Normally, the first post-tensioning stage requires only a minimum of post-tensioning strands to connect the segments together as a continuous piece. At this stage, the girder section is still non-composite. Therefore, not many post-tensioned strands can be applied. The first post-tensioning operation helps reduce cracking in the deck due to the

pre-compression force of the post-tensioning. The second post-tensioning operation is applied after the deck has already hardened and the girder/deck unit has become composite. Therefore, it is really only the additional post-tensioning beyond the initial stage that helps increase the span length of the system.

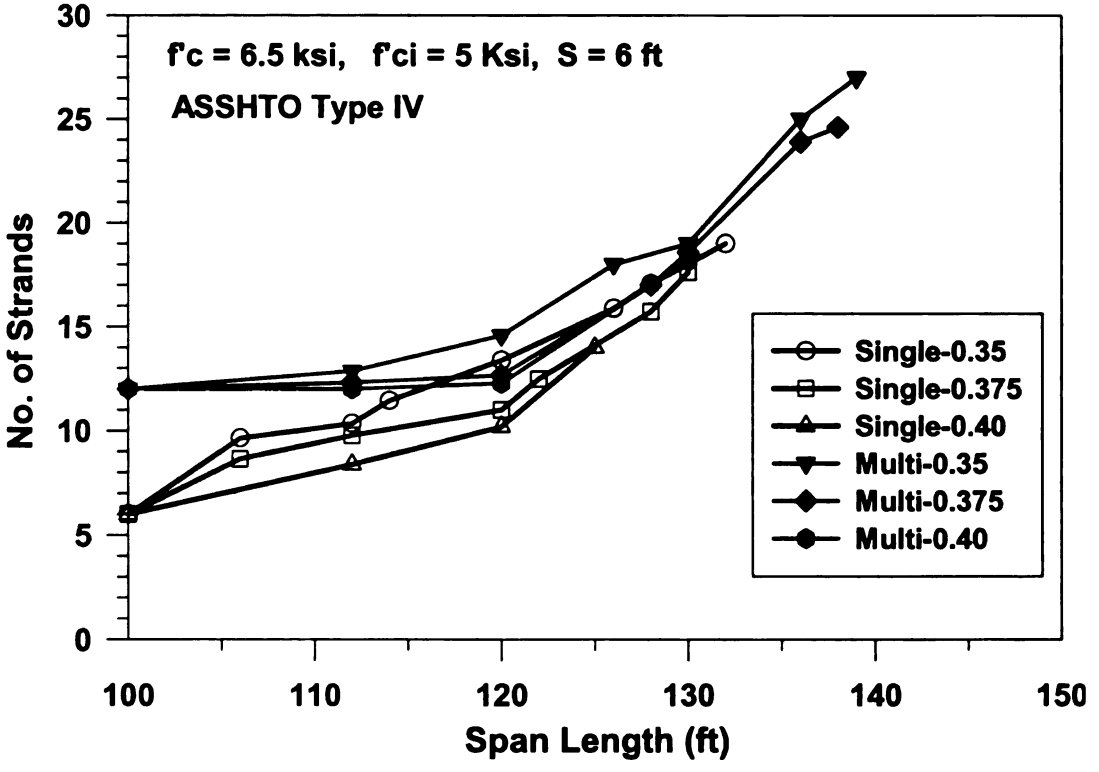

Figure 5-19 *Post-tensioning requirement of single- and multi-staged post-tensioning construction for S = 1.8 m (6 ft)*

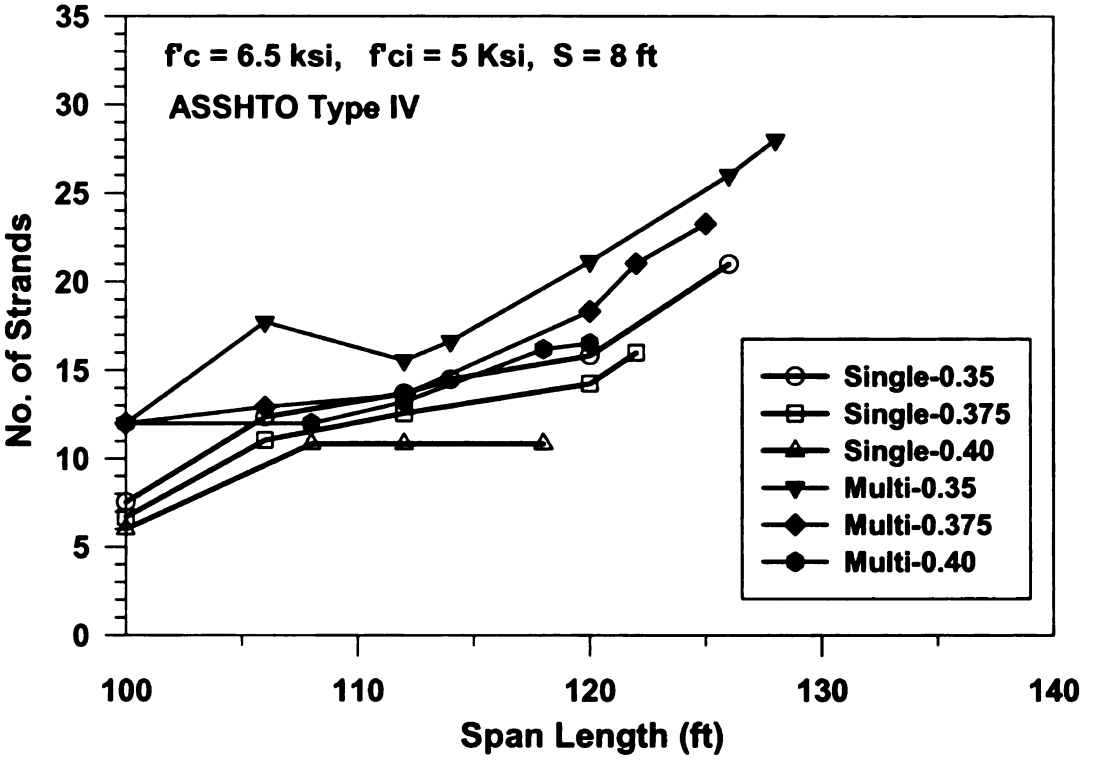

Figure 5-20 *Post-tensioning requirement of single- and multi-staged post-tensioning construction for S = 2.4 m (8 ft)*

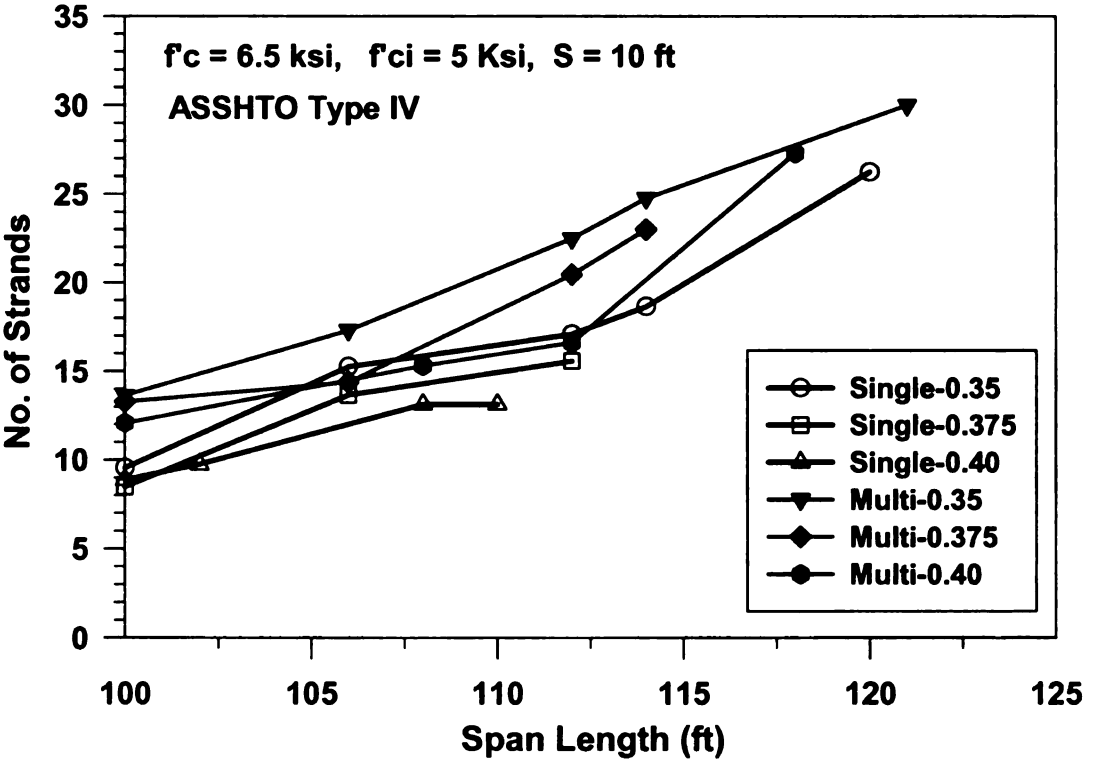

Figure 5-21 *Post-tensioning requirement of single- and multi-staged post-tensioning construction for S = 3.0 m (10 ft)*

The advantage of using a multi-stage post-tensioning construction method is the increase in the achievable span length. In addition, multi-stage post-tensioning is advantageous on projects where future deck replacement is anticipated since the deck can be removed without overstressing the existing girders. Although using a multi-stage post-tensioning approach is advantageous from a design point of view, the construction cost is more expensive. Staged post-tensioning would require that the post-tensioning supplier returns to the site a second (or more) times to complete the job. All post-tensioned strands need to be post-tensioned prior to having permanent connections. Construction time will thus increase since a detailed survey would be required after the first stage is done to define the grades for matching the girder cambers.

Single-stage post-tensioning allows the post-tensioning to be applied to the composite cross-section, thus making the system more efficient. Applying all of the post-tensioning after the deck is poured also has advantages over a multi-stage approach, among them the reduction in construction time. The post-tensioned subcontractor does not need to come back to the site since this method only requires a one-time application of the post-tensioning. Also, a larger prestressing force can be applied from pre-tensioning, resulting in reduced anchorage hardware costs. Thus, single-stage post-tensioning seems to be the favorable staged construction for spliced girder bridges since it is faster and less complex than multi-staged construction. However, this construction method has drawbacks in projects where future deck removal is anticipated. Removal of the deck during the lifetime of the bridge is complicated since the deck was present when the post-tensioning was applied. Thus, removal of the deck can overstress the

girders. One way to avoid this problem would thus be to use a multi-stage post-tensioning construction method.

5.8.2 Service moments for single- and multi-stage post-tensioning construction

The service moment diagrams for two-span continuous spliced girder bridges using AASHTO Type IV I-beams with a total span length of 68.6 m (225 ft) and a beam spacing of 1.8 m (6 ft) for a single-stage post-tensioning construction method are shown in Figure 5-22. This graph shows the moments acting on the non-composite and composite sections for comparison purposes. Moments acting on the non-composite girder section include those due to the girder/deck, haunch, deck, and construction loads; while moments acting on the composite girder section include those due to the temporary support loads, superimposed dead load and live load.

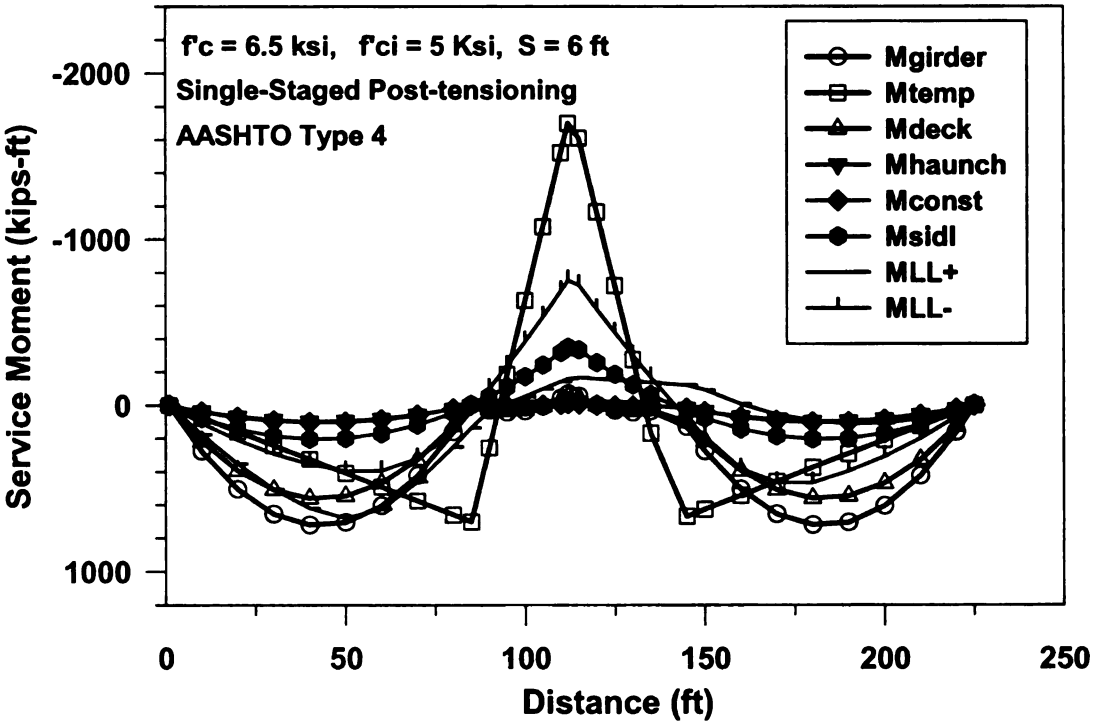

Figure 5-22 *Service moment demands on two-span continuous SGB built with single-staged post-tensioning with L = 68.3 m (224 ft) and S = 1.8 m (6 ft)*

Moment diagrams for the single-stage construction method are shown in Figure 5-23. Non-composite behavior was assumed for the spans between the abutment and the temporary supports for the positive segments and between the temporary support and a middle pier for the pier segment. Since the deck is cast before the post-tensioning, each segment still acts independently on the temporary supports. Consequently, moments caused by deck load are high in the positive segment and low in the negative segment. Temporary supports in single-stage post-tensioning construction have to carry all non-composite loads including the deck load before post-tensioning. Thus, the moment due to the removal of temporary supports is much higher than in multi-staged construction.

The moment demands along the 68.6 m (225 ft) span of a spliced girder system built through multi-staged post-tensioning construction are shown in Figure 5-23. Moments acting on the non-composite girder section include those due to the girder load, temporary support removal and secondary moments due to the first post-tensioning. The latter moment is not shown in Figure 5-23 since it is not a moment due to an external load. Rather, the secondary moment is an induced moment due to the first post-tensioning and was used in the stress calculations by considering it as part of the moment in the limit state stress calculation.

Moments acting on the composite girder section include those due to the girder/deck haunch, deck, construction loads, superimposed dead load and live load. For a multi-stage construction, the first post-tensioning operation makes all the separate segments become a continuous piece before applying the deck. Thus, the loads from the removal of temporary supports loads are much smaller than in the single-stage post-tensioning method, which yields smaller support removal moments. Since the external

moments for the multi-stage construction method are smaller than the external moments in single-staged construction, the flexural stresses at each critical stage are smaller and the maximum achievable span length should also be longer. This observations support the design optimization results that were shown in Figure 5-13 through Figure 5-22.

For a single-stage post-tensioning construction method, the pre-stressing forces are used to balance the non-composite dead loads; while the post-tensioning forces are used to resist the effects of the composite superimposed dead loads and live loads, which require larger pre-tensioning forces and a larger cross-section for the girder. For multi-stage post-tensioning construction, the initial pre-tensioning force and first stage post-tensioning are used to balance only the self-weight of the girder and the fresh concrete deck. The post-tensioning force from the second operation balances the additional dead and live loads. Therefore, smaller pre-tensioning forces and smaller first-stage post-tensioning forces are required, leading to smaller cross sections compared with the single-stage post-tensioning construction method.

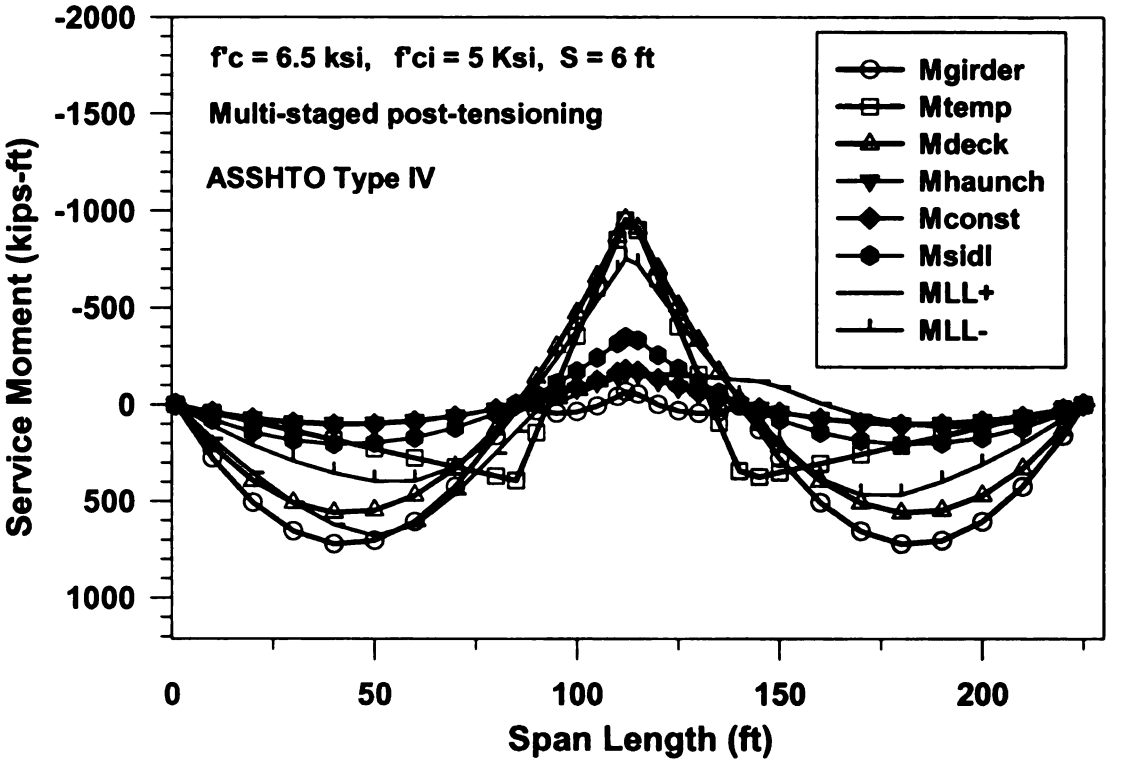

Figure 5-23 *Service moment of multi-staged post-tensioning with L = 68.3 m (224 ft) and S = 1.8 m (6 ft)*

5.8.3 Performance of pier segment option 1: standard beam with soffit

The efficiency of using a standard girder for both positive and negative spans (Option 1) in continuous two-span spliced girder bridges was evaluated by considering AASHTO's Type IV I-girder. The girder was provided with a tapering attached soffit on the negative segment. The maximum soffit thickness (over the pier center line) was increased from *0.1H* to *0.5H,* where *H* is the total height of the standard girder. The width of soffit was assumed to be equal to the width of girder bottom flange.

The objective function for the optimization problem was the minimization of superstructure construction cost. The AASHTO Type IV I-girders were spaced at 1.8 m (6 ft), 2.1 m (7 ft) and 2.4 m (8 ft) on center. Three splice locations were evaluated at

0.20L, 0.223L, and 0.25L 0.223L, where L is the total system span length. Only the results for maximum achievable span length for different beam spacing, the soffit requirement, and splice location are shown in this section. The prestressing requirements and their vertical locations along the span are provided in the form of design charts.

The maximum achievable span lengths for different soffit thicknesses at different splice locations and beam spacing were determined from the design optimization process (see Section 5.4) and the results are shown in Figure 5-24 through Figure 5-26. Figure 5-24 represents the relationship of maximum soffit thickness to achievable span length for 1.8 m (6 ft) beam spacing. The splice location at 0.35(L) was found to be the most efficient splice location since it yielded a longer span than any other splice locations with the same soffit thickness. Results show that span length is increased about 300 mm (1 ft) for every 137 mm (5.4in.) of added soffit thickness (maximum value at pier), which is about 10% of the total beam height (height of Type IV beam is 1220 mm (54 in.). The percent increase in span length compared to the total span length is less than 1%, which is very small. The results for 2.1 m (7 ft) and 2.4 m (8 ft) beam spacing are shown in Figure 5-25 and Figure 5-26, which illustrate the same trends as discussed above.

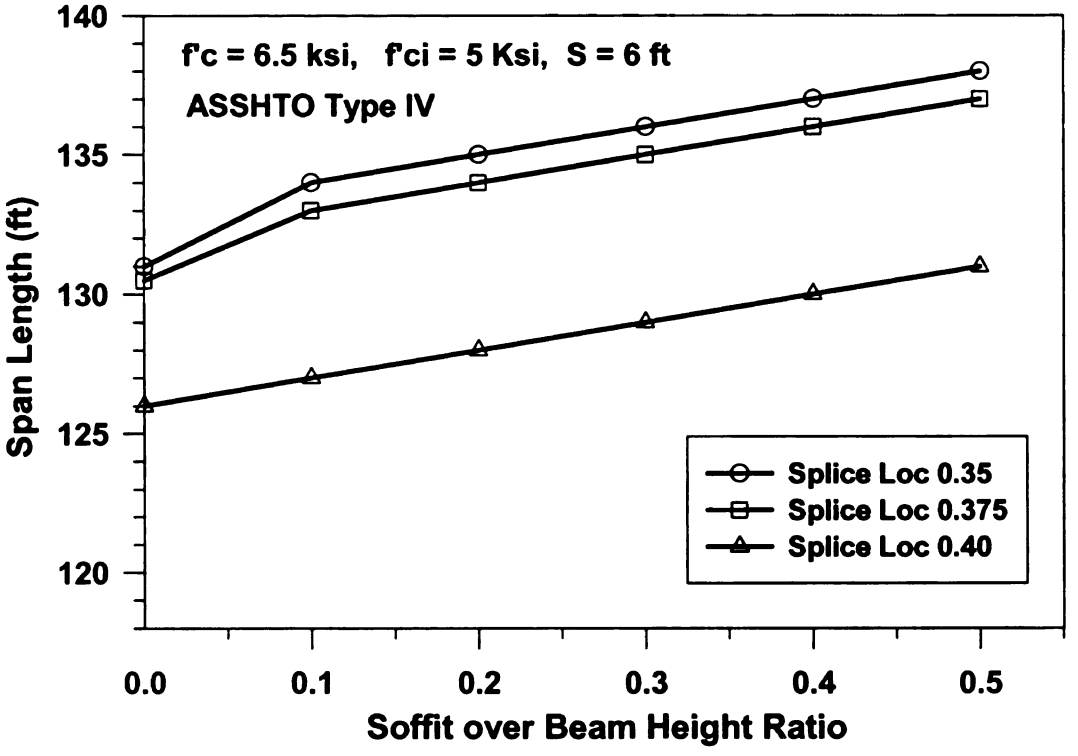

Figure 5-24 *Maximum span length of ASSHTO Type IV standard beam with soffit at beam spacing 1.8 m (6 ft)*

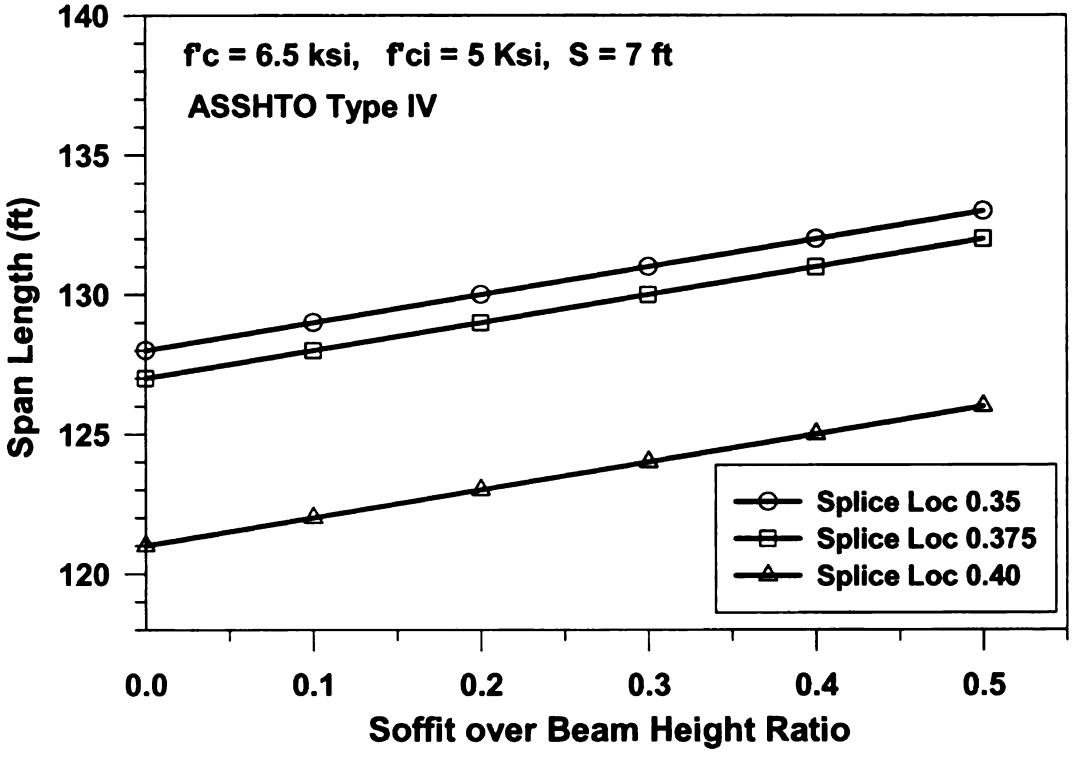

Figure 5-25 *Maximum span length of ASSHTO Type IV standard beam with soffit at beam spacing 2.1 m (7 ft)*

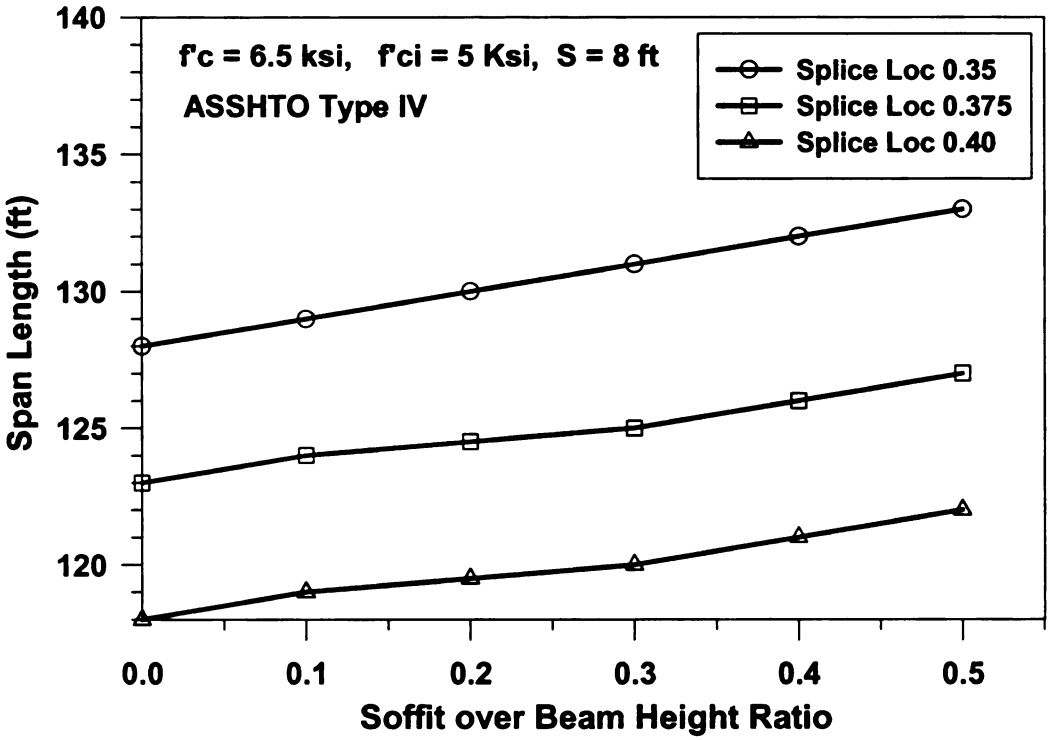

Figure 5-26 *Maximum span length of ASSHTO Type IV standard beam with soffit at beam spacing 2.4 m (8 ft)*

5.8.4 Dimensions and performance of optimized pier segments- options 2, 3 and 4

The objective function used to develop new optimal pier, or negative, segments was to minimize concrete volume, which is equivalent to minimizing girder weight. The new optimal negative sections include a new optimal non-prismatic section with varied web depth (option 2), a new optimal non-prismatic section with constant web depth (option 3), and a new optimal prismatic section (option 4). Minimum construction cost was not chosen as the main objective function here since there is no explicit cost

available for the modified girder. However, an objective function based on minimum concrete volume can be directly defined from the girder geometry.

The development of optimal *prismatic* pier sections (options 4 – see Figure 5-6 and Figure 5-10) was done in accordance to Section 5.4 for different span lengths, beam spacing, and the most efficient splice location (at 0.35L). Geometric design variables were those needed for the relevant component optimization together with those from the system optimization. The obtained optimal girder dimension results are listed in Table 5-6. These new sections were developed by increasing the span length in 3050 mm (10 ft) increment to obtain the beam height range. Designers and producers can use these values to develop standard beams by grouping them within desired span length and beam spacing ranges. The prismatic sections were used for both positive and negative segments.

Table 5-6 *Dimensions of optimized prismatic beams (option 4) for two-span continuous spliced girder bridges – SI units*

S (m)	L (m)	H (m)	b_1 (m)	b_2 (m)	t_1 (m)	t_2 (m)	t_3 (m)	t_4 (m)	D_w (m)	t_w (m)
1.8	**36.6**	1.27	0.61	0.46	0.13	0.13	0.13	0.13	0.76	0.20
1.8	**40.2**	1.55	0.61	0.46	0.13	0.13	0.13	0.13	1.03	0.20
1.8	**42.7**	1.65	0.61	0.46	0.13	0.13	0.13	0.13	1.14	0.20
1.8	**45.7**	1.91	0.61	0.46	0.13	0.13	0.13	0.13	1.38	0.20
1.8	**48.8**	2.13	0.61	0.46	0.13	0.13	0.13	0.13	1.63	0.20
1.8	**52.4**	2.51	0.65	0.46	0.13	0.13	0.13	0.13	2.01	0.20
1.8	**54.9**	2.72	0.65	0.46	0.13	0.13	0.13	0.13	2.20	0.20
2.1	**36.6**	1.37	0.61	0.46	0.13	0.13	0.13	0.13	0.86	0.20
2.1	**40.2**	1.66	0.61	0.46	0.13	0.13	0.13	0.13	1.15	0.20
2.1	**42.7**	1.78	0.61	0.46	0.13	0.13	0.13	0.13	1.27	0.20
2.1	**45.7**	2.08	0.61	0.46	0.13	0.13	0.13	0.13	1.56	0.20
2.1	**48.8**	2.34	0.61	0.46	0.13	0.13	0.13	0.13	1.83	0.20
2.1	**52.4**	2.64	0.71	0.46	0.13	0.13	0.13	0.13	2.13	0.20
2.1	**54.9**	2.90	0.68	0.46	0.13	0.13	0.13	0.13	2.37	0.20
2.4	**36.6**	1.47	0.61	0.46	0.13	0.13	0.13	0.13	0.97	0.20
2.4	**40.2**	1.78	0.61	0.46	0.13	0.13	0.13	0.13	1.25	0.20
2.4	**42.7**	1.93	0.61	0.46	0.13	0.13	0.13	0.13	1.40	0.20
2.4	**45.7**	2.18	0.61	0.46	0.13	0.13	0.13	0.13	1.68	0.20
2.4	**48.8**	2.49	0.62	0.47	0.13	0.13	0.13	0.13	1.98	0.20
2.4	**52.4**	2.79	0.76	0.46	0.13	0.13	0.13	0.13	2.26	0.20
2.4	**54.9**	3.02	0.74	0.46	0.13	0.13	0.13	0.13	2.50	0.20

Based on the component and system optimization results, new proposed girder dimensions for prismatic elements were obtained and are listed in Table 5-6, while the requirements and location of pre-tensioning and post-tensioning strands are partially shown in Chapter 6 in the form of design charts. For a complete design charts, please refer to MSU-CE report (Surakomol and Burgueno 2005).

Table 5-6 *Dimensions of optimized prismatic beams (option 4) for two-span continuous spliced girder bridges – US units (Cont...)*

S (ft)	L (ft)	H (in.)	b_1 (in.)	b_2 (in.)	t_1 (in.)	t_2 (in.)	t_3 (in.)	t_4 (in.)	D_w (in.)	t_w (in.)
6	**120**	50	24	18	5	5	5	5	30	8
6	**132**	61	24	18	5	5	5	5	41	8
6	**140**	65	24	18	5	5	5	5	45	8
6	**150**	75	24	18	5	5	5	5	54	8
6	**160**	84	24	18	5	5	5	5	64	8
6	**172**	99	26	18	5	5	5	5	79	8
6	**180**	107	26	18	5	5	5	5	87	8
7	**120**	54	24	18	5	5	5	5	34	8
7	**132**	66	24	18	5	5	5	5	45	8
7	**140**	70	24	18	5	5	5	5	50	8
7	**150**	82	24	18	5	5	5	5	61	8
7	**160**	92	24	18	5	5	5	5	72	8
7	**172**	104	28	18	5	5	5	5	84	8
7	**180**	114	27	18	5	5	5	5	93	8
8	**120**	58	24	18	5	5	5	5	38	8
8	**132**	70	24	18	5	5	5	5	49	8
8	**140**	76	24	18	5	5	5	5	55	8
8	**150**	86	24	18	5	5	5	5	66	8
8	**160**	98	24	18	5	5	5	5	78	8
8	**172**	110	30	18	5	5	5	5	89	8
8	**180**	119	29	18	5	5	5	5	98	8

It can be seen that the bottom flange width (b_1) has a larger value than the top flange width (b_2). Results for the thickness of the top flanges (t_1 and t_2), the bottom flanges (t_3 and t_4) and the web thickness (t_w) yielded the pre-defined lower bound values for these variables. The prismatic girder height varied from 1.27m (50.0in.) to 3.02m (119.0in.) depending on the desired span length and beam spacing. The percent increase in total beam height is about 8% of span length increase.

The same specified span lengths and beam spacing were used as parameters to develop optimal non-prismatic beams with constant web height and varied bottom flange thickness: pier segment option3 as shown in Figure 5-5 and Figure 5-9. Their resulting dimensions are given in Table 5-7.

Table 5-7 *Dimensions of optimized non-prismatic beams with constant web height and varied flange (option 3) for two-span continuous spliced girder bridges – US Units*

S (m)	L (m)	H (m)	b_1 (m)	b_2 (m)	t_1 (m)	t_2 (m)	t_3 (m)	t_4 (m)	D_w (m)	t_w (m)	S (m)
1.8	**36.6**	1.19	0.61	0.46	0.13	0.13	0.13	0.13	0.20	0.68	0.12
1.8	**40.2**	1.35	0.61	0.51	0.13	0.13	0.13	0.13	0.20	0.83	0.13
1.8	**42.7**	1.52	0.61	0.51	0.13	0.13	0.13	0.13	0.20	1.00	0.15
1.8	**45.7**	1.73	0.61	0.51	0.13	0.13	0.13	0.13	0.20	1.22	0.17
1.8	**48.8**	1.83	0.61	0.51	0.13	0.13	0.13	0.18	0.20	1.27	0.18
1.8	**52.4**	2.18	0.61	0.51	0.13	0.13	0.13	0.15	0.20	1.65	0.22
1.8	**54.9**	2.34	0.61	0.51	0.13	0.13	0.13	0.18	0.20	1.78	0.23
2.1	**36.6**	1.24	0.61	0.51	0.13	0.13	0.13	0.13	0.20	0.72	0.12
2.1	**40.2**	1.43	0.61	0.51	0.13	0.13	0.13	0.13	0.20	0.92	0.14
2.1	**42.7**	1.60	0.61	0.51	0.13	0.13	0.13	0.13	0.20	1.09	0.16
2.1	**45.7**	1.83	0.66	0.51	0.13	0.13	0.13	0.13	0.20	1.31	0.18
2.1	**48.8**	2.01	0.61	0.51	0.13	0.13	0.13	0.13	0.20	1.49	0.20
2.1	**52.4**	2.13	0.61	0.51	0.13	0.13	0.13	0.18	0.20	1.68	0.21
2.1	**54.9**	2.44	0.66	0.51	0.13	0.13	0.13	0.20	0.20	1.86	0.24
2.4	**36.6**	1.37	0.61	0.46	0.13	0.13	0.13	0.13	0.20	0.86	0.14
2.4	**40.2**	1.52	0.61	0.51	0.13	0.13	0.13	0.13	0.20	1.02	0.15
2.4	**42.7**	1.75	0.61	0.51	0.13	0.13	0.13	0.13	0.20	1.18	0.18
2.4	**45.7**	1.91	0.61	0.51	0.13	0.13	0.13	0.13	0.20	1.40	0.19
2.4	**48.8**	2.24	0.61	0.51	0.13	0.13	0.13	0.18	0.20	1.64	0.22
2.4	**52.4**	2.34	0.61	0.51	0.13	0.13	0.13	0.19	0.20	1.77	0.23
2.4	**54.9**	2.57	0.61	0.51	0.13	0.13	0.13	0.20	0.20	1.98	0.26

The obtained values for the bottom flange width (b_1) were similar to the developed optimal prismatic section (see Table 5-6). However, larger values of the top flange width (b_2) were obtained for this new non-prismatic section. Again, the obtained

values for the thickness of the top flanges (t_1 and t_2) and the web thickness (t_w) hit the pre-defined lower bound. As expected, the thickness values for the bottom flanges (t_3 and t_4) do vary as noted in the results table. The maximum total height over the negative span varied from 1.31 m (52.0 in.) to 2.82m (111.0 in.) for the different span lengths and beam spacings. The percent increase of maximum total beam height for the negative segment is about 10%.

Table 5-8 lists the maximum achievable span lengths and new girder dimension for optimal non-prismatic beams with varied web height and constant bottom flange thickness: option 2 as shown in Figure 5-4 and Figure 5-8. The same previously specified span lengths and beam spacings were used as parameters to develop these new girders. Similar results to the new prismatic section (see Table 5-6) were obtained for the bottom flange width (b_1), but various values of top flange width (b_2) were obtained for this new optimal non-prismatic section. The thickness of the top flange (t_1 and $t2$) and bottom flange (t_3 and t_4), and the web thickness (t_w) were all bounded by the predefined lower value. The maximum total height over the pier varied from 1.8 m (69.0 in.) to 3.1 m (120.0 in.) for the different span lengths and beam spacings. The percent increase of the maximum total beam height for the negative segment was approximately 10%.

Table 5-7 *Dimensions of optimized non-prismatic beams with constant web height and varied flange (option 3) for two-span continuous SGB – US units (Cont...)*

S (ft)	L (ft)	H (in.)	b_1 (in.)	b_2 (in.)	t_1 (in.)	t_2 (in.)	t_3 (in.)	t_4 (in.)	D_w (in.)	t_w (in.)	S (in.)
6	**120**	47	24	18	5	5	5	5	8	27	4.7
6	**132**	53	24	20	5	5	5	5	8	33	5.3
6	**140**	60	24	20	5	5	5	5	8	39	6.0
6	**150**	68	24	20	5	5	5	5	8	48	6.8
6	**160**	72	24	20	5	5	5	7	8	50	7.2
6	**172**	86	24	20	5	5	5	6	8	65	8.6
6	**180**	92	24	20	5	5	5	7	8	70	9.2
7	**120**	49	24	20	5	5	5	5	8	28	4.9
7	**132**	56	24	20	5	5	5	5	8	36	5.6
7	**140**	63	24	20	5	5	5	5	8	43	6.3
7	**150**	72	26	20	5	5	5	5	8	52	7.2
7	**160**	79	24	20	5	5	5	5	8	59	7.9
7	**172**	84	24	20	5	5	5	7	8	66	8.4
7	**180**	96	26	20	5	5	5	8	8	73	9.6
8	**120**	54	24	18	5	5	5	5	8	34	5.4
8	**132**	60	24	20	5	5	5	5	8	40	6.0
8	**140**	69	24	20	5	5	5	5	8	46	6.9
8	**150**	75	24	20	5	5	5	5	8	55	7.5
8	**160**	88	24	20	5	5	5	7	8	65	8.8
8	**172**	92	24	20	5	5	5	7	8	70	9.2
8	**180**	101	24	20	5	5	5	8	8	78	10.1

Table 5-8 *Dimensions of optimized non-prismatic beams with constant flange and varied web (option 2) for two-span continuous spliced girder bridges – SI units*

S (m)	L (m)	H (m)	b_1 (m)	b_2 (m)	t_1 (m)	t_2 (m)	t_3 (m)	t_4 (m)	D_w (m)	t_w (m)	S (m)
1.8	**36.6**	1.17	0.61	0.46	0.13	0.13	0.13	0.13	0.20	0.66	0.12
1.8	**40.2**	1.30	0.61	0.46	0.13	0.13	0.13	0.13	0.20	0.79	0.13
1.8	**42.7**	1.42	0.61	0.46	0.13	0.13	0.13	0.13	0.20	0.89	0.14
1.8	**45.7**	1.60	0.61	0.46	0.13	0.13	0.13	0.13	0.20	1.09	0.16
1.8	**48.8**	1.78	0.61	0.46	0.13	0.13	0.13	0.13	0.20	1.24	0.18
1.8	**52.4**	2.06	0.61	0.51	0.13	0.13	0.13	0.13	0.20	1.55	0.21
1.8	**54.9**	2.26	0.61	0.51	0.13	0.13	0.13	0.13	0.20	1.75	0.23
2.1	**36.6**	1.22	0.61	0.46	0.13	0.13	0.13	0.13	0.20	0.72	0.12
2.1	**40.2**	1.42	0.61	0.46	0.13	0.13	0.13	0.13	0.20	0.89	0.14
2.1	**42.7**	1.52	0.61	0.46	0.13	0.13	0.13	0.13	0.20	1.02	0.15
2.1	**45.7**	1.68	0.61	0.46	0.13	0.13	0.13	0.13	0.20	1.17	0.17
2.1	**48.8**	2.11	0.61	0.46	0.13	0.13	0.13	0.13	0.20	1.57	0.21
2.1	**52.4**	2.16	0.61	0.51	0.13	0.13	0.13	0.13	0.20	1.63	0.22
2.1	**54.9**	2.54	0.61	0.51	0.13	0.13	0.13	0.13	0.20	2.01	0.25
2.4	**36.6**	1.30	0.61	0.48	0.13	0.13	0.13	0.13	0.20	0.79	0.13
2.4	**40.2**	1.60	0.61	0.46	0.13	0.13	0.13	0.13	0.20	1.09	0.16
2.4	**42.7**	1.70	0.61	0.46	0.13	0.13	0.13	0.13	0.20	1.19	0.17
2.4	**45.7**	1.93	0.61	0.48	0.13	0.13	0.13	0.13	0.20	1.42	0.19
2.4	**48.8**	2.03	0.61	0.51	0.13	0.13	0.13	0.13	0.20	1.50	0.20
2.4	**52.4**	2.49	0.61	0.46	0.13	0.13	0.13	0.13	0.20	1.96	0.25
2.4	**54.9**	2.59	0.61	0.51	0.13	0.13	0.13	0.13	0.20	2.03	0.26

Table 5-8 *Dimensions of optimized non-prismatic beams with constant flange and varied web(option 2) for two-span continuous spliced girder bridges – US units (Cont...)*

S (ft)	L (ft)	H (in.)	b_1 (in.)	b_2 (in.)	t_1 (in.)	t_2 (in.)	t_3 (in.)	t_4 (in.)	D_w (in.)	t_w (in.)	S (in.)
6	**120**	46	24	18	5	5	5	5	8	26	23
6	**132**	51	24	18	5	5	5	5	8	31	22
6	**140**	56	24	18	5	5	5	5	8	35	27
6	**150**	63	24	18	5	5	5	5	8	43	29
6	**160**	70	24	18	5	5	5	5	8	49	34
6	**172**	81	24	20	5	5	5	5	8	61	40
6	**180**	89	24	20	5	5	5	5	8	69	26
7	**120**	48	24	18	5	5	5	5	8	28	14
7	**132**	56	24	18	5	5	5	5	8	35	26
7	**140**	60	24	18	5	5	5	5	8	40	29
7	**150**	66	24	18	5	5	5	5	8	46	30
7	**160**	83	24	18	5	5	5	5	8	62	15
7	**172**	85	24	20	5	5	5	5	8	64	42
7	**180**	100	24	20	5	5	5	5	8	79	19
8	**120**	51	24	19	5	5	5	5	8	31	10
8	**132**	63	24	18	5	5	5	5	8	43	10
8	**140**	67	24	18	5	5	5	5	8	47	20
8	**150**	76	24	19	5	5	5	5	8	56	12
8	**160**	80	24	20	5	5	5	5	8	59	38
8	**172**	98	24	18	5	5	5	5	8	77	19
8	**180**	102	24	20	5	5	5	5	8	80	18

Correlation between the maximum total beam height, including the soffit of negative segments, at a beam spacing of 1.8 m (6 ft) at different span lengths for all of the newly proposed optimized negative sections are shown in Figure 5-27. The total height of the optimal non-prismatic beam with varied web over the negative region (option 2) is the deepest beam while the new non-prismatic beam with varied bottom flange (option 3) yields the shallowest beam at the same span lengths. The height of the new prismatic girder (option 4) is bounded by the height of the new non-prismatic girder

beam with varied bottom flange (option 3) and the height of the new non-prismatic beams with varied web (option 2).

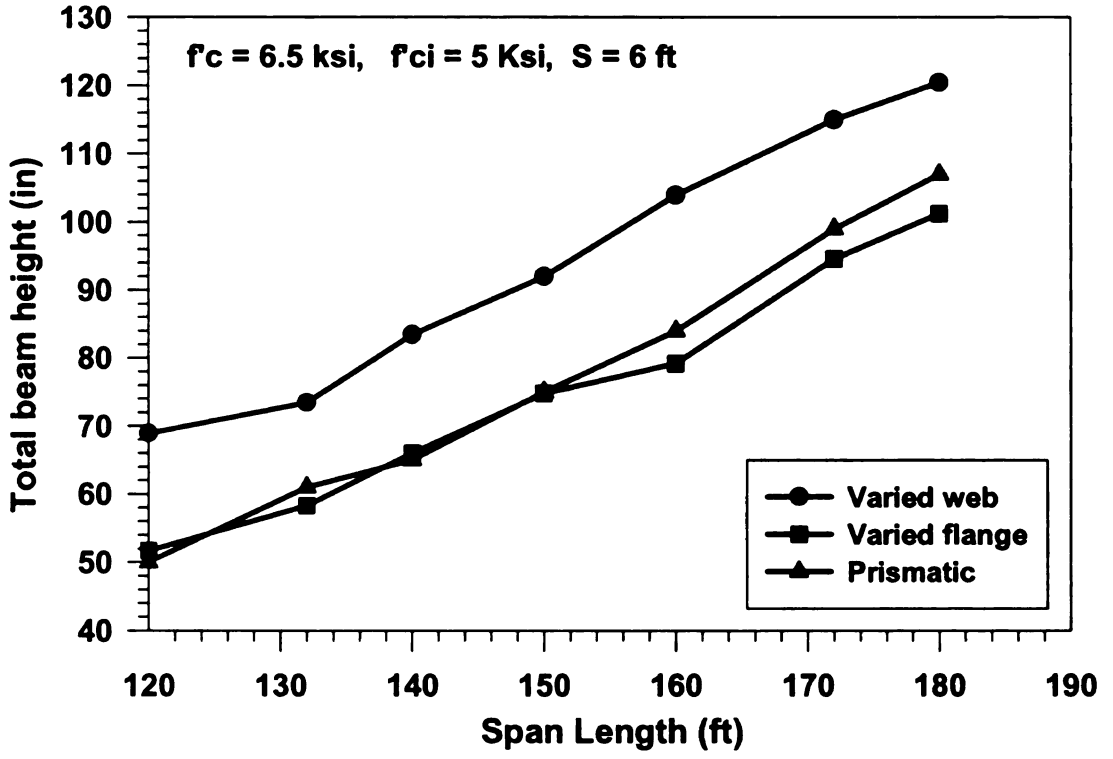

Figure 5-27 *Total beam height of new optimal negative segments for 1.8m (6ft) beam spacing*

When the same total height is used as a given parameter, the maximum achievable span length for each of the newly developed negative sections can be obtained and compared from Figure 5-27. For example, for a negative section at beam spacing of 1.8 m (6 ft) the new prismatic (option 4) and new non-prismatic beam with varied flange (option 3) can span longer than the new non-prismatic beam with varied web depth (option 2).

The above optimal results were based on the minimization of concrete volume, or equivalently to the minimum concrete weight of the girders. The proposed beam height

and dimension results can be used to develop standard negative pier segments for two-span continuous spliced girder bridges. Although the new non-prismatic sections with varied flange thickness were shown to be more efficient in the negative region than the prismatic segment, in practice, the contractor may prefer to develop a standard prismatic negative section since the manufacturing of a prismatic beam is most likely lower.

5.9 Multi-Criteria Optimum Design of Two-Span Continuous SGB

A three-lane two-span continuous PCI-BT 96 spliced girder bridge with single-stage post-tensioning after deck casting was chosen to study how multi-criteria optimization can improve the design of two-span continuous spliced girder bridges. A two-span continuous spliced girder bridge with a total width of 18.6 m (61 ft) and a maximum beam spacing of 2.7 m (9 ft) was used in this study. The total span length of 118.2 m (388 ft) consists of three segments: two equal end, or positive segments and a middle, or pier, segment. The splice location, which is the ratio of the end segment length (L_1) and the total span length (L), was chosen to be at 0.35 (L) since it was indicated by earlier studies to be the best splice location for the two-span system. Concrete with a final compressive strength of 62 MPa (9 ksi) and initial compressive girder strength of 34.5 MPa (5 ksi) was assumed for the girders.

5.9.1 Multi-criteria objective functions

The multi-criteria objective function was composed of a set of different single objective functions. $F_1(x)$ was a multi-criteria economics function defined by the combination of minimum superstructure cost $f_1(x)$, a minimum number of pre-tensioned

strands $f_2(x)$, and a minimum number of post-tensioned strands $f_3(x)$. Each single objective function was set to obtain their optimal design solution for the specified system. The objective functions are expressed as follows:

$$F_1(x)_{min} = \text{Economics Multi-criteria}$$

$$= [f_1(x)_{min}\ f_2(x)_{min} f_3(x)_{min}] \tag{5-17}$$

$$f_1(x) = \text{Minimum superstructure cost}$$

$$= C_{PS} + C_{PT} + C_{CD} + C_{TS} + C_B + C_R \tag{5-18}$$

$$f_2(x) = \text{Minimum number of pre-tensioning strands}$$

$$= npr_{11} + npr_{21} + npr_{31} + npr_{41} + npr_{12} + npr_{22} +$$

$$npr_{32} + npr_{42} + nprt_1 + nprt_2 \tag{5-19}$$

$$f_3(x) = \text{Minimum number of post-tensioning strands}$$

$$= npo \tag{5-20}$$

Each of the single objective functions was formulated separately to determine its optimal solution. Details of each of the parameters used to formulate the function of minimum superstructure cost in Equation 5-18 were described earlier in Table 5-2, while the objective function for the minimum number of pre-tensioned strands includes the total number of all pre-tensioning strands on the top and bottom girder flanges in all segments.

5.9.2 Results and comparison to single-objective optimizations

Optimal design variable solutions for each of the single objective functions were obtained for a total span length (L) of 118.2 m (388 ft) and are given in Table 5-9. Detailed design variable notations were specified in Section 5.6 and are not repeated here.

Table 5-9 *Optimization results for individual objective functions*

Design Variables	L =118.2 m (388 ft) Objective function		
	$f_1(x)$ **min npo**	$f_2(x)$ **min** npr_{ii}	$f_3(x)$ **min const cost**
npr_{11}	12	13	10
npr_{21}	11	5	10
npr_{31}	5	5	5
npr_{41}	1	2	2
npr_{12}	4	2	7
npr_{22}	2	0	0
npr_{32}	2	0	0
npr_{42}	2	0	0
npo	19	35	19
y_a	79 mm (3.1")	25 mm (1")	25 mm (1")
y_b	1.45 m (57")	736 mm (29")	1.45 m (57")
npt_1	7	6	6
npt_2	12	3	7
y_c	-229 mm (9")	-64 mm (2.5")	-211 mm (8.3")
y_d	-813 mm (32")	-453 mm (18")	-813 mm (32")
pra	0.35	0.35	0.35
Objective function	19	36	$9,160,000
npr_{ii} **(total)**	57	36	48

When the objective is to obtain a minimum number of post-tensioning strands, the maximum number of pre-tensioning strands was obtained and vice versa. Thus,

minimum construction cost provides a compromise between the minimum number of pre-tensioning strands and the minimum number of post-tensioning strands. Since these objectives contradict each other, a compromised solution is necessary. Multi-criteria optimization was thus used to obtain a compromised solution between these contradicting objective functions (see Section 3.5).

5.9.3 Pareto optima results

Once different single-objective solutions were obtained, these results were used as design constraints to determine a set of pareto optima (see Section 3.5.3). When all objective criteria are not equally important or conflicting, vector optimization can be used to select the preferred solution in a more rational way. Multi-criteria optimization techniques are used to generate a set of pareto optima, which are non-dominated solutions (see Section 3.5.3).

The range of minimum and maximum values for each objective function was determined after obtaining design variable solutions for each single objective function. The number of total pre-tensioning strands varied from 36 to 57, while the number of post-tensioning strands varied from 19 to 35, as shown in Table 5-9.

Different paired sets of objective functions were chosen to obtain the pareto sets. Pareto optima sets are generated by a constraint approach that is based on an adoption of one criterion as a scalar primary objective function and the transformation of other objective criteria into constraints bounded by some pre-determined constants (see Section 3.5.2). These scalar constraints are altered from the range of minimum to maximum values, and the subset of pareto optima is generated.

The multi-criteria objective is composed of three single objective functions (see Equation 5-17). The single objective functions were selected in pairs to determine the pareto optima set. Two pairs of objective functions were selected for this study. Each pair of objective functions had one objective function as a primary objective function and the other objective function was set as a constraint. The constraints were divided into arbitrary intervals. As the interval range reduces the accuracy of results is closer to the real compromised results. The constraints for this study were divided into five intervals.

The first pair of objective functions was set to minimize the total number of pre-tensioning strands as the main objective function while varying the total number of post-tensioning strands as a constraint. Pareto sets of the number of pre-tensioning strands as an objective and the numbers of post-tensioning strands as constraint are given in Table 5-10. The Euclidian distance and maximum distance of these Pareto sets is minimum at $L_2(x)$ = 0.18 and $L_\infty(x)$ = 0.23, respectively. These values correspond to Solution # 2, where npo = 22 (number of pos-tensioning strands) and npr_{ii} = 39 (total number of pre-tensioning strands).

Table 5-10 *Pareto sets of npr_{ii} as an objective and npo as a constraint*

Solution	Constraints	Objective function				
	$f_3(x)$ min npo	$f_2(x)$ min npr_{ii}	$\frac{(f_3-minf_3)}{df_1,max}$	$\frac{(f_2-minf_2)}{df_2,max}$	$L_\alpha(x)$ Maximum distance	$L_2(x)$ Euclidian distance
1	19	57	0.00	1.00	1.00	1.00
2	**22**	**39**	0.18	0.14	**0.18**	**0.23**
3	25	36	0.37	0.00	0.37	0.37
4	28	36	0.57	0.00	0.57	0.57
5	32	36	0.83	0.00	0.83	0.83
6	35	36	1.00	0.01	1.00	1.00

The second pair of objective functions was set to minimize the total number of post-tensioning strands as the main objective function while varying the number of total pre-tensioning strands as a constraint. The resulting Pareto sets are given in Table 5-11. The Euclidian distance and maximum distance of these Pareto sets is minimum at $L_2(x)$ = 0.22 and $L_\infty(x)$ = 0.30, respectively. These values correspond to Solution # 2 where npo = 22 (number of post-tensioning strands) and npr_{ii} = 41 (total number of pre-tensioning strands).

Table 5-11 *Pareto sets of npo as an objective and npr_{ii} as a constraint*

Solution	Objective function $f_2(x)$ min npo	Constraint $f_3(x)$ min npr_{ii}	$\frac{(f_2-minf_2)}{df_2,max}$	$\frac{(f_3-minf_3)}{df_1,max}$	$L_\alpha(x)$ Maximum distance	$L_2(x)$ Euclidian distance
1	35	36	1.00	0.00	1.00	1.00
2	**22**	**41**	0.20	0.22	**0.22**	**0.30**
3	20	45	0.08	0.41	0.41	0.42
4	19	49	0.00	0.60	0.60	0.60
5	19	53	0.00	0.79	0.79	0.79
6	19	57	0.00	1.00	1.00	1.00

A subset of pareto optima represented by six solutions is illustrated in Figure 5-28. This figure shows the relationship of pre-tensioning and post-tensioning strand requirements when one of them is the main objective function and the other is transformed to be a pre-determined constant constraint and vice versa. The best compromise solution of these objective functions is indicated by the dashed line in the figure and also highlighted (bold text) in Table 5-10 and Table 5-11.

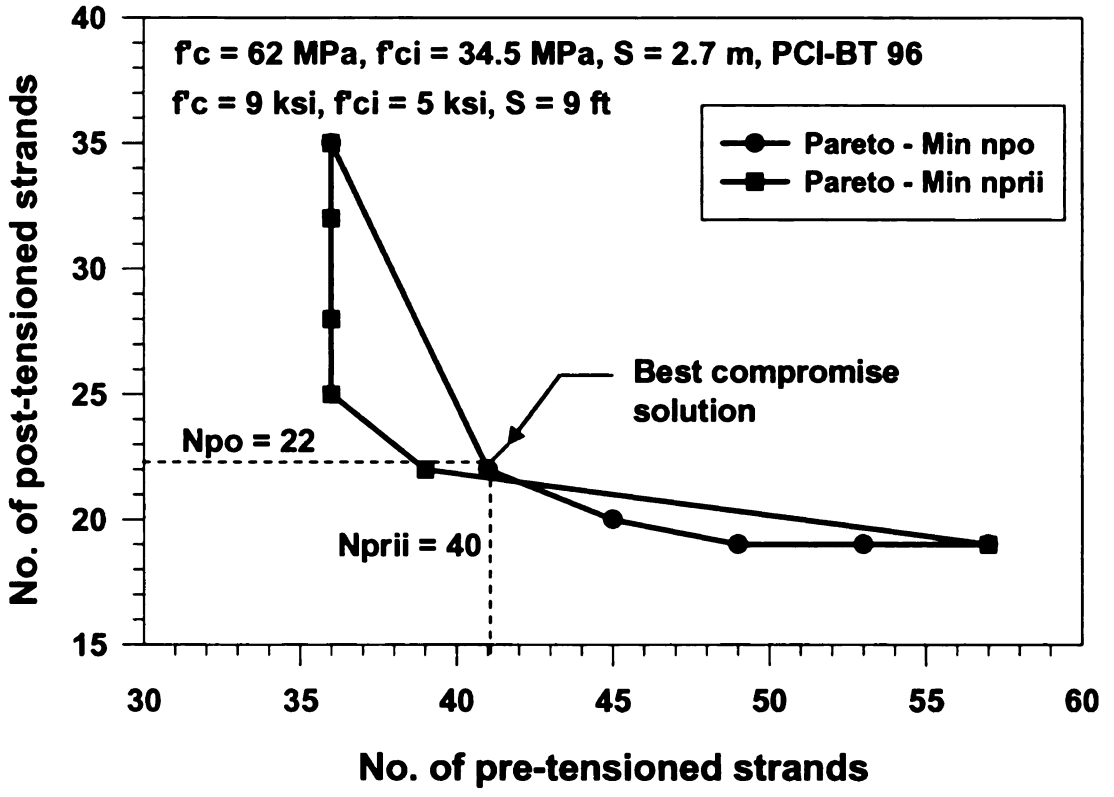

Figure 5-28 *Pareto set of pre-tensioning and post-tensioning strands*

A solution that corresponds to the best compromise between the optimized solutions can be directly obtained since they are part of the optimization results. The results for all design variables are given in Table 5-12. Thus, the optimal solution for the multi-criteria optimization is obtained when *npo* = 22 (number of post-tensioning strands) and np_{rii} = 40 (number of pre-tensioning strands) which is the best compromise solution. This solution is between the minimum and maximum range that was obtained in Section 5.9.2. The multi-criteria optimal solution from the compromised programming is non-dominated with regard to all criteria and ensures the best compromise between all competing criteria.

Table 5-12 *Best solutions to pareto sets*

Main objective Constant Constraint	1st Pair Min npr_{ii} npo	2nd Pair Min npo npr_{ii}
npr_{11}	11	11
npr_{21}	10	8
npr_{31}	4	5
npr_{41}	1	1
npr_{12}	3	3
npr_{22}	0	0
npr_{32}	0	0
npr_{42}	0	0
npo	22	22
y_a	25 mm (1")	51 mm (2")
y_b	1448 mm (57")	1422 mm (56")
y_c	-191 mm (7.5")	-84 mm (3.3")
y_d	-813 mm (32")	-760 mm (29.9")
npt_1	6	6
npt_1	5	6
npt	40	40

5.10 Summary

In this chapter, an integrated component and configuration optimization approach was applied to the design and optimization of two-span continuous spliced girder bridges. Different construction methods were investigated and the multi-staged construction sequence method was found to be the most efficient construction sequence for two-span continuous spliced girder bridges due to the maximum increase in their span length. Development of optimal pier segments was investigated and implemented. The minimization of concrete volume was used as an objective function to develop new

optimal pier segments since their objective function could be directly defined, unlike fabrication cost. Existing standard beams with increased soffits were used over the negative segment to increase span length. However the increase in maximum span length was found to be very small compared to the required increase in soffit thickness. New optimal prismatic and non-prismatic sections were thus developed to be used over the negative moment region section. With the same specified span length, a newly proposed optimal non-prismatic girder section with constant web depth yields the shallowest section than other newly developed girder sections. Results from multi-criteria optimization yielded a compromise solution for different single objective functions and should be used when decision-making must be made for several competing merit criteria.

6 Optimally-Derived Design Aids and Verification Example

6.1 Introduction

The proposed design aids in this research were developed to simplify the analysis and design of spliced girder bridges by providing guidance on variable sensitivity, facilitate the typical trial and error design process, and to expedite the design of this type of bridge systems. The availability of design aids for spliced girder bridges can be a great asset to bridge engineers to have more alternatives during the bridge type selection with less time effort, hopefully resulting in its wider use by state highway agencies.

In this chapter, the development of design aids for the preliminary design of spliced prestressed concrete girder bridges is demonstrated. Optimal design variables that were obtained from the nonlinear structural optimization techniques (see Section 4.5.1; Section 5.4.5; and Section 5.6.2) are shown as design aid charts. These optimal solutions were used in design examples to demonstrate how the developed design aids can be applied in the preliminary design of spliced girder bridges. In addition, the optimal solutions from design aid charts were verified by examining results from the NCHRP 517 report study (Castrodale and White 2004) and proven to be acceptable solutions.

6.2 Preliminary Design Example 1

In this section, Design Example 1 is used to demonstrate the preliminary design of a single-span spliced girder bridge. The optimal design variables from the optimization design were used in these problems. Design Example 1, detailed calculations for both service and the strength limit states are shown. For Design Example 2 only the service limit state calculations are shown since the strength limit state calculations for two-span continuous spliced girder bridges are similar to that of single-span spliced girder bridges.

6.2.1 Problem statement

A three-lane single-span spliced girder bridge with a total width of 18.59 m (61 ft), and a span length (L) of 60.35 m (198 ft) consisting of three segments, as illustrated in Figure 6-1, was used as a prototype structure in this study. The PCI-BT 96 girder was chosen in order to verify the present approach with the results documented for Design Example 1 of the NCHRP 12-57 report. (Castrodale and White 2004). Girder dimensions are shown in Figure 6-2.

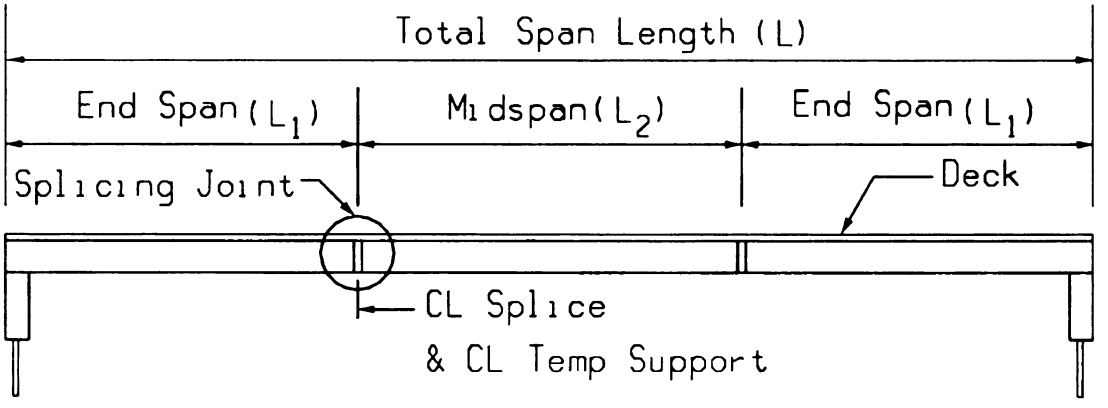

Figure 6-1 *Three-segment single-span spliced precast/prestressed girder bridge*

The end segments were assumed to be equal length (L_1). The splice location is defined as the ratio of the end segment length (L_1) to the total span length (L) and was assumed to be located at 0.223L. The length of the middle segment is thus defined as $L_2 = L - L_1$. The cast-in-place concrete slab thickness was assumed to be 216 mm (8.5 in.) with 50 mm (2 in.) built-up built on a 2.7 m (9 ft) girder spacing.

A single-staged post-tensioning construction was used in this evaluation. Segments are assumed to be placed on temporary supports and post-tensioning is assumed to be applied after the deck and splice joints are cast. A full depth diaphragm cast with the splice was assumed to be provided at the splice locations. No other intermediate diaphragms were assumed. The design study was conducted using the simplified design method of the AASHTO-LRFD Bridge Design Specifications (AASHTO 2003) and the recommendations of NCHRP 517 report (Castrodale and White 2004). Both service limit states and ultimate limit states were considered in the design.

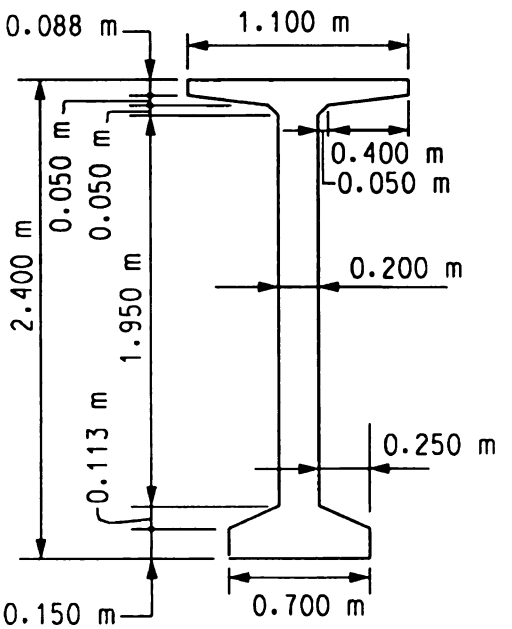

Figure 6-2 *System and girder cross sections for single-span spliced girder bridge study*

The purpose of this design example is to illustrate how the developed design charts can be used as an aid for the preliminary design of single-span spliced girder bridges. The same prototype structure as in Section 6.2 is used for this preliminary design example 1. The section at the mid-span section of Segment 2 (x = 30.175 m [99 ft] measured from the end span) of the spliced girder bridge is checked in this example.

6.2.2 Preliminary section properties

Non-composite PCI-BT 96 Girder Section Properties

y_{bg} = 1231 mm (48.47 in.)

S_{tg} = 434,486,615 mm^3 (26514 in.^{3})

S_{bg} = 425,981,729 mm^3 (25995 in.^{3})

A_g = 711,611 mm^2 (1103 in.^{2})

I_g = 5.2449e11 mm^4 (1260081 in.^{4})

Composite PCI-BT 96 Girder Section Properties

A_c = 1,204,514 mm^2 (1867 in.^{2})

I_c = 1.203e12 mm^4 (2474500 in.^{4})

S_{bc} = 582,117,675 mm^3 (35523 in.^{3})

S_{tc} = 1,539,368,018 mm^3 (93938 in.^{3})

S_{tcs} = 1,398,767,009 mm^3 (85358 in.^{3})

A_{cc} = 1,447,739 mm^2 (2244 in^2)

y_{bc} = 1,769 mm (69.66 in.)

y_{tc} = 669 mm (26.34 in.)

6.2.3 Preliminary material properties

Girder Material Properties

f_c' = 44.8 MPa (6.5 ksi)

f_{ci}' = 34.5 MPa (5 ksi)

E_{gi} = 29,558 MPa (4287 ksi)

E_g = 33,702 MPa (4888 ksi)

w_c = 2,400 kg/m^3 (150 lb/ft^3)

f_{cd}' = 24.1 MPa (4.5 ksi)

Deck Material Properties

f_{cdi}' = 31.0 MPa (3.5 ksi)

E_{cdi} = 24,731 MPa (3372 ksi)

E_{cd} = 28,041 MPa (3824 ksi)

w_{cd} = 2,400 kg/m^3 (150 lb/ft^3)

Pre-tensioning Strands Properties

a_{ps} = 140 mm^2 (0.217 in^2)

E_p = 196,502 MPa (28500 ksi)

f_{pu} = 1,861 MPa (270 ksi)

$f_{py} = 0.9f_{pu}$ = 1,675 MPa (243 ksi)

$f_{po} = 0.75f_{pu}$ = 1,396 MPa (202.5 ksi)

Post-tensioning Strands Properties

a_{ps} = 140 mm^2 (0.217 in.^{2})

E_p = 196,502 MPa (28500 ksi)

f_{pu} = 1,861 MPa (270 ksi)

$f_{py} = 0.9f_{pu}$ = 1,675 MPa (243 ksi)

$f_{pj} = 0.9f_{py}$ = 1,508 MPa (219 ksi)

6.2.4 General information

S = 2438 mm (8 ft)

t_s = 216 mm (8.5 in.)

Humidity = H = 75

t_r = 1 day

t_d = 60 days

t_{po} = 75 days

A_{set} = 9.53 mm (0.375 in.)

6.2.5 Use of design charts

The design variables in the optimization problem are those defining the amount and layout of the pre-tensioning and post-tensioning strands in the girders as described in Figure 6-3. The location of each strand layer is assumed to be 50 mm apart, including the distance of the first row of strands to the beam top and bottom. Normally, the number of post-tensioning strands requires the use of several ducts. To avoid having several ducts defined in the design variables, an effective post-tensioning profile is used to represent a group of ducts. The effective post-tensioning duct is assumed to follow the profile of a quadratic parabola.

Results from the optimization process were used to develop complete design aid charts for PCI-BT 96 single-span spliced girder bridges as shown in Figure 6-4 through Figure 6-7. These figures are used as an example to demonstrate how the developed design aids can be used. These design charts were developed based on beam spacing 2.7 m (9 ft), initial and final concrete compressive strength are 35 (5 ksi) and 45 MPa (6.5 ksi), respectively. These results are direct output from the optimization procedure (Section 4.5.1a), where the span length was kept as a design parameter.

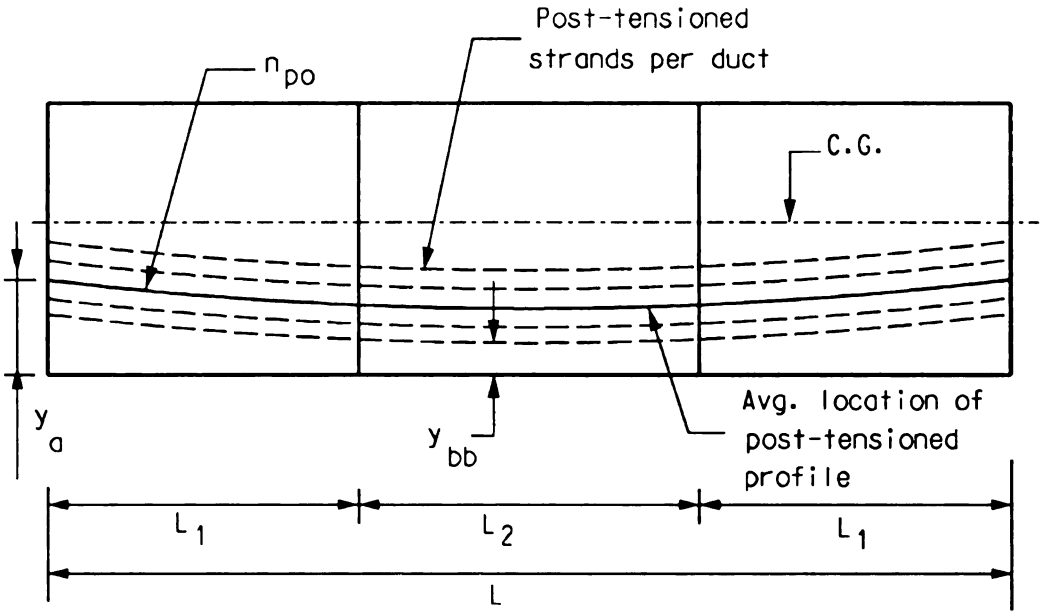

(a) *Post-tensioning Requirement*

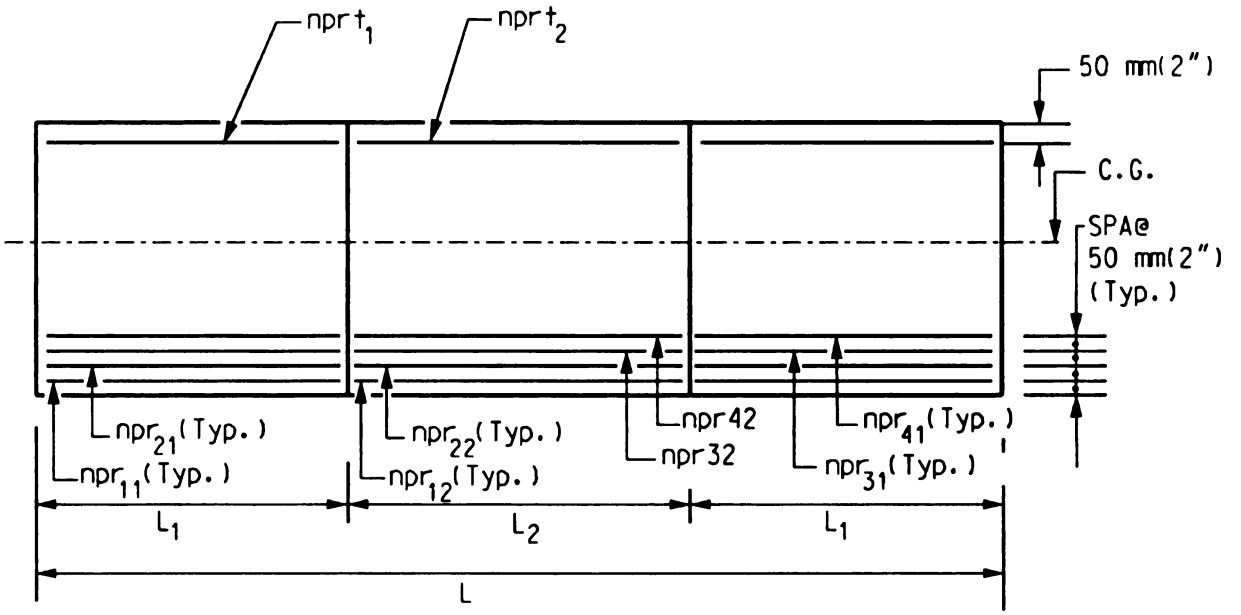

(b) Pre-tensioning Requirement

Figure 6-3 *Variables for the design optimization of single-span spliced girder bridges*

Figure 6-4 and Figure 6-5 provide traces that relate the optimal requirements of pre-tensioning strands per row in the end and middle girder segments, respectively. The relation between the amount of continuous post-tensioning to the achievable span length

is illustrated in Figure 6-6. The eccentricity locations of the effective post-tensioning duct at the bridge ends and at mid-span are shown in Figure 6-7. In addition to the solid lines in the figures, which represent the optimized results, dotted lines are projected from the x-axis which is the given span length 60.4 m (198 ft) and extended into the desirable trace in Figure 6-4 through Figure 6-7 to obtain the amount of prestress requirements and eccentricity locations of the effective post-tensioning duct in each segment from the y-axis. The resulting values (design variables) for the prototype structure are noted in the figures.

From the charts (Fig 6-4 to 6-7) the required amount of pre-tensioning for the end-segment is 2 strands on the first bottom layer and 2 strands on the first top layer, as illustrated in Figure 6-4. The mid-segment requires 8 strands on the first three bottom layers, 2 strands on the forth bottom layer, and 6 strands on the first top layer, as shown in Figure 6-5. The requirement for post-tensioning strand is 52 strands, as shown in Figure 6-6, which is assumed to be divided into 4 ducts as shown in Figure 6-8b. The location of the centroid the post-tensioning strands at the end-segment is 770 mm (30.31 in.) and is 400 mm (15.74 in.) at the mid-segment, as illustrated in Figure 6-7.

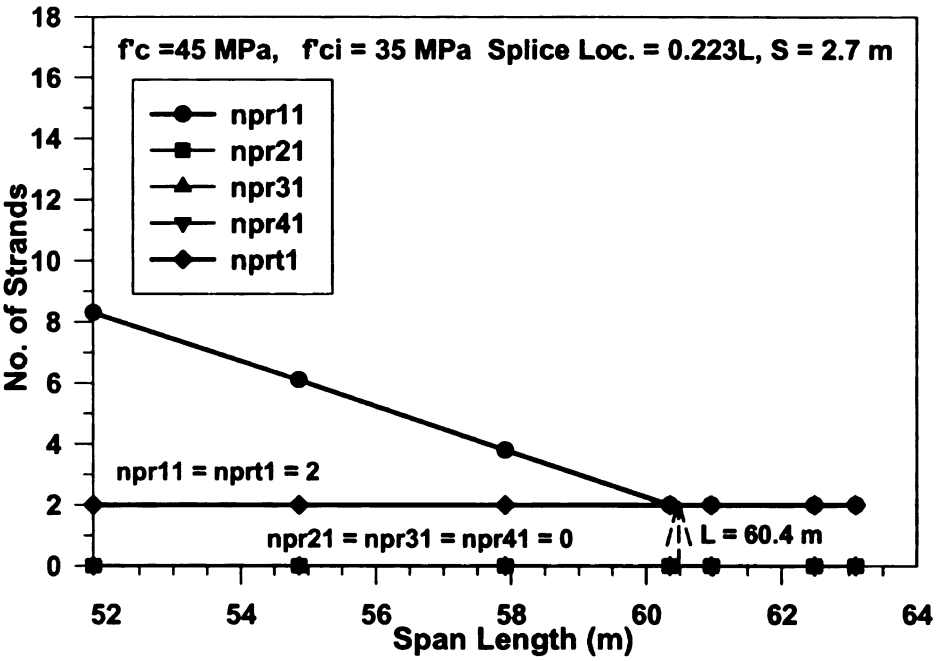

Figure 6-4 *Number of pre-tensioning strands per row in end-segment for PCI BT-96 beam*

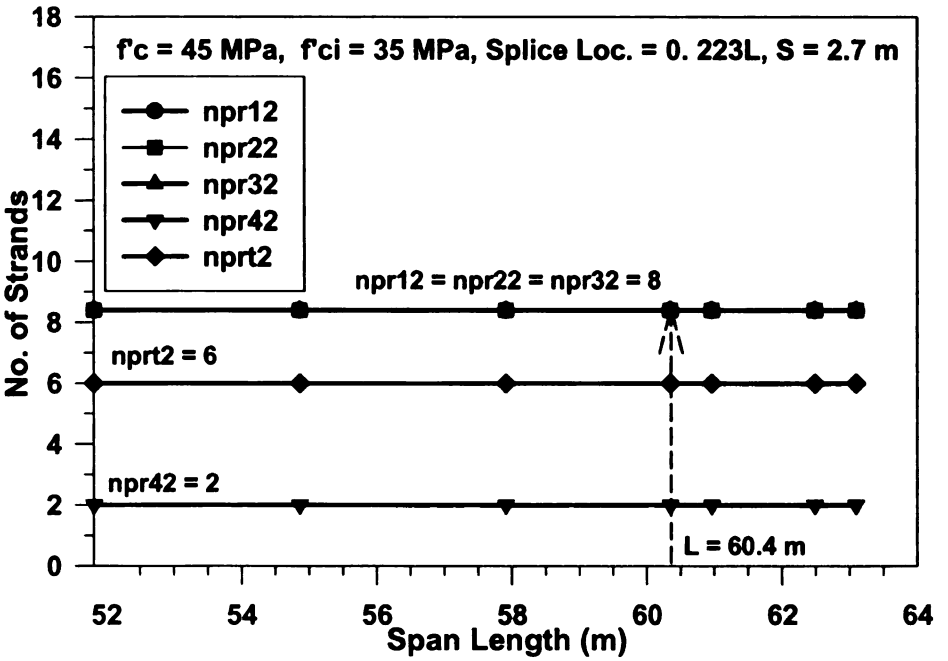

Figure 6-5 *Number of pre-tensioning strands per rows in mid-segment for PCI-BT 96 beam*

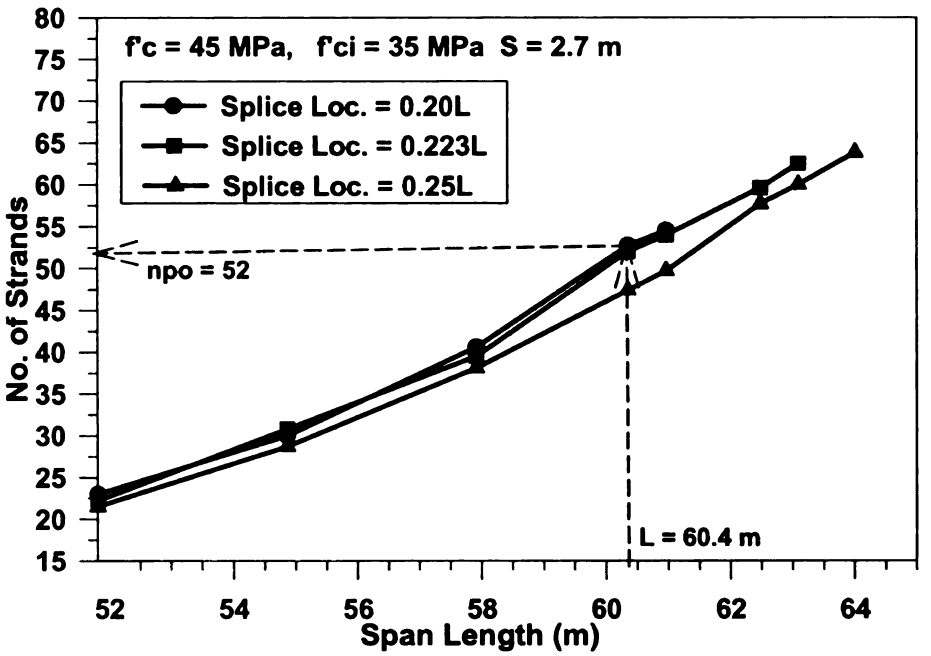

Figure 6-6 *Optimized total number of post-tensioning strands for PCI BT-96 beam for different splice locations*

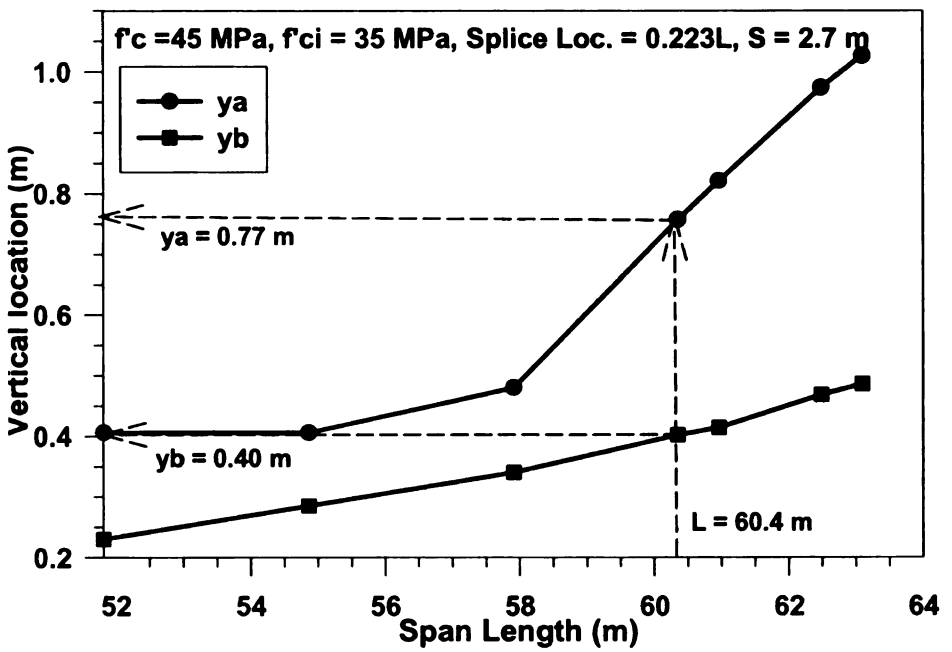

Figure 6-7 *Post-tensioning profile at end and mid-segments for PCI BT-96 beam*

The values for the variables used in this preliminary design calculation are obtained from the optimized design charts as shown in Figure 6-4 through Figure 6-7. These variable values are:

$npr_{11} = 2$; $npr_{12} = 0$; $npr_{13} = 0$;

$npr_{14} = 0$; $nprt_1 = 2$; $npr_{21} = 9$;

$npr_{22} = 8$; $npr_{23} = 8$; $npr_{24} = 2$;

$nprt_2 = 6$; $npo = 52$; $y_{bb} = 165$ mm (6.5 in.);

$y_a = 775$ mm (30.31 in.).

The service and ultimate limit states at the mid-span section of Segment 2 is checked herein to verify that the results provided by the design aids do in fact satisfy all serviceability and strength requirements.

6.2.6 Service limit state

Service limit states were defined in terms of flexural stress limits on the girder and deck. For flexure, service limit state requirements govern the required prestressing force. The stress limit states for each critical construction stage of the single-span spliced girder bridge when using a single-post-tensioning (see Section 4.5.1) are evaluated as follows:

Stage 1: Stress check at pre-tensioning

The end-segment, or segment 1, length is based on the spliced location and can be determined as:

L_1 = (splice location)(L) = (0.223)L = (0.223)(60.35) = 13.46 m.

End segments are assumed to be equal, therefore the mid-segment length can be computed as:

$L_2 = L - (2)(L_1) = 33.43$ m.

The centroid of all pre-tensioned strands is computed as follows:

$$y_{e2} = \frac{(npr_{12})(50) + (npr_{22})(100) + (npr_{32})(150) + (npr_{42})(200) + (nprt_2)(y_{bg} + y_{tg} - 50)}{(npr_{12} + npr_{22} + npr_{32} + npr_{42} + nprt_2)}$$

$y_{e2} = 522$ mm.

The eccentricity of the pre-tensioned strands at the midspan of mid-segment is computed as:

$e_{p2} = y_{bg} - y_{e2} = 709$ mm.

The total pre-tensioned strand areas include the area of all pre-tensioned strands in the top and bottom girder flanges:

$A_{ps2} = (a_{ps})(npr_{12} + npr_{22} + npr_{32} + npr_{42} + nprt_2) = 4{,}620$ mm^2.

The girder dead load moment a the midspan of Segment 2 is computed as

$$M_{g2} = \frac{1}{8} A_g w_c L_2^2 = 2{,}313 \text{ kN-m}$$

The stress at the centroid of the pre-tensioned strands of the mid-segment caused by pre-tensioning and girder dead loads is calculated as:

$$f_{cgp12} = \frac{0.7 A_{ps2} f_{pu}}{A_g} + \frac{0.7 A_{ps2} f_{pu} e_{p2}^2}{I_g} - \frac{M_{g2} e_{p2}}{I_g} = 11.11 \text{ MPa}$$

Elastic shortening prestress losses due to the pretensioning at the release stage can be determined as follows:

$$df_{ES2} = f_{cgp12}\frac{E_p}{E_{gi}} = 73.84 \text{ MPa.}$$

Relaxation prestress losses at release of the pretensioned strands are defined as:

$$df_{PR1} = \frac{\log(24t_{r1})}{40}[\frac{f_{pj}}{f_{py}} - 0.55]f_{pj} = 13.65 \text{ MPa.}$$

The effective prestress at the centroid of the pre-tensioned strands after all losses at release of pre-tensioning is calculated as follows:

$$f_{pe12} = f_{pei} - df_{ES2} - df_{PR1} = 1308.70 \text{ MPa.}$$

The total top girder stress at the mid-span of the mid-segment at Stage 1 is defined as:

$$\sigma_{t1} = \frac{M_{g2}}{S_{tg}} + \frac{A_{ps2}f_{pe12}}{A_g} - \frac{A_{ps2}f_{pe12}e_{p2}}{S_{tg}} = 3.95 \text{ MPa} < 0.6f'_{ci} = 20.68 \text{ MPa.}$$

The total bottom girder stress at the mid-span of the mid-segment at Stage 1 is calculated by:

$$\sigma_{b1} = -\frac{M_{g2}}{S_{bg}} + \frac{A_{ps2}f_{pe12}}{A_g} - \frac{A_{ps2}f_{pe12}e_{p2}}{S_{bg}} = 13.13 \text{ MPa} < 0.6f'_{ci} = 20.68 \text{ MPa.}$$

Stage 2: Stress check at placement of deck and splice

M_{d2} = Deck load moment at midspan of Segment 2

= 1925 kN-m

M_{h2} = Haunch load moment at midspan of Segment 2

= 356.58 kN-m

M_{s2} = Superimposed dead load moment at midspan of Segment 2

= 2017.46 kN-m

M_{c2} = Construction load moment at midspan of Segment 2

= 362 kN-m

M_{p2} = Removal of support moment at midspan of Segment 2

= 10928 kN-m

Shrinkage prestress losses are assumed to be calculated at 75% humidity and are determined according to AASHTO LRFD Equation 5.9.5.4.2-1 (AASHTO 2003):

$df_{pSR} = (17 - 0.15H) = 39.65$ MPa.

The creep coefficient during deck placement is based on the time at which the deck is poured and can be calculated according to AASHTO LRFD Equation 5.4.2.3.2-1 (AASHTO 2003):

$$K_{CRtd} = \frac{t_d^{0.6}}{10 + t_d} = 0.5384.$$

The shrinkage coefficient during deck placement is determined according to (AASHTO LRFD Equation 5.4.2.3.3-1(AASHTO 2003) :

$$K_{SHtd} = \frac{t_d}{35 + t_d} = 0.6316.$$

The initial post-tensioning stress is defined as:

$f_{p4} = 0.69 fpu = 1287$ MPa.

The total post-tensioning forces are determined from all post-tensioned ducts and can be calculated by:

$F_{PT12} = n_{po} a_{ps} f_{p4} = 9371$ kN.

The maximum number of strands in each duct is assumed to be 12. Therefore, the number of post-tensioning ducts is determined as:

$$NT = round(\frac{n_{po}}{12}) = 4 \text{ ducts.}$$

The location of the highest post-tensioning duct depends on the lowest centroid of the effective post-tensioned duct and is calculated as follows:

$$y_{bbb} = y_{bb} + (N-1) \times 150 = 622 \text{ mm.}$$

The average location of all post-tensioning ducts is determined by the summation of the lowest and highest post-tensioning duct locations as follows:

$$y_b = \frac{(y_{bb} + y_{bbb})}{2} = 394 \text{ mm.}$$

The eccentricity of pretensioned strands for the composite section is defined as:

$$e_{c2} = y_{bc} - y_{e2} = 1247 \text{ mm.}$$

The average eccentricity of all post-tensioning tendons for the composite section is calculated as:

$$e_{pt2} = y_{bc} - y_b = 1376 \text{ mm.}$$

The stress at the centroid of the pre-tensioned strands on the mid-segment caused by post-tensioning and temporary support removal loads can be determined as:

$$f_{cgpc2} = \frac{F_{PT12}}{A_c} + \frac{F_{PT12} e_{pt2} e_{c2}}{I_c} - \frac{M_{p2} e_{c2}}{I_c} = 10.16 \text{ MPa.}$$

The stress at the centroid of the pre-tensioned strands of the mid-segment caused by the deck, girder/deck haunch, and superimposed dead loads can be calculated as:

$$df_{cdp2} = \frac{M_{d2} + M_{h2}}{I_g} e_{p2} + \frac{M_{s2} e_{c2}}{I_c} = 5.53 \text{ MPa.}$$

Creep prestressing losses at this stage are computed according to the AASHTO-LRFD provisions (AASHTO 2003) and the recommendations from the NCHRP 517 report (Castrodale and White 2004). The first two terms of the following equation are determined according AASHTO-LRFD, Section 5.9.5.4 and the last term is added as recommended by the NCHRP 517 report.

$$df_{CR2} = 12f_{cgp12} - 7df_{cdp2} + 7f_{cgpc2} = 16.57 \text{ MPa.}$$

Final relaxation prestress losses, which include the loss due to elastic shortening, shrinkage, and creep, are determined according to AASHTO-LRFD Equation 5.9.5.4.4:

$$df_{PR22} = 0.3[20 - 0.4df_{ES2} - 0.2(df_{pSR} + df_{pCR2})] = 20.19 \text{ MPa.}$$

The total prestress losses at the placement of the deck and splice are calculated as follows:

$$df_{preTD2} = df_{ES2} + K_{CRtd}df_{CR2} + K_{SHtd}df_{pSR} + df_{PR22} = 208.29 \text{ MPa.}$$

The effective prestress at the centroid of the pre-tensioned strands after all losses at placement of the deck and splice stage is calculated as follows:

$$f_{pe22} = f_{pei} - df_{preTD2} = 1188 \text{ MPa.}$$

The total top girder stress at the mid-span of the mid-segment at Stage 2 is defined as:

$$\sigma_{t2} = \frac{M_{g2}}{S_{tg}} + \frac{M_{d2}}{S_{tg}} + \frac{M_{h2}}{S_{tg}} + \frac{M_{c2}}{S_{tg}} + \frac{A_{ps2}f_{pe22}}{A_g} - \frac{A_{ps2}f_{pe22}e_{p2}}{S_{tg}}$$

$$= 10.16\,MPa < 0.6fc' = 26.89 \text{ MPa.}$$

The total bottom girder stress at the mid-span of the mid-segment at Stage 2 is defined as:

$$\sigma_{b2} = -\frac{M_{g2}}{S_{bg}} - \frac{M_{d2}}{S_{bg}} - \frac{M_{h2}}{S_{bg}} - \frac{M_{c2}}{S_{bg}} + \frac{A_{ps2} f_{pe22}}{A_g} - \frac{A_{ps2} f_{pe22} e_{p2}}{S_{bg}}$$

$$= 5.21\,MPa < 0.6 fc' = 26.89\,\text{MPa}.$$

Stage 3: Stress check at post-tensioning

The creep coefficient during the post-tensioning stage is based on the time at which post-tensioning is applied and can be calculated as (AASHTO LRFD Equation 5.4.2.3.2-1):

$$K_{CRtp} = \frac{t_{po}^{0.6}}{10 + t_{po}} = 0.571.$$

The shrinkage coefficient during post-tensioning is determined as (AASHTO LRFD Equation 5.4.2.3.3-1):

$$K_{SHtp} = \frac{t_{po}}{35 + t_{po}} = 0.682.$$

Stressing of the post-tensioning tendons causes secondary elastic shortening prestress losses in the pre-tensioned strands in the girder segments. Additional elastic shortening losses due to post-tensioning are computed as:

$$df_{pESA2} = (\frac{E_p}{E_g}) f_{cgpc2} = 59.23 \text{ MPa}.$$

Total prestress losses at the centroid of pre-tensioned strands from the post-tensioning stage are calculated as follows:

$$df_{preTP2} = df_{ES2} + K_{CRtp} df_{CR2} + K_{SHtp} df_{pSR} + df_{PR22} + df_{pESA2} = 274.96 \text{ MPa}.$$

The effective prestress at the centroid of the pre-tensioned strands after all losses at the post-tensioning stage is calculated as follows:

$$f_{pe32} = f_{pei} - df_{preTP2} = 1121 \text{ MPa.}$$

The eccentricity of the effective post-tensioning duct at the end span of the composite section of Segment 1 is determined as:

$$e_{pt1} = e_{pt3} = y_{bc} - y_a = 995 \text{ mm.}$$

The eccentricity of the effective post-tensioning duct at the mid-span of composite section of Segment 2 is determined as:

$$e_e = e_{pt1} + (-3e_{pt1} + 4e_{pt2} - e_{pt3})\frac{x}{L} + 2(e_{pt3} - 2e_{pt2} + e_{pt1})\frac{x^2}{L^2} = 1376 \text{ mm.}$$

The friction losses are computed according AASHTO LRFD Equation 5.9.5.2.2 as shown below:

$$df_{pF} = f_{pj}(1 - e^{-(Kx+\mu\alpha)}) = 46.33 \text{ MPa.}$$

The stress at the centroid of all post-tensioned strands on the mid-segment caused by the post-tensioning and temporary support removal loads can be determined as:

$$f_{cgpo2} = \frac{F_{PT0}}{A_c} + \frac{F_{PT0}e_{pt2}^2}{I_c} - \frac{M_{r2}e_{pt2}}{I_c} = 10.49 \text{ MPa.}$$

Elastic shortening prestress losses at the centroid of the post-tensioning strands due to post-tensioning is computed as:

$$df_{PTES2} = \frac{(NT-1)}{2NT}\frac{E_p}{E_g} f_{cgpo2} = 22.95 \text{ MPa.}$$

Anchor set prestress loss is computed by estimating the loss that occurs when each tendon pulls into the anchorage due to seating. The maximum anchorage set loss, which is at the stressing anchorage, is computed using the NCHRP 517 report equation 7.3.1.1.2-3 (Castodale and White 2004) as follows:

$$df_A = 2\frac{df_{pF}}{x}\sqrt{\frac{A_{set}E_p x}{df_{pF}}} = 108.03 \text{ MPa.}$$

The distance along which the anchor set loss extends is computed using the NCHRP 517 report equation 7.3.1.1.2-2 (Castodale and White 2004) as shown below:

$$X_A = \frac{1}{12}\sqrt{\frac{A_{set}E_p x}{dfpF}} = 2888 \text{ mm.}$$

The total prestress losses at the post-tensioning stage are calculated as follows:

$$d_{PTPT2} = df_{pF} + df_{PTES2} + df_A\frac{(X_A - 0.5L)}{X_A} = 84.65 \text{ MPa.}$$

The effective prestress at the centroid of post-tensioned strands after all losses from the post-tensioning stage is calculated as follows:

$$f_{pof} = f_{po12} = f_{poi} - d_{PTPT2} = 1312 \text{ MPa.}$$

The total top girder stress at the mid-span of Segment 2 at Stage 3 is defined as:

$$\sigma_{t3} = \frac{M_{g2}}{S_{tg}} + \frac{M_{d2}}{S_{tg}} + \frac{M_{h2}}{S_{tg}} + \frac{M_{r2}}{S_{tc}} + \frac{A_{ps2}f_{pe32}}{A_g} - \frac{A_{ps2}f_{pe32}e_{p2}}{S_{tg}} +$$

$$\frac{n_{po}a_{ps}f_{pof}}{A_c} - \frac{n_{po}a_{ps}f_{pof}e_e}{S_{tc}}$$

$$= 15.89\,MPa < 0.6fc' = 26.89 \text{ MPa.}$$

The total bottom girder stress at the mid-span of Segment 2 at Stage 3 is defined as:

$$\sigma_{b3} = -\frac{M_{g2}}{S_{bg}} - \frac{M_{d2}}{S_{bg}} - \frac{M_{h2}}{S_{bg}} - \frac{M_{r2}}{S_{bc}} + \frac{A_{ps2} f_{pe32}}{A_g} + \frac{A_{ps2} f_{pe32} e_{p2}}{S_{bg}} + \frac{n_{po} a_{ps} f_{pof}}{A_c} + \frac{n_{po} a_{ps} f_{pof} e_e}{S_{bc}}$$

$= 16.84\,MPa < 0.6 fc' = 26.89$ MPa.

The total top deck stress at the mid-span of Segment 2 at Stage 3 is defined as:

$$\sigma_{ts3} = \frac{M_{r2}}{S_{tcs}} + \frac{n_{po} a_{ps} f_{pof}}{A_{cc}} - \frac{n_{po} a_{ps} f_{pof} e_e}{S_{tcs}} = 5.02 < 0.6 fcd' = 18.62 \text{ MPa.}$$

Stage 4: Stress check at Compression 1 limit state

M_{s2} = Superimposed dead load moment at midspan of Segment 2

= 2018 kN-m

M_{ll2} = Live load moment at midspan of Segment 2

= 6646 kN-m

Total prestress losses at the final condition for *Compression 1* are calculated as follows:

$$df_{preTPF2} = df_{ES2} + df_{CR2} + df_{pSR} + df_{PR22} + df_{pESA2} = 358.60 \text{ MPa.}$$

The effective prestress at the centroid of the pre-tensioned strands after all prestress losses for the final condition for Compression 1 is calculated as follows:

$$f_{pe42} = f_{pei} - df_{preTPF2} = 1037.60 \text{ MPa.}$$

The stress at the centroid of the post-tensioned strands of Segment 2 caused by deck, girder/deck haunch, and superimposed dead loads can be calculated as:

$$df_{cdpo2} = \frac{M_{d2} + M_{h2}}{I_g} e_{pt2} + \frac{M_{s2} e_{pt2}}{I_c} = 8.68 \text{ MPa.}$$

The stress at the centroid of the post-tensioned strands of Segment 2 caused by post-tensioning and girder loads can be calculated as:

$$f_{cgpco2} = \frac{F_{p2}}{A_g} + \frac{F_{p2} e_{pt2} e_{c2}}{I_g} - \frac{M_{g2} e_{pt2}}{I_g} = 22.09 \text{ MPa.}$$

Prestress loss due to creep at the centroid of the post-tensioning strands at this stage is computed according to the AASHTO-LRFD specifications and the recommendations from the NCHRP 517-12 report. The first two terms of the following equation are determined according to AASHTO-LRFD Section 5.9.5.4 (AASHTO 2003) and the last term is added as recommended by the NCHRP 517 report (Castrodale and White 2004).

$$df_{poCR2} = 12 f_{cgpo2} - 7 df_{cdpo2} + 7 f_{cgpco2} = 219.81 \text{ MPa.}$$

Shrinkage prestress loss in the post-tensioning is calculated at 75% humidity and according to AASHTO LRFD Equation 5.9.5.4.2-2 (AASHTO 2003) and is defined as:

$$df_{poSR} = (13.5 - 0.123H) = 29.47 \text{ MPa.}$$

Prestress loss due to final relaxation of the post-tensioned strand is calculated according to AASHTO-LRFD Equation 5.9.5.4.4 (AASHTO 2003):

$$df_{PR32} = 0.3(20 - 0.3 df_{pF} - 0.4 df_{PTES2} - 0.2(df_{poCR2} + df_{poSR}) = 19.49 \text{ MPa.}$$

Total prestress losses at the Compression 1 limit state for the final stage are calculated as follows:

$$d_{PTF2} = df_{pF} + df_{PTES2} + df_A \frac{(X_A - 0.5L)}{X_A} + df_{poCR2} + df_{poSR} + df_{PR32}$$

= 354 MPa.

The effective prestress at the centroid of the post-tensioned strands after all losses at the final Compression 1 stage is calculated as follows:

$$f_{poff} = f_{po22} = f_{poi} - d_{PTF2} = 1043 \text{ MPa.}$$

The total top girder stress at the mid-span of Segment 2 at Stage 4 is determined as:

$$\sigma_{t4} = \frac{M_{g2}}{S_{tg}} + \frac{M_{d2}}{S_{tg}} + \frac{M_{h2}}{S_{tg}} + \frac{M_{r2}}{S_{tc}} + \frac{M_{s2}}{S_{tc}} + \frac{M_{ll2}}{S_{tc}} + \frac{A_{ps2} f_{pe42}}{A_g} - \frac{A_{ps2} f_{pe42} e_{p2}}{S_{tg}} + \frac{n_{po} a_{ps} f_{poff}}{A_c} - \frac{n_{po} a_{ps} f_{poff} e_e}{S_{tc}}$$

$$= 21.73 MPa < 0.6 f_c^{'} = 26.89 \text{ MPa.}$$

The total bottom girder stress at the mid-span of Segment 2 at Stage 4 is defined as:

$$\sigma_{b4} = -\frac{M_{g2}}{S_{bg}} - \frac{M_{d2}}{S_{bg}} - \frac{M_{h2}}{S_{bg}} - \frac{M_{r2}}{S_{bc}} - \frac{M_{s2}}{S_{bc}} - \frac{M_{ll2}}{S_{bc}} + \frac{A_{ps2} f_{pe42}}{A_g} + \frac{A_{ps2} f_{pe42} e_{p2}}{S_{bg}} + \frac{n_{po} a_{ps} f_{poff}}{A_c} + \frac{n_{po} a_{ps} f_{poff} e_e}{S_{bc}}$$

$$= -5.48 MPa < 0.6 f_c^{'} = 26.89 \text{ MPa.}$$

The total top deck stress at the mid-span of Segment 2 at Stage 4 is defined as:

$$\sigma_{ts4} = \frac{M_{r2}}{S_{tcs}} + \frac{M_{s2}}{S_{tcs}} + \frac{M_{ll2}}{S_{tcs}} + \frac{n_{po} a_{ps} f_{poff}}{A_{cc}} - \frac{n_{po} a_{ps} f_{poff} e_e}{S_{tcs}}$$

$$= 11.78 < 0.6 f_{cd}^{'} = 18.62 \text{ MPa.}$$

Stage 5: Stress check at tension limit state

The total top girder stress at the mid-span of Segment 2 at Stage 5 is defined as:

$$\sigma_{t5} = \frac{M_{g2}}{S_{tg}} + \frac{M_{d2}}{S_{tg}} + \frac{M_{h2}}{S_{tg}} + \frac{M_{r2}}{S_{tc}} + \frac{M_{s2}}{S_{tc}} + 0.8\frac{M_{ll2}}{S_{tc}} + \frac{A_{ps2}f_{pe42}}{A_g} -$$

$$\frac{A_{ps2}f_{pe42}e_{p2}}{S_{tg}} + \frac{n_{po}a_{ps}f_{poff}}{A_c} - \frac{n_{po}a_{ps}f_{poff}e_e}{S_{tc}}$$

$$= 20.87MPa > -0.19\sqrt{fc'} = -3.34 \text{ MPa.}$$

The total bottom girder stress at the mid-span of Segment 2 at Stage 5 is obtained as:

$$\sigma_{b5} = -\frac{M_{g2}}{S_{bg}} - \frac{M_{d2}}{S_{bg}} - \frac{M_{h2}}{S_{bg}} - \frac{M_{r2}}{S_{bc}} - \frac{M_{s2}}{S_{bc}} - 0.8\frac{M_{ll2}}{S_{bc}} + \frac{A_{ps2}f_{pe42}}{A_g} +$$

$$\frac{A_{ps2}f_{pe42}e_{p2}}{S_{bg}} + \frac{n_{po}a_{ps}f_{poff}}{A_c} + \frac{n_{po}a_{ps}f_{poff}e_e}{S_{bc}}$$

$$= -3.199\,MPa > -0.19 \times \sqrt{fc'} = -3.34 \text{ MPa.}$$

The total top deck stress at the mid-span of Segment 2 at Stage 5 is calculated by:

$$\sigma_{ts5} = \frac{M_{r2}}{S_{tcs}} + \frac{M_{s2}}{S_{tcs}} + 0.8\frac{M_{ll2}}{S_{tcs}} + \frac{n_{po}a_{ps}f_{poff}}{A_{cc}} - \frac{n_{po}a_{ps}f_{poff}ee}{S_{tcs}}$$

$$= 10.83\,MPa < 0.6fcd' = 18.62 \text{ MPa.}$$

Stage 6: Stress check at Compression 2 limit state

The total top girder stress at the mid-span of Segment 2 at Stage 6 is defined as:

$$\sigma_{t6} = \frac{M_{g2}}{S_{tg}} + \frac{M_{d2}}{S_{tg}} + \frac{M_{h2}}{S_{tg}} + \frac{M_{r2}}{S_{tc}} + \frac{M_{s2}}{S_{tc}} + \frac{A_{ps2}f_{pe42}}{A_g} - \frac{A_{ps2}f_{pe42}e_{p2}}{S_{tg}} +$$

$$\frac{n_{po}a_{ps}f_{poff}}{A_c} - \frac{n_{po}\times a_{ps}\times f_{poff}\times e_e}{S_{tc}}$$

$= 17.42MPa < 0.45f_c^{'} = 20.17$ MPa.

The total bottom girder stress at the mid-span of Segment 2 at Stage 6 is computed as:

$$\sigma_{b6} = -\frac{M_{g2}}{S_{bg}} - \frac{M_{d2}}{S_{bg}} - \frac{M_{h2}}{S_{bg}} - \frac{M_{r2}}{S_{bc}} - \frac{M_{s2}}{S_{bc}} + \frac{A_{ps2}f_{pe42}}{A_g} + \frac{A_{ps2}f_{pe42}e_{p2}}{S_{bg}} +$$

$$\frac{n_{po}a_{ps}f_{poff}}{A_c} + \frac{n_{po}a_{ps}f_{poff}e_e}{S_{bc}}$$

$= 5.94MPa < 0.45fc' = 20.17$ MPa.

The total top deck stress at the mid-span of Segment 2 at Stage 6 is defined as:

$$\sigma_{ts6} = \frac{M_{r2}}{S_{tcs}} + \frac{M_{s2}}{S_{tcs}} + \frac{n_{po}a_{ps}f_{poff}}{A_{cc}} - \frac{n_{po}a_{ps}f_{poff}e_e}{S_{tcs}}$$

$= 7.03 < 0.45fcd' = 13.96$ MPa.

Stage7: Stress check at Compression 2 limit state

The total top girder stress at the mid-span of Segment 2 at Stage 7 is defined as:

$$\sigma_{t7} = 0.5(\frac{M_{g2}}{S_{tg}} + \frac{M_{d2}}{S_{tg}} + \frac{M_{h2}}{S_{tg}} + \frac{M_{r2}}{S_{tc}} + \frac{M_{s2}}{S_{tc}} + \frac{A_{ps2}f_{pe42}}{A_g} -$$

$$\frac{A_{ps2}f_{pe42}e_{p2}}{S_{tg}} + \frac{n_{po}a_{ps}f_{poff}}{A_c} - \frac{n_{po}a_{ps}f_{poff}e_e}{S_{tc}}) + \frac{M_{ll2}}{S_{tc}}$$

$= 13.02MPa < 0.4fc' = 17.92$ MPa.

The total bottom girder stress at the mid-span of Segment 2 at Stage 7 is determined as:

$$\sigma_{b7} = 0.5(-\frac{M_{g2}}{S_{bg}} - \frac{M_{d2}}{S_{bg}} - \frac{M_{h2}}{S_{bg}} - \frac{M_{r2}}{S_{bc}} - \frac{M_{s2}}{S_{bc}} + \frac{A_{ps2} f_{pe42}}{A_g} +$$

$$\frac{A_{ps2} f_{pe42} e_{p2}}{S_{bg}} + \frac{n_{po} a_{ps} f_{poff}}{A_c} + \frac{n_{po} a_{ps} f_{poff} e_e}{S_{bc}}] - \frac{M_{ll2}}{S_{tc}}$$

$$= -8.45 MPa < 0.4 fc' = 17.93 \text{MPa}.$$

The total top deck stress at the mid-span of Segment 2 at Stage 7 is defined as:

$$\sigma_{ts7} = 0.5(\frac{M_{r2}}{S_{tcs}} + \frac{M_{s2}}{S_{tcs}} + \frac{n_{po} a_{ps} f_{poff}}{A_{cc}} - \frac{n_{po} a_{ps} f_{poff} e_e}{S_{tcs}}) + \frac{M_{ll2}}{S_{tcs}}$$

$$= 8.27 < 0.4 \frac{fcd''}{1000} = 12.41 \text{ MPa}.$$

6.2.7 Strength limit state

After the design is completed for the service limit state, each critical section of girder needs to be checked for strength limit state requirements. The strength limit state included checks on moment and shear capacities. The ductility requirement was satisfied by ensuring that the relative neutral axis depth at the ultimate limit state c/d_e was less than 0.42 (AASHTO 2003).

a) Moment capacity at the midspan of segment 2

The flexural capacity at the midspan of the single-span spliced girder bridge is evaluated in this section. Optimal design variables at this stage include the number of pre-tensioned strands at the midspan of Segment 2, locations of the effective post-tensioning at the end span and at the midspan, and number of post-tensioning strands.

The total number of post-tensioning strands (n_{po}) obtained from the design chart (see Figure 6-6) is:

$$n_{po} = 52$$

The maximum number of strands in each duct is assumed to be 12. Therefore, the number of post-tensioning ducts is determined as:

$$\text{NT} = \text{round}\ (\frac{n_{po}}{12}) = 4$$

The location of the effective post-tensioning duct at the end of Segment 2 obtained from the design chart (see Figure 6-7) is:

$$y_a = 775 \text{ mm}$$

The location of effective post-tensioning duct at the midspan of Segment 2 obtained from the design chart (see Figure 6-7) is:

$$y_{bb} = 165 \text{ mm.}$$

The space between each post-tensioning duct is assumed to be 150 mm (6 in.) apart from each other. Therefore, the location of the highest post-tensioning duct depends on the lowest centroid of the effective post-tensioning duct and is calculated as follows:

$$y_{bbb} = y_{bb} + 150(NT - 1) = 622 \text{ mm.}$$

The average location of all post-tensioning ducts is determined by the summation of the lowest and highest post-tensioning duct locations as follows:

$$y_b = \frac{(y_{bb} + y_{bbb})}{2} = 394 \text{ mm.}$$

The total area of post-tensioned strands is determined as:

$$A_{PT} = n_{po} a_{ps} = 7280 \text{ mm}^2.$$

The total area of pre-tensioned strands at the midspan of Segment 2 is calculated as:

$$A_{preT} = (npr_{12} + npr_{22} + npr_{32} + npr_{42}) a_{ps} = 3780 \text{ mm}^2.$$

The distance from the location of effective post-tensioning duct to the extreme top fiber of composite section is calculated as:

$$d_{ppT} = H + t_s - y_b = 2254 \text{ mm}.$$

The centroid of all pre-tensioned strands at the mid-span of Segment 2 is defined as:

$$y_{cm} = \frac{(50npr_{12} + 100npr_{22} + 150npr_{32} + 200npr_{42})}{(npr_{12} + npr_{22} + npr_{32} + npr_{42})} = 107 \text{ mm}.$$

The distance from the centroid location of all pre-tensioning strands to the extreme top fiber of composite section is calculated as:

$$d_{ppret} = H + t_s - y_{cm} = 2541 \text{ mm}.$$

The centroid of prestress strands due to pre-tensioning and post-tensioning is determined as:

$$d_p = \frac{dp_{PT} A_{PT} + dp_{pret} A_{pret}}{A_{PT} + A_{pret}} = 2352 \text{ mm}.$$

The prestress stress in the post-tensioned strands is defined by:

$$f_{ps} = 0.92 f_{pu} = 1715 \text{ MPa}.$$

The total tension forces in the girder section due to the pre-tensioned and post-tensioned forces is computed as:

$$T = (A_{PT} + A_{PRET}) f_{ps} = 18965 \text{ kN}.$$

The concrete compression force in the top flange is defined as:

$$C_1 = 0.85 f_{cd} b_e h_f = 15160 \text{ kN}.$$

The concrete compression force in the web is determined as:

$$C_2 = 0.85 f_c b_f h_w = 6175 h_w .$$

The total concrete compression forces in the concrete girder must be equivalent to the total tension forces of the prestress steel and is computed as:

$$C = C_1 + C_2 = T .$$

The web height that is in the compression zone is obtained by trial and error until the tension and compression forces are equivalent. The portion of the web height under compression is:

$$h_w = 89.38 \text{ mm}.$$

The equivalent concrete compression stress block depth is then defined as:

$$a = h_f + h_w = 299 \text{ mm}.$$

The equivalent stress block coefficient used to determine the neutral axis of the girder section depends on the girder concrete compressive strength. The coefficient value of this example is:

$$\beta_1 = 0.725 .$$

The neutral axis of the girder section is determined as:

$$c = \frac{a}{\beta_1} = 412 \text{ mm}.$$

The nominal moment resistance of the T-section is calculated as:

$$M_n = 0.85 f_{cd} b_e h_f (d_p - \frac{h_f}{2}) + 0.85 f_c b_f h_w (d_p - h_f - \frac{h_w}{2}).$$

$$M_n = 42056\ kN - m.$$

The required moment must be less than the nominal moment resistance as shown below:

$$M_n = 42056\ kN - m > M_u = 33853\ kN - m.$$

The maximum reinforcement limit according to AASHTO LRFD Article 5.7.3.3.1 (AASHTO 2003) is checked as:

$$\frac{c}{d_e} = 0.175 < 0.42\ .$$

The moment capacity is thus adequate.

b) Shear resistance of the interface at spliced locations

There is a potential plane of weakness at the face of the splice, therefore shear at the splice must be considered. The interface shear capacity at the splice location is determined according to AASHTO LRFD Article 5.8.4 (AASHTO 2003). In this evaluation, the interface is considered to be a concrete to hardened concrete surface that has not been intentionally roughened.

The permissible stress at the surface is according to AASHTO LRFD Article 5.8.4.2 (AASHTO 2003) as:

$c = 0.517$ MPa.

The friction coefficient for normal weight concrete according to AASHTO LRFD Article 5.8.4.2 (AASHTO 2003) is calculated as

$$\mu = 0.6\lambda = 0.6.$$

The area of concrete engaged in shear transfer is determined as:

$$A_{cv} = t_w(h + t_s - d_t) = 486451 \text{ mm}^2.$$

The area of shear reinforcement crossing the shear plane is calculated as:

$$A_{vf} = t_w(h + t_s - d_t) = 7280 \text{ mm}^2.$$

The permanent net compressive force normal to the shear plane is computed as:

$$P_c = f_{pe} A_{vf} = 7028 \text{ kN}$$

The nominal shear resistance at the spliced is determined as:

$$V_n = cA_{cv} + \mu(A_{vf} f_y + P_c) = 6276 \text{ kN}$$

The factored nominal shear resistance at the splice most include the strength reduction factor of 0.90 and then compared with the ultimate shear requirement at the splice location as shown below:

$$\phi V_n = 0.9 V_n = 5649 \text{ kips} > V_u = 1899 \text{ kN}$$

c) Vertical shear at H/2

Calculation of the shear capacity of spliced girder bridges is as that for conventional prestressed concrete bridges. Nevertheless, the vertical shear capacity at H/2 from the support is also documented herein.

The computed vertical shear resistance from the concrete due to external loads is calculated as:

$$V_{ci-com} = 0.6\sqrt{f_c'} b' d' + V_d + \frac{V_i M_{cr}}{M_{\max}} = 1966 \text{ kips} = 8745 \text{ kN}$$

The minimum vertical shear resistance from the concrete is based on the modulus of rupture of concrete and can be determined as

$$V_{ci-\min} = MinV_{ci} = 1.7\sqrt{f_c'}b'd = 101.65 \text{ kips} = 452 \text{ kN}.$$

The maximum shear resisting force from concrete is determined as:

$$V_{ci} = Max(V_{ci-com}, V_{ci-\min}) = 8745\,\text{kN}.$$

The total prestress forces due to the pre-tensioned and post-tensioned forces can be defined as:

$$F = F_{post} + F_{pret} = 911 + 9012 = 9924 \text{ kN}.$$

The sine of the angle of the post-tensioned duct profile at the end with respect to the horizontal axis is equivalent to the tangent angle as shown below:

$$\sin\alpha = \tan\alpha = \frac{y_a - y_b}{L/2} = 0.012$$

The vertical shear force resistancecomponent due to the post-tensioning force is calculated as:

$$V_p = F\sin\alpha = 9924(0.012) = 119\,\text{kN}$$

The nominal vertical shear resistance at H/2 is determined as:

$$\phi V_n(H/2) = \phi(V_c + V_s + V_p) = 0.9(8745 + 119) = 7980 \text{ kN}.$$

The shear due to stirrup reinforcement is ignored in this calculation since the shear from the post-tensioning is much larger than the shear force from the stirrup reinforcement.

6.2.8 Design evaluation

The layout arrangement of pre- and post-tensioning requirements for design

Example 1 obtained from the design charts and those from the NCHRP 12-57 report (Castrodale and White 2004) are depicted in Figure 6-8 for comparison. Total prestress results obtained from the design charts and the NCHRP 12-57 for each segment are compared in Table 6-1. The provided nominal capacities of shear at the splice location and at H/2 as well as moments from the design charts and the NCHRP results are compared against the calculated demands also in Table 6-1.

Table 6-1 *Comparison of design requirements and capacities from NCHRP 517 and optimization chart results*

Prestressing Requirements			
	n_{po}	Npr_1	Npr_2
NCHRP 517	60	10	20
Design Charts	52	4	32
Design Capacities and Demands			
	M (kN-m)	V_Splice (kN)	V_h/2 (kN)
NCHRP 517	45,990	8,265	NA
Design Charts	41,115	5,440	7,980
Demand	33,858	1,900	3,648

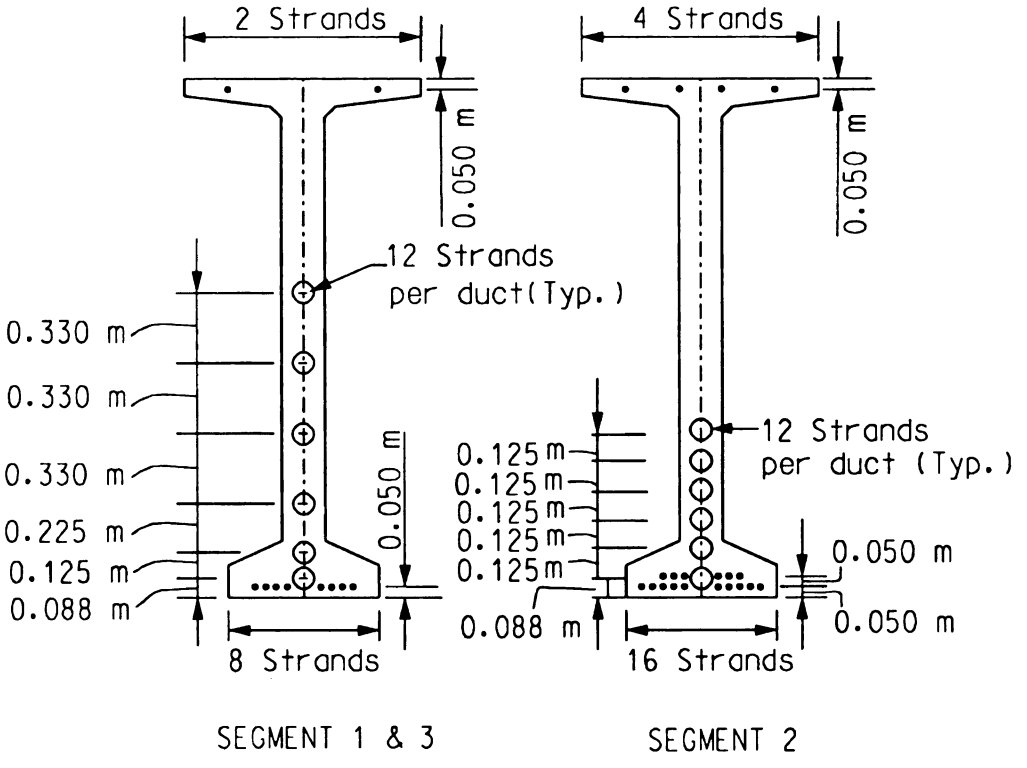

a) NCHRP Report 517-12 Example 1 result

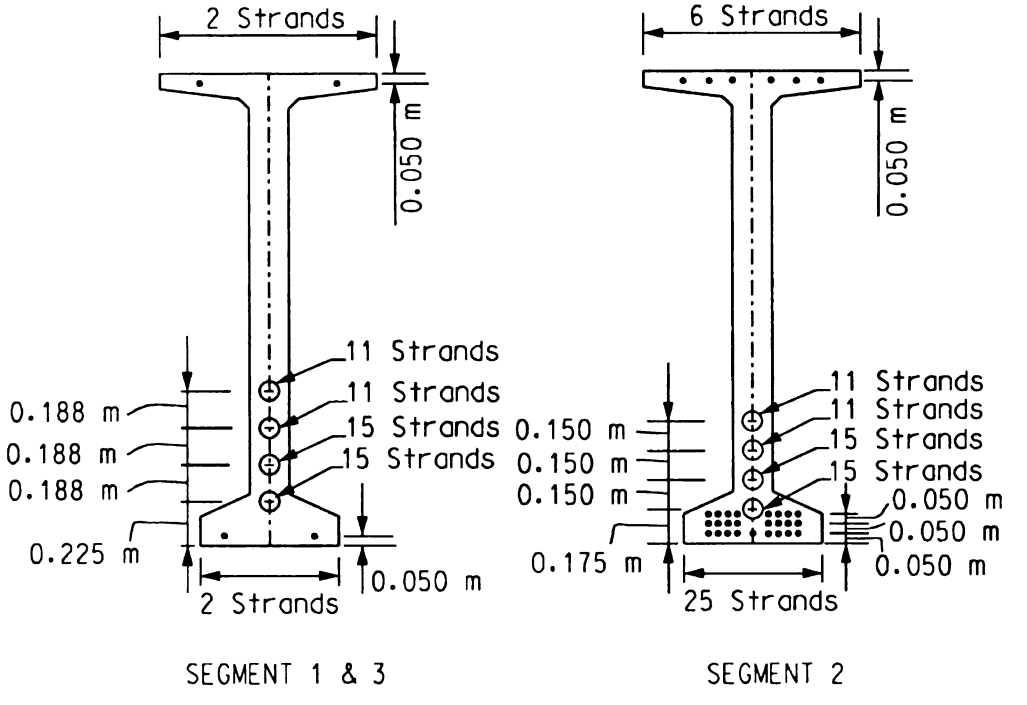

b) Optimized Design Aids result

Figure 6-8 *Pre- and post-tensioning strands requirement comparison between NCHRP and optimized aids results*

As one more measure of comparison between the results from the NCHRP report and those from the optimized charts, the flexural stresses from each critical construction stage were normalized in Figure 6-9. The normalized stresses for service limit states show that all results from the design charts are within the allowable limits for every construction stage. The required moment and shear of strength limit states were also compared with the nominal moment and shear results from the design charts, and they were found to be adequate.

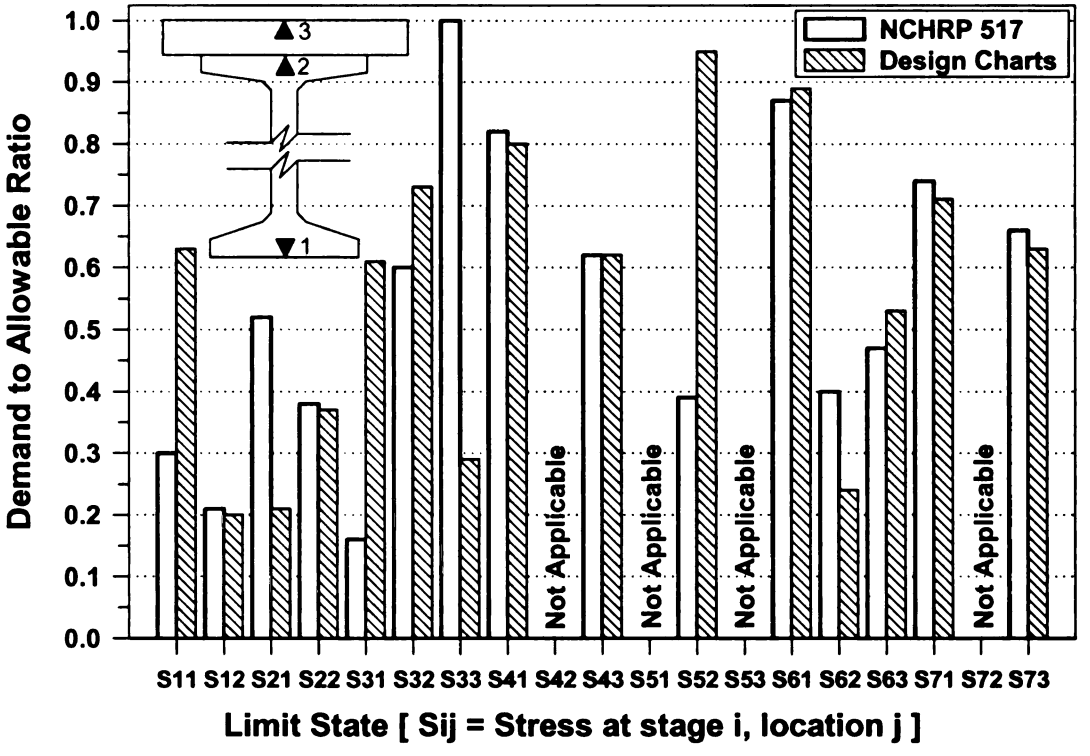

Figure 6-9 *Normalized stress results comparison between NCHRP and optimized aids designs*

The layout arrangement of pre- and post-tensioning requirements for design Example 1 obtained from the design charts and those from the NCHRP 12-57 report (Castrodale and White 2004) are depicted in Figure 6-8 for comparison.

6.3 Preliminary Design Example 2

6.3.1 Problem statement

A three-lane two-span continuous pliced girder bridge with a total width of 18.59 m (61 ft), and a span length (L) of 80.47 m (264 ft) consisting of three segments, as illustrated in Figure 6-10, was used as a prototype structure in this study. The new optimized girder was chosen in order to show how the service limit state of two-span continuous spliced girder bridge is different from single-span SGB. In addition, the total height of the new proposed beam obtained from the component optimization is used to compare with a prismatic spliced girder prestressed girder which is proposed by Lounis (1997).

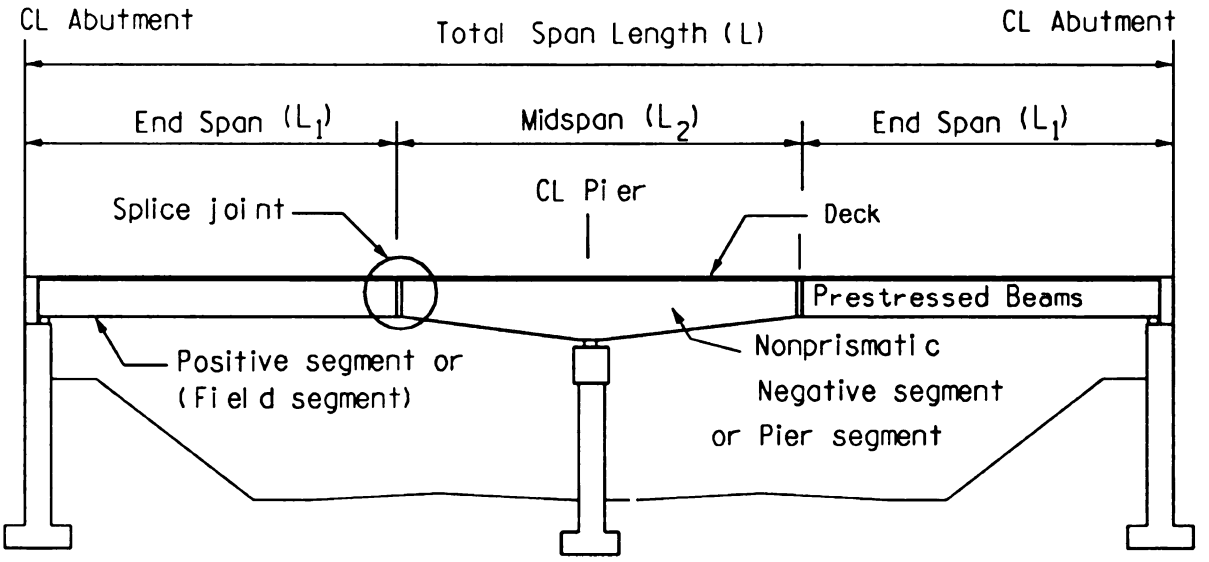

Figure 6-10 *Two-span spliced precast/prestressed bridge with non-prismatic pier segment*

The end segments were assumed to be equal length (L_1). The splice location is defined as the ratio of the end segment length (L_1) to the total span length (L) and was

assumed to be located at $0.35L$. The length of the middle segment is thus defined as $L_2 = L - L_1$. The cast-in-place concrete slab thickness was assumed to be 216 mm (8.5 in.) with 50 mm (2 in.) built-up built on a 1.8 m (6 ft) girder spacing.

The design study was conducted using the simplified design method of the AASHTO-LRFD Bridge Design Specifications (AASHTO 2003) and the recommendations of NCHRP 517 report (Castrodale and White 2004). Both service limit states and ultimate limit states were considered in the design.

The purpose of this design example is to illustrate how the developed design charts can be used as an aid for the preliminary design of two-span spliced girder bridges as shown in Figure 6-8. The non-prismatic negative segment with constant web height (option 3) obtained from the component optimization (see Section 5.4.3) for a bridge with total span length of 80.46 m [264 ft] was used in this example. A single-stage post-tensioning applied after deck casting construction is used in this study. The section at the mid-span section of negative segment (x = 40.23 m [132 ft] measured from the end span) of the spliced girder bridge is checked in this example.

6.3.2 Preliminary material properties

Girder Material Properties

f_c' = 44.8 MPa (6.5 ksi)

f_{ci}' = 34.5 MPa (5 ksi)

E_{gi} = 29,558 MPa (4287 ksi)

E_g = 33,702 MPa (4888 ksi)

w_c = 2,400 kg/m^3(150 lb/ft^3)

f_{cd}' = 24.1 MPa (4.5 ksi)

Deck Material Properties

f_{cdi}' = 31.0 MPa (3.5 ksi)

E_{cdi} = 24,731 MPa (3372 ksi)

E_{cd} = 28,041 MPa (3824 ksi)

w_{cd} = 2,400 kg/m^3(150 lb/ft^3)

Pre-tensioning Strands Properties

a_{ps} = 140 mm^2 (0.217 in^2)

E_p = 196,502 MPa (28500 ksi)

f_{pu} = 1,861 MPa (270 ksi)

$f_{py} = 0.9f_{pu}$ = 1,675 MPa (243 ksi)

$f_{po} = 0.75f_{pu}$ = 1,396 MPa (202.5 ksi)

Post-tensioning Strands Properties

a_{ps} = 140 mm^2 (0.217 in.^{2})

E_p = 196,502 MPa (28500 ksi)

f_{pu} = 1,861 MPa (270 ksi)

$f_{py} = 0.9f_{pu}$ = 1,675 MPa (243 ksi)

$f_{pj} = 0.9f_{py} = 1{,}508$ MPa (219 ksi)

6.3.3 Calculated section properties of optimized negative section

Non-composite Girder Section Properties (Negative Segments)

$y_{bg} = 637$ mm (25.08 in.)

$y_{tg} = 749$ mm (29.48 in.)

$S_{tg} = 122{,}902{,}980$ mm^3 (7500 in.^{3})

$S_{bg} = 146{,}418{,}417$ mm^3 (8935 in.^{3})

$A_g = 431{,}805$ mm^2 (669.3 in.^{2})

$I_g = 9.32899e10$ mm^4 (224,130 in.^{4})

Composite Girder Section Properties (Negative Segments)

$A_{ch} = 760{,}644$ mm^2 (1179 in.^{2})

$I_{ch} = 2.3155787e11$ mm^4 (556320 in^4)

$S_{bch} = 229{,}861{,}347$ mm^3 (14027 in.^{3})

$S_{tch} = 611{,}466{,}906$ mm^3 (37314 in.^{3})

$S_{tcsh} = 468{,}047{,}322$ mm^3 (28562 in.^{3})

$A_{cch} = 913{,}547$ mm^2 (1416 in.^{2})

$y_{bch} = 1007$ mm (39.66 in.)

$y_{tch} = 378$ mm (14.91 in.)

y_{tcsh} = 595 mm (23.41 in.)

6.3.4 General information

S = 1800 mm (6 ft)

t_s = 216 mm (8.5 in.)

Humidity = H = 75

t_r = 1 day

t_d = 60 days

t_{po} = 75 days

A_{set} = 9.53 mm (0.375 in.)

6.3.5 Use of design charts

The design optimization of two-span continuous SGB requires more design variables than those considered for the single-span system in Design Example 1. These include variables to define the sectional optimization options as shown in Figure 6-11, pre- and post-tensioning requirement and the definition of parabolic post-tensioning over the haunched negative segment as shown in Figure 6-12.

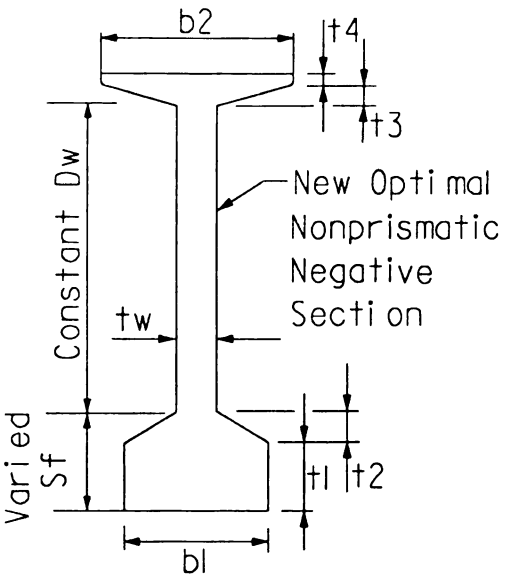

Figure 6-11 *Design variables for new non-prismatic section with constant web(option 3)*

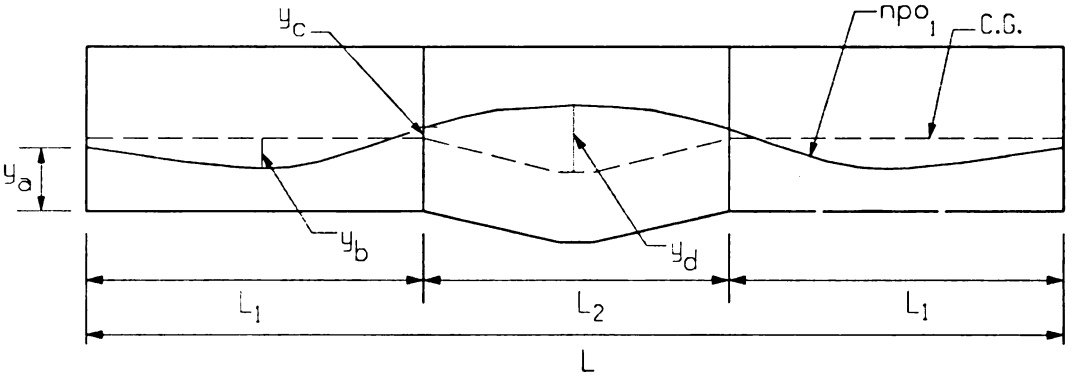

(a) Post-Tensioning Requirement

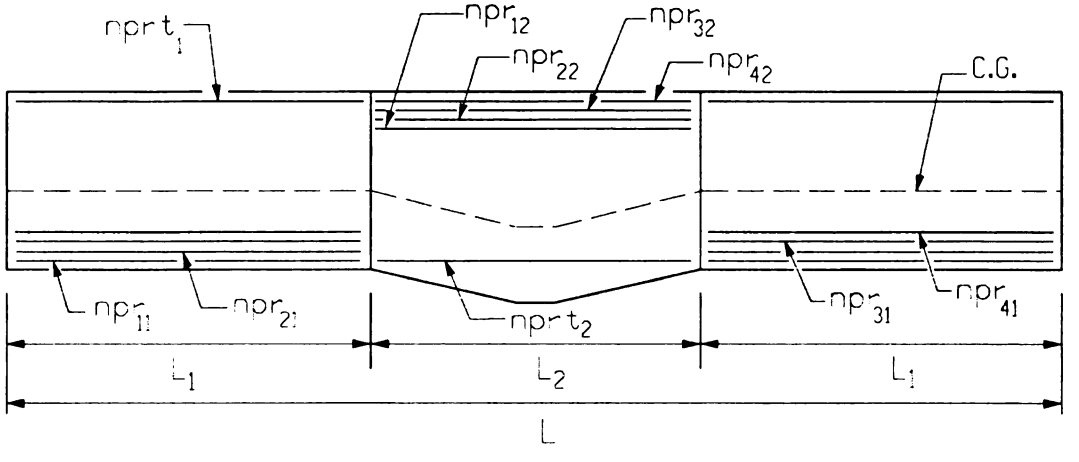

(b) Pre-Tensioning Requirement

Figure 6-12 *Variables for the design optimization of two-span continuous spliced girder bridge*

Design variables were obtained from the developed optimized design aid charts in the same way as explained for the single-span SGB (Example 1). Using design aid charts, the design variables are:

$npr_{11} = 5$; $npr_{12} = 5$; $npr_{13} = 3$;

$npr_{14} = 2$; $nprt_1 = 2$; $npr_{21} = 0$;

$npr_{22} = 0$; $npr_{23} = 0$; $npr_{24} = 0$;

$nprt_1 = 3$; $nprt_2 = 7$; $npo_1 = 20$;

t_1 = min 127 mm (5 in.) – max 178 mm (7 in.);

t_2 = 127 mm (5 in.); t_3 = 127 mm (5 in.);

t_4 = 127 mm (5 in.); b_1 = 610 mm (24 in.);

b_2 = 457 mm (18 in.); t_w = 200 mm (8 in.);

D_w=818 mm (32.2 in.);

y_a = 25 mm (1 in.); y_b = 635 mm (25 in.);

y_c = 50 mm (2 in.) upward from neutral axis;

y_d = 200 mm (8 in.) upward from neutral axis.

The service limit state and ultimate limit state at the mid-span section of the negative segment are now checked to verify that the results provided by the design aids do in fact satisfy all serviceability and strength requirements.

6.3.6 Service limit states

Service limit states were defined in terms of flexural stress limits on the girder and deck. For flexure, service limit state requirements govern the required prestressing force. The stress limit states for each critical construction stage of the single-span spliced girder bridge when using a single-post-tensioning (see Section 4.5.1) are evaluated as follows:

Stage 1: Stress check at pre-tensioning

The end-segment, or segment 1, length is based on the spliced location and can be determined as:

L_1 = (splice location)(L) = (0.35)L = (0.35)(80.47) = 28.16 m.

End segments are assumed to be equal, therefore the mid-segment length can be computed as:

$L_2 = L - (2)(L_1)$ = 24.15 m.

The centroid of all pre-tensioned strands measured from the top of the negative segment is computed as follows:

$$y_{e2} = \frac{(npr_{12})(50) + (npr_{22})(100) + (npr_{32})(150) + (npr_{42})(200) + (nprt_2)(y_{bg} + y_{tg} - 50)}{(npr_{12} + npr_{22} + npr_{32} + npr_{42} + nprt_2)}$$

y_{e2} = 1003 mm.

The eccentricity of the pre-tensioned strands at the midspan of negative segment is computed as:

$e_{p2} = (y_{tgm} - y_{e2})$ = 310 mm (measured above neutral axis).

The total pre-tensioned strand areas include the area of all pre-tensioning strands in the top and bottom girder flanges:

$$A_{ps2} = (a_{ps})(npn_{12} + npr_{22} + npr_{32} + npr_{42} + nprt_2) = 1{,}260 \text{ mm}^2.$$

The girder dead load moment at the midspan of the negative segment is computed as

M_{g2} = -186.4 kN-m

The cross-section area of the non-prismatic negative segment varies along its length. Therefore, the average cross-section area is used for the non-prismatic section and can be determined as:

$$A_{ge} = \frac{(A_g + A_{gm})}{2} = 413548 \text{ mm}^2.$$

Similarly, the average moment of inertia is used for the non-prismatic section and can be determined as:

$$I_{ge} = \frac{(I_g + I_{gm})}{2} = 8.53\text{e}10 \text{ mm}^4.$$

The stress at the centroid of the pre-tensioned strands of the negative segment caused by pre-tensioning and girder dead load is calculated as:

$$f_{cgp12} = \frac{0.7A_{ps2}f_{pu}}{A_{ge}} + \frac{0.7A_{ps2}f_{pu}e_{p2}^2}{I_{ge}} - \frac{|M_{g2}||e_{p2}|}{I_{ge}} = 5.143 \text{ MPa.}$$

Elastic shortening prestress losses due to the pre-tensioning at the release stage can be determined as follows:

$$df_{ES2} = f_{cgp12}\frac{E_p}{E_{gi}} = 34.2 \text{ MPa.}$$

Relaxation prestress losses at release of the pre-tensioned strands are defined as:

$$df_{PR1} = \frac{\log(24t_{r1})}{40}[\frac{f_{pj}}{f_{py}} - 0.55]f_{pj} = 13.65 \text{ MPa.}$$

The effective prestress at the centroid of the pre-tensioned strands after all losses at release of the pre-tensioning is calculated as follows:

$$f_{pe12} = f_{pei} - df_{ES2} - df_{PR1} = 1348 \text{ MPa.}$$

The total top girder stress at the mid-span of the mid-segment at Stage 1 is defined as:

$$\sigma_{t1} = \frac{M_{g2}}{S_{tge}} + \frac{A_{ps2}f_{pe12}}{A_{ge}} - \frac{A_{ps2}f_{pe12}e_{p2}}{S_{tge}} = 6.76 \quad \text{MPa} \quad < \quad 0.6f'_{ci} = 20.68$$

MPa.

The total bottom girder stress at the mid-span of the mid-segment at Stage 1 is calculated by:

$$\sigma_{b1} = -\frac{M_{g2}}{S_{bge}} + \frac{A_{ps2}f_{pe12}}{A_{ge}} - \frac{A_{ps2}f_{pe12}e_{p2}}{S_{bge}} = 1.59 \text{ MPa} < 0.6f'_{ci} = 20.68 \text{ MPa.}$$

Stage 2: Stress check at placement of deck and splice

M_{d2} = Deck load moment at midspan of negative segment

= -174.14 kN-m

M_{h2} = Haunch load moment at midspan of negative segment

= -29.91 kN-m

M_{s2} = Superimposed dead load moment at midspan of negative segment

= -663.92 kN-m

M_{c2} = Construction load moment at midspan of negative segment

= -32.78 kN-m

M_{p2} = Moment due to removal of supports at midspan of negative segment

= -3227 kN-m

M_{PT2} = Moment due to post-tensioning uniform loads

= 2027 kN-m

M_{wPT} = Moment due to post-tensioning uniform loads

= 283 kN-m

M_{SEC2} = Moment due to secondary effect of post-tensioned loads

= 233 kN-m

Shrinkage prestress losses are assumed to be calculated at 75% humidity and are determined according to AASHTO LRFD Equation 5.9.5.4.2-1 (AASHTO 2003):

$df_{pSR} = (17 - 0.15H) = 39.65$ MPa.

The creep coefficient during deck placement is based on the time that deck is poured and can be calculated according to AASHTO LRFD Equation 5.4.2.3.2-1 (AASHTO 2003):

$$K_{CRtd} = \frac{t_d^{0.6}}{10 + t_d} = 0.5384.$$

The shrinkage coefficient during deck placement is determined according to (AASHTO LRFD Equation 5.4.2.3.3-1(AASHTO 2003) :

$$K_{SHtd} = \frac{t_d}{35 + t_d} = 0.6316.$$

The initial post-tensioning stress is defined as:

$f_{p4} = 0.69 fpu = 1287$ MPa.

The total post-tensioning forces are determined from all post-tensioning ducts and can be calculated by:

$$F_{PT12} = n_{po} a_{ps} f_{p4} = 5587 \text{ kN}.$$

The maximum number of strands in each duct is assumed to be 12. Therefore, the number of post-tensioning ducts is determined as:

$$NT = round(\frac{n_{po}}{12}) = 2 \text{ ducts}.$$

The maximum eccentricity of the pre-tensioned strands for the composite section over the pier centerline is defined as:

$$e_{c2m} = -(y_{tch} - y_{e2}) = 625 \text{ mm}.$$

The eccentricity of the pre-tensioning strands for the composite section at the splice location is defined as:

$$e_{c2} = -(y_{tc} - y_{e2}) = 674 \text{ mm}.$$

The average eccentricity of the pre-tensioning strands for the composite section at the negative segment is defined as:

$$e_{c2e} = \frac{e_{c2m} + e_{c2}}{2} = 650 \text{ mm}.$$

The average top centroid of the haunched section with composite behavior for the negative segment is determined as:

$$y_{tche} = \frac{y_{tch} + y_{tc}}{2} = 354 \text{ mm}.$$

The average cross-sectional area of at the negative segment with composite behavior is determined as:

$$A_{ce} = \frac{A_{ch} + A_c}{2} = 741934 \text{ mm}^2.$$

The average moment of inertia of the composite section for the negative segment is determined as:

$$I_{ce} = \frac{I_{ch} + I_c}{2} = 2.13219\text{e}11 \text{ mm}^4.$$

The stress at the centroid of the pre-tensioned strands on the negative segment caused by post-tensioning, secondary effects, and temporary support removal loads can be determined as:

$$f_{cgpc2} = \frac{F_{PT12}}{A_{ce}} + \frac{F_{PT12} e_{ob} e_{c2e}}{I_{ce}} - \frac{|M_{RDL2}| e_{c2e}}{I_{ce}} + \frac{M_{SEC2} |e_{c2e}|}{I_{ce}}$$

$$+ \frac{M_{wPT} |e_{c2e}|}{I_{ce}}$$

$$= 6.72 \text{ MPa}.$$

The average moment of inertia of the non-composite section at the negative segment is calculated as:

$$I_{ge} = \frac{I_{gm} + I_g}{2} = 8.5307\text{e}10 \text{ mm}^4$$

The eccentricity of the pre-tensioned strands for the non-composite section over the pier centerline is defined as:

$$e_{p2} = -(y_{tg} - y_{e2}) = 310 \text{ mm}.$$

The stress at the centroid of the pre-tensioned strands of the negative segment caused by the deck, girder/deck haunch, and superimposed dead loads can be calculated as:

$$df_{cdp2} = \frac{|M_{d2} + M_{h2}|}{|I_{ge}|}|e_{p2}| + \frac{|M_{s2}\|e_{c2e}|}{I_{ce}} = 2.758 \text{ MPa.}$$

The creep prestressing losses at this stage are computed according to the AASHTO-LRFD provisions (AASHTO 2003) and the recommendations from the NCHRP 517 report (Castrodale and White 2004). The first two terms of the following equation are determined according to AASHTO-LRFD Section 5.9.5.4 and the last term is added as recommended by the NCHRP 517 report.

$$df_{CR2} = 12 f_{cgp12} - 7 df_{cdp2} + 7 f_{cgpc2} = 34.0 \text{ MPa.}$$

Final relaxation prestress losses, which include those due to elastic shortening, shrinkage, and creep, are determined according to AASHTO-LRFD Equation 5.9.5.4.4:

$$df_{PR22} = 0.3[20 - 0.4 df_{ES2} - 0.2(df_{pSR} + df_{pCR2})] = 32.84 \text{ MPa.}$$

The total prestress losses at the time of deck and splice placement are calculated as follows:

$$df_{preTD2} = df_{ES2} + K_{CRtd} df_{CR2} + K_{SHtd} df_{pSR} + df_{PR22} = 110.45 \text{ MPa.}$$

The effective prestress at the centroid of the pre-tensioned strands after all losses at the time of deck and splice is calculated as follows:

$$f_{pe22} = f_{pei} - df_{preTD2} = 1282 \text{ MPa.}$$

The total top girder stress at the mid-span of the negative segment at Stage 2 (current stage) is defined as:

$$\sigma_{t2} = \frac{M_{g2}}{S_{tge}} + \frac{M_{d2}}{S_{tge}} + \frac{M_{h2}}{S_{tge}} + \frac{M_{c2}}{S_{tge}} + \frac{A_{ps2} f_{pe22}}{A_{ge}} - \frac{A_{ps2} f_{pe22} e_{p2}}{S_{tge}}$$

$$= 4.4 MPa < 0.6 fc' = 26.89 \text{ MPa.}$$

The total bottom girder stress at the mid-span of the negative segment at Stage 2 is defined as:

$$\sigma_{b2} = -\frac{M_{g2}}{S_{bge}} - \frac{M_{d2}}{S_{bge}} - \frac{M_{h2}}{S_{bge}} - \frac{M_{c2}}{S_{bge}} + \frac{A_{ps2} f_{pe22}}{A_{ge}} - \frac{A_{ps2} f_{pe22} e_{p2}}{S_{bge}}$$

$$= 3.19\,MPa < 0.6 fc' = 26.89 \text{ MPa}.$$

Stage 3: Stress check at post-tensioning

The creep coefficient during the post-tensioning stage is based on the time at which post-tensioning is applied and can be calculated as (AASHTO LRFD Equation 5.4.2.3.2-1):

$$K_{CRtp} = \frac{t_{po}^{0.6}}{10 + t_{po}} = 0.571.$$

The shrinkage coefficient during post-tensioning is determined as (AASHTO LRFD Equation 5.4.2.3.3-1):

$$K_{SHtp} = \frac{t_{po}}{35 + t_{po}} = 0.682.$$

Stressing of the post-tensioning tendons causes secondary elastic shortening prestress losses in the pre-tensioned strands in the girder segments. Additional elastic shortening losses due to post-tensioning are computed as:

$$df_{pESA2} = (\frac{E_p}{E_g}) f_{cgpc2} = 39.21 \text{ MPa}.$$

Total prestress losses at the centroid of the pre-tensioned strands at the post-tensioning stage are calculated as follows:

$$df_{preTP2} = df_{ES2} + K_{CRtp} df_{CR2} + K_{SHtp} df_{pSR} + df_{PR22} + df_{pESA2} = 152.71 \text{ MPa}.$$

The effective prestress at the centroid of the pre-tensioned strands after all losses at the post-tensioning stage is calculated as follows:

$$f_{pe32} = f_{pei} - df_{preTP2} = 1243 \text{ MPa.}$$

The friction losses are computed according AASHTO LRFD Equation 5.9.5.2.2 as shown below:

$$df_{pF} = f_{pj}(1 - e^{-(Kx+\mu\alpha)}) = 55.6 \text{ MPa.}$$

Anchor set prestress loss is computed by estimating the loss that occurs when each tendon pulls into the anchorage at seating. The maximum anchorage set loss, which is at the stressing anchorage, is computed using the NCHRP 517 report Equation 7.3.1.1.2-3 (Castodale and White 2004) as follows:

$$df_A = 2\frac{df_{pF}}{x}\sqrt{\frac{A_{set}E_p x}{df_{pF}}} = 101.7 \text{ MPa.}$$

The distance along which the anchor set loss extends is computed using the NCHRP 517 report Equation 7.3.1.1.2-2 (Castodale and White 2004) as shown below:

$$X_A = \frac{1}{12}\sqrt{\frac{A_{set}E_p x}{dfpF}} = 1449 \text{ mm.}$$

The average eccentricity of the composite section over the pier is determined as:

$$e_{pt2} = kkk(4 - y_{tche}) - 2 = 303 \text{ mm (measured above neutral-axis).}$$

The total post-tensioning forces are determined from all of the post-tensioned ducts and can be calculated by:

$$F_{PT0} = n_{po}a_{ps}f_{p0i} = 5587 \text{ kN.}$$

The stress at the centroid of all post-tensioned strands on the negative segment caused by the post-tensioning and temporary support removal loads can be determined as:

$$f_{cgpo2} = \frac{F_{PT0}}{A_{ce}} + \frac{F_{PT0} e_{pt2}^2}{I_{ce}} - \frac{|M_{r2}||e_{pt2}|}{I_{ce}} + \frac{M_{SEC2} e_{pt2}}{I_{ce}} = 2.18 \text{ MPa.}$$

Elastic shortening prestress losses at the centroid of the post-tensioning strands due to post-tensioning are computed as:

$$df_{PTES2} = \frac{(NT-1)}{2NT} \frac{E_p}{E_g} f_{cgpo2} = 5.44 \text{ MPa.}$$

The total prestress losses at the post-tensioning stage are calculated as follows:

$$d_{PTPT2} = df_{pF} + df_{PTES2} + df_A \frac{(X_A - 0.5L)}{X_A} = 51.55 \text{ MPa.}$$

The effective prestress at the centroid of post-tensioned strands after all losses from the post-tensioning stage is calculated as follows:

$$f_{pof} = f_{po12} = f_{poi} - d_{PTPT2} = 1344 \text{ MPa.}$$

The total top girder stress at the mid-span of the negative segment at Stage 3 is defined as:

$$\sigma_{t3} = \frac{M_{g2}}{S_{tge}} + \frac{M_{d2}}{S_{tge}} + \frac{M_{h2}}{S_{tge}} + \frac{M_{r2}}{S_{tce}} + \frac{A_{ps2} f_{pe32}}{A_{ge}} - \frac{A_{ps2} f_{pe32} e_{p2}}{S_{tge}} +$$

$$\frac{n_{po} a_{ps} f_{pof}}{A_{ce}} + \frac{M_{PT2}}{S_{tce}} + \frac{M_{SEC2}}{S_{tce}} + \frac{M_{wPT}}{S_{tce}}$$

$$= 8.677 \, MPa < 0.6 fc' = 26.89 \text{ MPa.}$$

The total bottom girder stress at the mid-span of the negative segment at Stage 3 is defined as:

$$\sigma_{b3} = -\frac{M_{g2}}{S_{bge}} - \frac{M_{d2}}{S_{bge}} - \frac{M_{h2}}{S_{bge}} - \frac{M_{r2}}{S_{bce}} + \frac{A_{ps2} f_{pe32}}{A_{ge}} + \frac{A_{ps2} f_{pe32} e_{p2}}{S_{bge}} + \frac{n_{po} a_{ps} f_{pof}}{A_{ce}} - \frac{M_{PT2}}{S_{bce}} - \frac{M_{SEC2}}{S_{bce}} - \frac{M_{wPT}}{S_{bce}}$$

$= 11.11\,MPa < 0.6 fc' = 26.89$ MPa.

The total top deck stress at the mid-span of negative segment at Stage 3 is defined as:

$$\sigma_{ts3} = \frac{M_{r2}}{S_{ftcs}} + \frac{n_{po} a_{ps} f_{pof}}{A_{ccf}} - \frac{M_{PT2}}{S_{ftcs}} - \frac{M_{SEC2}}{S_{ftcs}} - \frac{M_{wPT}}{S_{ftcs}} = \quad 2.55 \quad \text{MPa}$$

$< 0.6 fcd' = 18.62$ MPa.

Stage 4: Stress check at Compression 1 limit state

M_{s2} = Superimposed dead load moment at midspan of negative segment

= -664 kN-m

M_{ll2} = Live load moment at midspan of negative segment

= -1945 kN-m

Total prestress losses at the final condition after all prestress losses for *Compression 1 limit state* are calculated as follows:

$$df_{preTPF2} = df_{ES2} + df_{CR2} + df_{pSR} + df_{PR22} + df_{pESA2} = 147.3 \text{ MPa.}$$

The effective prestress at the centroid of the pre-tensioned strands after all prestress losses for the final condition for the Compression 1 limit state is calculated as follows:

$$f_{pe42} = f_{pei} - df_{preTPF2} = 1249 \text{ MPa.}$$

The stress at the centroid of the post-tensioned strands on the negative segment caused by the deck, girder/deck haunch, and superimposed dead loads can be calculated as:

$$df_{cdp02} = \frac{|M_{d2} + M_{h2}|}{|I_{ge}|}|e_{p2}| + \frac{|M_{s2}||e_{c2e}|}{I_{ce}} = 1.669 \text{ MPa.}$$

The stress at the centroid of the post-tensioned strands of the negative segment caused by post-tensioning and girder dead loads can be calculated as:

$$f_{cgpc02} = \frac{0.7A_{ps2}f_{pu}}{A_{ge}} + \frac{0.7A_{ps2}f_{pu}e_{p2}e_{c2e}}{I_{ge}} - \frac{|M_{g2}||e_{p2}|}{I_{ge}} = 0.482 \text{ MPa}$$

Prestress loss due to creep at the centroid of the post-tensioning strands in this stage is computed according to the AASHTO-LRFD specifications and the recommendations from the NCHRP 517-12 report. The first two terms of the following equation are determined according to AASHTO-LRFD Section 5.9.5.4 (AASHTO 2003) and the last term is added as recommended by the NCHRP 517 report (Castrodale and White 2004).

$$df_{poCR2} = 12f_{cgpo2} - 7df_{cdpo2} + 7f_{cgpco2} = 34.4 \text{ MPa.}$$

Shrinkage prestress loss in the post-tensioning is calculated at 75% humidity and according to AASHTO LRFD equation 5.9.5.4.2-2 (AASHTO 2003) and is defined as:

$$df_{poSR} = (13.5 - 0.123H) = 29.47 \text{ MPa.}$$

Prestress loss due to final relaxation of the post-tensioning strands is calculated according to AASHTO-LRFD Equation 5.9.5.4.4 (AASHTO 2003):

$$df_{PR32} = 0.3(20 - 0.3df_{pF} - 0.4df_{PTES2} - 0.2(df_{poCR2} + df_{poSR}) = 31.87 \text{ MPa.}$$

Total prestress losses at the Compression 1 limit state for the final stage are calculated as follows:

$$d_{PTF2} = df_{pF} + df_{PTES2} + df_A \frac{(X_A - 0.5L)}{X_A} + df_{poCR2} + df_{poSR} + df_{PR32}$$

$$= 259 \text{ MPa.}$$

The effective prestress at the centroid of the post-tensioned strands after all losses at the final Compression 1 stage is calculated as follows:

$$f_{poff} = f_{po22} = f_{poi} - d_{PTF2} = 1137 \text{ MPa.}$$

The total top girder stress at the mid-span of the negative segment at Stage 4 is determined as:

$$\sigma_{t4} = \frac{M_{g2}}{S_{tge}} + \frac{M_{d2}}{S_{tge}} + \frac{M_{h2}}{S_{tge}} + \frac{M_{r2}}{S_{tce}} + \frac{M_{s2}}{S_{tce}} + \frac{M_{ll2}}{S_{tce}} + \frac{A_{ps2}f_{pe42}}{A_{ge}} - \frac{A_{ps2}f_{pe42}e_{p2}}{S_{tge}} + \frac{n_{po}a_{ps}f_{poff}}{A_{ce}} + \frac{M_{PT2}}{S_{tce}} + \frac{M_{SEC2}}{S_{tce}} + \frac{M_{wPT}}{S_{tce}}$$

$$= 3.17 MPa < 0.6f_c^{'} = 26.89 \text{ MPa.}$$

The total bottom girder stress at the mid-span of the negative segment at Stage 4 is defined as:

$$\sigma_{b4} = -\frac{M_{g2}}{S_{bge}} - \frac{M_{d2}}{S_{bge}} - \frac{M_{h2}}{S_{bge}} - \frac{M_{r2}}{S_{bce}} - \frac{M_{s2}}{S_{bce}} - \frac{M_{ll2}}{S_{bce}} + \frac{A_{ps2}f_{pe42}}{A_{ge}} + \frac{A_{ps2}f_{pe42}e_{p2}}{S_{bge}} + \frac{n_{po}a_{ps}f_{poff}}{A_{ce}} - \frac{M_{PT2}}{S_{bce}} - \frac{M_{SEC2}}{S_{bce}} - \frac{M_{wPT}}{S_{bce}}$$

$= 23.9 MPa < 0.6 f_c^{'} = 26.89$ MPa.

The total top deck stress at the mid-span of the negative segment at Stage 4 is defined as:

$$\sigma_{ts4} = \frac{M_{r2}}{S_{tcs}} + \frac{M_{s2}}{S_{tcs}} + \frac{M_{ll2}}{S_{tcs}} + \frac{n_{po} a_{ps} f_{poff}}{A_{cc}} - \frac{M_{PT2}}{S_{ftcs}} - \frac{M_{SEC2}}{S_{ftcs}} - \frac{M_{wPT}}{S_{ftcs}}$$

$$= -4.254 MPa < 0.6 f_{cd}^{'} = 18.62 \text{ MPa.}$$

Stage 5: Stress check at tension limit state

The total top girder stress at the mid-span of the negative segment at Stage 5 is defined as:

$$\sigma_{t5} = \frac{M_{g2}}{S_{tge}} + \frac{M_{d2}}{S_{tge}} + \frac{M_{h2}}{S_{tge}} + \frac{M_{r2}}{S_{tce}} + \frac{M_{s2}}{S_{tce}} + 0.8\frac{M_{ll2}}{S_{tce}} + \frac{A_{ps2} f_{pe42}}{A_{ge}} -$$

$$\frac{A_{ps2} f_{pe42} e_{p2}}{S_{tge}} + \frac{n_{po} a_{ps} f_{poff}}{A_{ce}} + \frac{M_{PT2}}{S_{tce}} + \frac{M_{SEC2}}{S_{tce}} + \frac{M_{wPT}}{S_{tce}}$$

$$= 5.85 MPa > -0.19\sqrt{fc'} = -3.34 \text{ MPa.}$$

The total bottom girder stress at the mid-span of the negative segment at Stage 5 is obtained as:

$$\sigma_{b5} = -\frac{M_{g2}}{S_{bge}} - \frac{M_{d2}}{S_{bge}} - \frac{M_{h2}}{S_{bge}} - \frac{M_{r2}}{S_{bce}} - \frac{M_{s2}}{S_{bce}} - 0.8\frac{M_{ll2}}{S_{bce}} + \frac{A_{ps2} f_{pe42}}{A_{ge}} +$$

$$\frac{A_{ps2} f_{pe42} e_{p2}}{S_{bge}} + \frac{n_{po} a_{ps} f_{poff}}{A_{ce}} - \frac{M_{PT2}}{S_{bce}} - \frac{M_{SEC2}}{S_{bce}} - \frac{M_{wPT}}{S_{bce}}$$

$$= -2.99 MPa > -0.19 \times \sqrt{fc'} = -3.34 \text{ MPa.}$$

The total top deck stress at the mid-span of the negative segment at Stage 5 is calculated by:

$$\sigma_{ts5} = \frac{M_{r2}}{S_{tcse}} + \frac{M_{s2}}{S_{tcse}} + 0.8\frac{M_{ll2}}{S_{tcse}} + \frac{n_{po}a_{ps}f_{poff}}{A_{cce}}$$
$$- \frac{M_{PT2}}{S_{ftcs}} - \frac{M_{SEC2}}{S_{ftcs}} - \frac{M_{wPT}}{S_{ftcs}}$$

$$= 11.25\,MPa < 0.6fcd' = 18.62 \text{ MPa.}$$

Stage 6: Stress check at Compression 2 limit state

The total top girder stress at the mid-span of the negative segment at Stage 6 is defined as:

$$\sigma_{t6} = \frac{M_{g2}}{S_{tge}} + \frac{M_{d2}}{S_{tge}} + \frac{M_{h2}}{S_{tge}} + \frac{M_{r2}}{S_{tce}} + \frac{M_{s2}}{S_{tce}} + \frac{A_{ps2}f_{pe42}}{A_{ge}} - \frac{A_{ps2}f_{pe42}e_{p2}}{S_{tge}} +$$

$$\frac{n_{po}a_{ps}f_{poff}}{A_{ce}} + \frac{M_{PT2}}{S_{tce}} + \frac{M_{SEC2}}{S_{tce}} + \frac{M_{wPT}}{S_{tce}}$$

$$= 6.38MPa < 0.45f_c' = 20.17 \text{ MPa.}$$

The total bottom girder stress at the mid-span of the negative segment at Stage 6 is computed as:

$$\sigma_{b6} = -\frac{M_{g2}}{S_{bge}} - \frac{M_{d2}}{S_{bge}} - \frac{M_{h2}}{S_{bge}} - \frac{M_{r2}}{S_{bce}} - \frac{M_{s2}}{S_{bce}} + \frac{A_{ps2}f_{pe42}}{A_{ge}} + \frac{A_{ps2}f_{pe42}e_{p2}}{S_{bge}} +$$

$$\frac{n_{po}a_{ps}f_{poff}}{A_{ce}} - \frac{M_{PT2}}{S_{bce}} - \frac{M_{SEC2}}{S_{bce}} - \frac{M_{wPT}}{S_{bce}}$$

$$= 15.4MPa < 0.45fc' = 20.17 \text{ MPa.}$$

The total top deck stress at the mid-span of the negative segment at Stage 6 is defined as:

$$\sigma_{ts6} = \frac{M_{r2}}{S_{tcse}} + \frac{M_{s2}}{S_{tcse}} + \frac{n_{po}a_{ps}f_{poff}}{A_{cce}} - \frac{M_{PT2}}{S_{ftcs}} - \frac{M_{SEC2}}{S_{ftcs}} - \frac{M_{wPT}}{S_{ftcs}}$$

$$= -0.097 < 0.45 fcd' = 13.96 \text{ MPa.}$$

Stage7: Stress check at Compression 3 limit state

The total top girder stress at the mid-span of the negative segment at Stage 7 is defined as:

$$\sigma_{t7} = 0.5\left(\frac{M_{g2}}{S_{tge}} + \frac{M_{d2}}{S_{tge}} + \frac{M_{h2}}{S_{tge}} + \frac{M_{r2}}{S_{tce}} + \frac{M_{s2}}{S_{tce}} + \frac{A_{ps2} f_{pe42}}{A_{ge}} - \frac{A_{ps2} f_{pe42} e_{p2}}{S_{tge}} + \frac{n_{po} a_{ps} f_{poff}}{A_{ce}}\right) + \frac{M_{ll2}}{S_{tce}} + \frac{M_{PT2}}{S_{tce}} + \frac{M_{SEC2}}{S_{tce}} + \frac{M_{wPT}}{S_{tce}}$$

$$= 0.63\, MPa < 0.4 fc' = 17.92 \text{ MPa.}$$

The total bottom girder stress at the mid-span of the negative segment at Stage 7 is determined as:

$$\sigma_{b7} = 0.5\left(-\frac{M_{g2}}{S_{bge}} - \frac{M_{d2}}{S_{bge}} - \frac{M_{h2}}{S_{bge}} - \frac{M_{r2}}{S_{bce}} - \frac{M_{s2}}{S_{bce}} + \frac{A_{ps2} f_{pe42}}{A_{ge}} + \frac{A_{ps2} f_{pe42} e_{p2}}{S_{bge}} + \frac{n_{po} a_{ps} f_{poff}}{A_{ce}}\right] - \frac{M_{ll2}}{S_{tce}} - \frac{M_{PT2}}{S_{bce}} - \frac{M_{SEC2}}{S_{bce}} - \frac{M_{wPT}}{S_{bce}}$$

$$= 17.88 MPa < 0.4 fc' = 17.93 \text{ MPa.}$$

The total top deck stress at the mid-span of the negative segment at Stage 7 is defined as:

$$\sigma_{ts7} = 0.5\left(\frac{M_{r2}}{S_{tcse}} + \frac{M_{s2}}{S_{tcse}} + \frac{n_{po} a_{ps} f_{poff}}{A_{cce}} - \frac{n_{po} a_{ps} f_{poff} e_e}{S_{tcse}}\right) + \frac{M_{ll2}}{S_{tcse}} - \frac{M_{PT2}}{S_{ftcs}} - \frac{M_{SEC2}}{S_{ftcs}} - \frac{M_{wPT}}{S_{ftcs}}$$

$$= 3.39 < 0.4\frac{fcd''}{1000} = 12.41 \text{ MPa.}$$

The strength limit state calculations for design Example 2, which include moment and shear capacities as well as shear resistance of the interface at the splice locations, are not shown here since their procedures are similar to the strength limit state calculations shown for Design Example 1.

6.3.7 Design evaluation

The comparison of negative girder depth of SGB obtained by our optimal design charts is compared with the prismatic girder depth proposed by Lounis (1997) as illustrated in Table 6-2. The total height of our negative girder segment is in the same range that obtained by Lounis (1997). In Lounis study, the prismatic girder section is used for both positive and negative segment while our optimized girder illustrated in this example is used for the nonprismatic negative girder section with a constant web depth.

Table 6-1 *Comparison of negative pier segment between our method and Lounis method*

Results	t_1 (mm)	t_2 (mm)	t_3 (mm)	t_4 (mm)	d_w (mm)	t_w (mm)	H (mm)
Lounis	180	150	100	100	870	150	1400
Our results	127	127	127	127	818	203	1326

Based on the presented design and analysis for the SGB with PCI BT-96 girders, it has been shown that the developed optimized design charts for single-span spliced girder bridges provide satisfactory results and can be efficiently utilized as preliminary design aids. The developed design charts can result in less time effort in the design, can lead to performance improvements of the bridge system and can provide guidance and insight to bridge designers into optimal solutions.

7 Conclusion and Future Research Needs

7.1 Overview

The research presented in this dissertation was possible due to the combination of elastic time-dependent analyses with structural optimization algorithms. This permitted understanding the behavior and performance of spliced girder bridges in terms of different component and system design variables. In addition, the use of standard precast girders and the used of newly proposed optimized sections were studied for improved system efficiency considering system geometry, construction staging and time-dependent effects.

The present study allowed the determination of efficient construction methods and splice locations. The efficiency of standard I-, Box, PCI-BT Beams and new optimal girder sections were determined to use in positive and/or negative segments. The developed optimal negative sections were found to be more efficient than using existing standard sections with attached soffit.

A significant research contribution to the bridge engineering industry is the development of design aids for the preliminary design of spliced girder bridge systems. These design tools can help expedite the design process and eliminate trial and error procedures. With the availability of achievable span lengths, the information in these charts can be a great asset to bridge engineers so that more alternatives during the bridge-type selection process can be available with less effort. The availability of alternative bridge types (i.e., spliced girder bridges) to steel plate girders, can lead to increased competition, which can result in lower cost to owners.

7.2 Conclusions

Conventional precast/prestressed concrete bridges have become the preferred type of bridge construction, primarily for reasons of economy, savings in life-cycle-cost, fast construction and low maintenance. However, the use of precast/prestressed concrete bridges for spans greater than 48.8 m (160 ft) has been limited due to girder transportation and handling weight limitations. Consequently, for medium-span bridges, steel plate girders are typically the chosen solution, although they have the drawback of higher material, construction, and maintenance costs.

In order to overcome these drawbacks and to have an alternative option to compete with steel superstructures, methods to achieve continuity with precast prestressed girders have become of great interest to increase the spanning capabilities of precast concrete bridges. With the advancement in design and material technologies, longitudinal splicing is allowing designers to overcome the limitations of fabrication, shipping, and erection that have prevented the use of very long precast/prestressed concrete girder bridges in the past. Much progress has been made over the past two decades to facilitate the analysis of spliced girder bridges by the development of research and commercial programs (Karim and Tadros 1993, LEAP 2004a). Unfortunately, in spite of these powerful tools, design aids of spliced girder bridges to help designers are not available.

Longitudinally spliced girder construction is not often considered as an option in the preliminary development of design alternates for conventional highway bridges. The reason primarily stems from the limited experience with this typically project-specific type of bridge as well as limited availability of preliminary analysis and design tools.

The availability of design aids for spliced girder bridges can be a great asset to bridge engineers to expedite the design process and promote this bridge system as an alternative during the preliminary design phase. Design aids can simplify the analysis and design of spliced girder bridges by providing guidance on variable sensitivity and reduce effort in the design process. In addition, the availability of achievable spliced span lengths for standard beam types would help the bridge engineer have more alternatives during the bridge type selection with less effort and time investment. Having more choices can lead to increased competition between bridge types and materials, which can result in lower cost to owners. Furthermore, the replacement of an existing multi-span structure with a single-span spliced prestressed girder bridge can reduce overall costs due to the reduction of substructure units.

Implementation of mathematical optimization algorithms can eliminate trial-and-error design procedures and thus lead to the design of more efficient systems. Optimization techniques have been used effectively before to develop design charts for conventional pre-tensioned girders. Computational optimization techniques (Arora 2004) can be used as a tool to produce design aids, charts, and tables based on optimal solutions to expedite the design process. Use of structural optimization for spliced girder bridge design is limited. For single-span spliced girder bridges, only the maximum achievable span lengths of standard 1800 mm (72 in.) girders with three-equal segment lengths by using custom spreadsheets and the program CONSPLICE were investigated (Collett and Saliba 2002). For two-span continuous spliced girder bridges, only studies on newly proposed sections for use in both pre- and post-tensioned construction and achievable span lengths have been performed (Lounis et al. 1997). Based on the authors'

knowledge, at this time there are no available design aids to determine the pre- and post-tensioning requirements and maximum achievable span lengths corresponding to different beam spacings for spliced girder bridges, which was thus the aim of the present study.

This study illustrated the potential of using nonlinear structural optimization approaches integrated with sequential time-dependent design and analysis to develop design aid charts for the preliminary design of spliced precast/prestressed girder bridges. The optimization procedure allowed the determination of design solutions for girder systems in a manner that satisfied a common single objective or a multi-objective when two or more objectives were to be simultaneously satisfied. Multicriteria optimization techniques were used to generate a set of pareto optima with non-dominated solutions to yield a compromise solutions for different single objective functions.

Longitudinal splicing of prestressed girders for single- and two-span continuous bridges were considered in this study. Existing standard sections used for simply supported bridges were used for section lengths under positive moment. Pier or negative segments normally consist of custom-designed sections for beam segments over intermediate supports for continuous bridge solutions. In addition to custom-design sections, existing standard sections with increased soffit were also investigated to use over intermediate supports.

A system optimization approach was used in this study since it provides a systematic approach to arrive at appropriate design solutions. Values that remain fixed in the optimization process, which included girder segment geometries, splice locations, construction sequences, and beams spacing, were considered as design parameters. The

design variables in the optimization problem of spliced girder bridges were those defining the amount and layout of the pre-tensioning and post-tensioning strands in each girder segment. The requirements of pre-tensioning strands, post-tensioning strands, and their locations along the span length were obtained from the optimization studies and presented in terms of design charts. Optimal solutions from design charts were also verified by comparing to the results from a recent NCHRP study (Castrodale and White 2004) and proven to be acceptable solutions.

In the exploration of using standard precast/prestressed girders in single-span spliced girder systems, results showed that shallow girder sections have higher span gain in percentage increase than deeper girder sections. Also, large beam spacing was determined to be more efficient than tight beam spacing for use in a spliced girder system. The use of standard girder sections with increased soffit as the negative segment in two-continuous span bridges was also evaluated. However, the increase in maximum span length is small compared with the increase in the soffit thickness.

In addition to the investigation of standard beams, component optimization was coupled with the system optimization and used as a tool to develop optimal girder shapes for the negative segment of two-span continuous systems. New optimal pier sections were developed for different span lengths, beam spacings, and splice locations. These new optimal negative sections included prismatic sections, non-prismatic sections with varied web depth, and non-prismatic sections with constant web depth.

The developed optimal prismatic girder section has uniform cross-section for both the positive and negative segments. This girder section was developed since the fabrication cost of prismatic girders is lower than for non-prismatic sections when

dealing with negative segments. As compared to the other developed girder sections, the new prismatic girder has a deeper section over the positive moment region and its section height over the negative moment region is bounded by the heights of the optimal non-prismatic girder sections.

The developed optimal non-prismatic girder section with varied web height for the negative segment in continuous systems has a uniform bottom flange thickness and varied web height. The web height increased linearly from the depth of the prismatic positive section to a maximum web height over the pier. Based on the comparison of different developed girder sections, the non-prismatic girder section with varied web depth used over the negative region yields the shallowest section over the positive moment region and the deepest section over the negative moment region.

The developed optimal non-prismatic girder section for the negative segment with uniform web height and a variable bottom flange thickness has a bottom flange with variable thickness that increases linearly from the prismatic positive girder section to its maximum value over the pier. This cross-section approach yields the shallowest negative section as compared to the other developed girder sections. The height of the positive section developed for this non-prismatic negative section is deeper than those required for the girder section with varied web height and shallower than that required for the optimal prismatic girder solution.

The effects of construction sequence for single- and two-span continuous spliced girder bridges were also studied. It was learned that single-staged post-tensioning applied after pouring the deck is the most efficient construction method for single-span

spliced girder bridges, while multi-staged post-tensioning was determined to best for two-span continuous systems due to their longer span length.

Furthermore, the maximum achievable span lengths for spliced girder bridges using existing standard girders and developed optimal girders at different splice locations and beam spacing were obtained and provided as a part of design charts. The most efficient splice locations were determined to be at $0.25(L)$, where L is the total system span length, for a single-span three-segment spliced girder bridge with equal end segments; and at $0.35(L)$ for two-span continuous spliced girder bridge systems.

Material parametric studies were investigated to determine the most efficient option to increase the spanning length of spliced girder bridges. The maximum span length increase was obtained when using lightweight concrete for both girders and deck. However, using a lightweight concrete deck generates less design issues of concern than when using lightweight concrete on the girders, especially regarding prestress losses. Therefore, using lightweight concrete on the deck might be a better option to increase span length for these systems.

The structure's service lifetime in combination with the life-cycle cost of a spliced prestressed girder bridge was integrated into the design optimization process by considering the variation of concrete cover to increase the structure's durability to chloride attach. The studies showed that with an increase in the clear cover of concrete of less than 25 mm (1 in.) the service lifetime of a single-span spliced girder bridge structure can be increased more than twice.

Given the added complexity in the design and analysis of spliced girder bridges, the availability of design aids for spliced prestressed concrete girder bridges could facilitate a reduction of the typical trial and error process in design and be a great asset to bridge engineers to expedite the design process of this bridge type, potentially resulting in its wider use by state highway agencies.

7.3 Future Research

The research presented in this dissertation for new optimal negative sections of two-span continuous spliced girder bridges has not yet been verified by means of experimental testing. Only analytical models were developed and investigated in this study. Thus, the proposed optimal negative sections presented here attempt only to serve as new feasible standard sections for this bridge system. Verification of the analytical results with experimental evaluation can lead to the full development and use of new standard negative sections for continuous spliced girder bridges.

The investigation of using lightweight concrete on the girders could also increase the span length dramatically. However, the execution of a full-scale experimental research program would be needed before accepting the use of this material in a complex design concept such as spliced bridges, especially considering prestress losses and transfer length issues.

The proposed design aids in this research were developed for use only in regions where seismic effects are not an issue. However, the same optimization concept can be used to develop design aids for spliced prestressed girder bridges in seismic zones.

REFERENCES

Chapter 1

American Association of State Highway and Transportation Officials 2003, Bridge design specifications, 2nd edition

Anderson, A. R 1973, " Stretched-out AASHTO-PCI beams types III and IV for longer span highway bridges," PCI Journal, V.18, No. 5, pp 32-49

Arora, J. S. 1997, "Guide to structural optimization," ASCE Manuals and Reports on Engineering Practice No. 90, Reston, VA, American Society of Civil Engineer

Arora, J.S. 1989, "Introduction to optimum design," New York, McGraw-Hill

Arora, J. S. and Haug, E.J. 1979, "Methods of design sensitivity analysis in structural optimization," AIAA Journal, No. 17, pp 970-974

Caroland, W.B., Depp, D., Janssen, H., and Spaans, L. 1992, "Spliced Segmental Prestressed Concrete I-Beams for Shelby Creek Bridge," PCI Journal, V., No., September-Octobe, pp. 22-33.

Castrodale, R.W. and White, C.D. (2004). *Extending Span Ranges of Precast Prestressed Concrete Girders*, NCHRP Report 517, National Cooperative Highway Research Program, Transportation Research Board, Washington, D.C.

Collett B.S., and Saliba, J.E., " Post-tensioning and Splicing of Precast/Prestressed bridge beams to extend spans," Smart Structures and Materials, Proceedings of SPIE, V. 4696, 2002, pp 363-375

Comite Euro-International du Beton (CEB) and the Federation Internationale de la Precontrainte (FIP) "Model code for concrete structures (MC-90).", Thomas Telford, London, Nov 1993

Fitzgerald, J.B., and Stelmack, T.W., "Spliced Bulb-Tee Girders Bring Strength and Grace to Pueblo's Main Street Viaduct," PCI Journal, V., No., November-December 1996, pp 40-54.

Holombo, J., Priestley, M.J.N., and Seible, F., "Continuity of Precast Prestressed Spliced-Girder Bridges under Seismic Loads," PCI Journal, V. No., March-April 2000, pp 40-63.

Janssen, H.H., and Spaans, L., "Record Span Spliced Bulb-Tee Girders Used in Highland View Bridge," PCI Journal, V., No., Januaray-February 1994, pp 12-19.

Leap Software Inc. (2004). *CONSPAN LA®*, < http://www.leapsoft.com>.

Leap Software Inc. (2004). *CONSPLICE PT®*, < http://www.leapsoft.com>.

Lounis,Z., Mirza, M.S., and Cohn, M.Z. " Segmental and Conventional Precast Prestressed Concrete," Journal of bridge engineering, August 1997, pp 73-81

Mathworks Inc. (2004). *MATLAB 6*, Release 13, < http://www.mathworks.com>.

Ronald, H.D., "Design and Construction Considerations for Continuous Post-Tensioned Bulb-Tee Girder Bridges," PCI Journal, V., No., May-June 2001, pp.44-66.

Tadros, M.K., Ficenec, J.A., Elinea, A., and Holdsworth, S., "A new Technique to Create Continuity in Prestressed Concrete Members," PCI Journal, V.38, No.5, September-October 1993, pp 30-37.

Tanase, L.D., Tomley, D.A., Pueschel, G., Zokaie, T., Leap Software Inc., "Precast/Prestressed Spliced-Girder Bridges," International Bridge Conference Special Interest Session at Pittsburgh, Pennsylvania, June 10th 2002.

Chapter 2

American Association of State Highway and Transportation Officials, Bridge design specifications, 2nd edition, 2003

American Concrete Institute (ACI), "Prediction of Creep, Shrinkage, and Temperature Effects in Concrete Structures, ACI 209R-92, ACI Manual of Concrete practice part 1, 2002

Castrodale, R.W. and White, C.D. (2004).*Extending Span Ranges of Precast/PrestressedConcrete Girders*, NCHRP Report 517, National Cooperative Highway Research Program, Transportation Research Board, Washington, D.C.

Collins and Mitchell (1991). "Prestressed Concrete Structures", Prentice Hall, Upper Saddle River, NJ, 1991

Comite Euro-International du Beton (CEB) and the Federation Internationale de la Precontrainte (FIP) "Model code for concrete structures (MC-90).", Thomas Telford, London, Nov 1993

Dilger, H.W., "Creep Analysis of Prestressed Concrete Structures using Creep-Transformed Section Properties," PCI Journal, V.27, No.1, January-February 1982, pp 98-117

Leap Software Inc. (2004). *CONSPAN LA*®, < http://www.leapsoft.com>.

Leap Software Inc. (2004). *CONSPLICE PT*®, < http://www.leapsoft.com>.

Lounis, Z., Mirza, M.S., and Cohn, M.Z. (1997). "Segmental and Conventional Precast

Mathworks Inc. (2004). *MATLAB 6*, Release 13, < http://www.mathworks.com>.

Precast/Prestressed Concrete Institute (PCI), " PCI Design Handbook," Precast and Prestressed Concrete, 4th edition, PCI, Chicago, IL, 1992

Ronald, H.D., "Design and Construction Considerations for Continuous Post-Tensioned Bulb-Tee Girder Bridges," PCI Journal, V., No., May-June 2001, pp.44-66.

Wollmann, G.P., Anderson, R.B., and Wollmann, C.L., "Creep and Shrinkage Effects in Spliced Prestressed Concrete Girder Bridges," PCI Journal, V., No., November-December 2003, pp.92-105

Chapter 3

American Association of State Highway and Transportation Officials, Bridge design specifications, 2nd edition, 2003

Arora, J. S. and Haug, E.J., "Methods of design sensitivity analysis in structural optimization," AIAA Journal, No. 17, pp 970-974, 1979

Arora, J.S., "Introduction to optimum design," New York, McGraw-Hill,1989

Arora, J. S., "Guide to structural optimization," ASCE Manuals and Reports on Engineering Practice No. 90, Reston, VA, American Society of Civil Engineer, 1997

Carmichael, D.G., "Computation of Pareto optima in structural design", International Journal Numerical Methods Engineering, V. 15, No. 6, pp 925-929, 1980

Duckstein, L., "Multiobjective optimization in structural design", New Deirection in Optimum Structural Design, eds. Atrek et al., Wiley, New Yorkpp 459-81, 1984

Lounis, Z., and Cohn., M.Z. " An Engineering Approach to Multicriteria Optimization of Bridge Structures," Microcomputers in Civil Engineering 10, 1995, pp 233-238

Lounis, Z., and Cohn., M.Z., " Multiobjective Optimization of Prestressed Concrete Structures," Journal of Structural Engineering, V. 119, No. 3, March, 1993, pp 794-808

Lounis, Z., " Multilevel & Multiovjective Optimization of Prestressed Concrete Bridge Superstructure Systems," Dissertation, Waterloo, Ont.,University of Waterloo, 1993

Mathworks Inc. (2004). *MATLAB 6*, Release 13, < http://www.mathworks.com>.

Chapter 4

American Association of State Highway and Transportation Officials, Bridge design specifications, 2nd edition, 2003

Castrodale, R.W. and White, C.D. (2004). *Extending Span Ranges of Precast/PrestressedConcrete Girders*, NCHRP Report 517, National Cooperative Highway Research Program, Transportation Research Board, Washington, D.C.

Cohn, M.Z., and Lounis, Z., "Optimal Design of Structural Concrete Bridge Systems", Journal of Structural engineering, V. 120, No.9, Sept 1994, pp 2653-2674

Lounis Z., and Cohn., M.Z., " An approach to Preliminary Design of Precast Pretensioned Concrete Bridge Girders," Microcomputers in Civil Engineering 11, 1996, pp 381-393

Lounis,Z., Mirza, M.S., and Cohn, M.Z. " Segmental and Conventional Precast Prestressed Concrete," Journal of bridge engineering, August 1997, pp 73-81

Leap Software Inc. (2004). *CONSPAN LA®*, < http://www.leapsoft.com>.

Leap Software Inc. (2004). *CONSPLICE PT ®*, < http://www.leapsoft.com>.

Mathworks Inc. (2004). *MATLAB 6*, Release 13, < http://www.mathworks.com>.

Stephen L. Amey; Dwayne A. Johnson; Matthew A.Miltenberger; and Hamid Farzam, "Predicting the Service life of Concrete Marine Structures: An environmental Methodology," ACI Structural Journal, March-April 1998, pp. 205-214

Yoshiki Tanaka, Hirotaka Kawano, Hiroshi Watanabe, "Study on Required Cover Depth of Concrete Highway Bridges in Coastal Environment," 17th U.S.-Japan Bridge Engineering Workshop, 2001, Tsukuba, pp.1-16

Chapter 5

American Association of State Highway and Transportation Officials, Bridge design specifications, 2nd edition, 2003

Castrodale, R.W. and White, C.D. (2004). *Extending Span Ranges of Precast Prestressed Concrete Girders*, NCHRP Report 517, National Cooperative Highway Research Program, Transportation Research Board, Washington, D.C

Surakomol and Burgueno (2005). *Preliminary design aid charts for Spliced Precast/Prestressed Concrete Girder Bridges Report*, Michigan State University, Civil and Environmental Engineering Department

Chapter 6

American Association of State Highway and Transportation Officials, Bridge design specifications, 2nd edition, 2003

Castrodale, R.W. and White, C.D. (2004). *Extending Span Ranges of Precast Prestressed Concrete Girders*, NCHRP Report 517, National Cooperative Highway Research Program, Transportation Research Board, Washington, D.C

Chapter 7

Arora, J. S. (2004). *Introduction to Optimal Design*, 2nd Ed., Elsevier Academic Press, San Diego, CA.

Castrodale, R.W. and White, C.D. (2004). *Extending Span Ranges of Precast Prestressed Concrete Girders*, NCHRP Report 517, National Cooperative Highway Research Program, Transportation Research Board, Washington, D.C.

Collett B.S., and Saliba, J.E. (2002). "Post-tensioning and Splicing of Precast/prestressed bridge beams to extend spans." *Proc., Smart Structures and Materials*, SPIE, 4696, 363-375.

Karim, A. M., and Tadros, M.K., "Computer Analysis of Spliced Girder Bridges," ACI Structural Journal, V., No., January-February 1993, pp 21-31.

Leap Software Inc. (2004). *CONSPAN LA®*, < http://www.leapsoft.com>.

Leap Software Inc. (2004). *CONSPLICE PT ®*, < http://www.leapsoft.com>.

Lounis,Z., Mirza, M.S., and Cohn, M.Z. " Segmental and Conventional Precast Prestressed Concrete," Journal of bridge engineering, August 1997, pp 73-81